Jagiellonian University
Department of Physics, Astronomy and Applied Computer Science

A thesis submitted for the degree of Doctor of Philosophy in Astronomy

Outbursts in Close Binary Systems

by

Iwona Kotko

written under the supervision of

Prof. Jean-Pierre Lasota-Hirszowicz

Cracow, 2012

Acknowledgements

I would like to express my deepest gratitude to my supervisor, prof. Jean-Pierre Lasota, for his confidence and enormous patience and for all his knowledge and experience he has been willing to share with me. He made me realize what are the important conditions to be a good scientists and what one should work on to head in that direction.

I owe my gratitude to prof. Marek Abramowicz, for that he gave the right direction to my scientific path.

I thank all I had opportunity to work with and who contributed to this thesis, especially to dr Guillaume Dubus.

I would like to thank my husband Piotrek, for his trust in me and his support. Without him I wouldn't be at this point.

I also thank his family for their heart and understanding.

Finally, I thank my family:
my brother Marek and his wife Ela, for supporting me and motivating me especially in hard moments,
and my Father, especially to him, for everything.

The preparation of this thesis was supported by doctoral dissertation grant awarded by the Ministry of Science and Higher Education, grant number PSP/K/PBP/000392.

Preface

Since the discovery of U Gem in the middle of 19^{th} century the outbursts of dwarf novae attracted attention of astronomers. The origin of these eruptions of amplitudes up to ~ 5 mag showing up with various recurrence times (from 1 day to even 33 years) remained a puzzle until the beginning of the eighties when the theory explaining them begun to crystallize and was eventually formulated by Meyer and Meyer-Hofmeister (1981); Smak (1982, 1984); Cannizzo et al. (1982); Faulkner et al. (1983); Mineshige and Osaki (1983).

The model proposed (the Disc Instability Model, DIM) describes outbursts in close binary systems as the result of thermal-viscous instability in accretion disc surrounding the more massive among the two stars of the close binary. In the case of dwarf novae this more massive star is a white dwarf. During the time between the outbursts the disc gradually accumulates the matter which is transferred to it from the second, low-mass component of the binary. The instability sets in when at some point in the disc the density and temperature become so high that the dominant chemical element of the disc matter becomes partially ionized and the opacities dependence on temperature changes rapidly. This leads to the formation of the steep gradients of temperature and surface density which start to propagate through the disc, rising its luminosity. One observes this as the beginning of an outburst.

Since the star which transfers the matter is a late-type main-sequence star the discs in dwarf novae consist mainly of hydrogen and the instability develops at the temperature of hydrogen ionization. However, the mechanism leading to the instability should be universal with respect to the chemical composition of the disc what we confirm in this work.

There is a group of close binaries which is a perfect testbed for the model of outbursts - the AM CVn stars. This class of stars is very peculiar: they have helium-dominated spectra in which no hydrogen lines are detected and their extremely short orbital periods span the range from ~ 5.4 to 65.1 minutes. The light curves of outbursting AM CVn stars are very complex. Not only they combine the characteristic features of different kinds of dwarf novae (SU UMa, ER UMa, Z Cam and WZ Sge-type systems) but also show a variety of properties never observed in their hydrogen-rich cousins.

Up to now there are only a few papers considering the AM CVn stars from the theoretical point of view (Tsugawa and Osaki (1997a); Lasota et al. (2008); Cannizzo (1984); Smak (1983)) and in our opinion this subject desires more detailed treatment. Most of the literature is devoted to the investigations of the influence of helium on the local thermal equilibrium in the disc and its consequence

for stability limits of the disc and, as far as we know, there has been only one attempt of modeling the AM CVn light curves (Tsugawa and Osaki (1997b)).

We also investigate the influence of helium on the local thermal equilibrium of the disc which connected with opacities and ionization temperatures and we test how the conditions in the helium-dominated disc impact the viscous-thermal instability. We compare the results with those for the hydrogen-dominated discs. But additionally we complement these information with the detailed analysis how the atomic structure of helium manifests itself in the structure and properties of the fronts propagating in a helium disc. The big part of our work considers the modeling of the AM CVn light curves within the framework of the Disc Instability Model supplemented by additional components which are: the additional sources of the disc heating (hot spot and the primary white dwarf), the primary white dwarf's magnetic field and the enhanced mass transfer rate. We use our results to explain at least some of the features seen in the outburst pattern of helium-rich compact binaries.

The physical mechanisms driving angular momentum transport in accretion discs rise more questions than there are reliable answers. Despite the big uncertainties regarding its description in the terms of the basic physics, the modeling of accretion disc behavior is still possible owing to the Shakura-Sunyaev prescription (Shakura and Sunyaev, 1973). It assumes that the "viscosity" in the disc is turbulent in origin and that it can be parametrized with α which takes the values between 0 and 1. The simulations of dwarf nova outbursts have shown that α should have different value in outburst ($\alpha_{\rm h}$) and in quiescence ($\alpha_{\rm c}$) (Smak, 1984) in order to reproduce outbursts of amplitudes corresponding to observations. Moreover, from the comparison between models and observations it can be deduced that the value of $\alpha_{\rm h}$ should be $0.1 - 0.2$ (Smak, 1999).

Nowadays the best candidate to explain the origin of the turbulence in accretion discs is the model of the Magneto-Rotational Instability (MRI). But one of the most serious problems of this mechanisms is that the numerical simulations of MRI predict the values of the stress-to-pressure ratio (the α "viscosity" parameter) in hot accretion discs (above the temperature of the dominant chemical element ionization) an order of magnitude lower than those deduced from observations of outbursting discs ($\alpha_{\rm h} \sim 0.01$).

This discrepancy between values of $\alpha_{\rm h}$ obtained from MRI simulations and deduced from observations and models of dwarf nova outbursts is a serious problem for theory which intends to explain the angular momentum transport in the disc. There are also not many attempts to evaluate α empirically and to our knowledge the main work considering this subject has been done by Smak (1999).

We therefore repeat the reasoning of Smak (1999) but with new set of data consisting not only from dwarf novae but also supplemented with one AM CVn star what give a hint about the dependence of the results on the chemical composition of the disc. We also use different code for numerical simulations. Additionally we derive semi-analytically the decay time of an outburst (which depends on $\alpha_{\rm h}$) and check which α value would give the time corresponding to decay time measured in dwarf nova and AM CVn star outbursts.

We consider also the Kukarkin-Parenago relation which is the empirical relation between outburst amplitudes and recurrence times in dwarf novae. Motivated by the fact that such a relation should

result also from the model which describes the outbursts in those systems we find that it is possible to derive a similar relation from the DIM. We show that it applies also to helium discs what is an additional argument in favor of universality of DIM with respect of chemical properties of the disc. As $\alpha_{\rm h}$ is an explicit parameter in the derived relation it supplements us with another tool for verification of $\alpha_{\rm h}$ both in hydrogen-rich and helium-dominated discs.

This thesis is organized as follows: in Chapter 1 we introduce briefly the history of discovery of close binary systems and their classification. We also describe the paths of their evolution which lead to the formation of dwarf novae and AM CVn stars. Chapter 2 is devoted to description of the Disc Instability Model. We introduce and explain the equations describing the vertical structure of the disc and its time evolution and the consequences of their solutions - the so called S-curves and the behavior of the disc during one outburst cycle. In the last section of this chapter we analyze the impact of helium on the properties of the DIM. The numerical methods and the description of the scheme of operation of the Fortran code used for simulations of the thermal-viscous instability in hydrogen- and helium-rich discs are presented in Chapter 3. Chapter 4 presents our results considering modeling of the AM CVn star light curves and it is based on our paper which is in press (Kotko et al., 2012). The results regarding the value of α in hot accretion discs are described in Chapter 5. This chapter is based on our second paper which has been recommended for publication, however has not been yet formally accepted. The conclusions are given in Chapter 6 and additional expressions for the critical values in accretion discs of various chemical compositions are listed in Appendix.

Contents

Chapter 1

Introduction

1.1 History of Cataclysmic Variables observations

According to the latest investigations (Jetsu et al., 2012) the history of variable binary stars may have started yet in ancient times when the Egyptians have recorded the period of Algol brightness changes into the Cairo Calendar. In 17th century John Goodrick, a young British amateur astronomer (re)discovered the variability of Algol and suggested that it is caused by the body passing in front of the companion star making it the first ever observed eclipsing binary system.

There are mentions of nearly 100 suddenly occurring "novae stelle" (novae and supernovae) visible with naked-eye in the dynastic chronicles of Far East empires between 200 B.C. and 1600 A.D. . Meanwhile astronomers in Western Europe had to await for the observations of supernovae by Tycho Brahe in 1572 and Johannes Kepler in 1604, and the outburst of P Cygni (which is nowadays known to be a Luminous Blue Variable star) by Willem Blaue in 1600 to realize that stars are not immutable and still but that their nature can be violent and eruptive. The first star (in Europe) confirmed strictly as nova was Nova Vulpecula (CK Vul) discovered by Père Dom Anthelme, a Carthusian monk in Dijon, in 1670. This was a beginning of the discoveries of stars which at present are generally classified as Cataclysmic Variable Stars (hereafter CVs).

In December 1855 John Russell Hind observed a star which suddenly brightened by about 4 magnitudes. This blue variable star, named U Geminorum, faded away after about 9 days and three months later brightened again. This clearly showed that U Gem is not an ordinary nova but a member of a new class of CVs - the Dwarf Novae (hereafter DN).

1.2 Classification of close binaries

The basic criterion which divides the binaries in general into classes is connected with their geometry.

The geometry of binaries was first studied by Edouard Roche. He considered the motion of a test particle in the gravitational field of two stars orbiting each other on a circular orbit. The circular

orbit approximation is relevant in many cases because the tidal forces tend to circularize the initially eccentric orbits on a time scale which is short comparing to the time scale over which the mass transfer between stars sets in.

The binary orbital separation a is defined through the III Kepler law by the binary orbital period $P_{\rm orb}$ and masses M_1, M_2 of the components:

$$4\pi^2 a^3 = G(M_1 + M_2)P_{\rm orb}^2 \tag{1.1}$$

where G is the gravitational constant.

In what follows we always define M_1 as the mass of the primary (considering the binary in the final stage of its evolution) and M_2 as the mass of its companion.

The gravitational potential $\Phi_{\rm R}(\vec{r})$ generated by above described configuration of two stars is known as the Roche potential. Assuming that the binary system rotates with respect to the observer with the angular velocity $\vec{\omega}$ and that $\vec{r}_1$, $\vec{r}_2$ are the position vectors of the centers of the stars with respect to their center of mass, the potential takes the form:

$$\Phi_{\rm R}(\vec{r}) = -\frac{GM_1}{|\vec{r}-\vec{r}_1|} - \frac{GM_2}{|\vec{r}-\vec{r}_2|} - \frac{1}{2}(\vec{\omega}\times\vec{r})^2. \tag{1.2}$$

There is one special case among all the surfaces of constant $\Phi_{\rm R}(\vec{r})$. This special critical equipotential surface has a figure-of-eight shape. Its two parts are called the *Roche lobes* and each of them surrounds one binary component. The point at which the Roche lobes join is the *Lagrangian point* L_1. The motion of a gas inside the Roche lobe is dominated by the gravitational field of the star to which this lobe is connected but as the gas approaches the L_1 (which is the saddle point) it may eventually pass through it and flow into the Roche lobe of the second star (Frank et al., 2002). Therefore, the form $\Phi_{\rm R}(\vec{r})$ and existence of the critical equipotential surface enables transfer of mass between stars in binaries.

The radius of the Roche lobe of the less massive star is given by the formula found by Eggleton (1983):

$$\frac{R_2}{a} = \frac{0.49\,q^{2/3}}{0.6\,q^{2/3} + \ln(1+q^{1/3})} \tag{1.3}$$

where $R_2$is a star radius and $q \equiv M_2/M_1$ is the ratio of the considered star mass to the mass of the second component.

According to the degree at which the stars fill their Roche lobes the binaries fall into three categories:

(a) *detached binaries* - both stars have sizes smaller than their Roche lobes and the mass transfer between them may occur inly via stellar wind. All binaries are formed as detached binaries.

(b) *semi-detached binaries* - only one of the stars fills its Roche lobe and the mass starts to pass through the L_1 point onto the second star.

(c) *contact binaries* - both stars fill their Roche lobes. In opposite to the common envelope which is

the unstable phase of the close binary evolution (see below) the contact binaries form a stable configuration lasting billions of years. The examples of the systems belonging to this category are the contact eclipsing binaries called W UMa.

The term *close binary* refers to the semi-detached binaries in which a low-mass companion star transfers the mass onto the compact object - white dwarf (in short WD), neutron star (in short NS) or stellar-mass black hole (in short BH). For this reason the compact object is also called *accretor* or *primary* while the star from which the mass is transferred is called *donor* or *secondary*.

Close binary stars with white dwarfs accreting matter from donors filling their Roche lobe are called the *Cataclysmic Variables* (CVs) while those with neutron stars or black holes are *X-ray binaries.*

With respect to the character of the light curves one can distinguish different types of CVs:

1. *Novae*

They show very large eruptions (up to 12 mag) which are caused by the thermonuclear explosions of hydrogen[1] on the surface of white dwarf when the temperature of accreted material crosses reaches the ignition temperature and unstable hydrogen burning set in. The *classical novae* erupt only once during their observational history while *recurrent novae* repeat the outburst at least one more time.

2. *Dwarf Novae*

Their outbursts are of lower amplitude than those in novae and occur much more often. But the crucial difference is that the DN outbursts are the result of *the thermal-viscous instability* in accretion disc (see Chap. 2). DN can be further divided into three subgroups depending on the characteristic features observed in their light curves :

(a) *U Gem-type*

They show only *normal* outbursts which show up in a quasi-periodic way. The normal outbursts have amplitudes from 2 to 5 mag and their recurrence times may be as short as few days. Usually they appear every several tens of days.

With respect to their duration times normal outbursts may be divided into *narrow* and *wide*. The distinction between them follows from the observational comparisons not from the strict definition but one can adopt that the narrow are these which last $\sim 1-5$ days while wide ones are longer, up to ~ 20 days.

Most of the observed U Gem-type stars have orbital periods above the *period gap*, i.e. $P_{\rm orb} > 3\,{\rm hr}$ (see Sect.1.3).

(b) *SU UMa-type*

All SU UMa stars have orbital periods below ~ 2 hr (below the period gap). Their light curves consist of normal outbursts and *superoutbursts.* Superoutbursts are the eruptions which are usually brighter by $\sim 0.5-1$ mag than normal outbursts and last $5-10$ times

[1] There are also known cases of helium novae, e.g. V445 Pup.

longer (Warner, 1995). The characteristic feature of superoutbursts, which does not appear during normal outbursts, are the low-amplitude short-period light variations called *superhumps*.

Among SU UMa-type dwarf novae there can be singled out two groups of stars which differ by the *supercycle* duration (the supercycle is the time which passes from the onset of one superoutburst to the onset of the next superoutburst):

(i) *ER UMa*

They are the SU UMa stars which supercycles are very short (e.g. $\sim$ 43 days for ER UMa itself, $\sim$ 32 days for DI UMa or even $\sim$ 19 days in the case of RZ LMi). Between superoutbursts several normal outbursts usually appear.

(ii) *WZ Sge-type*

Their orbital periods $P_{\rm orb}$ are near the orbital period minimum for DN ($\sim$ 80 min) and their superoutbursts (and outbursts in general) are very rare: the recurrence times may reach even $\sim$ 30 yr (like in the case of WZ Sge itself). The interesting feature of WZ Sge- type star light curves is the appearance of the so called *cycling state* during the superoutburst decline: after the first phase of brightness decay from superoutburst maximum the system, instead of fading to the minimum luminosity, brightens again to the level $\sim$ 2 mag below the maximum and starts to outburst on the short time scale ($\sim$ 1 day) with amplitude up to $\sim$ 1 mag. This phase may be as long as superoutburst itself and when it ends the system falls back to the minimum light.

(c) *Z Cam-type*

Z Cam stars are DN with very high mass transfer rates which are close to their critical values (see Sect. 2). In their light curves there are periods of elevated brightness which is lower by $\sim$ 1 mag from the normal outburst maximum. Those periods may last for months or even years and are called *standstills*. After the standstill Z Cam-type systems returns to its low luminosity state.

3. *AM CVn stars*

AM CVn stars are the binaries with ultra-short orbital periods ($\sim 5.4-65$ min) and with spectra which do not show any hydrogen lines. They are also called the helium dwarf novae because the mechanism of their outbursts is believed to be the same as in the case of DN. Their light curves are very complex and combine features of all dwarf nova classes. The detailed description of AM CVn stars is given in Chap. 4.

With regard to the strength of accretor magnetic field, CVs can be divided into:

1. *Non-magnetic* CVs

These are all systems specified above.

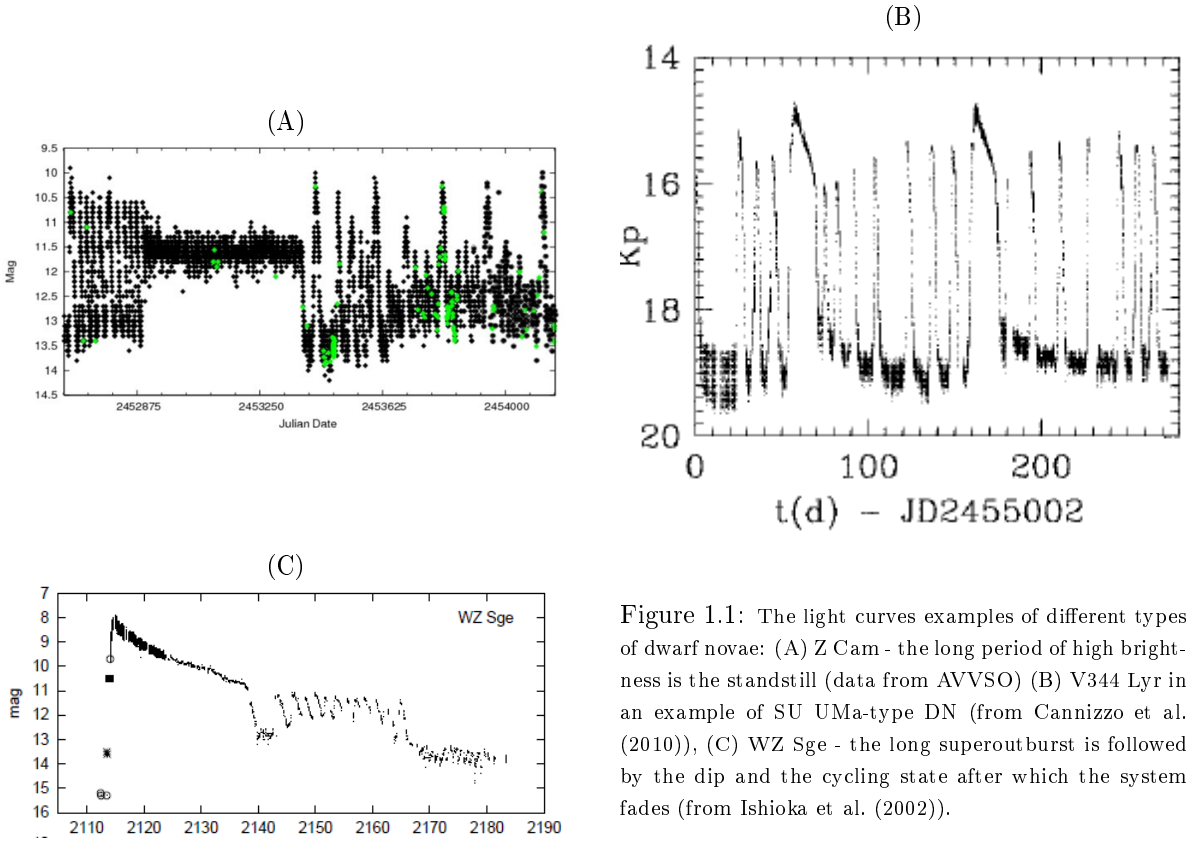

Figure 1.1: The light curves examples of different types of dwarf novae: (A) Z Cam - the long period of high brightness is the standstill (data from AVVSO) (B) V344 Lyr in an example of SU UMa-type DN (from Cannizzo et al. (2010)), (C) WZ Sge - the long superoutburst is followed by the dip and the cycling state after which the system fades (from Ishioka et al. (2002)).

2. *Polars* (the magnetic CVs)

   In these systems the magnetic field of primary is strong enough to prevent the formation of accretion disc and accretion stream falls onto the white dwarf following the lines of its magnetic field (e.g. AM Her).

3. *Intermediate polars*

   The strength of their magnetic fields allows the formation of the narrow accretion disc farther away from the primary but as the distance to the WD decreases the accretion disc is truncated (e.q. DQ Her).

1.3 Evolution

The distribution of the orbital periods in CVs is determined by their evolution. The DN have $P_{\rm orb}$ between 75 min and 8 hr (Ritter, 2008) with the famous period gap between 2 and 3 hr. At the short end of the orbital period range ($P_{\rm orb} \sim 8 - 65$ min) are the AM CVn stars.

White dwarfs in binaries form from the stars of initial masses $M_i \lesssim 10\,{\rm M}_\odot$ which have not started the carbon burning in their cores yet. The progenitors of WDs obey the core mass-radius relation,

which means that the more massive WD is to be formed the more space its progenitor star needs. This has a consequence for binaries in which the orbital separation a sets the limits for the mass of WD which can be formed.

The investigations of the Algol system by Gerard Kuiper in 1941 revealed the problem which became known as the "Algol paradox". The paradox lied in the fact that the more massive star was found to be still a main-sequence star of early type, i.e. it appeared to be younger than its less massive companion classified as Roche-lobe filling subgiant. From the laws of the stellar evolution it was known that the more massive is the star the faster it evolves, i.e. the star with higher mass should be older. The first to suggest the solution to this problem was Crawford (1955) who claimed that the subgiant had been originally more massive but then it lost his mass for the benefit of its younger companion.

It appeared that the mass transfer from one component to another in a binary system is a critical factor for the binary evolution.

1.3.1 General evolution of CVs

The possible scenarios of binary stars origin which are nowadays taken into account consider (i) the capture mechanism when two initially isolated stars become bound through the two- or three-body encounter and (ii) the different processes of a rotating gas cloud fragmentation (Tohline, 2002), however, the formation of such systems is still far from being understood.

Once a binary consisting of two main sequence stars has formed the subsequent evolution depends on the masses of its components and their mutual distance.

The first mass transfer event may take place depending on the evolution phase of the stars and their orbital separation. There are three cases (Paczyński, 1971) :

(A) One of the stars expands on the nuclear time scale determined by hydrogen burning process. It reaches its Roche lobe if the initial size of the binary is equivalent to the orbital period $P_{\rm i,orb}$ of $\sim 0.65 - 1.5$ d.

(B) The star has finished hydrogen burning and its core rapidly contracts just before the onset of helium burning. The binary will become semi-detached binary if $P_{\rm i,orb} \approx 1.5 - 87$ d.

(C) The similar situation to case (B) will appear just before the onset of the core carbon burning by one of the stars, for binaries with initial orbital periods > 87 d.

Once the mass transfer sets in it proceeds in two stages. During the first stage the mass transfer rate is very violent and takes place on Kelvin-Helmholtz time-scale $t_{\rm K-H}$ which gives the maximum rate at which mass can be transferred

$$\dot{M}_{\rm tr,max} \equiv \frac{M_2}{t_{\rm K-H}} = 3.2 \times 10^{-8}\,{\rm M}_\odot/{\rm yr}\ \frac{R_2 L_2}{M_2} \tag{1.4}$$

where M_2, R_2, L_2 are the mass, radius and luminosity of the donor respectively. This stage is the same for the onset of mass transfer in all three phases (A-C) of the star's evolution. What happens

next depends on the phase of the star's evolution at which the mass transfer started and on the masses of the binary components:

(1) In general the more massive star evolves faster. Therefore considering case (A) (above) the donor is initially more massive star burning hydrogen which expands and fills its Roche lobe first. When the rapid mass exchange takes place the mass ratio is inverted. The occurring semi-detached binary evolves slowly, the donor (which is now less massive) fills the Roche lobe as a subgiant which is still burning hydrogen in its core.

(2) If the initial mass of the donor is $M_{\rm i,2} \gtrsim 3.0\,{\rm M}_\odot$ the rapid mass transfer stage ends up with the helium ignition in its core. The fusion of helium releases the energy which drives the core expansion. At the same time the rate of hydrogen burning in the layers surrounding the core decreases and the star's envelope contracts. The size of the star becomes smaller than the size of its Roche lobe what inhibits the mass transfer. The donor settles near the helium main sequence track.

(3) If $M_{\rm i,2} < 3.0\,{\rm M}_\odot$ then the electron degeneracy pressure will balance the donor core contraction at some point of the rapid mass transfer phase. The mass exchange rate slows down while the donor slowly burns hydrogen in the shell at the bottom of its envelope. When the hydrogen reserve depletes the star radius decreases while it loses its envelope and the white dwarf forms.

This description is valid in the case of conservative mass transfer rate, i.e. when all mass transferred from the secondary is accreted by the primary. The stable mass transfer from a donor is possible if the mass ratio $q \equiv M_2/M_1 \lesssim 1.2$ and if the donor is not a star with a convective envelope (Podsiadlowski, 2008).

The CV progenitor has to be a binary which is wide enough to accommodate the WD progenitor, i.e. the red giant (or supergiant) star of $R \sim 10 - 100\,R_\odot$. As the red giant is a star with convective envelope and $q > 1.2$ the criteria for stable mass transfer are not satisfied. In fact the formation of a system with short orbital period of order of hours from such a wide binary needs high mass and angular momentum losses from the system. The phase during which it happens is called *the common envelope (CE)* phase (Paczynski, 1976).

At the very beginning of the mass transfer from the red giant onto the less massive star both the orbital separation a and Roche lobes shrink. It follows from the formula (Frank et al., 2002):

$$\frac{\dot{a}}{a} = \frac{2\,\dot{J}}{J} + \frac{2\,(-\dot{M}_2)}{M_2}\left(1 - \frac{M_2}{M_1}\right) \tag{1.5}$$

where $\dot{M}_2 < 0$ and the total angular momentum of a binary J:

$$J = M_1 M_2 \sqrt{\frac{a\,G}{(M_1 + M_2)}}. \tag{1.6}$$

At the same time the massive donor (a giant or supergiant) tends to expand with response to

the mass loss. This leads to the unstable mass transfer phase during which the huge amount of gas passing through L_1 can not be incorporated by the accretor and instead it starts to piles up and expand. Eventually the matter excess overfills the accretor Roche lobe and forms the common envelope around the accretor and the core of the donor. At this point the degenerate core of the giant star and the low-mass star do not fill their Roche lobes. It is supposed that the evolution of the core and the star inside the envelope is driven by the dynamical friction drag and leads to the gradual shrinkage of the components orbit (Postnov and Yungelson, 2006). Finally the CE is ejected leaving behind the detached MS-WD binary - the pre-CV system. The subsequent evolution is determined by a rate at which the angular momentum is being lost from the system and by the evolution of a low-mass component.

When enough angular momentum is lost from the system and/or low mass star has evolves to the stage at which it fills its Roche lobe, the binary components enter into the contact again forming a cataclysmic variable star.

There are two mechanisms which can be responsible for angular momentum loss (hereafter AML) from the binary: *gravitational radiation* (GR) and *magnetic stellar wind* (MSW) (i.e. *Magnetic Braking* (MB)).

In general the AML by GR acts in every binary and sets the minimum rate at which the binary angular momentum J is drained. The rate at which J is removed from the system by GR, under the assumption that binary orbit is circular, is given by Landau and Lifshitz (1975)

$$\left(\frac{\dot{J}}{J}\right)_{\rm GR} = -\frac{32}{5}\frac{G^3}{c^5}\frac{M_1 M_2 (M_1+M_2)}{a^4} \tag{1.7}$$

However, CVs with orbital periods above ~ 3 hr have much higher AML rates than predicted from GR theory and the additional mechanism for AML is needed. The widely accepted candidate is the magnetic stellar wind.

The magnetic braking is believed to be effective mechanism of AML for the stars with masses $M = 0.3 - 1.5\,{\rm M}_\odot$ (dwarfs of G-M type) (Postnov and Yungelson, 2006) which all posses weak stellar winds. Above and below this limits the dynamo mechanism which drives the magnetic activity is suppressed: when $M > 1.5$ M$_\odot$ the convective zone in the star disappears and for $M < 0.3$ M$_\odot$ the star becomes fully convective.

When the stellar wind is highly ionized it is forced by the magnetic field of the star to co-rotate with it up to the Alfvén radius. The torque which the corotating wind exerts spins the star down. At the same time the tidal forces tend to keep the synchronization between the binary orbit and the spin of the Roche-lobe filling donor. Thus the result of the magnetic wind is the extraction of the angular momentum from the system as a whole.

The change of J due to magnetic braking describes the formula (Postnov and Yungelson, 2006)

$$\left(\frac{\dot{J}}{J}\right)_{\rm MSW} \sim -\frac{R_2^4}{M_1}\frac{G(M_1+M_2)}{a^5}. \tag{1.8}$$

The characteristic time scale for angular momentum removal due to GR is $\tau_{\rm GR} \equiv \left(\dot{J}/J\right)^{-1}_{\rm GR} \propto a^4$, and the same time scale in the case of MB is $\tau_{\rm MSW} \propto a$ (because the radius R_2 of the donor filling its Roche lobe should be proportional to a). The comparison between $\tau_{\rm GR}$ and $\tau_{\rm MSW}$ shows that angular momentum loss by gravitational radiation will be dominant for binaries with short $P_{\rm orb}$ while for binaries of larger sizes the magnetic braking will dominate. However, one should keep in mind that the prescription for MB is still the matter of debate.

The gap in the period distribution of the observed CVs which appears between $P_{\rm orb} = 2\,{\rm hr}$ and $P_{\rm orb} = 3\,{\rm hr}$ is supposed to be connected with the MB mechanism and the evolution of a donor. According to this the donor in a binary at 3 hr becomes fully convective. The stellar wind in such a star is strongly reduced and the efficiency of MB sharply decreases and so does the mass loss rate. As the secondary shrinks it disconnects from its Roche lobe, the system becomes the detached binary and evolves to shorter $P_{\rm orb}$ through the angular momentum loss driven by the gravitational radiation. Near $P_{\rm orb} \sim 2$ hr the extend of the Roche lobe approaches the size of the donor and the mass transfer is restored.

There is a minimum value of orbital period for CVs $P_{\rm orb,min} \sim 80$ min connected with the evolution of the donor and loss of angular momentum from the binary through the gravitational radiation.

1.3.2 The possible evolution channels of AM CVn stars

One of the possible outcome of the CVs evolutionary tracks are AM CVn stars. They may form if in the course of the CV evolution the second CE event appears. After this second CE phase the binary keeps loosing its angular momentum, the low-mass secondary (most probably helium white dwarf) fills its Roche-lobe and the AM CVn star is born.

From the spectroscopic observations of AM CVn stars it is clear that the donor has to be helium-rich. The possibility that the donor is a zero-age helium star of mass $0.4 - 0.5\ {\rm M}_\odot$ can be discarded because otherwise the observed AM CVn star spectra would be dominated by its contribution while this is not observed. The second candidate for a donor in the considered binaries is a low-mass ($\lesssim 0.3\,{\rm M}_\odot$) helium white dwarf (He-WD) (Nelemans et al., 2010). He-WD can not be more massive as the system has to fulfill the criterion $q \equiv M_2/M_1 < 0.2$ to avoid the unstable mass transfer leading to the coalescence of the binary components.

He-WD is created when the star of initial mass $M_i \lesssim 2.2\,{\rm M}_\odot$ has lost the hydrogen-rich envelope before it reaches the stage of He-flash. The formation of He-WD is possible only due to the mass transfer rate between the components in close binaries because the mass loss through the stellar wind by a single star on the first giant branch is not strong enough to lead to the complete loss of the star's envelope.

There have been proposed three formation channels for AM CVn stars depending on the character of the donor progenitor (Nelemans et al., 2010).

1.3.2.1 The WD channel.

In this evolution channel the AM CVn star forms from the initially detached double white dwarf binary of relatively short orbital period. The orbital separation between the low-mass He-WD secondary and more massive CO-WD primary decreases as the angular momentum is taken away from the system by gravitational radiation.

Within the lifetime of the Galactic disc the He-WD and the CO-WD are brought into the contact and the Roche lobe overflow from the lower mass He-WD starts. This moment is the origin of AM CVn star under the condition that the mass transfer from the donor is stable. This condition depends on the mass ratio q and the mass-radius relation of the donor which implicitly incorporates the information about donor temperature and chemical composition (Paczyński, 1969)

$$q \equiv \frac{M_2}{M_1} < \frac{5}{6} + \frac{\zeta(M_2)}{2} \tag{1.9}$$

where $\zeta(M_2) \equiv d\ln R_2/d\ln M_2$ is the mass-radius index.

If one adopts the mass-radius relation for degenerated stars in the form $R \sim M^{-1/3}$ than the criterion for the stability of the mass transfer becomes: $q \leq 2/3$.

From theoretical considerations of the evolution through the WD channel it seems that none of the AM CVn stars has an accretion disc formed at the beginning of its existence. It can happen only after $\sim 10^7$ years when the mass of the donor becomes lower than $\sim 0.05\,\mathrm{M}_\odot$ and the binary orbit extends enough that the primary Roche lobe can incorporate the disc (Nelemans et al., 2001).

1.3.2.2 The helium star channel.

Another possibility is that the donor transferring mass onto the WD primary evolves from the low-mass ($\sim 0.4-0.6$ $\mathrm{M}_\odot$) burning core helium star. The progenitor of such helium star is the $2.3-5.0\,\mathrm{M}_\odot$ mass star which undergoes the mass transfer. Such a star and WD are at first in detached binary. If the initial $P_{\mathrm{i,orb}}$ is short enough the components will approach each other due to gravitational radiation before the time when helium in the donor star core will be exhausted. The mass transfer which will appear as a consequence of this process will be stable if $q < 1.2$ (Nelemans et al., 2001). The helium burning stops when the donor mass falls below $0.2\,\mathrm{M}_\odot$ and the helium star becomes semi-degenerate. So far positive exponent in the $M-R$ relation for donor changes the sign and P_{orb} starts to increase with the further mass loss from the donor. The orbital period has a minimum value around ~ 10 min which is determined by the changes in the structure of the transferring mass star. In several Gyr the donor mass falls down to $0.01\,\mathrm{M}_\odot$ and P_{orb} of the binary approaches ~ 1 hr.

In this channel the accretion disc forms always because the orbit is sufficiently wide at the onset of the mass transfer.

1.3.2.3 The evolved main-sequence star channel.

It is possible that after the first CE event the binary is too large to undergo the second CE event in reasonable time. In this case the progenitor of AM CVn star may be the CV with an evolved main-sequence star donor ($M \sim 1.0\,\mathrm{M}_{\odot}$) which fills its Roche-lobe just at the end of the hydrogen-burning phase of its evolution (Podsiadlowski et al., 2003). During mass transfer the donor eventually unveils its helium-dominated core and the subsequent evolution is similar to the evolution in the helium-star channel.

The evolution through the WD channel and through the He-star channel follows roughly by the same path after the He-star becomes degenerated. The MS-star channel may be still distinguished from the other two until the binary reaches the orbital period minimum because the donor envelope should contain observable amounts of hydrogen. After P_{orb} minimum, however, all three channels of AM CVn stars evolution are hard to separate.

Chapter 2

Disc instability model

In this chapter we present the basic version of the Disc Instability Model. We start with the brief description of accretion disc formation where we introduce the quantities defining the disc and the basic problem of angular momentum transport. Next we outline the disc structure and evolution equations and their consequences for local and global behavior of the disc . The last part of this chapter accounts for the detailed characteristics of helium influence on the properties of accretion discs.

2.1 The formation of accretion discs

In the semi-detached binaries in which the Roche-lobe overflow takes place the gas flowing through the L_1 point has non-zero specific angular momentum with respect to the accretor which we denote as j_2. The continuous stream entering the primary potential follows an elliptical orbit around the accretor and after the first circuit it starts to intersect itself. Due to the strong dissipation of the energy at the point of intersection (e.g. via collisions and shocks) the gas settles on a Keplerian orbit, i.e. the orbit of minimum energy for a given angular momentum and forms a ring of matter around the primary. The radius of such an orbit for angular momentum j_2 is called the *circularization radius* $R_{\rm circ}$ (Frank et al., 2002)

$$R_{\rm circ} = a(1+q)(0.500 - 0.227 \log q)^4 \tag{2.1}$$

where a is the binary separation and $q \equiv M_2/M_1$.

The dissipation processes inside the ring (collectively called "viscosity") force the gas to lose its energy. The cooling mechanisms in the gas are assumed to be efficient enough that the dissipated energy in the ring is radiated away on the time scale much shorter then the time scale on which the gas angular momentum $j_{\rm K}$ decreases (here we denote by $j_{\rm K}$ the angular momentum corresponding to the given Keplerian orbit). In result the gas gets rid of as much energy as possible at an orbit of a given $j_{\rm K}$.

The angular velocity $\Omega_{\rm K}$ and the angular momentum $j_{\rm K}$ of a Keplerian orbit are

$$\Omega_{\rm K} = \sqrt{\frac{GM_1}{R^3}} \tag{2.2}$$

$$j_{\rm K} = \sqrt{GM_1 R} \tag{2.3}$$

where R is the distance from the accretor of mass M_1, and G is the gravitational constant.

As the process of energy dissipation continues the gas energy drops and at some point the gravitational prevails pulling the gas in. The gas has to lose its angular momentum to follow deeper into the accretor potential and settles on the Keplerian orbit of smaller radius until the energy drain forces it to move closer to the central object. Because of the viscous processes the matter transferred from the secondary spirals inwards the primary Roche lobe through the set of Keplerian orbits. In the absence of the mechanisms which may truncate the disc (magnetic field of the primary or strong irradiation by the primary) the inner disc radius is taken on the surface of the white dwarf $R_{\rm in} = R_1$.

Because of the conservation laws the angular momentum which is lost by the gas has to be passed to some portion of matter which in consequence will be pushed to the orbits of larger radii. This causes the outer parts of the disc to extend over $R_{\rm circ}$ up to the point at which the tidal force between the disc and the secondary removes all the angular momentum from the disc outer edge and feeds it back to the orbital motion of the binary (Lin and Papaloizou, 1979).

The mechanism by which the gas loses its angular momentum, or in other words: by which its angular momentum is transported outwards, remains the outstanding question of astrophysics.

To gain some information about the viscosity one has to consider the hydrodynamical description of the accretion flow.

Between the adjacent annuli of the differentially rotating fluid the viscous stresses are generated. These stresses act in the direction orthogonal to the motion of the gas and in general they are called *the shear viscosity*. The shearing torques exist as long as $d\Omega/dr \neq 0$.

The viscosity originating from the interactions between the fluid molecules is far too low to account for the rate at which the angular momentum is transported in accretion discs. The Reynolds number Re (which is the ratio of inertia forces to viscous forces in the fluid) calculated in the case of molecular viscosity in accretion discs is very large ($Re_{\rm mol} > 10^{14}$, Frank et al. (2002)) and it can not be significantly lowered for any reasonable set of parameters describing the disc.

The laboratory experiments show that there exists the critical value of Re above which in the stationary stable laminar flow the turbulence sets in. Considering the order of magnitude of Re estimated for accretion discs it is believed that the nature of viscosity in the disc is turbulent, however, its origin remains a matter of debate. Presently the most serious candidate for the source of the turbulence is the Magneto-Rotational Instability (MRI) arising due to the presence of a weak magnetic field in the disc (see Balbus and Hawley (1998)).

The Disc Instability Model (in short DIM) uses the α-prescription for viscosity introduced by Shakura and Sunyaev (1973) (SS73) and below we remind its origin.

To describe the accretion flow in the disc one can use the equations describing motion of the fluid

in the presence of the turbulence. In this case the tangential stresses in the disc are given by

$$\tau_{\mathrm{R}\phi} = \eta R \frac{d\,\Omega_{\mathrm{K}}}{dR} = \nu\rho\, R \frac{d\,\Omega_{\mathrm{K}}}{dR} = -\frac{3}{2}\nu\rho\,\Omega_{\mathrm{K}} \tag{2.4}$$

where R is the radius, η and ν are the dynamical and kinematic viscosity coefficients respectively and ρ is the fluid density.

According to Shakura and Sunyaev the tangential stresses in the disc are connected both to the turbulence of the velocity v_t and the magnetic field B present in the matter transferred from the secondary (Shakura and Sunyaev, 1973)

$$-\tau_{\mathrm{R}\phi} \sim \rho\, c_s^2 \left(\frac{\mathrm{v}_t}{c_s}\right) + \rho\, c_s^2 \left(\frac{B^2}{4\pi\mu_{\mathrm{mag}}^2\,\rho\, c_s^2}\right) = \alpha\rho\, c_s^2 \tag{2.5}$$

where c_s is the speed of sound and μ_{mag} is the permeability.

The crucial assumption of SS73 is that the efficiency of the angular momentum transport for both mechanisms can be parametrized by only one parameter α. For the turbulent mechanism $\alpha < 1$ because otherwise the supersonic turbulence would lead to rapid heating of the plasma and to decrease of α below unity anyway. Also in the case of magnetic transport the energy of magnetic field is likely to be smaller than the thermal energy of matter and so $\alpha < 1$ is a good approximation.

Since $c_s = \sqrt{P/\rho}$ the equation (2.5) can be written in terms of total pressure P

$$\tau_{\mathrm{R}\phi} = -\alpha P \tag{2.6}$$

The total pressure P is the sum of the gas and radiation pressures

$$P = \frac{\rho\, k_{\mathrm{B}} T_{\mathrm{c}}}{\mu\, m_{\mathrm{H}}} + \frac{4\sigma}{3c} T_{\mathrm{c}}^4 \tag{2.7}$$

where k_{B} is the Boltzmann constant, μ is the mean molecular molecular weight and m_{H} is the atomic mass of hydrogen.

From Eq.(2.4) and (2.6) one can calculate the kinematic viscosity coefficient ν in the case of α-parametrization:

$$\alpha P = \frac{3}{2}\nu\rho\Omega_{\mathrm{K}} \Rightarrow \nu = \frac{2}{3}\alpha\frac{c_{\mathrm{s}}^2}{\Omega_{\mathrm{K}}} \tag{2.8}$$

The familiar form of ν widely used in literature is

$$\nu = \frac{2}{3}\alpha\, c_{\mathrm{s}} H \tag{2.9}$$

where H is the pressure height scale of the disc: $H = c_{\mathrm{s}}/\Omega_{\mathrm{K}}$.

If instead of pressure height scale one uses the height of the disc h, defined for example as the distance from the disc mid-plane to the point at which the disc becomes optically thin, than α_1 used in equation $\nu = 2/3\alpha_1 c_{\mathrm{s}} h$ will not have the same meaning as α defined by SS73. In this work only α

determined by pressure height scale is used.

The parametrization of the viscosity in the disc with α enables to investigate the disc structure, evolution and emission properties without really knowing the exact description of the physical processes standing behind the angular momentum transport in the disc.

The α-prescription gives the formula for viscosity which has to be known if one wants to solve the equations describing accretion discs.

2.2 The disc vertical structure equations

The very important assumption is that the cooling processes are efficient enough relative to the rate of energy dissipation in the disc that the radial pressure gradients are negligibly small and the viscously dissipated energy is radiated away locally. This is the necessary condition for the thin disc approximation to hold.

The thin disc approximation states that the height scale of the disc is much smaller than its radius ($H/R \ll 1$) and that the angular velocity of the gas is highly supersonic. This approximation extremely simplifies the numerical investigations of accretion discs because it allows to decouple the vertical structure equations from the time evolution equations and consider them separately.

In the case of thin disc the vertical gravitational acceleration due to self-gravity of the disc may approximated by the gravitational acceleration produced by the infinite plane $g_{\rm disc} = -2\pi\Sigma G$ while the vertical component of gravitational acceleration due to primary is $g_{\rm z} \approx -G\,M_1 H/R^3$. Therefore, the criterion for non self-gravitating disc is

$$\Sigma \ll \frac{M_1 H}{R^3} \tag{2.10}$$

or expressing Eq.(2.10) it in the disc mass

$$\frac{M_{\rm disc}}{M_1} \ll \frac{H}{R} \tag{2.11}$$

For typical parameters of the discs in cataclysmic variables this always holds: $M_{\rm disc}/M_1 \sim 10^{-11} - 10^{-8}$ and $H/R \sim 10^{-3} - 10^{-4}$. As long as self-gravity of the disc can be neglected the only component of the gravitational force comes from the primary.

Since the gas flow in the thin accretion disc is essentially only plane-parallel the only force to balance the gravitational influence of the primary in the vertical direction is the pressure force and the disc is assumed to be in hydrostatic equilibrium in each radius R which for Keplerian disc can be written as

$$\frac{dP}{dz} \approx -\rho\Omega_{\rm K}^2 z \tag{2.12}$$

where z is the distance from the disc mid-plane.

The Eq. (2.12) results from the consideration of the z-component of Eq. (2.27) (see below Sect. 2.3).

The surface density ς at any distance z from the central disc plane $z = 0$ is defined as the density of the gas ρ integrated between $-z$ and $+z$

$$\frac{d\varsigma}{dz} = 2\rho. \tag{2.13}$$

At the disc mid-plane $\varsigma = 0$, while at the disc photosphere $\varsigma = \Sigma$.

To investigate the vertical energy transport one has to determine the temperature gradient

$$\frac{d\ln T}{d\ln P} = \nabla \tag{2.14}$$

which can be either radiative $\nabla_{\rm rad}$ or convective $\nabla_{\rm conv}$ depending on the energy transport mechanism which dominates in the disc. The decisive role plays here the Schwarzschild criterion which states that the medium is stable against convection if the radiative gradient is sub-adiabatic: $\nabla_{\rm ad} > \nabla_{\rm rad}$. In the disc region where this condition holds the energy is transported radiatively from the mid-plane to the disc surface.

The radiative energy transport can be treated as the diffusion process as long as the mean free path of photons is much smaller than the characteristic length (here it is the disc height scale) over which the energy is transported. This is true for optically thick discs we consider (Sect.2.4) so we can write the energy flux

$$F_{\rm z} = -D\,\nabla U \tag{2.15}$$

with the diffusion coefficient defined as

$$D = \frac{1}{3}\,c\,\frac{1}{\kappa_{\rm R}\rho} \tag{2.16}$$

where c is the speed of light and the mean free path has been substituted by the mean Rosseland opacity $\kappa_{\rm R}$ and density ρ.

Substituting to Eq.(2.15) the density of radiation energy $U = aT^4$ (a is the radiation-density constant) and neglecting the radial and azimuthal components one obtains

$$F_{\rm z} = -\frac{16\,\sigma\,T^3}{3\kappa_{\rm R}\,\rho}\frac{\partial T}{\partial z} \tag{2.17}$$

where $\sigma \equiv ac/4$ is the Stefan-Boltzmann constant.

The form of radiative temperature gradient results from Eqs.(2.7), (2.12), (2.14) and (2.17):

$$\nabla_{\rm rad} = \frac{P\kappa_{\rm R}\,F_{\rm z}}{4\,P_{\rm rad}c\,g_{\rm z}}. \tag{2.18}$$

The convection sets in whenever the radiative gradient becomes superadiabatic: $\nabla_{\rm rad} > \nabla_{\rm ad}$. There are two effects which lead to the violation of the Schwarzschild criterion. The first one is the increase of $\nabla_{\rm rad}$ with the increase of the opacity: (i) H^- ion opacity in the case of a cool disc and (ii) bound-free opacity when the increase of temperature and density leads to the onset of disc matter

ionization.

The second one is the decrease of $\nabla_{\rm ad}$ in the region where the partial ionization of the matter takes place. The specific heat C_V in this region becomes large ($\nabla_{\rm ad} = 1 - C_V/C_P$) because the energy supplied to this region rises the degree of ionization of the gas and does not affect significantly its temperature until the major part of the gas becomes ionized.

If we consider the element of the fluid which has the temperature excess δT over its surrounding and moves upwards with the velocity v and maintains the pressure balance with its surroundings then the local convective flux may be written as

$$F_{\rm conv} = \rho {\rm v} c_{\rm P} \delta T \tag{2.19}$$

where $c_{\rm P}$ is the specific heat under the constant pressure and δT.

This element will move until it expands so much that it will finally dissolve and mix with the surroundings. The distance it travels to this point is called the mixing length $\ell_{\rm ml}$. If one sets certain height z and considers the elements which pass through the surface parallel to the disc mid-plane at height z they will have different temperatures δT and velocities v as different elements start to move at different points, not necessarily at $z = 0$. Lets assume that random element has traveled the distance $\ell_{\rm ml}/2$ when it passes the surface z. One can define the temperature difference $\delta T/T$ and the density difference $\delta\rho/\rho$ between element and the surroundings Assuming that half of the work done by the buyoncy force acting on the fluid element goes into its kinetic energy and half goes into the surroundings then the average velocity of the element which passes the surface at height z is (Kippenhahn and Weigert, 1990)

$${\rm v}_{\rm e}^2 = g_{\rm z} \frac{\ell_{\rm ml}^2}{8\,H} \left(\frac{\partial \rho}{\partial T}\right)_P (\nabla - \nabla_{\rm e}) \tag{2.20}$$

where $\nabla_{\rm e} \equiv \left(\frac{d\ln T}{d\ln P}\right)_{\rm e}$ is defined for an element of a fluid.

Putting Eq.(2.20) and the expression for $\delta T/T$

$$\frac{\delta T}{T} = \frac{1}{T}\frac{\partial(\delta T)}{\partial z}\frac{\ell_{\rm ml}}{2} = \frac{1}{H}(\nabla - \nabla_{\rm e})\frac{\ell_{\rm ml}}{2} \tag{2.21}$$

into Eq.(2.19) one obtains the formula for average convective flux (Kippenhahn and Weigert, 1990)

$$F_{\rm conv} = \rho\, c_{\rm P} T \sqrt{g_{\rm z}\left(\frac{\partial \rho}{\partial T}\right)_P} \frac{\ell_{\rm ml}^2}{4\sqrt{2}} \left(\frac{\nabla - \nabla_{\rm e}}{H}\right)^{3/2} \tag{2.22}$$

which is used to find the convective temperature gradient $\nabla_{\rm conv}$ calculated in the mixing length approximation following Paczyński (1969).

To complete the equations of the local structure of the disc one has to determine the vertical energy flux $F_{\rm z}$ and find the relation between $T_{\rm c}$ and $T_{\rm eff}$. In general case the vertical energy flux $F_{\rm z}$ generated locally by the viscous dissipation should be complemented by the flux F_t resulting from the

heating/cooling followed by the expansion/contraction of the disc

$$\frac{dF_{\rm z}}{dz} = \frac{3}{2}\alpha\,\Omega_{\rm K}P + \frac{dF_{\rm t}}{dz}. \tag{2.23}$$

The exact form of the term $dF_{\rm t}/dz$ is unknown but it can be assumed to be proportional to pressure P and crudely approximate by $dF_{\rm t}/dz \approx 3/2\,\alpha_{\rm t}\,\Omega_{\rm K}P$ (Smak, 1984):

$$\frac{dF_{\rm z}}{dz} = \frac{3}{2}(\alpha+\alpha_{\rm t})\Omega_{\rm K}P = \frac{3}{2}\alpha_{\rm eff}\,\Omega_{\rm K}P \tag{2.24}$$

where $\alpha_{\rm eff}$ may be considered as parameter which describes certain "effective" viscosity.

With Eq.(2.24) one can obtain $T_{\rm eff}$ at any R in the disc assuming that the disc is in thermal equilibrium defined by $\alpha_{\rm eff}$. This "effective" equilibrium differs from the thermal equilibrium resulting only from the viscous dissipation term. The difference $\alpha - \alpha_{\rm eff}$ determines how far from the viscous thermal equilibrium is the disc annulus described by the given solution (Σ and $T_{\rm eff}$) of Eq.(2.24).

The boundary conditions which close the set of vertical structure equations assume that (i) at the disc mid-plane ($z = 0$) the vertical energy flux vanishes ($F_{\rm z} = 0$) and the temperature is equal to the disc central temperature ($T = T_{\rm c}$), (ii) the energy flux at the photosphere defines the effective temperature of the disc: $F_z(\tau = 2/3) = \sigma T_{\rm eff}^4$ where the photosphere is assumed to start at the point where the optical depth τ becomes equal to 2/3.

2.3 Time evolution equations

Once the vertical structure of the disc is determined one can solve the disc evolution equations.

The time evolution of an accretion disc is described by the equations of viscous fluid dynamics: the continuity equation and the Navier-Stokes equations. In this context the most suitable is to write those equations using the cylindrical coordinate system with the origin placed on the primary white dwarf. Since the disc is to a good approximation axisymmetric the mass conservation equation takes the form

$$\frac{\partial\Sigma}{\partial t} + \frac{1}{R}\frac{\partial}{\partial R}(R\,\Sigma\,{\rm v_R}) = 0 \tag{2.25}$$

where $\rm v_R$ is the radial velocity of the inwardly diffusing matter.

The Eq. (2.25) is vertically averaged according to the thin disc approximation and so the density ρ is replaced here by the surface densityΣ. In the case of the semi-detached binaries one has to take into account in Eq. (2.25) the additional mass flux flowing through each element of the disc (Smak, 1984; Lasota, 2001):

$$\frac{\partial\Sigma}{\partial t} + \frac{1}{R}\frac{\partial}{\partial R}(R\,\Sigma\,{\rm v}_R) = \frac{1}{2\pi R}\frac{\partial\dot{M}_{\rm ext}}{\partial R} \tag{2.26}$$

where $\dot{M}_{\rm ext}$ is the rate at which the mass is fed into the outer edge of the disc from the secondary.

The velocity $\rm v_R$ is defined by the fluid equations of motion which are the Navier-Stokes equations if the viscosity is taken into account. Their general form (in the presence of gravitational potential)

integrated over z-direction is

$$\Sigma\left(\frac{\partial\overrightarrow{\mathrm{v}}}{\partial t}+(\overrightarrow{\mathrm{v}}\nabla)\overrightarrow{\mathrm{v}}\right)=-\nabla P+\nabla W_{R\phi}-\Sigma\nabla\Phi \tag{2.27}$$

where P is the total pressure, Φ is the gravitational potential and W is the vertically integrated stress tensor

$$W_{R\phi}=\nu\Sigma\, R\frac{d\Omega}{dR} \tag{2.28}$$

Considering only the azimuthal component of Eq.(2.27) and using Eq.(2.25) one arrives to the angular momentum conservation equation

$$\frac{\partial(\Sigma R\,\mathrm{v}_\phi)}{\partial t}+\frac{1}{R}\frac{\partial}{\partial R}(R\,\mathrm{v}_\mathrm{R}\Sigma\,\mathrm{v}_\phi R)=\frac{1}{R}\frac{\partial}{\partial R}(\nu\Sigma\, R^3\frac{d\Omega}{dR}) \tag{2.29}$$

where $R\,\mathrm{v}_\phi=R^2\Omega=j_\mathrm{K}$ is the Keplerian angular momentum if $\Omega\equiv\Omega_\mathrm{K}$.

The right hand side of Eq.(2.29) is the the torque $G(R)$ exerted by the ring at $R+\delta R$ on the neighboring inner radius R. One can derive $G(R)$ from the consideration of chaotic motions of gas elements in two adjacent disc annuli resulting in the angular momentum transport (Frank et al., 2002)

$$G(R)=2\pi\nu\Sigma R^3\frac{d\Omega_\mathrm{K}}{dR}=-3\pi\nu\Sigma\, R^2\Omega_\mathrm{K} \tag{2.30}$$

From Eq. (2.29) and (2.30)

$$\frac{\partial(\Sigma j_\mathrm{K})}{\partial t}+\frac{1}{R}\frac{\partial}{\partial R}(R\mathrm{v}_\mathrm{R}\Sigma j_\mathrm{K})=\frac{1}{2\pi R}\frac{\partial^2 G}{\partial R^2} \tag{2.31}$$

In the case of binary where the mass transfer from the secondary takes place Eq.(2.31) has to be supplemented by the term which describes the amount of angular momentum carried by the matter flowing through the L_1 point and the term which account for the extraction of angular momentum from the disc due to the tidal interaction between disc and secondary. The complete angular momentum conservation equation is (Smak, 1984; Lasota, 2001)

$$\frac{\partial(\Sigma j_\mathrm{K})}{\partial t}=-\frac{1}{R}\frac{\partial}{\partial R}(R\,\mathrm{v}_\mathrm{R}\Sigma j_\mathrm{K})+\frac{1}{2\pi R}\frac{\partial^2 G}{\partial R^2}+\frac{j_2}{2\pi R}\frac{\partial\dot{M}_\mathrm{ext}}{\partial R}-\frac{1}{2\pi R}T_\mathrm{tid} \tag{2.32}$$

where j_2 is the angular momentum of the matter transferred from the secondary and T_tid is the tidal force acting between the disc and the secondary.

The prescription for the tidal torque was first derived by Papaloizou and Pringle (1977). The form adopted by Smak (1984) for the time evolution equations is

$$T_\mathrm{tid}=C\omega R\nu\Sigma\left(\frac{R}{a}\right)^5 \tag{2.33}$$

where ω is the angular velocity of the binary orbital motion and C is the numerical coefficient defining

the time averaged disc radius.

For small q (appropriate for the close binaries) the tidal torque from the secondary dominates over the viscously driven disc expansion at some tidal radius $R_{\rm tid}$ and truncates the disc before it expands over the primary Roche lobe. $R_{\rm tid}$ defines the outer disc radius $R_{\rm d}$ and it is assumed that the maximum radius to which the disc can expand is $R_{\rm d,max} = 0.9\,R_{\rm tid}$ (what seems to be confirmed by observations (Harrop-Allin and Warner, 1996)).

The full description of the time evolution of the disc needs another conservation equations: the energy conservation equation. The total energy produced in the disc (kinetic and internal) has to be equal to the total energy lost from the disc:

$$\frac{\partial}{\partial t}(E_{\rm kin} + E_{\rm in}) + \nabla[\vec{\mathrm{v}}(E_{\rm kin} + E_{\rm in})] + L_{\rm tot} = 0 \tag{2.34}$$

where the kinetic energy $E_{\rm kin} = \rho \mathrm{v}^2/2$, the total internal energy of the gas $E_{\rm in} = 3P/2\rho$ and $L_{\rm tot}$ is the total energy produced and lost by the disc locally by the viscous heating Q^+, cooling Q^-, expansion/contraction $Q_{\rm pdV}$, radial energy transport viscous or radiative J and advective energy transport $Q_{\rm adv}$.

To find $L_{\rm tot}$ lets consider the slab of the disc of height dz at distance z above the disc mid-plane. The net flux of energy passing through surface z is $l(z)$, the net energy flux leaving the slab is $l + dl$ where the surplus energy dl is provided by the processes specified above which we designate as $\epsilon_{\rm tot}$. In the case when the slab can change its internal energy and exchange the work pdV with the neighboring slabs one can write:

$$\frac{dQ}{dt} = \epsilon_{\rm tot} - \frac{\partial l}{\partial z}. \tag{2.35}$$

The heat added to the slab dQ is given by the first law of thermodynamics $dQ = du + pdV$. Using thermodynamical relations and substitute the internal energy du and pdV and rewrite Eq.(2.35)

$$\frac{\partial l}{\partial z} = \epsilon_{\rm tot} - C_{\rm P}\frac{\partial T}{\partial t} - \frac{P}{\rho^2}\frac{\partial \rho}{\partial t}, \tag{2.36}$$

where $C_{\rm P}$ is the specific heat at the constant pressure.

Integrating Eq.(2.36) over z one arrives to the formula for $L_{\rm tot}$ which can be incorporated in Eq. (2.34). After several transformations and with the use of mass and angular momentum conservation equations Eq.(2.25) and (2.31) the equation for the time evolution of the energy in the disc is

$$C_{\rm P}\Sigma\frac{\partial T_{\rm c}}{\partial t} = 2(Q^+ - Q^- + \frac{1}{2}Q_{\rm i} + J) - \Sigma\frac{\Re T_{\rm c}}{\mu R}\frac{\partial(R\,\mathrm{v}_{\rm R})}{\partial R} - \Sigma\,C_{\rm P}\mathrm{v}_{\rm R}\frac{\partial T_{\rm c}}{\partial R} \tag{2.37}$$

and $\Re$ is the gas constant.

The term Q^+ is the rate at which the energy is produced by viscous dissipation per unit surface

$$Q^+ = \frac{9}{8}\nu\Sigma\Omega_{\rm K}^2 \tag{2.38}$$

To achieve the thermal equilibrium in the disc the heating rate has to be balanced by the rate at

which the energy is transported away due to the cooling mechanisms. The cooling rate is defined as $Q^- = \sigma T_{\rm eff}^4$ where $T_{\rm eff}$ is the effective temperature.

The term J represents the radial energy flux transported either by radiation or by viscous mechanisms. However, following the conclusions of Smak (1984) and Ludwig and Meyer (1998) we neglect the radial energy flux carried by radiative diffusion but retain the radial energy flux carried by viscous processes as it becomes important during the propagation of the heating front (see Sect.2.5). In this case the assumption that viscosity is given by α-prescription allows to estimate J as (Ludwig and Meyer, 1998; Hameury et al., 1998):

$$J = \frac{1}{R}\frac{\partial}{\partial R}\left(\frac{3}{2}R\,\nu\,C_P\Sigma\,\frac{\partial T_{\rm c}}{\partial R}\right). \tag{2.39}$$

The additional heating sources like the "hot spot" or the dissipation due to the tidal torque $T_{\rm tid}$ are given by the term Q_i and are described in separate section (see Sect. 4.5.2).

To solve the differential equations (2.26)-(2.37) one has to impose the appropriate boundary conditions.

The description of the way the stream of matter from secondary interacts with the outer edge of the disc is far from being completed. It is complicated by the fact that the large fraction of the stream may in fact overflow the disc edge what seem to be confirmed by the newest analysis of the eclipses in Z Cha and OY Car light curves (Smak, 2012). However, for our purposes it is reasonable to assume that the matter is supplied to the disc in the narrow region such that $\dot{M}_{\rm ext}(R)$ can be defined by Diracδ-function and Σ by the Heaviside Y-function: $\dot{M}_{\rm ext}(R) = \dot{M}_{\rm tr}\delta[R_o(t) - R]$ and $\Sigma = \Sigma_o Y[R_o(t) - R]$, where R_o and Σ_o are evaluated at the disc outer edge. Applying this to Eq.(2.26) and (2.32) at R_o leads to two boundary conditions:

$$\dot{M}_{\rm tr} = 2\pi R\Sigma_o(\dot{R}_o - {\rm v}_{R,o}) \tag{2.40}$$

$$\dot{M}_{\rm tr}\left[1 - \left(\frac{R_{\rm circ}}{R_o}\right)^{1/2}\right] = 3\pi\nu\Sigma_o \tag{2.41}$$

It is important to stress that those boundary conditions take into account the variations of the outer disc radius under the operation of the tidal force from secondary.

It is justified by the observations showing that the disc expands during the dwarf nova outbursts and contracts while returning to the quiescence (Harrop-Allin and Warner, 1996). The situation in which R_o is fixed should be considered as unphysical. In addition the consequence of applying $R_o = $ const. as a boundary condition in numerical calculations of DN outbursts is that one can obtain only the outbursts which start at the inner edge of the disc. This also is in contradiction with the observations which show that outbursts start in the outer parts of the disc as well.

As the inner boundary condition it is assumed that the stress vanishes at $R_{\rm in}$ ($\Sigma \to 0$). In the standard case when the mechanisms which lead to the truncation of the inner disc radius (e.g. the influence of the accretor magnetic field or evaporation, see Sect.4.5.2.1) are neglected the disc extends

down to the surface of the white dwarf ($R_{\rm in} = R_1$ where R_1 is the WD radius).

During the outburst phase the thermal equation is dominated by Q^+ and Q^- while terms with higher order derivatives in R can be neglected except for the regions of the disc where steep gradients in Σ and T form. Therefore, one can safely assume $\partial T_c/\partial R = 0$ both at the inner and outer edge.

2.3.1 Time scales

It is important to identify the time scales which characterize the accretion flow in the disc.

The dynamical time scale, i.e. the time scale at which the gas particle at given R encircles the primary, is defined as:

$$t_{\rm dyn} \equiv \frac{1}{\Omega_K} \tag{2.42}$$

It may range from fraction of seconds at the inner disc radius around massive white dwarf (e.g $M_1 = 1.2\,{\rm M}_\odot$) up to tens of minutes at large radii (e.g. $\sim 5.0 \times 10^{10}$ cm) of discs around less massive primaries (e.g. $M_1 = 0.6\,{\rm M}_\odot$). The dynamical time scale is the shortest time scale which characterizes the accretion disc.

If the disc was subjected to perturbation in the vertical direction it returns to the hydrostatic equilibrium on the time scale t_z

$$t_{\rm z} = \frac{H}{c_{\rm s}} \tag{2.43}$$

but since $H = c_{\rm s}/\Omega_{\rm K}$ the deviations from hydrostatic equilibrium are smoothed out on the dynamical time scale $t_{\rm dyn} \sim t_z$.

The thermal time scale measures how fast the disc recovers its thermal equilibrium after the dissipation rate has changed. The time it takes is defined as the ratio of the heat content per unit area (enthalpy) $E_{\rm t}$ to the dissipation rate per unit area Q^+. For perfect gas:

$$E_{\rm t} = \int \frac{\gamma P}{\gamma - 1} dz \sim PH \sim \Sigma c_{\rm s}^2 \tag{2.44}$$

Since $Q^+ = \frac{9}{8}\nu\Sigma\Omega_{\rm K}^2$ the thermal time

$$t_{\rm th} \sim \frac{c_{\rm s}^2}{\nu\Omega_{\rm K}^2} \sim \frac{1}{\alpha\Omega_{\rm K}} \tag{2.45}$$

The thermal time scale is about order of magnitude longer than dynamical time scale in hot accretion discs (where $\alpha \sim 0.1 - 0.2$) and up to 100 times longer in the cold discs (for which$\alpha \sim 0.01 - 0.05$).

The longest is the time scale which defines how much time needs the gas to drift radially over the distance R under the viscous torques. This is the time scale on which the gas redistributes its angular momentum in the disc

$$t_{\rm visc} \sim \frac{R}{{\rm v}_R} \sim \frac{R^2}{\nu}. \tag{2.46}$$

The viscous time scale is of order of days or even weeks for typical disc parameters.

The expression (2.46) does not hold in the region where the strong Σ gradient is present. In such regions the viscous time scale is defined by the lenghtscale L characterizing the spatial extend of the rapid Σ changes and the viscous time scale is defined as

$$t_{\rm visc,1} \sim \frac{L^2}{\nu}. \tag{2.47}$$

Eq.(2.47) implies that the strong density gradients ($L \ll R$) propagate faster in the disc than the matter in the disc parts of the smooth density distribution.

The different time scales result in two different types of instabilities: thermal and viscous. If the thermal balance is perturbed the instability will grow on the thermal time scale, but since $t_{\rm th} \ll t_{\rm visc}$ then the temperature variations at given R will take place at Σ that may be treated as fixed. The disc maintains also the hydrostatic equilibrium while the thermal instability develops since $t_{\rm th} > t_{\rm z}$.

The second type of instability is the viscous instability which arises slowly on time scale $t_{\rm visc}$ under the perturbations of Σ. Because $t_{\rm visc} \gg t_{\rm th}, t_{\rm z}$ there is enough time for the disc to adjust its vertical structure to the changes ofΣ, and the thermal and hydrostatic equilibria hold.

The last important time scale to mention here is the accumulation time. It defines how fast the mass piles-up in a given disc annulus during the quiescence until it reaches $\Sigma^-_{\rm crit}$. Assuming that the matter accumulated in a torus which width is determined by the process of viscous spreading (Eq.(2.46)) $\Delta R \sim \sqrt{\nu t_{\rm accum}}$ the expression for the accumulation time takes the form (Lasota, 2001)

$$t_{\rm accum} \approx \frac{4\pi^2 R^2 \nu \, \Sigma^-_{\rm crit}}{\dot{M}_{\rm tr}{}^2} \tag{2.48}$$

where $\dot{M}_{\rm tr}$ is the mass transfer rate from the secondary and $\Sigma^-_{\rm crit}$ is the minimum critical value of Σ (see Sect.2.4 below).

2.3.2 Steady disc case

When the changes in the radial disc structure take place on a time scale much longer than the viscous time scale the disc can be considered as steady. This is the case which allows to investigate accretion disc properties in the simplest way because the disc equations (2.26,2.32,2.37) can be solved analytically. This was first done by Shakura and Sunyaev who assumed that ν is given by equation (2.9). Their solutions, known as α-discs or Shakura-Sunyaev discs, consider three different regions of the accretions disc around black hole which are characterized by different pressures and opacities (Shakura and Sunyaev, 1973). The solutions which are applicable for hot discs around white dwarfs are those for region where the gas pressure dominates the radiation pressure ($P_{\rm g} > P_{\rm rad}$) and where the opacity has the Kramer's form. We derive here the expression for luminosity of the hot disc which is used in Sect.5.2.

When $\partial/\partial t = 0$ in the mass conservation equation (2.26) one obtains the prescription for the

constant mass accretion rate $\dot{M}_{\rm acc}$ (with $\mathrm{v}_R < 0$)

$$\dot{M}_{\rm acc} = 2\pi R\,\Sigma(-\mathrm{v}_R) \tag{2.49}$$

Because $\dot{M}_{\rm accr}$ is the same at each radius of the hot disc it has to be everywhere equal to the mass transfer rate from the secondary which determines $\dot{M}_{\rm accr}$ at the outer disc radius: $\dot{M}_{\rm accr}(R_{\rm d}) = \dot{M}_{\rm tr}$.

The angular momentum conservation equation (2.31) takes the form

$$-\nu\Sigma\,\frac{d\Omega_{\rm K}}{dR} = \Sigma(-\mathrm{v}_R)\Omega_{\rm K} + \frac{C}{2\pi R^3} \tag{2.50}$$

where constant C is calculated at the inner edge where $d\Omega_{\rm K}/dR = 0$

$$C = -\dot{M}_{\rm acc}\sqrt{GMR_1} \tag{2.51}$$

Substituting C to Eq.(2.50)

$$\nu\Sigma = \frac{\dot{M}_{\rm acc}}{3\pi}\left(1 - \sqrt{\frac{R_1}{R}}\right) \tag{2.52}$$

Eq.(2.52) can be substituted in the expression for dissipation (2.38):

$$Q^+ = \frac{3\,G\,M_1\dot{M}_{\rm acc}}{8\,\pi R^3}\left(1 - \sqrt{\frac{R_1}{R}}\right) \tag{2.53}$$

The viscous heating written in the form above is independent of viscosity and is determined by quantities which can be found observationally. The luminosity coming from both sides of the disc is

$$L(R_1, R_{\rm d}) = 2\int_{R_1}^{R_{\rm d}} 2\pi Q^+ R dR. \tag{2.54}$$

After integrating Eq.(2.54) with the use of Eq.(2.53) one arrives to the expression for the luminosity of the whole hot disc:

$$L_{\rm max} = \frac{GM_1\dot{M}_{\rm acc}}{2R_1}\left[1 - \frac{R_1}{R_{\rm d}}\left(3 - 2\sqrt{\frac{R_1}{R_{\rm d}}}\right)\right]. \tag{2.55}$$

2.4 S-curves

The solutions of the equations (2.12)-(2.24) give the effective temperatures and surface densities for which the given disc annulus is in the thermal equilibrium. Once the solution of the energy transfer equation (2.24) is found it gives the relation between $T_{\rm c}$ and $T_{\rm eff}$ for the optically thick disc. For radiative transfer

$$T_{\rm c}^4 = \frac{3}{8}\tau_{\rm tot}T_{\rm eff}^4 \tag{2.56}$$

where the total optical depth is $\tau_{\rm tot} = \int_0^\infty \kappa_{\rm R}\rho\,dz$.

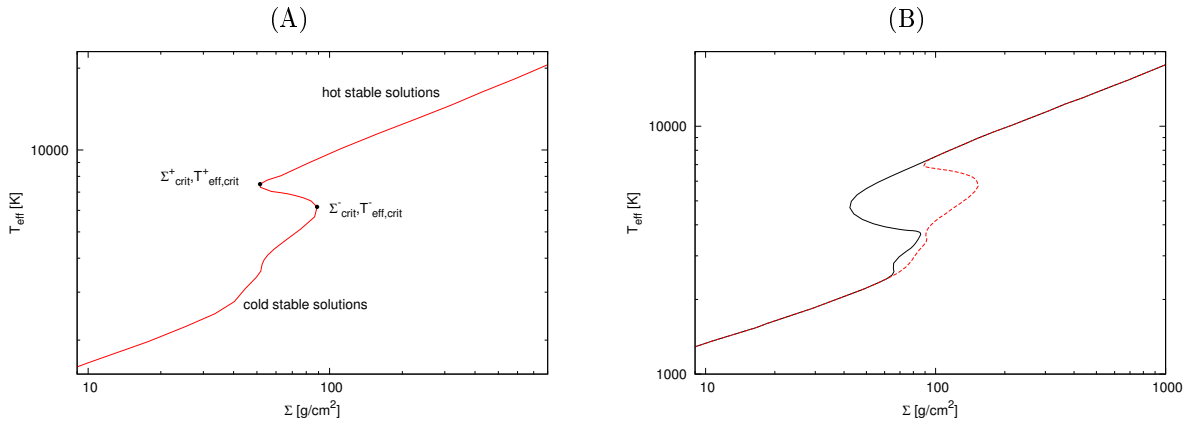

Figure 2.1: *(A):* The solutions of disc structure equations plotted on the $\Sigma - T_{\rm eff}$ plane form the S-curve. The S-curve presented on the plot is calculated at $R = 6.0 \times 10^9$ cm with $\alpha = 0.04$ and $M_1 = 1.0\,{\rm M}_\odot$ (solar composition disc). The upper and lower bands (at which Σ and $T_{\rm eff}$ have the critical values) divide the S-curve into three parts: upper and lower corresponds respectively to the hot stable and the cold stable solutions and the middle part is formed by the unstable solutions. *(B):* The comparison of the S-curves calculated with (red line) and without (black line) convection included in the energy transfer equation. Both S-curves are calculated in $R = 1.0 \times 10^{10}$ cm with $\alpha = 0.04$ and $M_1 = 1.0\,{\rm M}_\odot$ for solar composition disc.

The solutions of the vertical structure equations plotted on the $\Sigma - T_{\rm eff}$ (or $\Sigma - T_{\rm c}$equivalently) plane form the curves of the characteristic S-shape seen in Fig.2.1.

The stable solutions form the positive-slope branches of the S-curve: the lower (upper) branch corresponds to the disc which is in the cold (hot) stable state in given R. The equilibrium solutions which build the middle part of the S-curve (with the negative slope) are thermally and viscously unstable. The existence of these solutions is the source of the *thermal-viscous instability* in the accretion discs which is the core of the Disc Instability Model.

The upper and lower bend of the S-curve are the two transition points between stable and unstable branches. The cool stable solutions terminate at the point where surface density and temperature reach the critical values $\Sigma^-_{\rm crit}$, $T^-_{\rm crit}$ above which the stable cold state is no longer maintained. The second transition point is where the upper branch of the S-curve turns into the unstable, middle part. It is where the surface density and the temperature decreasing along the hot branch reach their minimum values, $\Sigma^+_{\rm crit}$ and $T^+_{\rm crit}$ for which the hot stable solutions are possible (see Fig.2.1A).

The position of the critical values of Σ and T on the S-curve depends on the cooling mechanisms which are taken into account in the calculations. Fig.2.1B illustrates what happens in the case when the convection is neglected. The lack of convection means that the disc cooling is less efficient and the instability starts in the disc which is cooler and less dense than the disc in which convection operates (the critical values $\Sigma^-_{\rm crit}$ and $T^-_{\rm eff,crit}$ are lower). Clearly the disc also reaches the hot stable state earlier (i.e. $\Sigma^+_{\rm crit}$ and $T^+_{\rm eff,crit}$ are lower) when only radiative cooling is considered.

The disc never follows the unstable part of the S-curve because in this regime of temperatures and surface densities even a small perturbation of Σ drives the disc from thermal equilibrium and leads to

the rapid grow of instability.

The Eq.(2.26) can be written in the form of the diffusion equation assuming $\dot{M}_{\rm ext}$ = const. and using Eq.(2.29)

$$\frac{\partial \Sigma}{\partial t} = \frac{3}{R}\frac{\partial}{\partial R}\Big[\sqrt{R}\,\frac{\partial}{\partial R}(\nu\Sigma\sqrt{R})\Big]. \tag{2.57}$$

The viscous instability is the consequence of the form of equation (2.57) describing the surface density fluctuations in the disc. If one introduces a perturbation $\Delta\Sigma$ to Σ and defines the quantity $\mu \equiv \nu\Sigma$ then $\Sigma \to \Sigma + \Delta\Sigma$ and $\mu \to \mu + \Delta\mu$ (in general ν is a function of R and Σ: $\nu = \nu(R, \Sigma)$). Since the perturbation of μ can be written as $\Delta\mu = (\partial\mu/\partial\Sigma)\Delta\Sigma$ or $\Delta\mu = \nu(\Sigma + \Delta\Sigma)$ one can write the diffusion equation for the growth of the perturbation in the gas flow (see Pringle (1981); Frank et al. (2002))

$$\frac{\partial(\Delta\mu)}{\partial t} = \frac{\partial\mu}{\partial\Sigma}\frac{3}{R}\frac{\partial}{\partial R}\Big[\sqrt{R}\,\frac{\partial}{\partial R}(\Delta\mu\sqrt{R})\Big] \tag{2.58}$$

where the diffusion coefficient $D \propto \partial\mu/\partial\Sigma$.

For ν given by SS73 prescription ($\nu \sim \alpha c_{\rm s} H$) the parameter μ has the dimension of the mass accretion rate: $\mu = \nu\Sigma \propto \dot{M}_{\rm acc}$. Since $\dot{M}_{\rm acc}$ in general case ($\dot{M}_{\rm acc} \neq$ const) is given by (Lasota, 2001)

$$\dot{M}_{\rm acc} = 3\pi\nu\Sigma\left(2\frac{\partial \ln(\nu\Sigma)}{\partial \ln R} + 1\right) \tag{2.59}$$

one can write $D \propto \partial\dot{M}_{\rm acc}/\partial\Sigma$.

The perturbation will smooth out in the viscous time if $D > 0$. In the opposite case ($D < 0$) the small local increase of Σ will lead to the effect of a "snowball" - the higher will be Σ at some point of the disc the more matter will accumulate there. Defining D with $\dot{M}_{\rm acc}$ makes it even more evident: the condition $\partial\dot{M}_{\rm acc}/\partial\Sigma < 0$ means that the mass accretion at given R decreases when Σ in this radius increases. In other words the dense parts of the viscously unstable disc build up their density while their less dense surroundings become more and more rarefied as the mass outflow there is more intense.

In the case of optically thick discs the dominant cooling mechanism near ($\Sigma^-_{\rm crit}$, $T^-_{\rm c,crit}$) point is convection. The thermal instability starts when the local density attains $\Sigma^-_{\rm crit}$ and the overdense region becomes so hot ($T = T^-_{\rm c,crit}$) that the efficiency of convection falls rapidly. It is induced by the increasing degree of matter ionization (which rises the adiabatic gradient) and by the decreasing bound-free opacity. Above $T^-_{\rm c,crit}$ even small changes in Σ lead to the sharp temperature increase - the thermal instability grows rapidly on the thermal time scale as there is no efficient cooling process to balance the viscous heating. The disc annulus follows the path (marked in Fig.2.2 with red points) passing through the region where $Q^+ > Q^-$, located on the right from the S-curve. It regains the thermal equilibrium when its the temperature reaches the value lying on the upper S-curve branch and the rate of the cooling balances the rate of the heating again.

When the underdense region becomes less dense than $\Sigma^+_{\rm crit}$ the temperature there falls below $T^+_{\rm c,crit}$ and the recombination of the dominant chemical element in the disc starts. The recombination results in the rapid change of the opacities and enhances the radiative cooling efficiency. In this case the disc

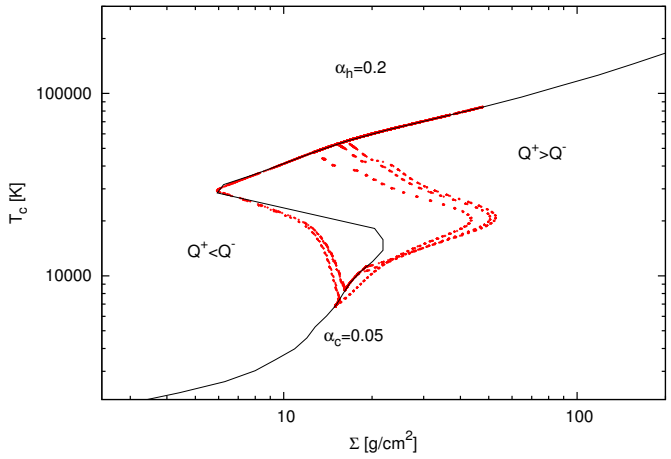

Figure 2.2: The local behavior of the disc at $R = 2.15 \times 10^9$ cm during the outburst cycle (red points) calculated for $\alpha_c = 0.05$, $\alpha_h = 0.2$, $M_1 = 1.0\,M_\odot$, $\dot{M}_{tr} = 0.1 \times 10^{16}$ g/s, solar composition disc. The black line represents the effective S-curve for $\alpha_c = 0.05$, $\alpha_h = 0.2$, $R = 2.15 \times 10^9$ cm and $M_1 = 1.0\,M_\odot$.

annulus follows the solutions which lie in T_c and Σ regime where $Q^+ < Q^-$ (red points on the left of the S-curve in Fig.2.2). This region of the disc is again thermally unstable and cools until the thermal equilibrium corresponding to the solutions on the lower part of the S-curve is found.

The behavior of Σ in the regimes where $Q^+ < Q^-$ and $Q^+ > Q^-$ in Fig.2.2 is the manifestation of the global disc evolution - it mirrors the passage of the cooling and heating front respectively through the given radius. The rise of Σ with decreasing T_c in the regime where $Q^+ < Q^-$ is the effect of the outflow of mass which appears at the cooling front while the initial rise of Σ followed by its decrease with increasing T_c in the regime where $Q^+ > Q^-$ reflects the temporary increase of the surface density caused by the passage of the mass accumulated in the heating front.

The described response of the disc to the perturbations in certain temperatures and densities regime is believed to be the origin of the outbursts of dwarf novae.

At this point it is important to point out the connection between the efficiency of convection and α assumed in the disc. The high values of α ($\alpha \geq 0.3$ according to Cannizzo and Wheeler (1984)) result in lower Σ in the disc. In effect the convective flux decreases while radiative flux becomes more important. Therefore higher α lowers the significance of convection as a mean of energy transport. In this situation Σ^-_{crit} is no longer connected with efficiency of convection but is defined as the point where the change of κ_R becomes less steep with decreasing temperature and T_c becomes less sensitive to change in T_{eff} (see Eq.(2.56)). At that point the S-curve slope changes from negative to positive and Σ starts to decrease with decreasing T_{eff} along the cold part of the S-curve. For $\alpha < 0.3$ the surface density is high enough for convection to dominate at Σ^-_{crit} and to determine the $T_c - T_{eff}$ dependence (Eq.(2.56) is no longer valid). The strong convection decreases the temperature gradient and induces that $\Sigma^-_{crit,conv} > \Sigma^-_{crit,rad}$ as can be seen on the right panel of Fig.2.1.

The S-curve presented with black line on Fig.2.2 is the effective S-curve which results from joining

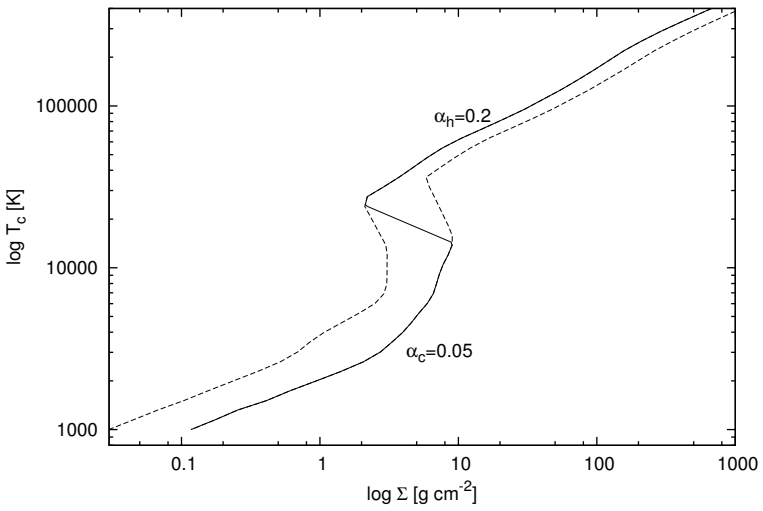

Figure 2.3: The example of an effective S-curve (solid line) used in DN outbursts calculations. The lower branch of this S-curve overlaps with the lower branch of the S-curve calculated for $\alpha = 0.05$ and upper branch overlaps with the upper branch of the S-curve with $\alpha = 0.2$. The S-cruves are calculated for solar composition disc at radius $R = 1.0 \times 10^9$ cm and for $M_1 = 1.0\,\mathrm{M}_\odot$.

two S-curves calculated for different α. The cold branch of the effective S-curve presented on Fig. 2.3 corresponds to $\alpha_\mathrm{c} = 0.05$, the hot branch to $\alpha_\mathrm{h} = 0.2$ and the middle part is the transition region from α_c to α_h (see Eq. (2.60) and the description below).

The necessity of changing α appeared during the first attempts of reproducing DN outbursts in the DIM framework. It was realized by Smak (1984) that in order to obtain outbursts with amplitudes similar to those observed one has to use two different values of α for cold and hot state of the disc, i.e. α_c and α_h respectively. The relation between outburst amplitude and the difference between Σ^+_crit and Σ^-_crit is explained in Sect. 2.6.

The general formulae for $\Sigma^\pm_\mathrm{crit}$, $T^\pm_\mathrm{c,crit}$ and $T^\pm_\mathrm{c,eff}$ in terms of R, α and M_1 for a disc with a given chemical composition are found by numerical fitting. In addition one can calculate critical mass accretion rates $\dot{M}^\pm_\mathrm{crit}$ corresponding to $\Sigma^\pm_\mathrm{crit}$. Those formulae for discs of 4 different chemical compositions: solar, purely helium, $Y = 0.98$ $Z = 0.02$ and $Y = 0.96$ $Z = 0.04$ has been kindly delivered us by Guillaume Dubus and are given in Appendix (A).

The change of α from the cold to the hot branch in the effective S-curve is given by the expression which assures that the transition will be numerically smooth

$$\log(\alpha) = \log(\alpha_\mathrm{c}) + [\log(\alpha_\mathrm{h}) - \log(\alpha_\mathrm{c})] \times \left[1 + \left(\frac{2.5 \times 10^4\,\mathrm{K}}{T_0}\right)^8\right]^{-1} \tag{2.60}$$

where T_0 is the temperatures which defines when α should start to change.

The transition of α should start at the point where the gas starts to recombine, the opacities

change and the disc is no longer in a hot state. The problem with the choice of T_0 arises in the case of helium-dominated discs due to the two helium ionization levels.

It appears that if one sets $T_0 = 0.5(T^+_{\rm c,crit} + T^-_{\rm c,crit})$ then the transition from $\alpha_{\rm h}$ to $\alpha_{\rm c}$ starts in the regime of temperatures and surface densities below the temperature of the second helium ionization. Therefore the value of $\alpha_{\rm eff}$ in this temperature regime is higher than the value $\alpha_{\rm eff}$ would have if it started to change at $T^+_{\rm c,crit}$ and it mimics the continuation of the hot branch (see Fig.2.4B). It can be understood in terms of the thermal balance written as $Q_{\rm eff}\alpha_{\rm eff} = \sigma T^4_{\rm eff}$ (see Eq.(2.24)). In the temperature regime below $T^+_{\rm c,crit}$ the helium atoms are only singly ionized and they start to recombine for the second time - Σ decreases quickly again. This local drop of Σ is stronger than the non-local effect of the mass outflow generated by the passage of the cooling front through the given radius which in turn tends to increase Σ. So instead of rising Σ with decreasing temperature (as it is seen in the plots illustrating the limit cycles during transition from the hot to the cold S-curve branch, e.g. Fig.2.2, Fig.2.4A) one sees further drop of Σ (Fig.2.4B). In the considered case $\alpha_{\rm eff}$ is high enough to compensate the decrease of Σ and the disc "finds" the solutions which correspond to the "artificial" thermal equilibrium which in fact should not be found in the regime where the disc matter is partially ionized. When the temperature falls below the level of the first helium ionization the Σ drop is strongly restrained and the non-local effect of the mass outflow from the cooling takes over.

The consequence of the above described situation is that the critical values of Σ and $T_{\rm c}$ are lowered what affects the stability conditions in the disc and the appearance of the calculated light curves. The difference in the local behavior of the ring as well as its global consequence manifesting in the light curves between various definitions of T_0 is illustrated in Fig.2.4. Fig.2.4B,C show the S-curves for $\alpha_{\rm c} = 0.05$ and $\alpha_{\rm h} = 0.1$ and the limit cycle which undergoes the helium-rich disc ($Y = 0.98$ $Z = 0.02$) at $R = 2.15 \times 10^9$ cm during the outburst cycle. Fig.2.4B shows the limit cycle with $T_0 = 0.5(T^+_{\rm c,crit} + T^-_{\rm c,crit})$ and Fig.2.4C with $T_0 = T^+_{\rm c,crit}$. Note the artificial prolongation of the hot branch on the panel (B). The influence of T_0 on the outbursts is presented on Fig.2.4D. The outbursts in the model with $T_0 = 0.5(T^+_{\rm c,crit} + T^-_{\rm c,crit})$ (black line) have higher amplitude and longer recurrence times than outbursts produced by the model with $T_0 = T^+_{\rm c,crit}$. This is because in the first case the middle branch is more extended: the more matter has to be accreted from the disc to bring it to the cold state and consequently more mass has to be accumulated before the new outburst is triggered (see Sect.2.5).

The plot on the panel (A) in Fig.2.4 is the cycle for the same parameters as the cycles on panels (B) and (C) but for the solar composition disc with $T_0 = 0.5(T^+_{\rm c,crit} + T^-_{\rm c,crit})$. As can be seen the problem with prescription for T_0 does not exist in the case of hydrogen-rich discs because hydrogen has only one ionization state and there is no phase between different ionization levels analogical to that in helium case.

To avoid the effect of the artificially prolongated hot branch we adopt $T_0 = T^+_{\rm c,crit}$.

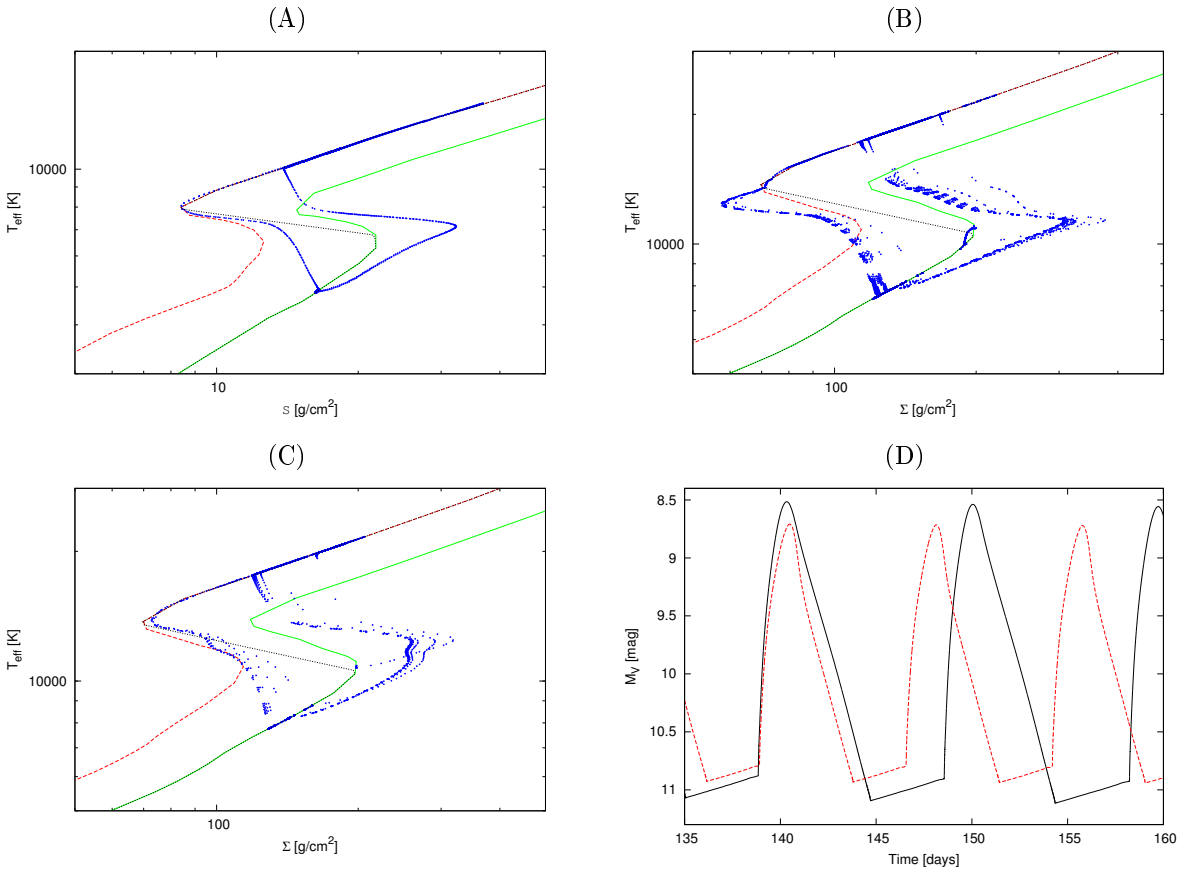

Figure 2.4: The outburst cycle at $R = 2.15\times10^9$ cm for $\alpha_{\rm h} = 0.1$, $\alpha_{\rm c} = 0.05$, $M_1 = 1.0\,{\rm M}_\odot$. The green lines are the S-curves for $\alpha_{\rm c} = 0.05$, red lines are the S-curves for $\alpha_{\rm h} = 0.1$ and the black lines are appropriate effective S-curves. (A) solar composition disc with $T_0 = 0.5(T^+_{\rm c,crit} + T^-_{\rm c,crit})$; (B) $Y = 0.98$ $Z = 0.02$ with $T_0 = 0.5(T^+_{\rm c,crit} + T^-_{\rm c,crit})$; (C) $Y = 0.98$ $Z = 0.02$ with $T_0 = T^+_{\rm c,crit}$; (D) The local behavior of the disc presented on plots (B) and (C) corresponds to the light curves shown on this plot. The black line represents the change of α defined with $T_0 = 0.5(T^+_{\rm c,crit} + T^-_{\rm c,crit})$ and red line represents the prescription with $T_0 = T^+_{\rm c,crit}$.

2.5 The outburst cycle

The local stability described in the previous section translates into the disc global behavior and results in the outburst cycles of dwarf novae and AM CVn stars.

The dwarf nova cycle starts when the instability in the disc triggers an outburst. The luminosity of the system rises until the outburst reaches its maximum. At this point according to the DIM the whole disc is hot and stable till the moment when the outburst decay starts. When the luminosity reaches its minimum the disc becomes everywhere cold and stable and the system enters the quiescent state. The cycle ends with the beginning of the next outburst.

2.5.1 The start of an outburst

In the cold disc the surface density profile is almost parallel to the line representing the critical surface density $\Sigma^{-}_{\rm crit} \sim R$ (see A). The mass accretion rate in the quiescence is not constant so the matter accumulates in the disc increasing its temperature - each disc annulus goes up the lower branch of its local S-curve. The surface density and temperature cross their critical values $\Sigma^{-}_{\rm crit}(R_0)$ and $T^{-}_{\rm c,crit}(R_0)$ at the radius R_0 at which the accumulation time is shorter than viscous time (Sect.2.3.1). The ionization of the gas becomes so significant there that the cooling mechanisms (convection or radiation, see Sect.2.4) are no longer efficient enough to keep the thermal equilibrium in R_0. At this point the considered disc annulus leaves the lower branch of its S-curve undergoing rapid heating which pushes it towards the S-curve upper branch (hot state) (see Fig.2.2 or 2.4) - the narrow fully-ionized region of high viscosity appears in R_0. At the same time the neighboring annuli ($R_0 - \triangle R$ and $R_0 + \triangle R$) are still in the cold state what induces the steep temperature gradient and the formation of a heating front. The spike which arises in Σ profile is a consequence of the different viscosity in the hot and the cold parts of the disc: the low viscosity outside the hot annulus is unable to transfer the angular momentum outwards at the rate which would prevent further accumulation of mass in R_0. The formation of the heating front marks the beginning of an outburst.

The radius at which the front starts to propagate depends on the mass transfer rate from the secondary, the efficiency of viscosity in the cold state defined by parameter $\alpha_{\rm c}$ and the size of the disc. The front is of *outside-in* type if it develops in the outer parts of the disc (black line in Fig.2.6) and propagates inwards, in the opposite case the front is of the *inside-out* type (black line in Fig.2.5).

The higher $\dot{M}_{\rm tr}$ the closer to the outer disc edge the front starts. In large discs one needs much higher $\dot{M}_{\rm tr}$ to trigger the outside-in front than in the small discs because $\Sigma^{-}_{\rm crit}$ rises with R. Therefore in large $R_{\rm d}$ a lot of mass has to be accumulated to cross $\Sigma^{-}_{\rm crit}$ in a period of time shorter than the viscous time. Also low $\alpha_{\rm c}$ may lead to the creation of the outside-in front inasmuch as it inhibits the rate at which the mass diffuses through the disc.

2.5.2 Heating front propagation - rise to an outburst

The steep Σ and $T_{\rm c}$ gradients in the heating front induce the rapid diffusion of matter and heat to the adjacent annuli forcing their transition to the hot state. The inner (i.e. closer to the inner disc

radius) and outer edge of the expanding high-temperature region are the transition zones between high and low viscosity regions. The mass accumulation at the inner transition zone is the consequence of the elevated accretion rate in the hot region while the density spike at the outer transition zone is created by the mass which carries the excess of angular momentum from the inner disc. Therefore the expansion of the fully-ionized region leads to the formation of two spikes in Σ profile traveling in the opposite directions (Fig.2.5 and 2.6).

One of those spikes dies out at the early stage of the front propagation. It is the one which has the shorter distance to cover from the site of its origin to the nearest disc edge (for example if the front starts close to the inner disc radius then the one which travels inwards will vanish first, see for example blue lines in Fig.2.5 and 2.6). In the following the *outside-in/inside-out front* or in general *the heating front* refers to the front which "survives" and propagates through the disc heating it up and rising its luminosity.

It is easier for the front to propagate to smaller radii because it travels down the decreasing density gradient, in the direction of accretion flow, and the high viscosity in the front eases the outward drain of angular momentum. The shape of the outburst which is the result of the outside-in front (resulting in the *outside-in* outburst) is asymmetrical because the fast front propagation leads to the fast rise of luminosity to its maximum after which slower decay takes place (see Sect.2.5.3).

For the inside-out front it is more difficult to pass through the whole disc up to the outer radius. The diffusion of the matter carrying angular momentum excess is being slowed down by the low rate at which the angular momentum is transported in the cold outer disc parts. The rise of the *inside-out* outburst is slower and its shape is symmetrical.

The elevated mass accretion rate reduces the surface density just behind the heating front and enhances the mass inflow to the inner disc regions. It may happen that the post-front surface density $\Sigma(R_{\rm p-f})$ will drop below $\Sigma^{-}_{\rm crit}(R_{\rm p-f})$ and the cold, low-viscosity zone will form behind the inside-out front (i.e. the cooling front, see Sect.2.5.3). This cold zone will start to move inwards and the inside-out front will be suppressed before completing its journey through the disc in the result of the outward angular momentum transfer reduction. The heating front will be "reflected" (see also Sect.2.7.3.1).

2.5.3 The outburst decay

Once the heating front reaches the disc edge (inner or outer depending on the front type) each disc radius is on the upper branch of its S-curve, the disc is fully ionized and its luminosity reaches the maximum. The mass accretion rate everywhere in the disc is increased and it outweighs the mass transfer rate from the secondary. The high temperatures induced by increasing $\dot{M}_{\rm accr}$ at $R_{\rm in}$ cause that the boundary layer between the disc and the primary white dwarf is the source of the UV radiation (also of the soft X-rays which flux depends on the intensity of $\dot{M}_{\rm accr}$). The rest of the disc is the main source of the optical flux emitted by the system.

The mass stored in the outer parts of the disc during the quiescence keeps diffusing inwards with high viscous velocity. Because the highest $\Sigma^{-}_{\rm crit}$ is near the outer disc edge the amount of matter accumulated there during the quiescence and during the outburst rise has to be higher than elsewhere

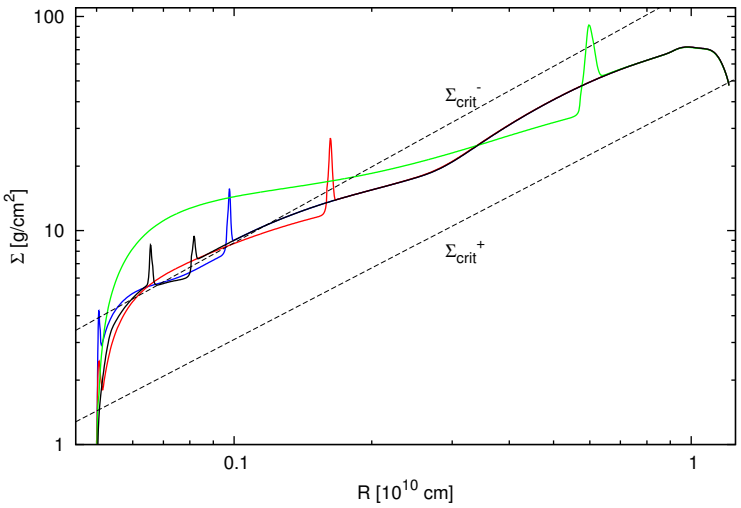

Figure 2.5: The evolution of the surface density profile during the propagation of the inside-out heating front. The black dashed lines represent $\Sigma^{+}_{\rm crit}(R)$ and $\Sigma^{-}_{\rm crit}(R)$ calculated from the formulae for critical values in solar composition disc given in Appendix A for $\alpha_{\rm c} = 0.05$, $\alpha_{\rm h} = 0.1$, $\dot{M}_{\rm tr} = 1.0 \times 10^{15}$ g/s , $M_1 = 1.0\,{\rm M}_{\odot}$ and $\langle R_{\rm d} \rangle \approx 1.15 \times 10^{10}$ cm. The subsequent moments of the front propagation are marked with solid lines: (1) *black* - at the onset of instability fronts are created which propagate in the opposite directions, the one going outwards will heat up the disc and rise its luminosity while the one going inward will vanish at the inner edge and will give no contribution to the luminosity of the disc; (2) *blue* - the inside-out heating front propagates up the density gradient, the second front arrives to the inner edge; (3) *red* - the front which arrived to the inner radius disappears; (4) *green* - the inside-out heating front approaches to the outer disc edge, the density in the inner disc region rises due to the high rate of diffusion of the hot matter in the disc.

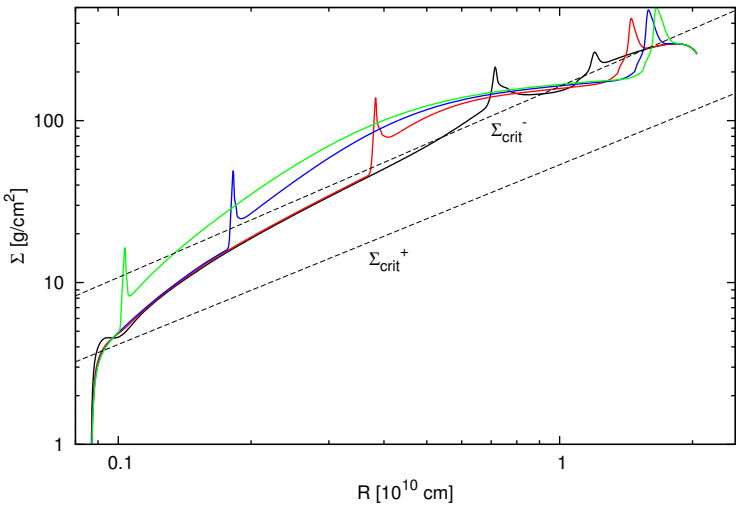

Figure 2.6: The evolution of the surface density profile during the propagation of the outside-in heating front. The black dashed lines represent $\Sigma^{+}_{\rm crit}(R)$ and $\Sigma^{-}_{\rm crit}(R)$ (see Appendix A) calculated for $\alpha_{\rm c} = 0.05$, $\alpha_{\rm h} = 0.1$, $\dot{M}_{\rm tr} = 1.0 \times 10^{16}$ g/s, $M_1 = 0.6\,{\rm M}_{\odot}$ and $\langle R_{\rm d} \rangle \approx 2.0 \times 10^{10}$ cm . The subsequent moments of the front propagation are marked with solid lines: (1) *black* - the high-temperature region forms near the outer disc edge and fronts start to propagate in the opposite directions, this time the disc will be heated by the front which propagates inward ; (2) *red* - the inside-out heating front slowly approaches the outer disc radius while the second front propagates through the disc towards the inner edge; (3) *blue and green* - as the outside-in heating front approaches the inner disc edge, the density in the middle disc region rises, because this time the outer disc parts were heated first.

in the disc in order Σ could cross $\Sigma^+_{\rm crit}$. This means that Σ manages to rise only slightly above $\Sigma^+_{\rm crit}$ near the outer disc edge during the heating front passage and it falls below this critical value almost immediately after the heating front disappears. At the radius where it happens the cooling is strongly enhanced by the change in the opacities when $T_{\rm c} < T^+_{\rm c,crit}$ and the steep Σ and $T_{\rm c}$ gradients lead to the formation of the *cooling front* (black line in Fig.2.7A). Thus, right after the maximum the outburst starts to decay as the outer radii of the disc leave the upper branch of their S-curves unless other additional heating mechanisms are present (Sect.4.5).

Because the cooling front develops at the outer disc edge almost at the same time as the heating front disappears, the mass excess from the outer parts of the heated disc has no time to arrive to the inner disc radius before the cooling front sets in. The surface density profile at the outburst maximum is not yet proportional to $R^{-3/4}$ as expected for a hot stable disc. Therefore, despite the start of the cooling front propagation the mass accretion rate at $R_{\rm in}$ still increases until the mass excess from the outer disc region has traveled through the whole disc and has been accreted.

The maximum of the mass accretion rate at $R_{\rm in}$ is delayed with respect to the maximum brightness in the optical band. Therefore the DIM predicts the delay of the maximum in the UV flux with respect to the optical flux for both types of outbursts (outside-in and inside-out) and may be the explanation for the observed *UV-delay*.

When $\dot{M}_{\rm accr}(R_{\rm in})$ reaches its maximum it exceeds the critical mass transfer rate at $R_{\rm d}$ (black and red line in Fig.2.7B) and the mass accretion rate throughout the disc is not constant. It becomes constant in the hot parts of the disc ahead the cooling front after the initial phase of its propagation.

The diffusion of the hot matter into the cold region behind the front from the adjacent annulus enables the propagation of the cooling front and causes the strong outflow - the matter is "shoved" from the hot region near the front to the already cold, outer parts of the disc behind it.

The outburst ends when the cooling front fades away at the inner radius and the disc settles again in the cold and stable state. The outburst cycle enters into the quiescence phase during which the matter starts to accumulate in the disc again.

2.6 The outbursts - general considerations

The outbursts are the observational effect of the propagation of the fronts in the disc and their properties depend on the parameters characterizing the binary. The size of the disc defined by the mass of the primary and the mean disc radius, the mass transfer rate from the secondary and the viscosity parameters α are the basic quantities which shape the light curves. To predict their possible values from observations and to consciously use them in simulations to obtain the desired results one has to know how each of them separately influences the outburst.

2.6.1 α- parameters

The viscosity defines the time scales in the disc. From Eq.(2.46) and (2.9) it follows that $t_{\rm visc} \propto \alpha^{-1}$.

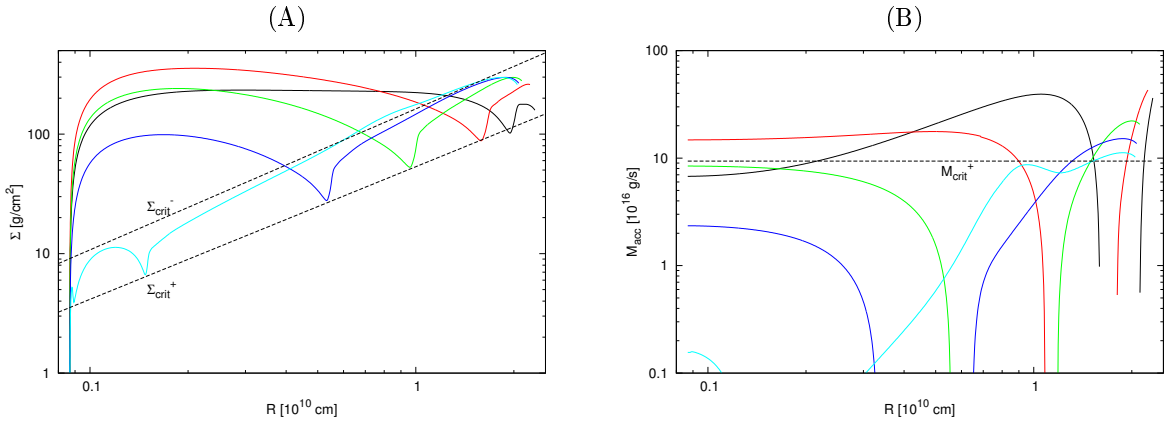

Figure 2.7: (A)*:* The evolution of Σ profile during the propagation of the cooling front. The model parameters are the same as in Fig. 2.6. The subsequent moments of the front propagation are marked with solid lines: (1) *black* - the moment right after the cooling front onset, Σ profile is almost flat and it is not proportional to $R^{-3/4}$ yet; (2) *red* - the next moment of the front propagation, Σin the inner disc parts rises, (3) *green and blue* - at this stage of the front propagation the hot parts of the disc (ahead the front) fulfill Shakura-Sunyaev solutions: $\dot{M}_{\rm accr}$ across these regions is constant and $\Sigma \propto R^{-3/4}$; (4) light blue - the cooling front approaches the inner disc radius leaving behind cold, stable disc. (B) The profiles of $\dot{M}_{\rm accr}$ in subsequent moments of the cooling front propagation. The same colors on both plots correspond to the same moments of the front propagation. The horizontal dashed line corresponds to $\dot{M}^{+}_{\rm crit}(R_{\rm d,max})$. It should be noticed that the mass accretion rate at the inner radius is still rising and crosses $\dot{M}^{+}_{\rm crit}(R_{\rm d,max})$ at the beginning of the front propagation (line black and red) and only later starts to fall down to the very low level when the front is near inner edge (light blue line).

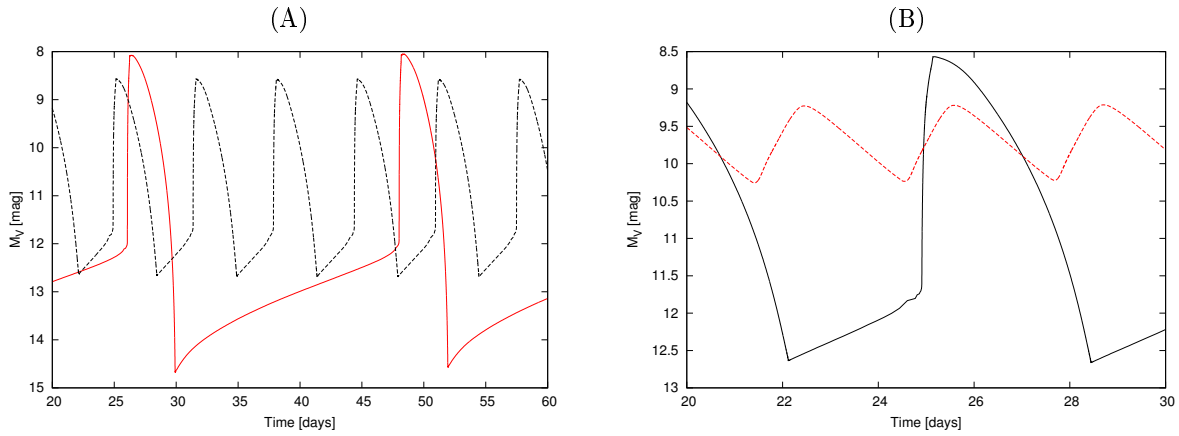

Figure 2.8: The result of changing α_c (A) and α_h (B) on the light curves of solar composition disc. All light curves are calculated for $M_1 = 1.0\,M_\odot$, $\dot{M}_{tr} = 1.0 \times 10^{16}$ g/s and $\langle R_d \rangle = 1.2 \times 10^{10}$ cm. Black lines on both figures are for: $\alpha_c = 0.05$, $\alpha_h = 0.2$. Red lines: (A)$\alpha_c = 0.02$, $\alpha_h = 0.2$; (B) $\alpha_c = 0.05$, $\alpha_h = 0.1$.

When α_c is low it takes longer for matter to diffuse through the disc. The lower efficiency of viscous heating means also that in order to reach the temperature at which an outburst can be triggered the disc has to be denser ($\Sigma^-_{crit} \propto {\alpha_c}^{-0.8}$, see Appendix A). A disc with low α_c spends more time in quiescence and has sparser outbursts than the disc with higher α_c. The difference is shown in the panel (A) of Fig.2.8 where the red line corresponds to the model calculated for $\alpha_c = 0.02$ and black line for $\alpha_c = 0.05$. Other parameters are the same for both models: $\alpha_h = 0.2$, $M_1 = 1.0\,M_\odot$, $\dot{M}_{tr} = 1.0 \times 10^{16}$ g/s and $\langle R_d \rangle = 1.2 \times 10^{10}$ cm, the disc has the solar composition.

High α_h shortens t_{visc} in the hot disc. In other words it controls the rate at which the mass is accreted during the outburst decay. Higher efficiency of the mass accretion with higher α_h means that the disc will be less massive at the beginning of the quiescence. It can be seen in Fig.2.8B where the disc with $\alpha_h = 0.2$ plotted with black line needs time after the outburst to accumulate the mass and start a new cycle. On the contrary, in the light curve calculated for $\alpha_h = 0.1$ (red line) the quiescent state is absent for two reasons. First is that for lower α_h the cooling front starts at higher Σ ($\Sigma^+_{crit} \propto {\alpha_h}^{-0.8}$, see Appendix A) which is therefore closer to Σ^-_{crit}. Second is that in this case the viscosity in the hot gas is so ineffective that the cooling front is not able to arrive to the inner radius because it is "reflected" somewhere on its way (see "reflares", Sect.2.7.3.1).

In general the ratio of Σ^-_{crit} and Σ^+_{crit} controls the amplitude and the recurrence time of an outburst. It determines how much mass is accreted and accumulated during the outburst cycle what decides about the disc luminosity in the high and the low state. Σ^-_{crit} and Σ^+_{crit} in the same R differ only by constant and by α so it is useful to define the ratio $\beta \equiv \alpha_h/\alpha_c$. The higher is β the larger is the outburst amplitude and the longer is its recurrence time. The dependence of the light curves on β can be clearly seen in Fig.2.8: in the diagram (A) the red line corresponds to $\beta = 10$ and the black line to $\beta = 4$, in the diagram (B) the red line corresponds to $\beta = 2$ and the black line to $\beta = 4$. β influences also the appearance of the reflares (Sect.2.7.3.1).

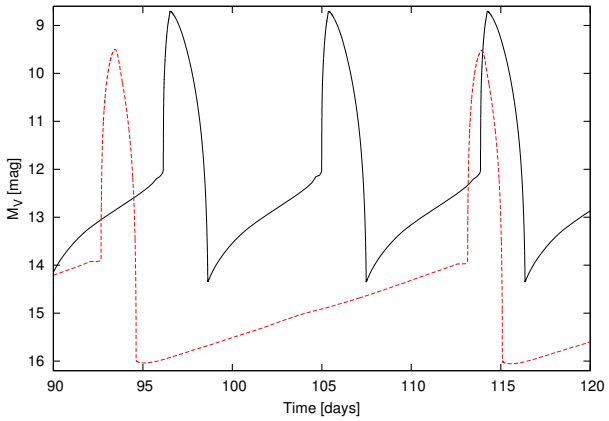

Figure 2.9: The result of changing $\dot{M}_{\rm tr}$ on the light curves of solar composition disc. Both light curves are calculated for $M_1 = 0.6\,{\rm M}_\odot$, $\alpha_{\rm c} = 0.05$, $\alpha_{\rm h} = 0.2$ and $\langle R_{\rm d}\rangle = 1.2 \times 10^{10}\,{\rm cm}$. Black line: $\dot{M}_{\rm tr} = 1.0 \times 10^{16}\,{\rm g/s}$; red line $\dot{M}_{\rm tr} = 0.1 \times 10^{16}\,{\rm g/s}$.

2.6.2 The mass transfer rate

The rate at which the matter is supplied to the disc has an influence on the disc luminosity. When all other parameters are fixed the increased $\dot{M}_{\rm tr}$ makes the disc hotter and denser - the luminosity both in the cold and in the hot state is augmented. The outburst is also longer because more mass is being fed into the disc during the outburst maximum what delays the onset of the cooling front. The difference in outburst amplitudes between $\dot{M}_{\rm tr} = 1.0 \times 10^{16}$ g/s (black line in Fig.2.9) and $\dot{M}_{\rm tr} = 0.1 \times 10^{16}$ g/s (red line in in Fig.2.9) is the effect of the location at which the heating front is triggered. Eventually for the very high $\dot{M}_{\rm tr}$ the outburst changes its character from the inside-out to the outside-in outburst. The higher $\dot{M}_{\rm tr}$ the farther away from the inner edge of the disc the heating front starts to propagate. In the model with $\dot{M}_{\rm tr} = 0.1 \times 10^{16}$ g/s the surface density in the disc is lower than in the disc in the model with $\dot{M}_{\rm tr} = 1.0 \times 10^{16}$ g/s. In consequence the disc luminosity in quiescence is lower and the front forms closer to $R_{\rm in}$ than in the former case. Thus the amplitude is higher for lower $\dot{M}_{\rm tr}$.

Higher luminosity at the outburst maximum in the light curve plotted in black in Fig.2.9 follows from Eq.(2.55) which states that the luminosity of the hot disc is proportional to $\dot{M}_{\rm tr}$. However, the relation between $L_{\rm max}$ and $\dot{M}_{\rm tr}$ is more complex than that. Eq.(2.55) depends also on $R_{\rm d}$ or, more precisely, on $R_{\rm d,max}$ which in turn depends on $\dot{M}_{\rm tr}$ through the outer boundary condition - Eq.(2.41). Higher rate at which the matter is incorporated into the disc and higher surface density at R_d imply that more angular momentum has to be transported outwards - the disc during the outburst expands to larger $R_{\rm d,max}$ what gives small contribution to increase of $L_{\rm max}$.

2.6.3 The size of the disc: M_1 and $\langle R_{\rm d}\rangle$

Unless the processes which may truncate the inner parts of the disc are taken into account (the accretor magnetic field or the inner disc evaporation) the primary mass defines the inner disc radius

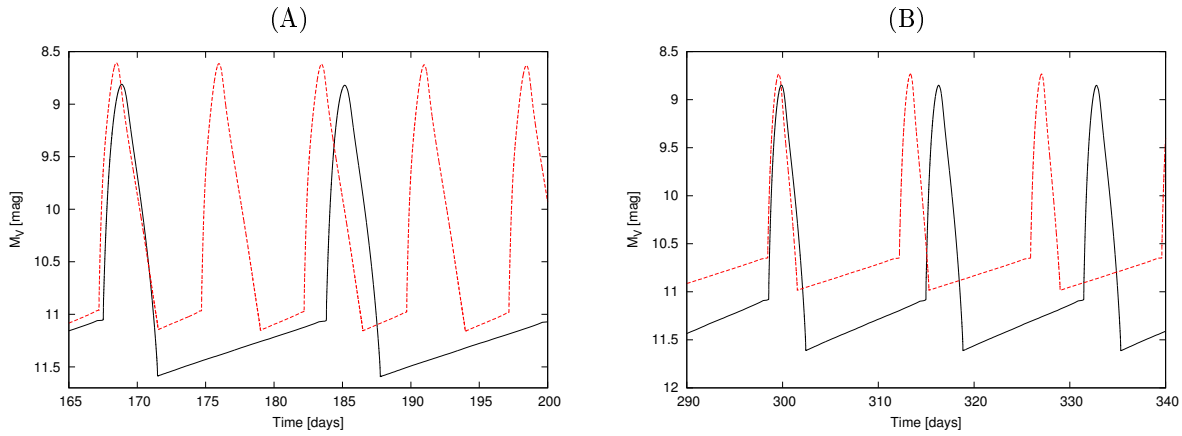

Figure 2.10: The results of changing M_1 (A) and $\langle R_{\rm d}\rangle$ (B) in the light curves of $Y = 0.98$ $Z = 0.02$ disc. All light curves were calculated for $\alpha_{\rm c} = 0.05$, $\alpha_{\rm h} = 0.1$ and $\dot{M}_{\rm tr} = 1.0 \times 10^{16}$ g/s. (A): $M_1 = 0.6\,{\rm M}_\odot$ (black line) and $M_1 = 1.0\,{\rm M}_\odot$ (red line), $\langle R_{\rm d}\rangle = 1.2{\times}10^{10}$ cm in both; (B): $\langle R_{\rm d}\rangle = 1.2{\times}10^{10}$ cm (black line) and $\langle R_{\rm d}\rangle = 3.0{\times}10^{10}$ cm (red line), $M_1 = 0.6\,{\rm M}_\odot$ in both.

and, together with $\langle R_{\rm d}\rangle$, defines the disc extent. The inner disc radius is smaller in the system with massive primary (due to the mass-radius relation for the degenerate stars (Nauenberg, 1972)) what enables the onset of the inside-out outburst at lower densities because $\Sigma^{-}_{\rm crit} \propto R$. It leads to the more frequent outbursts with lower amplitude because during short quiescence less mass is accumulated in the disc and less mass has to be accreted during the outburst decay. $L_{\rm max}$ is mainly defined by $\dot{M}_{\rm tr}$ but the weak dependence on M_1 makes it a little higher for more massive accretor. This results are presented in Fig.2.10A.

The diffusion of matter through the larger disc takes longer what suggests that the large disc should spend more time in quiescence. But the things are more complicated as the large disc is also more massive: (i) first, the propagation of the cooling front in denser disc is more prone to reflections and it may not arrive to the inner edge, (ii) second, the higher density left in the disc after cooling front passage eases the triggering of the new heating front at larger radii, just as in the case of increased $\dot{M}_{\rm tr}$. This is the reason of higher luminosity in quiescence and slightly more frequent outbursts for the model with $\langle R_{\rm d}\rangle = 3.0 \times 10^{10}$ cm shown in Fig.2.10B (red line).

2.7 Impact of helium on the disc properties

The existence of two electrons in helium atom induces 2 ionization states and leads to a wide range of different atomic transitions. We analyze the consequences of the atomic structure of helium for the solutions of the vertical structure equations and the heating and cooling fronts properties in the helium-dominated discs.

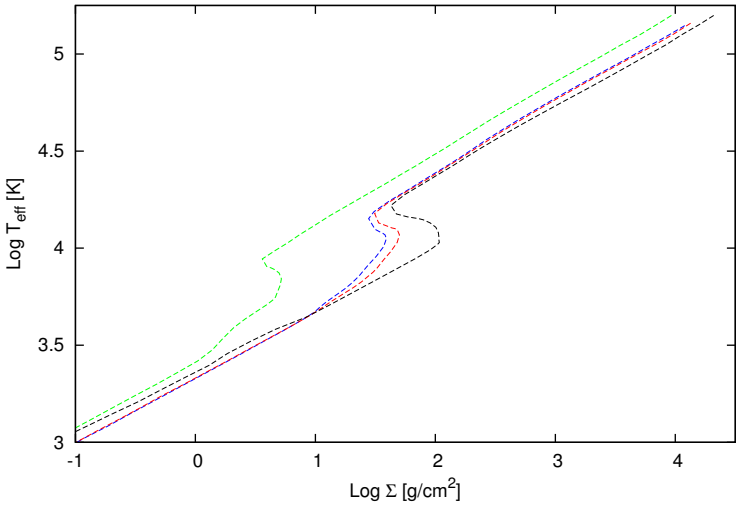

Figure 2.11: The S-curves for 4 different chemical compositions of the disc calculated in $R = 1.0 \times 10^9$ cm, for $\alpha = 0.1$ and $M_1 = 1.0\,\mathrm{M}_\odot$: black: $Y = 1.0$, red: $Y = 0.98$ $Z = 0.02$, blue: $Y = 0.96$ $Z = 0.04$, green: solar composition.

2.7.1 S-curves

The opacities in the temperature range found in the optically thick accretion discs are dominated by the bound-bound, bound-free and free-free processes. For the last two the mean Rosseland opacity takes the Kramers form:

$$\kappa = \kappa_{\mathrm{R}} \propto \rho T^{-3.5} \tag{2.61}$$

Since the opacity in purely helium discs is much smaller than the opacity in the helium disc with admixture of metals or the opacity of the solar composition disc (Table 2.2) the radiative gradient of temperature becomes too small to dominate over the adiabatic temperature gradient and the convection is suppressed. It has the same effect on $\Sigma^{-}_{\mathrm{crit}}$ as has $\alpha > 0.3$ (see Sect.2.4)

The reason for the rise of κ_{R} when even small amount of metals is added to the pure helium lies in the helium ionization temperatures and is explained below.

To calculate the ionization temperatures corresponding to the given ionization energies one has to use the Saha equation which describes the degree of ionization of plasma as a function of its density ρ, temperature T and ionization energy E_i of atoms.

For two successive stages of ionization Saha equation takes the form

$$\frac{N_{i+1}N_e}{N_i} = \frac{2}{\Lambda^3}\frac{U_{i+1}(T)}{U_i(T)}\exp\left(\frac{-(E_{i+1}-E_i)}{k_{\mathrm{B}}T}\right), \tag{2.62}$$

where N_i is the number density of atoms in i^{th} ionization state, N_e is the number density of electrons, E_i is the ionization potential between states $i+1$ and i, and Λ is the thermal de Broglie wavelength

z	$T_{\rm zII}$	$T_{\rm zIII}$	$T_{\rm zIV}$	$T_{\rm zV}$
O	14 416	37 191	58 182	81 981
C	11 926	25 825	50 710	68 303
N	15 339	31 240	50 075	81 760

Table 2.1: The first four ionization temperatures of three chemical elements: oxygen, carbon and nitrogen, calculated from Eq. (??) with $\gamma \approx 11$. The temperatures are in K.

of electrons of temperature T

$$\Lambda = \frac{h}{(2\pi m_e k_{\rm B} T)^{1/2}} \tag{2.63}$$

where h is the Planck constant.

The partition function U_i can be found from Boltzmann law:

$$U_i = \sum_i g_i e^{-\beta E_i} \tag{2.64}$$

where g_i is the degeneration of $i^{\rm th}$ level and $\beta \equiv \frac{1}{k_{\rm B}T}$.

The degree of ionization can be measured by the number of electrons in the cube of the volume Λ^3. After some algebraic transition the temperature T at which the ionization changes from level i to level $i+1$ can be found from

$$k_{\rm B} T \sim \frac{(E_{i+1} - E_i)}{\gamma} \tag{2.65}$$

where $\gamma \equiv -\ln(N_e \Lambda^3)$.

The evaluated γ for different helium content in the disc is $\gamma \approx 10$ and $\gamma \approx 11$ for $Y = 1.0$ and $Y = 0.96,\ Z = 0.04$ respectively. To find N_e we used the EOS tables from OPAL calculated following Paczyński (1969) and temperatures and densities from our numerical calculations of the disc vertical structures.

The first and second ionization energy of helium is $E_{\rm HeII} = 24.6$ eV and $E_{\rm HeIII} = 54.4$ eV. Using Eq.(2.65) we found the ionization temperatures of helium for (i) purely helium plasma ($Y = 1.0$): $T_{\rm HeII} \approx 28\,560$ K, $T_{\rm HeIII} \approx 63\,150$ K, (ii) for plasma consisting of 96% of helium and 4% of metals ($Y = 0.96\ Z = 0.04$): $T_{\rm HeII} \approx 25\,920$ K, $T_{\rm HeIII} \approx 57\,410$ K.

The calculated temperatures of different ionization levels for O, N and C (for $\gamma \approx 11$) are listed in Table 2.1. It shows that metals are highly ionized at the temperature of the second helium ionization and their contribution to the plasma free electrons population is significant. Therefore, even though their abundances are assumed to be low ($Z = 0.02$ or $Z = 0.04$) their impact on the opacities in the disc is noticeable. As the main opacity sources in the disc are f-f and b-f transitions, the additional electrons change the efficiency of the cooling and heating mechanisms what has the influence on $T^{+}_{\rm c,crit}$ and $T^{-}_{\rm c,crit}$.

Since the ionization temperature of hydrogen, $T_{\rm HII} \sim 18\,000$ K, is significantly lower then those of helium the metals contribution to the opacities in the case of hydrogen-dominated discs is negligible.

The difference in ionization temperatures influences the stability criteria of the disc of different

	Y = 1.0	Y = 0.98	Y = 0.96	solar
$\Sigma^{+}_{\rm crit}$ [g/cm^2]	42.1	30.8	27.8	3.5
$\Sigma^{-}_{\rm crit}$ [g/cm^2]	108.0	50.2	39.0	5.2
$Teffcrm$ [K]	10 700	11 700	11 200	6 960
$Teffcrp$ [K]	15 600	14 250	14 200	8 210
$\kappa(\Sigma, T_c^{-})$ [cm^2/g]	4.2×10^{-1}	4.5×10^{2}	5.4×10^{2}	1.3×10^{3}
$\tau_{\rm tot}(\Sigma, T_c^{-})$	45.3	2.24×10^{4}	2.11×10^{4}	7.03×10^{3}

Table 2.2: S-curve's critical points for 4 disc chemical compositions. Their values are calculated for $R = 1.0 \times 10^9\, cm$, $\alpha = 0.1$ and $M_1 = 1.0\,{\rm M}_\odot$

chemical compositions and it can be clearly understood when one looks at the S-curves.

In Fig.2.11 four S-curves are shown, each of them for different chemical composition of the disc: hydrogen-dominated ($X = 0.7$, $Y = 0.28$, $Z = 0.02$), pure helium, $Y = 0.98$, $Z = 0.02$ and $Y = 0.96$, $Z = 0.04$. All of them are calculated in radius $R = 1.0 \times 10^9$cm, for $M_1 = 1.0\,{\rm M}_\odot$ and $\alpha = 0.1$.

The numerical fits for critical values of T, Σ and $\dot{M}_{\rm accr}$ were calculated by Guillaume Dubus (private communication) and are given in Appendix A. Their values for $R = 1.0 \times 10^9$ cm, and $\alpha = 0.1$ are listed in Table 2.2.

The temperatures and surface densities in helium discs are much higher than in hydrogen-rich discs, moreover the ratio $\beta_c \equiv \Sigma^{+}_{\rm crit}/\Sigma^{-}_{\rm crit}$ in helium discs is twice that in solar composition discs.

The ratio of the critical surface densities determines how much mass in the disc will be accumulated and accreted during the outburst cycle and thus decides how luminous will be the disc in the maximum and minimum light - it decides about the outburst amplitude. It has the same effect on the local properties of helium disc as has the change of α from $\alpha_{\rm h}$ to $\alpha_{\rm c}$ - increasing $\beta_{\rm c}$ it stretches the middle part of the S-curve. It is then possible to get outbursts of amplitude up to 2.5 mag without changing α in helium discs. But still, as will be shown in Sect.2.7.3, to get the outburst amplitudes observed in AM CV stars (i.e. up to $4-5$ mag) one needs to retain two different α values: $\alpha_{\rm h}$ and $\alpha_{\rm c}$.

In Fig.2.12 is shown how $\kappa_{\rm R}$ changes with density and temperature. In the diagram (A) is presented the $\kappa_{\rm R} - T$ relation in purely helium gas for different parameter $R_{\rm OPAL} \equiv \rho/T_6$, where $T_6 = T/10^6$ K (data has been taken from the OPAL website). The densities ρ in the accretion discs considered are of the order $\sim 10^{-5} - 10^{-6}$ g/cm^3 what corresponds to the region between blue and green lines. The shape of those lines in the temperature range $10^4 - 10^5$ K corresponds to the two peaks present in Fig.2.13A. The diagram (B) of Fig.2.12 shows the difference in $\kappa_{\rm R} - T$ relations for various values of $R_{\rm OPAL}$ between purely helium disc (solid lines) and $Y = 0.98$ $Z = 0.02$ disc (dashed lines). It clearly demonstrates how the addition of only 2% of metals to helium increases the opacity.

In Fig.2.13 is shown how $\kappa_{\rm R}$ changes with $T_{\rm c}$ during the outburst cycle in $R = 2.15 \times 10^9$ cm for three different chemical composition of the disc: $Y = 1.0$ (A), $Y = 0.98$ $Z = 0.02$ (B) and $X = 0.7$ $Y = 0.28$ $Z = 0.02$ (C). In all three models: $\alpha_{\rm h} = 0.1$, $\alpha_{\rm c} = 0.05$, $M_1 = 1.0\,{\rm M}_\odot$. The lower line on each plot corresponds to the transition of the annulus from the upper branch to the lower branch of the S-curve while the upper line corresponds to the transition in the opposite direction -

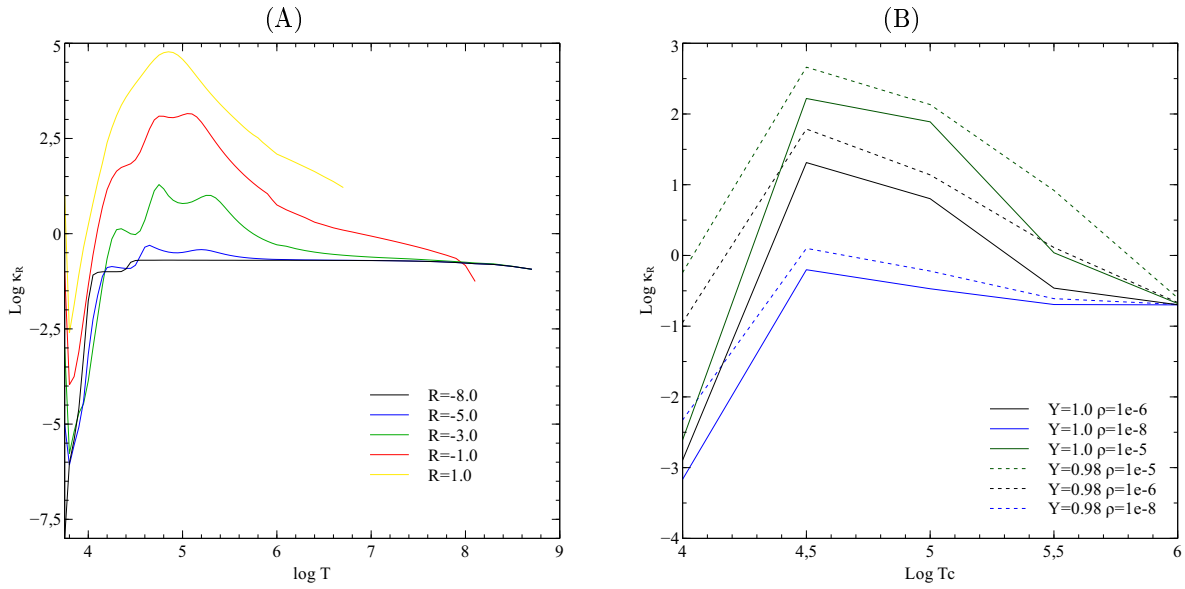

Figure 2.12: (A) The relation between the mean Rosseland opacity κ_{R} and temperature T for different values of parameter $R_{\mathrm{OPAL}} \equiv \rho/T_6$. For high densities the structure of the plotted lines smooth out and the opacity has a peak near the temperature of the second ionization of He. (B) The same relations as in (A) but for $Y = 1.0$ (solid lines) and $Y = 0.98$ $Z = 0.02$ (dashed lines). The structure of the lines is less detailed because of less points taken for the plots. The data has been taken from the OPAL project website.

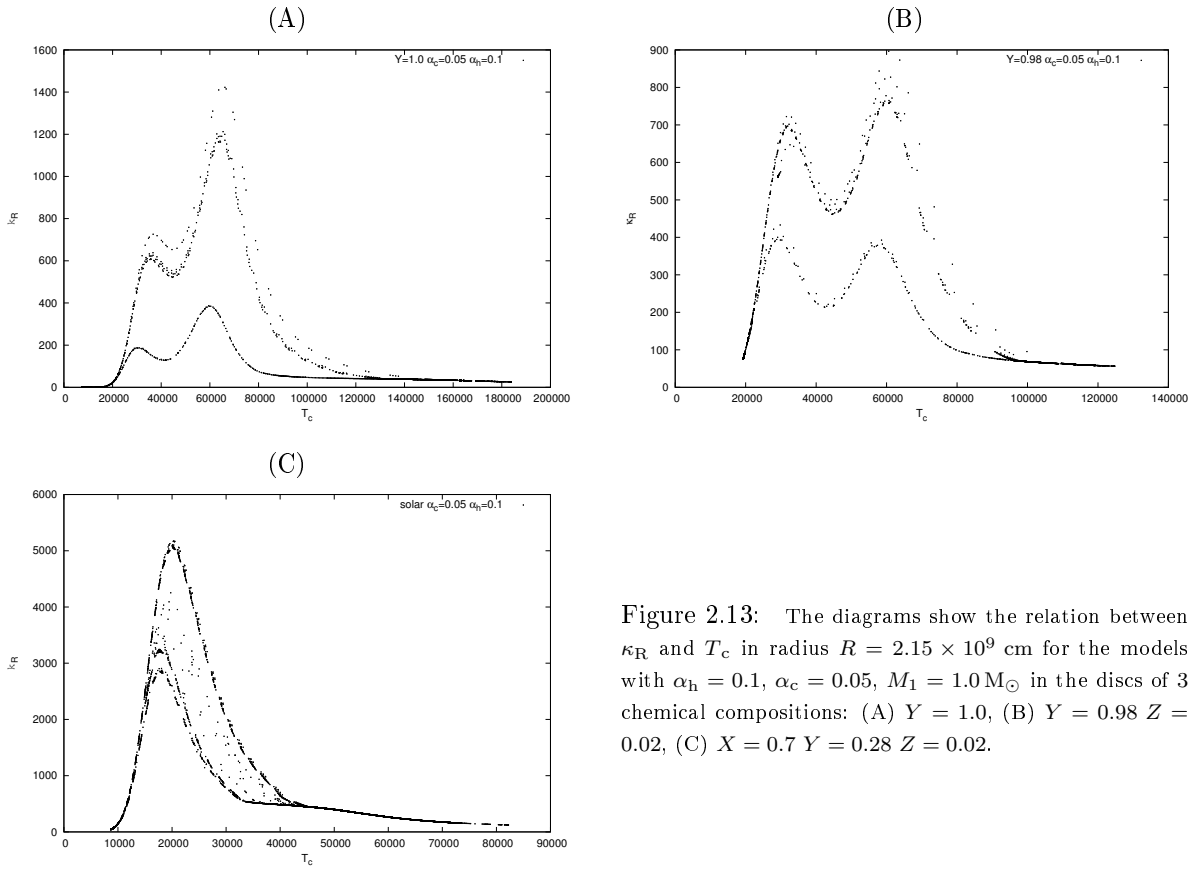

Figure 2.13: The diagrams show the relation between $\kappa_{\rm R}$ and $T_{\rm c}$ in radius $R = 2.15 \times 10^9$ cm for the models with $\alpha_{\rm h} = 0.1$, $\alpha_{\rm c} = 0.05$, $M_1 = 1.0\,{\rm M}_\odot$ in the discs of 3 chemical compositions: (A) $Y = 1.0$, (B) $Y = 0.98$ $Z = 0.02$, (C) $X = 0.7$ $Y = 0.28$ $Z = 0.02$.

from the cold to the hot branch. The conclusions from Fig.2.13 are:

- the higher is Z the higher is $\kappa_{\rm R}$ connected with $T^-_{\rm c,crit}$ (left peak on the upper line of $\kappa_{\rm R} - T_{\rm c}$ relation) - the ionization of metals has the deciding influence on the opacity in ($\Sigma^-_{\rm crit}$, $T^-_{\rm c,crit}$) point
- higher Z does not influence $\kappa_{\rm R}$ connected with $T^+_{\rm c,crit}$ (right lower peak on the lower line of $\kappa_{\rm R} - T_{\rm c}$ relation) - the opacities in ($\Sigma^+_{\rm crit}$, $T^+_{\rm c,crit}$) point are determined by the second ionization of helium
- in general the rise of Z rises the opacities in the low-temperature regime (below the temperature of 2nd He ionization)
- in the hydrogen-dominated disc the opacities are controlled by hydrogen ionization, the influence of He or metals on $\kappa_{\rm R}$ is unnoticeable (only one peak in $\kappa_{\rm R}$ appears, near by the temperature of hydrogen ionization)

We have investigated also how various α-parameters which we choose in the model influence $\kappa_{\rm R}(T_{\rm c})$ relation (which is different from the previous one in a sense that the previous considered the influence

of intristic, atomic properties of plasma). The impact of different sets of $\alpha_{\rm h}$ and $\alpha_{\rm c}$ on $\kappa_{\rm R}$ in radius $R = 2.15 \times 10^9$ cm in the models calculated for the helium dominated discs with $Z = 0.02$ for $\dot{M}_{\rm tr} = 0.1 \times 10^{16}$ g/s, $M_1 = 1.0$ M$_\odot$ is shown in Fig.2.14. These plots show several properties which can be noticed:

- the increase of $\alpha_{\rm c}$ (while $\alpha_{\rm h}$ is fixed) lowers the opacities during the transition of the disc ring from cold to hot state (compare upper plots in diagrams (A) and (C) in Fig.2.14) and has no effect on the opacities during the transition from the hot to the cold state (lower plots in diagrams (A) and (C) in Fig.2.14). Similar effect has the increase of Z in helium dominated disc (see Fig.2.13A and B) although Z additionally influences opacities near $T^-_{\rm c,crit}$ regime.

- the change of $\alpha_{\rm h}$ from 0.1 to 0.4 impacts the shape of $\kappa_{\rm R} - T_{\rm c}$ relation (Fig.2.14A and B): higher $\alpha_{\rm h}$ decreases $\kappa_{\rm R}$ around $T^+_{\rm c,crit}$, i.e. the opacities connected with the second ionization of helium. This happens because by setting $\alpha_{\rm h} = 0.4$ one lowers $\Sigma^+_{\rm crit}$ ($\Sigma^+_{\rm crit} \propto {\alpha_{\rm h}}^{-0.8}$) while $T^+_{\rm c,crit}$ remains unchaned as it does not depend on $\alpha_{\rm h}$. Therefore with the same $T^+_{\rm c,crit}$ but lower $\Sigma^+_{\rm crit}$ one leaves the regime where the opacities related to the 2nd helium ionization dominate. The elevated left upper peak for $\alpha_{\rm h} = 0.4$ (Fig.2.14A) is the consequence of the higher amount of mass which has to be accumulated in the given ring during quiescence to cross $\Sigma^-_{\rm crit}$ (when $\alpha_{\rm h}$ is higher more mass is accreted from the disc during the outburst decay).

The cautious conclusions which can be drawn are:

1. Since $\Sigma^-_{\rm crit}$ is determined by the metallicity of the helium-dominated disc and it is inversely proportional to $\alpha_{\rm c}$ the alteration of $\alpha_{\rm c}$ in the model may mimic changing Z in the disc.

2. Since $\Sigma^+_{\rm crit}$ is connected with amount of helium in the disc (for helium-dominated disc, in H-rich disc it would be hydrogen) and it is inversely proportional to $\alpha_{\rm h}$ the change of $\alpha_{\rm h}$ may imitate the change in the amount of the dominant chemical element in the disc.

2.7.2 The fronts

The transition fronts are the means by which the instability which is triggered locally spreads through the disc and affects its global evolution. The times (or equivalently the velocities) of the front propagation through the disc define the time scales observed in outbursts: the time it takes the heating front to travel through the disc determines the time of the rise of an outburst and the time of the cooling front propagation fixes the outburst decay time. The investigations of the fronts properties give the insight to what happens in the disc during the outburst and the significance of different terms in thermal equation.

2.7.2.1 Front structure

The atomic structure of the dominant chemical elements affects the structure of the cooling and heating fronts (the front origin and propagation is described in Sect. 2.5).

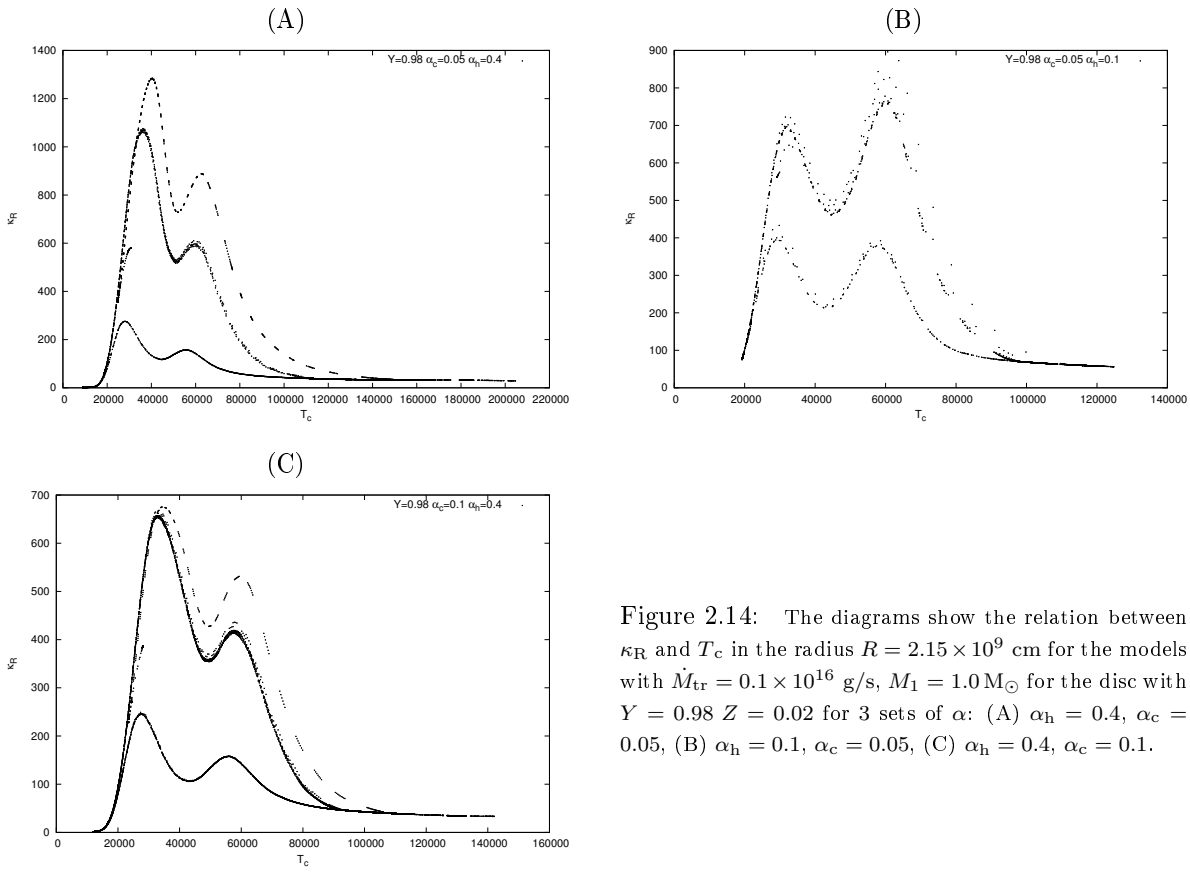

Figure 2.14: The diagrams show the relation between $\kappa_{\rm R}$ and $T_{\rm c}$ in the radius $R = 2.15 \times 10^9$ cm for the models with $\dot{M}_{\rm tr} = 0.1 \times 10^{16}$ g/s, $M_1 = 1.0\,{\rm M}_\odot$ for the disc with $Y = 0.98$ $Z = 0.02$ for 3 sets of α: (A) $\alpha_{\rm h} = 0.4$, $\alpha_{\rm c} = 0.05$, (B) $\alpha_{\rm h} = 0.1$, $\alpha_{\rm c} = 0.05$, (C) $\alpha_{\rm h} = 0.4$, $\alpha_{\rm c} = 0.1$.

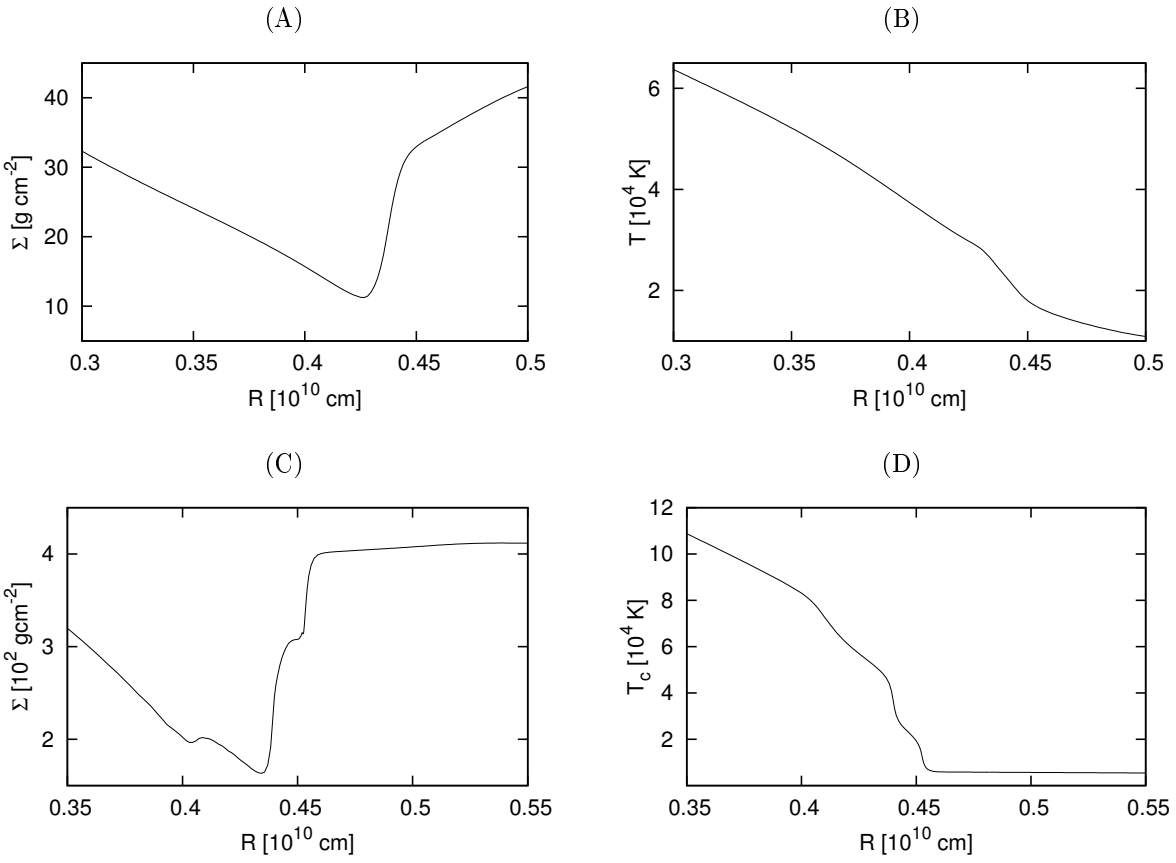

Figure 2.15: The structure of a cooling fronts in solar composition disc and in purely helium disc. *Top panels* (A), (B): solar disc, *Bottom panels* (C), (D): pure helium disc. *Left column* (A), (C): front seen in Σ profile, *Right column* (B), (D): $T_{\rm c}$ profile. Models calculated for $\alpha_{\rm h} = 0.1$, $\alpha_{\rm c} = 0.05$, $\dot{M}_{\rm tr} = 0.1 \times 10^{16}$ g/s, $M_1 = 1.0\,{\rm M}_\odot$ and $\langle R_{\rm d} \rangle \approx 1.1 \times 10^{10}$ cm.

The analysis of a cooling and heating front structure in the solar composition disc were pursued by Menou et al. (1999). It was found that general properties of the fronts do not depend on viscosity and front location in the disc.

The temperature gradients of both heating and cooling front in solar composition discs are smooth (upper panels of Fig.2.15 and 2.7.2.2). In comparison the fronts in helium discs exhibit additional features, which can be seen as "humps" in the profiles of $\mathrm{T_c}(R)$ and $\Sigma(R)$ plotted in Fig.2.15 C&D and Fig.2.16C&D.

The breaks in the slope of the temperature gradient appear at roughly the same temperatures both for the heating and cooling fronts. Using the Saha equation one can convert these temperatures to energies and attempt to identify them with the energies corresponding to the different atomic transitions in helium.

The first characteristic hump appears at $T \sim 26\,000$ K. At this temperature one electron is

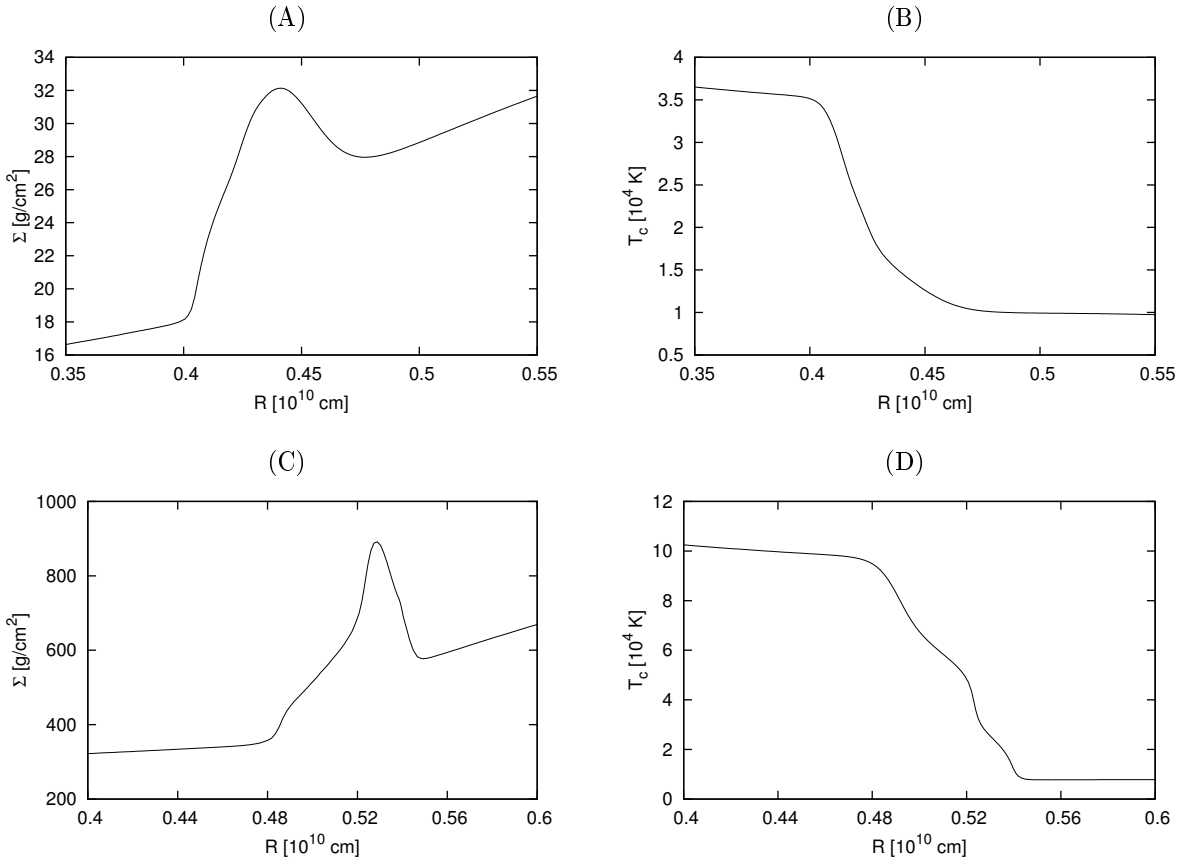

Figure 2.16: The structure of heating fronts in solar composition disc and purely helium disc. *Top panels (A), (B)*: solar disc, *Bottom panels* (C), (D): pure helium disc. *Left column* (A), (C): front seen in Σ profile, *Right column* (B), (D): $T_{\rm c}$ profile. Models calculated for $\alpha_{\rm h} = 0.1$, $\alpha_{\rm c} = 0.1$, $\dot{M}_{\rm tr} = 0.1 \times 10^{16}$ g/s, $M_1 = 1.0\,{\rm M}_\odot$ and $\langle R_{\rm d} \rangle \approx 0.8 \times 10^{10}$ cm.

in the state $1s$ and the second electron starting from orbital $3s$ gradually passes to higher states $(3p, 3d, 4p, ..)$ as the temperature rises and finally at $T \sim 28\,560$ K it becomes ionized. With further rise of temperature the first electron which was in the ground state is excited to states: $n = 2$ (at $T \sim 47\,000$ K), $n = 3$ (at $T \sim 56\,000$ K), $n = 4$ (at $T \sim 59\,000$ K). At temperature of $\sim 63\,150$ K helium becomes double-ionized. The hump in the temperature profile appearing for T $\sim 80\,000 - 92\,000$ K ($\sim 69 - 80$ eV) can be assigned to double-photoionization and different negative-ion resonances.

These transitions of helium electrons between different energy levels cause the changes in the opacities and the breaks seen in Σ profile.

In the case of solar composition discs we do not see any features from atomic transitions of helium and metals, because the fronts there start to propagate at lower temperatures and much lower densities (i.e. hydrogen ionization temperature $\sim 15\,000$ K and $\Sigma \sim 30$ g cm^{-2}) at which these transition do not take place or are negligible because of small contribution of metals to overall disc composition (like single ionization of carbon at $T \sim 12\,000$ K).

2.7.2.2 Front width and velocity

The width of the heating/cooling front defines the temperature and surface density gradients and (mass and angular momentum) fluxes in the front. It is also closely connected to the thermal time scales in the disc.

The width of a front is the distance it travels during several thermal time scales. We approximate it following Menou et al. (1999) as 90% of width of the region in which the transition of α between its cold and hot value takes place (the α "jump" is given by Eq.(2.60)). This region is marked in all three panels of Fig.2.17 between points 1 and 2.

We adopt the definition of the front location in the disc from Menou et al. (1999) as the radius $R_{\rm F}$ at which the central temperature reaches the value lying in the instability regime, i.e. where the disc matter becomes partially ionized. For the solar composition disc $R_{\rm F}$ is defined where $T_{\rm c} = 1.8 \times 10^4$ K (Menou et al., 1999) and for helium discs we define $R_{\rm F}$ where $T_{\rm c} = 4.0 \times 10^4$ K (Fig.2.17).

The front velocity is calculated from the formulae given by Menou et al. (1999). We also calculate it by differentiating the front location in time in the numerical simulations of the light curves.

According to Menou et al. (1999) the cooling front velocity is

$$\mathrm{v}_{\rm front,cool} = \alpha_{\rm h}\, c_{\rm s} \left(\frac{H}{R}\right)^{0.7} \tag{2.66}$$

where $\alpha_{\rm h}$ is the viscosity parameter in a hot state,$c_{\rm s}$ is a speed of sound and H is a disc height scale in a given radius R (the similar formula was derived by Vishniac and Wheeler (1996))

Substituting $c_{\rm s} = \sqrt{kT_{\rm c}/4\,m_{\rm H}}$ (in the case of helium) and $H = c_{\rm s}/\Omega_{\rm K}$ into equation (2.66) we get that

$$\mathrm{v}_{\rm front,cool} = \alpha_{\rm h} \left(\frac{k}{4m_{\rm H}}\right)^{0.85} \left(\frac{R}{G\,M_1}\right)^{0.35} T_{\rm c}^{0.85}. \tag{2.67}$$

The calculated values of $\mathrm{v}_{\rm front,cool}$ for three different chemical compositions of the disc and three

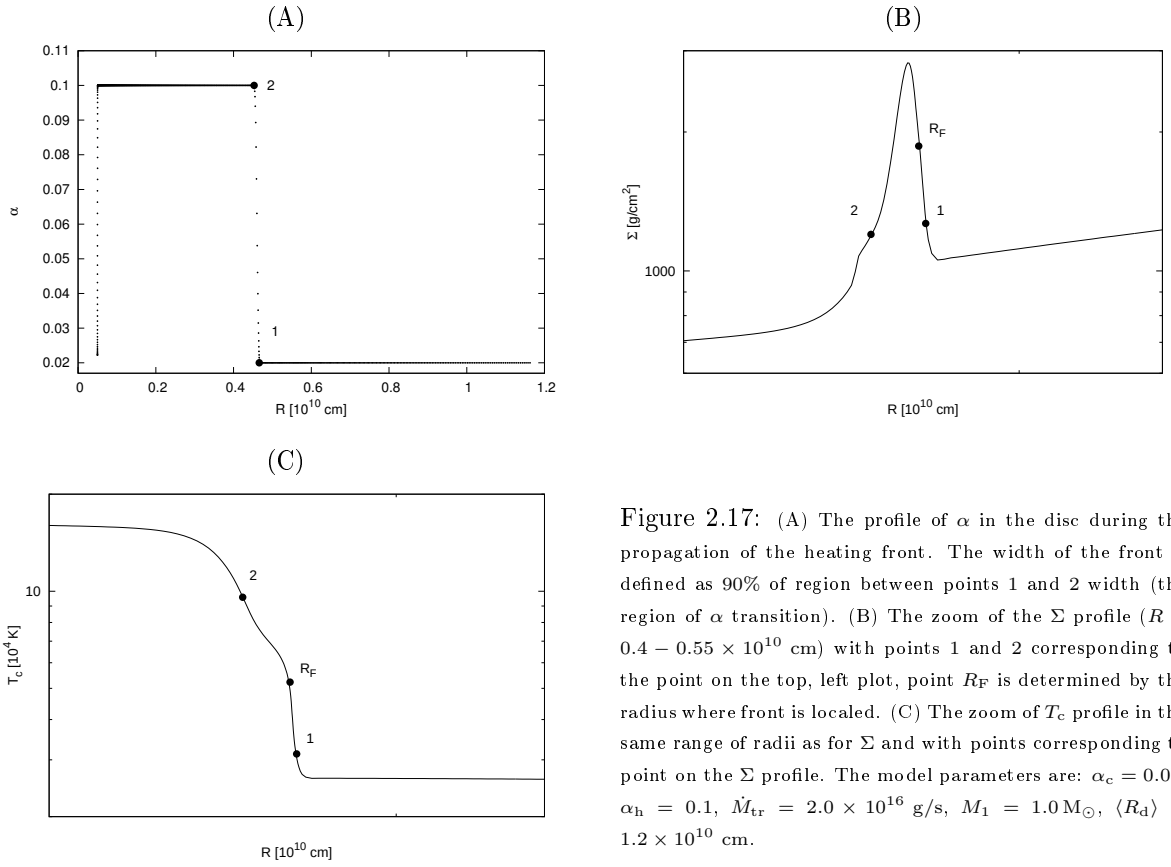

Figure 2.17: (A) The profile of α in the disc during the propagation of the heating front. The width of the front is defined as 90% of region between points 1 and 2 width (the region of α transition). (B) The zoom of the Σ profile ($R = 0.4 - 0.55 \times 10^{10}$ cm) with points 1 and 2 corresponding to the point on the top, left plot, point $R_{\rm F}$ is determined by the radius where front is localed. (C) The zoom of $T_{\rm c}$ profile in the same range of radii as for Σ and with points corresponding to point on the Σ profile. The model parameters are: $\alpha_{\rm c} = 0.02$, $\alpha_{\rm h} = 0.1$, $\dot{M}_{\rm tr} = 2.0 \times 10^{16}$ g/s, $M_1 = 1.0\,{\rm M}_\odot$, $\langle R_{\rm d} \rangle = 1.2 \times 10^{10}$ cm.

different pairs of $\alpha_{\rm h}$ and $\alpha_{\rm c}$ are listed in Table 2.4. It can be seen that the velocity of the cooling fronts in the hydrogen-rich discs are about twice that of fronts in helium-dominated discs. This difference is shown in Fig.2.18D where blue line is the velocity of the cooling front in solar composition disc while lines red and green lying below it are for helium-dominated discs. This differenece in velocities results from the molecular mass of helium which is 4 times that of hydrogen and from the values of the central temperatures which in helium-rich discs are about 2 times higher than $T_{\rm c}$ in solar composition discs.

The cooling front in solar composition disc in the model shown with the blue line in Fig.2.18D is reflected before it arrives to the inner disc edge. Moreover it forms not exactly at the outer edge but at smaller radius. This is the reason for its slightly different behavior from that of two other fronts shown on the diagram - it has not time to establish its velocity to the asymptotic value and the rapid acceleration near the outer edge is the effect of the transition from cooling to heating front.

Fig.2.18C illustrates the impact of $\alpha_{\rm h}$ and $\alpha_{\rm c}$ on the cooling front velocity in the helium disc with $Z = 0.02$. There is almost no difference in $\rm v_{front}$ for $\alpha_{\rm c} = 0.05$ and $\alpha_{\rm c} = 0.02$ (green and red line respectively) but the change from $\alpha_{\rm h} = 0.1$ to $\alpha_{\rm h} = 0.2$ rises $\rm v_{front}$ almost two times in the middle region of the disc.

The general characteristic of the cooling front is that it strongly deccelerates at the initial stage of its propagation down to the "asymptotic regime" where its velocity is roughly constant until it approaches the inner disc edge where it accelerates again due to the boundary condition (the rapid increase in $\rm v_{front}$ in solar composition disc at larger radii than in the case of green and red line, means that the cooling front has been reflected before arriving to the inner disc radius). In Menou et al. (1999) the gas velocity at the front is approximated as $\rm v_F \sim 1/7 \alpha_F c_F$, where $\alpha_{\rm F}$ and $c_{\rm F}$ are the values at the front. We find that $\rm v_F \sim 1/7 \alpha_h c_s$ is comparable to the velocity of the cooling front ($\rm v_{front}$) in the asymptotic regime: the rate at which the gas outflows from the hot to the cold region at the transition zone determines the speed at which the cooling front can penetrate into the hot gas. However, in general $\rm v_F \neq v_{front}$.

When the inside-out heating front starts to propagate it rapidly slows down just as the cooling front does but then it does not travel with the approximately constant $\rm v_{front}$ but keeps slowly deccelerating until it arrives to $R_{\rm d}$ where it rapidly vanishes. Fig.2.18A and B the strong decceleration of $\rm v_{front}$ appears at different radii what marks the location at which the heating front starts.

The initial decceleration of both types of the fronts is induced by the fact that in both cases the front propagates into the direction of increasing Σ.

The dependence on α is similar for the velocity of the heating fronts what is shown in Fig.2.18A (colors of lines correspond to the parameters as in the case of the cooling front). The increase of heating front velocity is proportional to the increase of $\alpha_{\rm h}$ value. In the case of a heating front the impact of $\alpha_{\rm c}$ is more noticable (compare green and red lines) because the onset and the propagation of the heating front depends on the $\Sigma^{+}_{\rm crit}$ and the surface density in the disc at the end of the quiescence - for $\alpha_{\rm c} = 0.05$ front starts at larger R (green line). The blue line in Fig.2.18B shows that the heating front starts very close to the outer edge in the solar composition disc (for the same paramets critical values of Σ for solar case are much lower from those in the helium discs).

$Y = 0.98$ $Z = 0.02$	$\alpha_{\rm h}$	$\alpha_{\rm c}$	$R_{\rm F}$	$v_{\rm F}$	$v_{\rm front}$	$c_{\rm s}$
Heating front	0.2	0.05	0.536	-	2.06	~ 9.1
	0.1	0.05	0.289	-	1.15	
	0.1	0.02	0.208	-	1.57	
Cooling front	0.2	0.05	0.384	~ 0.26	0.30	~ 9.1
	0.1	0.05	0.329	~ 0.13	0.19	
	0.1	0.02	0.498	~ 0.13	0.15	

Table 2.3: The different velocities connected with the heating and cooling fronts in the disc with $Y = 0.98$ $Z = 0.02$. $R_{\rm F}$ is the front location in $R_{\rm F} = 1.0 \times 10^{10}$ cm, $v_{\rm F}$ is the velocity at the cooling front calculated according to formula given by Menou et al. (1999) ($v_{\rm F} \sim 1/7\alpha_{\rm h} c_{\rm s}$) in km/s, $v_{\rm front}$ is the front velocity at $R_{\rm F}$ (in the asymptotic regime) in km/s obtained from the numerical calculations and $c_{\rm s}$ is the speed of sound in the temperature $T_{\rm c} \sim 4.0 \times 10^4$ K.

From Table 2.3 it can be seen that the velocity of the heating front is roughly proportional to $\alpha_{\rm h} c_{\rm s} \propto \alpha_{\rm h} T_{\rm c}^{0.5}$ in analogy to the velocity of an ignition front (Menou et al., 1999; Meyer, 1984). The higher temperatures in the purely helium disc are the reason why the heating front in the purely helium disc is faster from the front in the disc with $Z = 0.02$ (green and red line in Fig.2.18B).

	solar			100% He			98 % He		
$\alpha_{\rm h}$	0.2	0.1	0.1	0.2	0.1	0.1	0.2	0.1	0.1
$\alpha_{\rm c}$	0.05	0.05	0.02	0.05	0.05	0.02	0.05	0.05	0.02
$W_{\rm cool}/R_{\rm F}$	~ 0.09	~ 0.06	~ 0.05	~ 0.09	~ 0.06	~ 0.06	~ 0.12	~ 0.08	~ 0.08
$W_{\rm heat}/R_{\rm F}$	~ 0.03	~ 0.03	~ 0.02	~ 0.024	~ 0.025	~ 0.01	~ 0.03	~ 0.03	~ 0.02

Table 2.4: The widths W of the cooling and heating fronts for three sets of α parameters in the discs of three different chemical compositions: solar, purely helium and helium with 2% of metals. The front width are normalized to the radius in which the front is located and are in units days/cm.

The width W of the fronts is devided by the radius in which they are located, $R_{\rm F}$. The cooling fronts are broader and slower than the heating fronts which is connected with the slower diffusion of the matter in the cold region inside and behind the cooling front. We find that in helium-dominated disc $W \propto H$ for any value of $\alpha_{\rm h}$ and $\alpha_{\rm c}$, similar to what has been found by Menou et al. (1999) in hydrogen-dominated discs. The slope of the linear fit of the form $W = A\,H$, where A is the constant, differs between the discs of different composition and different values of α. The relation between $W/R_{\rm F}$ and $H/R_{\rm F}$ for the cooling front propagating in solar, purely helium and helium with $Z = 0.02$ for $\alpha_{\rm h} = 0.2$, $\alpha_{\rm c} = 0.05$ is shown in Fig.2.19.

The cooling front widths are similar for all disc compositions and all set of α. The same is true for the heating fronts.

All models presented in Fig. 2.18 have been calculated for $M_1 = 1.0\,{\rm M}_\odot$, $\langle R_{\rm d} \rangle \approx 1.2 \times 10^{10}$ cm and $\dot{M}_{\rm tr} = 2.0 \times 10^{16}$ g/s.

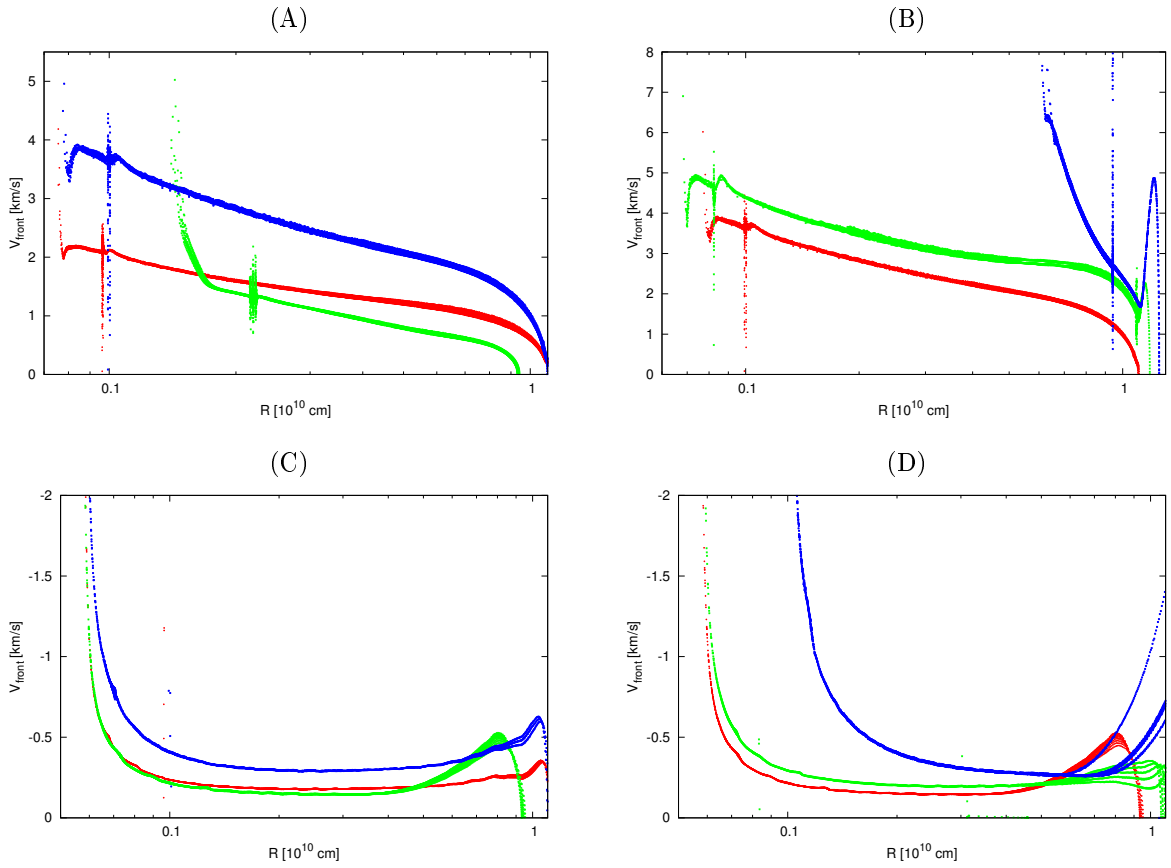

Figure 2.18: (A): The heating front velocity in the helium disc with $Z = 0.02$ for 3 sets of α's: $\alpha_{\rm h} = 0.2$, $\alpha_{\rm c} = 0.05$ (blue), $\alpha_{\rm h} = 0.1$, $\alpha_{\rm c} = 0.05$ (green), $\alpha_{\rm h} = 0.1$, $\alpha_{\rm c} = 0.02$ (red); (B): The heating front velocity for $\alpha_{\rm h} = 0.2$, $\alpha_{\rm c} = 0.05$ for 3 different disc chemical compositions: $Y = 0.98$ $Z = 0.02$ (red), $Y = 1.0$ (green), solar (blue). (C): The cooling front velocity in the helium disc with $Z = 0.02$ for 3 sets of α's: $\alpha_{\rm h} = 0.2$, $\alpha_{\rm c} = 0.05$ (blue), $\alpha_{\rm h} = 0.1$, $\alpha_{\rm c} = 0.05$ (green), $\alpha_{\rm h} = 0.1$, $\alpha_{\rm c} = 0.02$ (red); (D): The cooling front velocity for $\alpha_{\rm h} = 0.1$, $\alpha_{\rm c} = 0.05$ for 3 different disc chemical compositions: $Y = 0.98$ $Z = 0.02$ (red), $Y = 1.0$ (green), solar (blue). All models have been calculated for $M_1 = 1.0\,{\rm M}_\odot$, $\langle R_{\rm d} \rangle \approx 1.2 \times 10^{10}$ cm and $\dot{M}_{\rm tr} = 2.0 \times 10^{16}$ g/s.

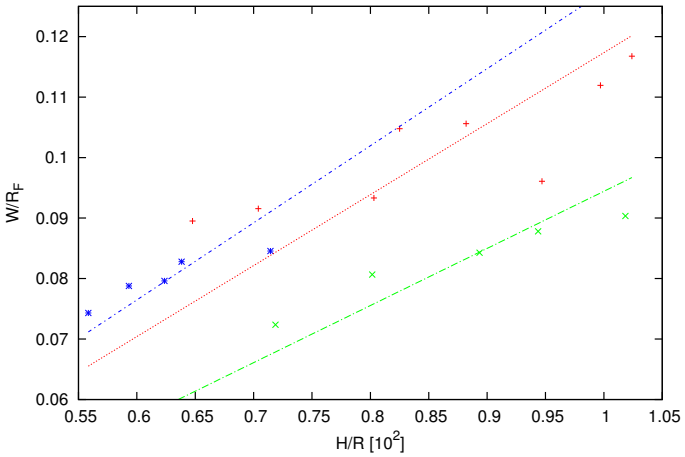

Figure 2.19: The relation of the normalized width of the cooling front to the normalized height of the disc at the radius in which the front is located. The points are $W/R_{\rm F}$ and $H/R_{\rm F}$ read out from simulations for the cooling front caught at different locations $R_{\rm F}$ during its propagation through the disc. The lines are the linear fit to the points of the corresponding color: hydrogen-dominated disc (blue), purely helium disc (green) and $Y = 0.98$ $Z = 0.02$ (red). In all cases $\alpha_{\rm h} = 0.2$, $\alpha_{\rm c} = 0.05$, $M_1 = 1.0\,{\rm M}_\odot$, $\dot{M}_{\rm tr} = 2.0 \times 10^{16}$ g/s, $\langle R_{\rm d} \rangle \approx 1.2 \times 10^{10}$ cm.

2.7.3 The outbursts

The DIM is supposed to describe both dwarf novae outbursts and AM CVn star outbursts (see Chap.4). The best way to see how the chemical composition of the disc can influence the observational light curves is to investigate what are the differences between the normal outbursts in helium- and hydrogen-dominated discs.

In the case of solar composition discs to obtain outbursts of an observed amplitude one has to assume $\alpha_c \neq \alpha_h$ (Smak, 1984). Yet the first look at Fig.(2.20), which shows the synthetic light curves calculated for discs of the same parameters but different chemical compositions, suggests that this condition may no longer be necessary in the case of helium-dominated discs.

The light curves in Fig. 2.20 are calculated for solar composition, pure helium and helium-dominated ($Y = 0.98$ $Z = 0.02$, $Y = 0.96$ $Z = 0.04$) discs. In all cases α is assumed to be constant through the outburst cycle: $\alpha_{\rm c} = \alpha_{\rm h} = 0.1$ and the parameters are: $\dot{M}_{\rm tr} = 1.0 \times 10^{15}$ g/s, $\langle R_{\rm d} \rangle \approx 1.2 \times 10^{10}$ cm and $M_1 = 1.0\,{\rm M}_\odot$.

The light curve for a solar composition disc shows (Fig.2.20C) the low-amplitude (~ 0.5 mag) fast (with period of ~ 1.2 d) light variations hardly resembling the dwarf novae outbursts. Things are different for purely helium disc (Fig.2.20A) where outbursts have amplitudes up to 2.0 mag and repeat about every 9 d. The addition of metals ($Z = 0.02$, $Z = 0.04$) to helium decreases $A_{\rm n}$ to around 1 mag (Fig.2.20B) and rises their frequency to ~ 2 d but also changes their shape.

Those differences in the light curves mirror the different critical surface density ratios $\beta_{\rm c} = \Sigma^{+}_{\rm crit}/\Sigma^{-}_{\rm crit}$ for different disc chemical compositions. The critical values calculated for $\alpha_{\rm h} = \alpha_{\rm c} = 0.1$, $M_1 = 1.0\,{\rm M}_\odot$ in radius $R = 5.0 \times 10^9$ cm, together with corresponding $\beta_{\rm c}$ and opacities $\kappa_{\rm R}$ are listed

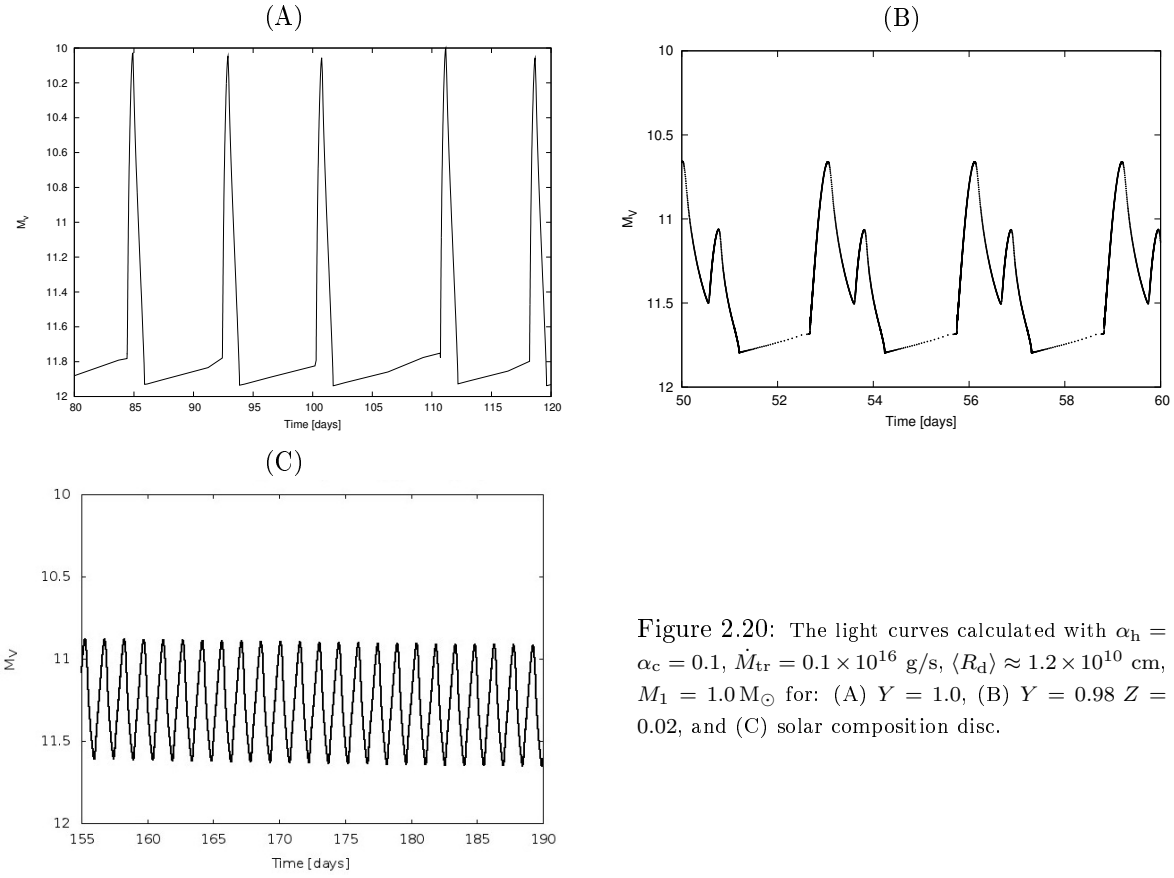

Figure 2.20: The light curves calculated with $\alpha_{\rm h} = \alpha_{\rm c} = 0.1$, $\dot{M}_{\rm tr} = 0.1 \times 10^{16}$ g/s, $\langle R_{\rm d} \rangle \approx 1.2 \times 10^{10}$ cm, $M_1 = 1.0\,{\rm M}_\odot$ for: (A) $Y = 1.0$, (B) $Y = 0.98$ $Z = 0.02$, and (C) solar composition disc.

in Table 2.2. For given parameters $\beta_c \sim 3$ in a helium disc while for solar composition disc: $\beta_c \sim 1.4$. Therefore, to have A_n of the same order in both cases β_c has to be increased in the solar case and the only way to obtain this is to change α between the hot and cold states of the disc. In general β_c in helium discs decreases with the increasing metallicity (see Sect.2.7.1) what decreases the amplitude of the outbursts.

Despite that the outburst amplitudes in pure helium discs with constant α resemble the dwarf nova outbursts, α still has to have two different values for hot and cold helium-dominated disc because:

- the observed A_n in AM CVn stars are much higher than 2 mag (up to 5 mag) and without changing α such amplitudes can not be attained even for purely helium discs
- the observations show that discs in AM CVn stars are definitely not pure helium (Sect.4.3), therefore the maximum outburst amplitude for constant α would be even lower than 2 mag.

Besides the amplitude β_c influences also the recurrence times of the outbursts. A β_c higher in pure helium than in hydrogen-dominated disc prolongates quiescence and so the outbursts are less frequent.

From our results it also follows that we can not say anything new about α from the differences in AM CVns and DN light curves, because the chemical composition of the discs has an important impact on their characteristics.

However, the conclustion of Sect.2.7.1 should have their reflection in the modeled light curves:

1. The increase of Z in the He-dominated disc has the same effect as decrease of the ratio α_h/α_c- it decreases the outburst amplitudes and recurrence times. This effect is presented in Fig.2.21: blue line is the model of the purely helium disc, green line is He-rich disc with $Z = 0.02$ and red line is for model with $Y = 0.96$ $Z = 0.04$. All three models are calculated for $\alpha_c = 0.05$, $\alpha_h = 0.1$, $\dot{M}_{tr} = 0.1 \times 10^{16}$ g/s , $M_1 = 1.0\,M_\odot$ and $\langle R_d \rangle \approx 1.2 \times 10^{10}$ cm.
2. In order to obtain similar shapes of the light curves for H-rich and He-rich discs (with the same model parameters) one should take higher values of α_h and α_c for He-rich disc what is shown in Fig.2.22.The diagrams A and C show similar shape of the light curves for solar composition disc with $\alpha_h = 0.1$, $\alpha_c = 0.05$ and He-rich disc with $Z = 0.04$ with $\alpha_c = 0.4$, $\alpha_h = 0.9$, the amplitudes differ by about ~ 0.5 mag. However, the time scales are completely different so the idea that α could be estimated from the shape of the light curves of two systems having similar parameters and known chemical composition of the disc would not work.

2.7.3.1 Reflares

Since the cooling front and inside-out front propagate against the surface density gradient they both can be stopped before arriving to the either of two disc edges. This is especially probable when the disc has accumulated a lot of mass during the quiescence and during the rise to an outburst (this is the situation when $\dot{M}_{tr}$ is high and α_c low, it can be also the case in the large discs) and/or when the hot state viscosity is not efficient enough to shuffle this mass excess to the inner region where it can be accreted (when α_h is relatively low).

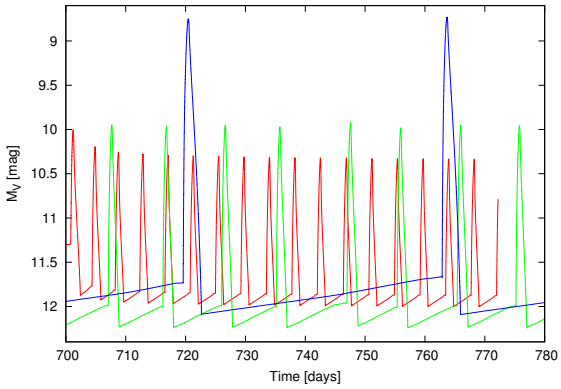

Figure 2.21: The light curves calculated for 3 different amounts of metals in He-dominated disc: $Z = 0.0$ (blue line), $Z = 0.02$ (green line) and $Z = 0.04$ (red line). The models parametes are: $\alpha_{\rm c} = 0.05$, $\alpha_{\rm h} = 0.1$, $\dot{M}_{\rm tr} = 0.1 \times 10^{16}$ g/s, $M_1 = 1.0\,{\rm M}_\odot$ and $\langle R_{\rm d} \rangle \approx 1.2 \times 10^{10}$ cm.

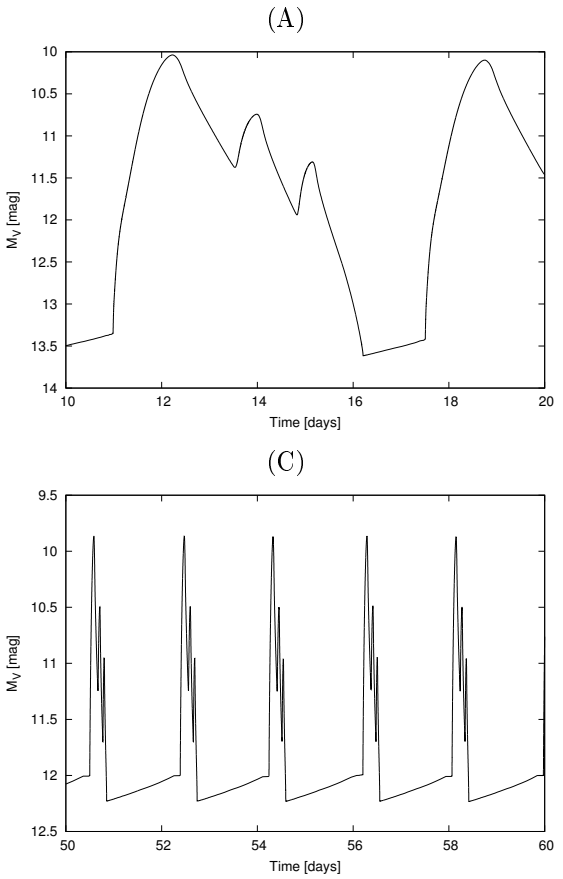

Figure 2.22: The light curves for the models with $\dot{M}_{\rm tr} = 0.1 \times 10^{16}$ g/s, $M_1 = 1.0\,{\rm M}_\odot$ and $\langle R_{\rm d} \rangle \approx 1.2 \times 10^{10}$ cm: (A) solar composition disc with $\alpha_{\rm h} = 0.1$, $\alpha_{\rm c} = 0.05$, (B) disc with $Y = 0.96$ $Z = 0.04$ with $\alpha_{\rm h} = 0.1$, $\alpha_{\rm c} = 0.05$, (C) disc with $Y = 0.96$ $Z = 0.04$ with $\alpha_{\rm h} = 0.9$, $\alpha_{\rm c} = 0.4$.

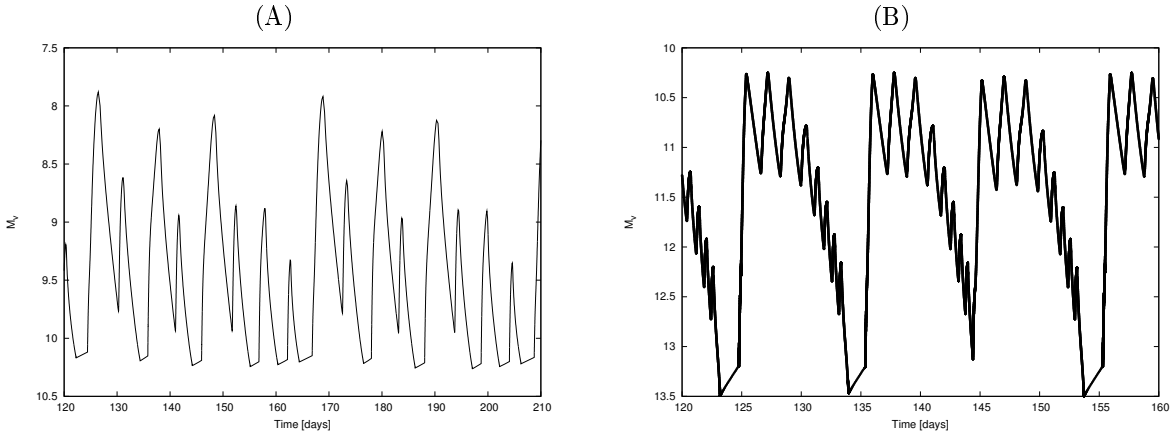

Figure 2.23: The examples of reflares present in the light curves calculated for: (A) $\alpha_{\rm h} = 0.1$, $\alpha_{\rm c} = 0.05$, $\dot{M}_{\rm tr} = 1.0 \times 10^{16}$ g/s, $M_1 = 1.3\,{\rm M}_\odot$, $\langle R_{\rm d} \rangle \approx 3.0 \times 10^{10}$ cm, disc with $Y = 0.98$ $Z = 0.02$; (B) $\alpha_{\rm h} = 0.1$, $\alpha_{\rm c} = 0.05$, $\dot{M}_{\rm tr} = 0.1 \times 10^{16}$ g/s, $M_1 = 1.3\,{\rm M}_\odot$, $\langle R_{\rm d} \rangle \approx 0.7 \times 10^{10}$ cm, solar composition disc.

The mass outflow present during the cooling front propagation leads to the increased Σ in the cold region behind the front. In Menou et al. (1999) the authors show that the $\Sigma(R)$ profile is self-similar when the cooling front propagates in the almost constant velocity in the asymptotic regime. Hence, as the cooling front moves to the lower radii at some point the post-front Σ may become high enough to cross $\Sigma^-_{\rm crit}$. In this situation the new heating front arises and starts to move outwards. The matter heated by this newly formed front flows at the high rate into the zone of the cooling front, rising its temperature and surface density. This inflow of the hot gas eventually "kills" the cooling front and only a heating front is left. It looks like the cooling front had been reflected before it arrived to the inner edge.

A similar mechanism explains the reflections of the inside-out heating fronts. If the post-front Σ remains close to $\Sigma^+_{\rm crit}$ the elevated accretion rate in the hot region behind the propagating inside-out front may cause that at certain radius $\Sigma < \Sigma^+_{\rm crit}$ and the cooling front will start to form. The reduced transport of the angular momentum through the emerging cold zone finally stops the propagation of the heating front and the newly formed cooling front will diffuse inwards.

The examples of manifestation of the cooling and heating front reflections in the light curves are presented in Fig.2.23 for helium-dominated disc (A) and solar composition disc (B) (the reflares are also present in the light curves in Fig.2.20B, and Fig.2.20A and C). The reflares show up as the low-amplitude light variations of short duration and recurrence times superimposed on the "main" outburst-decay which gradually fade. This gradual decrease of the reflares magnitude comes from the consecutive reflections of heating and cooling fronts at smaller and smaller radii in the disc in course the disc losses its mass.

As it was mentioned the $\Sigma(R)$ profile in the case of cooling front is self-similar in the asymptotic regime of $v_{\rm front}$. In this case the post-front surface density $\Sigma(R_{\rm p-f})$ is comparable to $K\Sigma^+_{\rm crit}(R_{\rm p-f})$, where K is the self-similarity constant which depends on the primary mass and both parameters α

(Menou et al. (1999)). The reflares will occur whenever the condition $K\Sigma^{+}_{\rm crit}(R_{\rm p-f}) > \Sigma^{-}_{\rm crit}(R_{\rm p-f})$ is fulfilled. It is less likely that the reflection of a cooling front will appear when M_1 is smaller because according to Menou et al. (1999) K decreases with M_1.

Because of the decrease of $\beta_{\rm c}$ with higher Z, the higher the metal content in the He-dominated disc the more prone this disc is to reflares. Also reflares are more probable to appear in a solar composition disc than in a He-rich disc when they both have similar system parameters.

These considerations about the reflares may give a hint on what causes the observed "sawtooth" shape of the light curve of some dwarf novae, for example V794 Aql (see e.g. Honeycutt and Robertson (1998)) - the reason may be that the disc is overabundant in metals comparing to the solar composition disc.

Chapter 3

Numerical tools

The code used for the numerical studies of dwarf nova behavior is based on the method of Eggleton Eggleton (1971) which was originally used for calculations of stellar evolution. This method is a version of the Henyey method to which the adaptive grid is applied.

3.1 The Henyey method

There are two types of numerical methods for approximating the time derivatives: the implicit and the explicit scheme. Lets consider the time interval $[t_n, t_{n+1}]$ and assume that the variables x_n at time t_n are known while the variables in the next time step t_{n+1}, x_{n+1}, are to be calculated. If the time derivatives depend only on variables x_n the method is *explicit*. If in turn the time derivatives depend both on variables x_n and x_{n+1} the method is *implicit* - the time derivatives are evaluated simultaneously to the variables x_{n+1} on which they depend. The advantage of the implicit scheme is that it converges for larger time steps for the given spacing of the mesh points. In the explicit method the Courant–Friedrichs–Lewy condition has to be fulfilled to ensure the convergence of the numerical solution. According to this condition the time step Δt has to be smaller than $\Delta x/c_{\rm s}$, where Δx is the smallest space interval between two neighboring mesh points and $c_{\rm s}$ is the speed of sound. In our case, in which we have to deal with steep spatial gradients of Σ and $T_{\rm c}$ the explicit method would require very small Δt to be numerical stable and would be very time-consuming.

The Henyey method is an implicit iterative procedure. In this method the initial solution in the sequential time moment $t_{\rm n+1}$ is "guessed". Then in each iteration the corrections to all variables at all points of the mesh are calculated. The new solution is improved during each consecutive iteration until it reaches the desired degree of accuracy. But before solving the equations one has to define the distribution of the mesh points on which the solutions will be calculated.

The spacing of the mesh points has to be such that any physical quantity within each interval should change rapidly - no important information about changes of the physical conditions in the system should be lost . To achieve that lets define $f^{(i)}$ as the i-th function which varies slowly from

point to point, x^i as the i-th variable and k as the label of the mesh points ($k = 1, 2, ..N$). The mesh intervals should minimize the expression:

$$\sum_{k=2}^{N}\sum_{i=1}^{I}(f_k^{(i)} - f_{k-1}^{(i)})^2 \tag{3.1}$$

where I is the number of equations to solve.

Following Eggleton (1971) we replace the variable R by the parameter q which runs from 0 to 1 through the disc ($q = 0$ at $R = R_{\rm in}$ and $q = 1$ at $R = R_{\rm d}$) with equal increments between the mesh points. If in the Eq.(3.1) the sum is approximated by the integral the problem reduces to finding the extremum of the functional

$$\delta \int_0^R \sum_{i=1}^{I} \left(\frac{df^{(i)}}{dR}\right)^2 \frac{dR}{dq}\, dq = 0. \tag{3.2}$$

If only $f^{(i)}$ are known functions of R the solution consists of the pair of differential equations

$$\frac{dq}{dR} = \Phi \cdot W(x^1, x^2, ..,), \tag{3.3}$$

$$\frac{d\Phi}{dR} = 0 \tag{3.4}$$

where

$$W(x^1, x^2, ..,) = \left[\sum_{i=1}^{I} \left(\frac{df^{(i)}}{dR}\right)^2\right]^{1/2} \tag{3.5}$$

The boundary conditions are given by $q = 0$ and $q = 1$. The function $W(x^1, x^2, ...)$ becomes small when the space derivatives of $f^{(i)}$ become large. Φ is the normalization constant and its role is to adjust the grid to the range covered by R (Eq.(3.4)).

The above prescription gives the mesh which adjusts its intervals to the function $f^{(i)}$ which changes the most rapidly in a given region of the disc. If for example in the certain region of the disc the most rapidly changes temperature $T_{\rm c}$ then the mesh will be distributed so that the changes of $T_{\rm c}$ within each mesh interval were not too large.

As soon as the mesh is defined the differential equations can be solved with the procedure proposed by Henyey and which general form is presented below.

At the beginning the set of first-order differential equations, of the general form

$$\frac{dx^i}{dR} = f^i(x^1, ..., x^I) \qquad (i = 1, .., I), \tag{3.6}$$

has to be discretized on the given mesh what means that they have to be replaced by difference form for finite radius interval $[R_{\rm k}, R_{\rm k+1}]$. $x^i_{\rm k}$ and $x^i_{\rm k+1}$ are the variables at the both ends of the interval. If one defines the functions

$$A_k^i := \frac{x_k^i - x_{k+1}^i}{R_k - R_{k+1}} - f^{(i)}(x_{k+1/2}^1, ..., x_{k+1/2}^I), \tag{3.7}$$

where functions $f^{(i)}$ are taken for some arguments $x_{k+1/2}^i$ of value between x_{k}^i and $x_{\mathrm{k+1}}^i$, then the differential equations (3.6) take the from

$$A_j^i = 0 \text{ for } [R_k, R_{k+1}]. \tag{3.8}$$

The first approximation of the solution of Eq.(3.8) has to be "guessed" for example by extrapolation of the foregoing solution (i.e. calculated at $t_{\mathrm{n-1}}$) and we denoted it by $(x_k^i)_1$. Substitution of $(x_k^i)_1$ into Eq.(3.8) gives $A_i^j(1) \neq 0$ where "1" stands for $(x_k^i)_1$. Next one has to search for the corrections δx_k^i to $(x_k^i)_1$ (the corrections for all variables on all mesh points) to obtain the second approximation $(x_k^i)_2 = (x_k^i)_1 + \delta x_k^i$ for which A_k^i vanishes $A_k^i(2) = 0$ (i.e. $A_k^i(1) + \delta A_k^i = 0$). If $A_k^i(2) \neq 0$ again the next approximation has to be found with the new correction: $(x_k^i)_3 = (x_k^i)_2 + (\delta x_k^i)_1$ and substituted to Eq.(3.8) to check if $A_k^i(3) = 0$. If not the procedure repeats. Usually A_k^i does not equals exactly zero and one has to set the accuracy ϵ within which A_k^i should be approach zero with the reasonable number of iterations. Thus the iterations will be repeated until $A_k^i < \epsilon$.

The corrections δx_k^i are found using Newton-Raphson method. It is the fast converging method to find the roots of the real-valued function , however, it may diverge if the "guessed" solution is too far from the real one.

In this method the function $A_k^i(1)$ is first approximated by its tangential $A_k^{'i}(1)$

$$A_k^{'i}(1) = \frac{A_k^i(1) - 0}{(x_k^i)_1 - (x_k^i)_2}, \tag{3.9}$$

and then one calculates the point in which this tangential intersects with x axes

$$(x_k^i)_2 = (x_k^i)_1 - \frac{A_k^i(1)}{A_k^{'i}(1)}. \tag{3.10}$$

$(x_k^i)_2$ is the next approximation of the solution and it lies closer to the function root. One proceeds with iterations until the desired accuracy is achieved. After $n+1$ iterations the form of the solution is

$$(x_k^i)_{n+1} = (x_k^i)_n - \frac{A_k^i(n)}{A_k^{'i}(n)}. \tag{3.11}$$

Once the roots of A_k^i are found one can calculate the functions f^i at the given time t_{n}. Those function become the initial guess for the solutions of Eq.(3.7) in the next time step $t_n + \Delta t$ and the whole procedure repeats from the beginning.

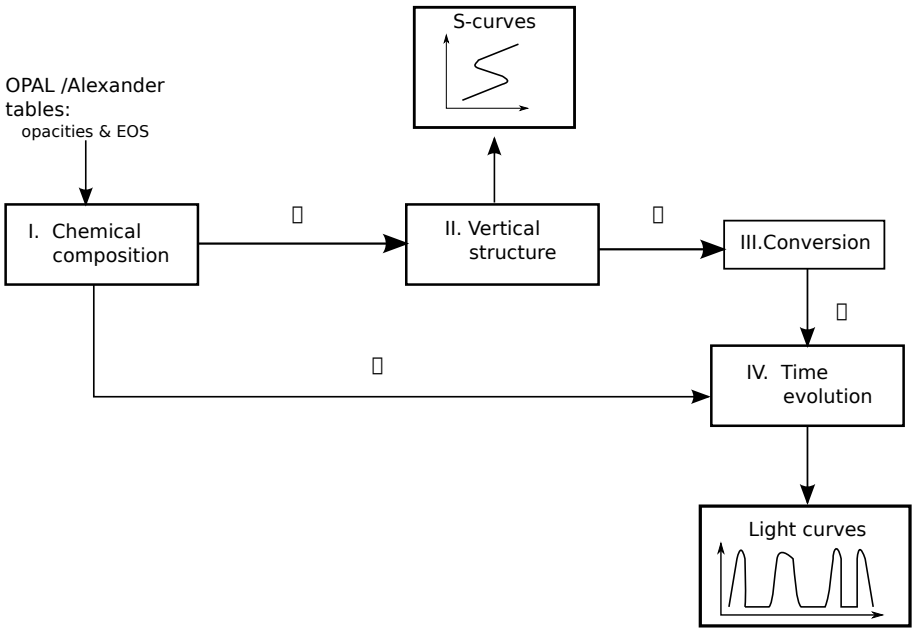

Figure 3.1: The numerical procedure of calculating the light curves described in following subsections.

3.2 The code

The code we use has been written by Jean-Marie Hameury, Guillaume Dubus and Kristen Menou in Fortran77 with some elements of Fortran95 introduced. The use of adaptive grid allows very high resolution of the transition fronts which propagate in the disc what makes this code unique among all others used for dwarf nova outbursts calculations.

The calculation of the light curves proceeds in two stages: (i) first one has to solve the vertical structure equations to obtain all possible values of Q^+ and $T_{\rm eff}$ for given Σ and $T_{\rm c}$ in the given R; (ii) the second stage considers the calculations of the solutions for the disc time evolution equations. These solutions are found in the cube of solutions $(R, \alpha_{\rm eff}, T_{\rm eff})$ produced in the first stage.

3.3 Stage I - the vertical structure code

3.3.1 Chemical composition

To start with the calculations of the disc vertical structure first one has choose the chemical composition of the disc and calculate corresponding tables of opacities and thermodynamical quantities.

The mean Rosseland opacities for temperatures $\log T = 4.0 - 8.7$ K are taken from OPAL tables (Iglesias and Rogers, 1996) and for lower temperatures ($\log T < 4.0$ K) from Alexander tables (Alexander and Ferguson, 1994).

The thermodynamical quantities such as total pressure, adiabatic gradient and $(d\log T/d\log\rho)_P$,

are calculated in two temperatures regimes: for higher temperature the equation of state is interpolated from OPAL tables and for lower temperatures the Saha equations are solved following Paczyński (1969).

The chemical composition is defined by the hydrogen mass fraction X, helium mass fraction Y and metals mass fraction Z. We use the tables where the metals relative distribution is set to be solar (Grevesse and Noels, 1993).

To calculate the thermodynamical quantities characterizing the given chemical composition of the disc one has only to set desired X and Z in the code which produces the data table consisting if total pressure, adiabatic gradient and $(d\log T/d\log\rho)_P$. This table is then used as the input data file in calculations of the vertical disc structure and the disc time evolution. The quantities in the table are calculated for 70 values of temperature T from $\log T = 3.75\,\mathrm{K}$ to $\log T = 8.7\,\mathrm{K}$ and 19 values of parameter $R \equiv \rho/T_6^3$ (where $T_6 = T * 10^{-6}$ K) which lies in the range $\log R = -8.0 - 1.0$ g cm^{-3}K^{-3}.

3.3.2 Vertical structure cube

Once the chemical composition of the disc is determined the vertical structure equations can be solved.

At the beginning one has to fix the mass of the primary M_1, the number of mesh points N, the accuracy of the solution ϵ and the maximum number of iterations $i_{\max}$ within which this accuracy should be achieved, the ranges of R, Σ and $T_{\rm c}$and the number of equidistant values taken in each range for which the solutions will be found.

If one considers the irradiation of the disc by the primary white dwarf then one has to recalculate the vertical disc structure every time one changes the mass of the primary M_1 because it affects the irradiation temperature defined by Eq.(4.9) what modifies the solutions. When no irradiation is taken into account M_1 enters into calculations of the vertical structure only via Keplerian velocity.

For investigations of DN and AM CVn stars we typically set 50 values of R from the range $\log R = 8.5 - 11$ cm, 50 values of Σ running from $\Sigma_1 = 0.001$ g/cm^2 to $\Sigma_{50} = 1000$ g/cm^{2}and 100 values of $T_{\rm c}$ from 10^3 K to 10^6 K . This parameter space is sufficient for the range of values found in evolution calculations. We also adopt $N = 101$, $\epsilon = 0.01$ and $i_{\max} = 500$.

The routine starts with the choice of the lowest value from the R-range and fixing it as the radius R_1. Then for R_1 the lowest value from $T_{\rm c}$ range is taken. For fixed R_1 and $T_{\rm c,1}$ the vertical structure equations are solved for each value from the Σ-range. When solutions for all values of Σ are found the next value $T_{\rm c,2}$ is taken (with the same R_1) and the calculation are made for each Σ again. When solutions for all values of $T_{\rm c}$ and Σ in R_1 are found the radius changes to R_2 and the whole procedure repeats. Thus the result is the $50 \times 50 \times 100$ cube of $(T_{\rm eff}, \alpha_{\rm eff})$ points.

In the case of the vertical code the grid is defined as Hameury et al. (1998)

$$W = \frac{4}{H^2} + \left(\frac{1}{\Sigma}\frac{d\varsigma}{dz}\right)^2 + \left(\frac{d\ln P}{dz}\right)^2 (1 + 2\nabla^2) \tag{3.12}$$

where $H = (\Re T_{\rm c}/\Omega_{\rm K}^2)^{1/2}$ is the scale height of the disc.

If the temperature gradient ∇ is radiative one calculates from expression (see Sect.2.2 Eq.(2.17))

$$\nabla = \nabla_{\rm rad} = \frac{\kappa_{\rm R} P_{\rm tot} F_{\rm z}}{4 P_{\rm rad} c g_{\rm z}} \tag{3.13}$$

where c is a speed of light, $g_{\rm z}$ is the vertical component of gravity.

To find $\nabla_{\rm conv}$ one has to follow the derivation given in Kippenhahn and Weigert (1990) and then calculated it in the mixing length approximation following Paczyński (1969).

The set of equations which has to be solved in order to find $\nabla_{\rm conv}$ (see Sect.2.2) is

$$F_{\rm conv} = c_{\rm P} \rho T_{\rm c} {\rm v}_{\rm ml} \frac{\ell_{\rm ml}}{H} (\nabla_{\rm conv} - \nabla'), \tag{3.14}$$

$${\rm v}_{\rm ml}^2 = -\frac{g_{\rm z} \ell_{\rm ml}^2}{8H} \left(\frac{\partial \ln \rho}{\partial \ln T} \right)_{\rm P} (\nabla_{\rm conv} - \nabla'), \tag{3.15}$$

$$\frac{\nabla_{\rm conv} - \nabla'}{\nabla' - \nabla_{\rm ad}} = \gamma_0 {\rm v}_{\rm ml}, \tag{3.16}$$

where

$$\gamma_0 = \frac{c_{\rm P} \rho}{8 \sigma T_{\rm c}^3} \frac{1 + \frac{1}{3} (\kappa_{\rm R} \rho \ell_{\rm ml})^2}{\kappa_{\rm R} \rho \ell_{\rm ml}}. \tag{3.17}$$

The expression $\kappa_{\rm R} \rho \ell_{\rm ml}$ stands for the optical depth of convective eddies: $\tau_{\rm ml} = \kappa_{\rm R} \rho \ell_{\rm ml}$.

The Eq.(3.14)-(3.16) can be reduced to one cubic equation if one introduces the parameters

$$C = \frac{g_{\rm z} \ell_{\rm ml}^2}{8H} \left(\frac{\partial \ln \rho}{\partial \ln T} \right)_{\rm P}, \qquad V = \frac{1}{\gamma_0 \sqrt{C(\nabla_{\rm rad} - \nabla_{\rm ad})}}, \qquad A = \frac{9}{8} \frac{\tau_{\rm ml}^2}{3 + \tau_{\rm ml}^2}, \tag{3.18}$$

and the variable

$$y = {\rm v}_{\rm ml} V \gamma_0. \tag{3.19}$$

The final equation to solve to is

$$2Ay^3 + Ay^2 + V^2 y - V = 0. \tag{3.20}$$

It turns out that there is only one real root of the Eq.(3.20) which can be found with the iterative method and which gives the sought $\nabla_{\rm conv}$

$$\nabla = \nabla_{\rm conv} = \nabla_{\rm ad} + (\nabla_{\rm rad} - \nabla_{\rm ad}) y (y + A). \tag{3.21}$$

The mixing length $\ell_{\rm ml}$ is proportional to the pressure scale height H where the proportionality constant is marked with $\alpha_{\rm ml}$ in the literature, but it should not be confused with $\alpha_{\rm h}$, $\alpha_{\rm c}$ or $\alpha_{\rm eff}$. For the calculations of the stellar models the value of $\alpha_{\rm ml}$ is usually assumed to range from 1.0 to 2.2 depending on the star effective temperature and surface gravity. For the Sun it is found to be $\alpha_{\odot{\rm ml}} = 1.76 \pm 0.08$ (Trampedach and Stein, 2011). Here we take $\alpha_{\rm ml} = 1.5$ following Hameury et al.

(1998).

To determine the vertical disc structure one has to solve 7 differential equations (2.12), (2.13), (2.14), (2.23), (3.3), (3.4), (3.24) which can be written in the general form

$$\frac{dF_i(x^j)}{dq} = G_i(x^j) \quad (i = 1, .., 7) \tag{3.22}$$

The variables x^j for which the equations are to be solved are: $T_{\rm c}$,ρ, z, F_z,ς ,$\alpha_{\rm eff}$, and Φ.

The general form of the discretized equations (3.22) is

$$F_i(x_k^j) - F_i(x_{k-1}^j) - \delta q\,[\beta_i\, G(x_k^j) + (1-\beta_i)\, G(x_{k-1}^j)] = 0, \tag{3.23}$$

where $\delta q = 1/(N-1)$ is the mesh spacing, x_k^j is the value of the quantity x^j at the grid point k, and $\beta_i \in [0,1]$ are weights. We assume $\beta_i = 0.5$ what leads to the second-order scheme for solving the equations.

The solutions of the set of equations of the form of Eq.(3.23) give all possible values of $T_{\rm eff}$ and $\alpha_{\rm eff}$ for radius R in thermal equilibrium for given ranges of $T_{\rm c}$ and Σ, where $\alpha_{\rm eff}$ is the parameter described in Sect.2.2. It is the condition for $\alpha_{\rm eff}$:

$$\frac{d\alpha_{\rm eff}}{dz} = 0 \tag{3.24}$$

which stands for the 7th equation defining the disc vertical structure.

To sum up - the output of the vertical structure code is a cube $100 \times 50 \times 50$ of all possible values of $T_{\rm eff}$ and $\alpha_{\rm eff}$ in each R for assumed ranges of $T_{\rm c}$ and Σ.

Before this table is incorporated into the evolution code it is first converted into the binary format and the solutions are redefined from $(\alpha_{\rm eff}, T_{\rm eff})$ into $(\sigma T_{\rm eff}^4/\alpha_{\rm eff}, T_{\rm eff})$.

3.4 Stage II - time evolution code

The initial parameters in this part of the code are: the number of grid points N, the primary mass M_1, parameters $\alpha_{\rm h}$ and $\alpha_{\rm c}$, the mass transfer rate from the secondary $\dot{M}_{\rm tr}$, the inner disc radius $R_{\rm in}$, the circularization radius $R_{\rm circ}$, and the parameter c from Eq.(2.33) which, together with $R_{\rm circ}$, determines the mean disc radius $\langle R_{\rm d}\rangle$.

As it was mentioned above the solutions of the vertical structure are calculated for thermal equilibrium with some effective viscosity parametrized by $\alpha_{\rm eff}$

$$\frac{3}{2}\alpha_{\rm eff}\Omega_{\rm K}^2 P = \sigma T_{\rm eff}^4. \tag{3.25}$$

$\alpha_{\rm eff}$ is the measure of the disc departure from the thermal equilibrium defined by $\alpha_{\rm TE}$ (given by Eq.(2.60)) in course of its time evolution (in the hot disc $\alpha_{\rm TE} = \alpha_{\rm h}$ and in the cold disc $\alpha_{\rm TE} = \alpha_{\rm c}$). $\alpha_{\rm eff}$ includes the contribution of the non-equilibrium terms (we denote them as "NE") of thermal

equation (see. Sect.2.3 and Hameury et al. (1998))

$$\alpha_{\rm eff} = \alpha_{\rm TE} + \frac{NE}{3/2\,\Omega_{\rm K}^2 P} \tag{3.26}$$

We define $Q^+_{\rm eff}$ as

$$Q^+_{\rm eff} = \frac{\sigma T^4_{\rm eff}}{\alpha_{\rm eff}}. \tag{3.27}$$

which is the solution of the vertical structure code.

In the evolution code the viscous heating term in each radius is evaluated as $Q^+ = Q^+_{\rm eff}\alpha_{\rm TE}$ (the cooling term is as always $Q^- = \sigma T^4_{\rm eff}$). If $\alpha_{\rm TE} < \alpha_{\rm eff}$ then $Q^+ < Q^-$ and the disc in the given R cools down, if $\alpha_{\rm TE} > \alpha_{\rm eff}$ the opposite happens: the heating dominates over cooling, and when $\alpha_{\rm TE} = \alpha_{\rm eff}$ the given disc radius is in a thermal equilibrium.

The grid for time evolution equations is defined as

$$W = 1 + c_1\left[\frac{\partial \ln(\nu\Sigma\sqrt{R})}{\partial \ln R}\right]^2 + c_2\left[\frac{\partial \ln T_{\rm c}}{\partial \ln R}\right]^2 \tag{3.28}$$

where constants c_1 and c_2 determine the relative importance of the two variables $(\nu\Sigma\sqrt{R})$ and $T_{\rm c}$. $(\nu\Sigma\sqrt{R})$ is the variable which describes the distribution of radial velocity of matter in the disc (see Eq.(2.57)). Setting c_1 and c_2 one decides how much mesh should be devoted to the region of the disc where the radial gradient of $(\nu\Sigma\sqrt{R})$ is steeper than the radial gradient of $T_{\rm c}$ and how much of the mesh should be devoted to the disc region where the opposite situation has place. Typically in the calculations we use the value of c_1 from the range $[0.001 - 0.1]$ and the value of c_2 lying between 0.01 and 0.2.

In the time evolution code there are 6 differential equations to solve (2.26), (2.32), (2.37), (2.39), (3.3), (3.4) where variables are R, Φ, $T_{\rm c}$, Σ, $\partial(\nu\Sigma\sqrt{R})/\partial R$ and $\partial T_{\rm c}/\partial R$.

The first thing to do before running the code is to set the initial parameters and find the solutions for these new parameters. The calculations should start with the solutions for a stable disc (hot or cold) with arbitrary Σ distribution and for very large time step ($\Delta t = 10^{12}$ s). Such initial guess usually allows the code to converge to the solutions for the stable disc with the new parameters. However, one has to be careful not to change the initial parameters too drastically and not to change all of them at once - it may cause that the guessed solution will be too far from the real solutions and the code will diverge.

If the new parameters are sufficiently close to the previous ones and the code converges then the results are used as the initial state for the calculations of the disc evolution for the same parameters but with smaller time step (typically $\Delta t = 10^4$ s).

Usually it is sufficient to set the resolution of the grid to 400 points. As it is shown in Hameury et al. (1998), this is a border number of points in the grid: for $N \geq 400$ the grid does not affect the outbursts appearance. However, if the fronts become particularly narrow this number has to be enlarged and usually 800 points is sufficient for our purposes. At the same time the constants c_1 and

c_2 (Eq.(3.28)) have to be increased in order that more points of the mesh were intended for resolving the propagating front. In some cases the solutions are easier to find when the time step is smaller, for example $\Delta t = 10^2$ s.

We have encountered two main problems while running the code. First is the lack of convergence that appears when one sets the initial parameters such that the code tries to find the solutions which are out of the input data cube from the vertical part. The second is a not sufficient number of grid points to resolve the fronts, especially the heating ones. This is either because the grid is too sparse, or because there are too few points from grid devoted to the front (c_1 or c_2 in Eq. (3.28)). The latter is particularly important when the front arrives at the inner disc edge and it is the most frequent reason why the evolution code crashes during calculations.

Chapter 4

AM CVn stars

4.1 Introduction

The first to suggest that the star called HZ 29 may be a peculiar helium binary star with short orbital period of ~ 18 min was Smak (1967). Nowadays this star is known as AM CVn and it gave the name for the whole group of the very close binaries which do not show any hydrogen lines in their spectra.

Because these binaries are rather faint ($\sim 14 - 20$ mag) their observed number has been growing very slowly until recently. The biggest contribution to the observational knowledge about AM CVn have two surveys: the Sloan Digital Sky Survey (SDSS) which has been operating since year 2000 and till now has discovered 14 AM CVn systems; and the Palomar Transient Factory (PTF) which first light was achieved 13 Dec 2008 and since then it has delivered the light curves of unprecedent quality of 8 new AM CVn systems. The important thing about PTF is that it is able to detect the objects down to ~ 23 mag. Therefore, the future of the AM CVn stars observations seems to be very promising.

At this moment there are 36 systems classified as AM CVn stars. The outbursts are detected in the light curves of 20 systems, only 6 are permanently bright and 9 are permanently faint. The state of the remaining 1 (SDSSJ1525) is not clear yet (P.Groot, 3rd workshop on AM CVn stars). Their orbital periods are extremely short ranging from 5.4 min for HM Cnc to 65.1 min for V396 Hya. The periods of 10 systems have not been determined yet.

The primary is a He/CO white dwarf (Bildsten et al., 2006) while the secondary is the most probably also a He white dwarf.

4.2 Observational light curves characteristics

AM CVn stars are observed in three distinct luminosity states. The state when they are persistently bright and the outbursting state resemble the states observed in DN. The third state during which their brightness is persistently in the low level has no a

nalog among CVs.

All high state AM CVn stars have orbital periods below 20 min . HM Cnc and V407 Vul which orbital periods are even below 10 min are probably the direct impact systems (Roelofs et al., 2010).

Based on the available database of AM CVn light curves one can conclude that all these systems show outbursts of amplitudes in the range from 3.5 to 6 mag with recurrence times from ~ 14.7 to ~ 450 d but this latter parameter has been determined only for 5 systems (with orbital periods between 24.5 and 28.3 min) for which more than one outburst cycle has been observed. The determination of the outburst recurrence times is hampered by the selection effect - some short outbursts may be missed in observations. One should also stress that significant variation of the large outbursts (i.e. the superoutbursts, see below) recurrence time has been observed in CR Boo: from 46.3 to 14.7 d (Kato et al., 2001) and in KL Dra: from ~ 65 to ~ 44 d (Ramsay et al., 2012). The change of the supercycles (the periods of time between two consecutive superoutbursts, see below) duration is also observed in ER UMa-type dwarf novae: V1159 Ori (Kato, 2001) and DI UMa (Rutkowski et al., 2009).

One can classify these outbursts as *superoutbursts* because they resemble the superoutbursts observed in SU UM-type dwarf novae (Warner, 1995). The most important similarity is the presence of the superhumps - the low-amplitude ($[1] \lesssim 0.3$ mag) light variations with period a few percents longer (positive superhumps) or shorter (negative superhumps) than the orbital period of the binary. The superoutbursts in AM CVn stars can be as short as 9 d but they typically last ~ 20 d. In some cases they can be prolongated by a series of frequent ($\sim 1-2$ d period) outbursts of amplitude~ 1 mag: the so called cycling state which may last as long as the "smooth" superoutburst itself Patterson et al. (2000); Kato et al. (2004b). This state is very similar to what is observed in the WZ Sge-type dwarf novae (e.g. Patterson et al. (2002)) or in some of the SU UMa-type DN like EG Cnc Kato et al. (2004a). There is another characteristic feature often present in the light curves of the AM CVn stars - a well pronounced dip which appears suddenly in the middle of the "smooth" superoutburst and which has also its double in the WZ Sge-type binaries. It is not satisfactorily explained if there is a relation between dip and cycling state and, if it is, what is its nature.

It seems that the shortness of orbital period has a decisive impact on the presence of the superoutburst: all SU UMa stars have orbital periods below the period gap ($P_{\rm orb} < 2$ hr) and they all show the superoutbursts intermittent by the normal outbursts, the binaries of WZ Sge-type with $P_{\rm orb}$ close to the minimum orbital period of DN show superoutbursts only and the AM CVns seems to follow this trend[1].

The dip is observed in the light curves of KL Dra ($P_{\rm orb} = 25$ min), SDSS J0926 ($P_{\rm orb} = 28.32$ min), CP Eri ($P_{\rm orb} = 28.35$ min) or PTF1J0719 ($P_{\rm orb} = 26.8$ min). The same feature is found in DN of WZ Sge-type: WZ Sge ($P_{\rm orb} = 82$ min), AL Com ($P_{\rm orb} = 81.6$ min) or V485 Cen ($P_{\rm orb} = 59$ min). It brings into the mind that the dip is connected with the size of the disc.

The narrow eruptions corresponding to those observed in U Gem-type dwarf novae are called *normal outbursts*. They are very common in the light curves of hydrogen-rich binaries but are relatively

[1]However, so far there seems to be one exception to the rule - U Gem itself. In its light curve one large outburst has been observed (Mason et al., 1988) in which the superhumps were later identified what classifies this outburst as superoutburst (Smak and Waagen, 2004).

rare in the helium-dominated outbursting systems. In DN the normal outbursts have the bimodal distribution considering their width: the classification of the narrow ones is quite straightforward but from the observational point of view the distinction between the wide normal outbursts and the superoutbursts may be ambiguous. Therefore, the normal outbursts are defined as the outbursts during which no superhumps are present (however, in some cases during normal outbursts following superoutbursts the superhumps are still detectable).

Another characteristics of the normal outbursts in DN is that they follow the empirical *Kukarkin-Parenago relation* (hereafter K-P relation) connecting the outburst amplitude with its recurrence time. Since this relation should be universal for all outbursts triggered by the same mechanism in the disc it should describe also normal outbursts in AM CVn stars (see Chap.4).

The light curves of AM CVn stars are complex and they avoid simple classification into distinct groups. Thus, we characterize the outbursting AM CVn stars with the specific examples of the systems which light curves are the best covered.

4.2.1 CR Boo and V803 Cen

V803 Cen (discovered in 1975, Elvius (1975)) and CR Boo (discovered in 1986, Wood et al. (1987)) were the first outbursting AM CVn stars for which an extended observational campaigns were conducted.

The long-term light curve of V803 Cen consists of two main different states of outburst activity:

1. The state in which the system shows the bright outbursts of amplitudes $\sim 3.7-4.3$ mag (up to ~ 12.7 mag) and durations $\sim 3-12$ d, and the faint phases during which the system brightness stays near $V = 17.0$ for at least $10-30$ d. The low state is interrupted by short (~ 1 d), faint outbursts (~ 1 mag) which seem to appear every 5 d (Patterson et al., 2000). Because there are detectable superhumps associated with the bright outbursts the latter can be classified as the superoutbursts. Thus the considered state consists of the supercycles which period has been estimated to ~ 77 d (Kato et al., 2000b).

2. The state during which the binary brightness is at intermediate level and varies rapidly between $V = 14.5-13.0$ mag. Patterson et al. (2000) call this "the cycling state" (we will refer to this as the state observed in April 1997).

In June 2000 and in June 2003 the superoutbursts had place after which V803 Cen behaved in a non-standard manner.

After the superoutburst in 2000 the system did not fade to the low state but it stopped at $V = 13.3-14.0$ mag for a long time. The disappearance of the 77-day supercycles suggests that this state may refer to the standstill states observed in Z Cam-type DN. However, the luminosity changes by $0.5-1.0$ mag and with period ~ 20 h present during this state in V803 Cen are not observed in DN standstills.

The superoutburst in 2003 appeared to be yet different from all the previous ones. This time the star after spending 3 days in the brightness maximum suddenly faded by ~ 2.5 mag. This "dip"

System	$P_{\rm orb}$ (min)	M_1 ($M_\odot$)	M_2 ($M_\odot$)	V range (mag)	$\log \dot{M}_{\rm tr}{}^{(*)}$ [g/s]	Ref.
HM Cnc	5.4	0.55	0.27	21.1	?	[1]
V407 Vul	9.5	?	?	19.9	?	[1]
ES Cet	10.3	$0.60-0.69$	$0.062-0.26$	$16.8-16.5$	$17.27^{+0.07}_{-0.19}$	[2], [3]
SDSSJ1908+34	15.8	?	?	16.1	$17.35-17.73$	[4]
AM CVn	17.1	0.71 ± 0.07	0.13 ± 0.01	14.0	$17.65^{+0.12}_{-0.1}$	[5]
HP Lib	18.4	$0.80-0.49$	$0.048-0.088$	$13.6-13.7$	$16.98^{+0.17}_{-0.27}$	[5], [6]
CR Boo	24.5	$1.10-0.67$	$0.044-0.087$	$17.5-13.0$	$16.7^{+0.18}_{-0.32}$	[5]
KL Dra	25	?	?	$17.0-13.8$	?	[7], [8]
V803 Cen	26.6	$1.17-0.78$	$0.059-0.109$	$16.8-12.2$	$16.75^{+0.13}_{-0.19}$	[5], [9]
PTF1J0719+48	26.8	?	?	$19.4-15.9$	?	[10]
SDSSJ0926+36	28.3	0.85 ± 0.04	0.035 ± 0.003	$19.6-16.6$	$15.79^{+0.08}_{-0.1}$	[11], [12]
CP Eri	28.4	?	?	$20.2-16.2$	?	[13]
V406 Hya	33.8	?	?	$19.7-14.5$	?	[14]
SDSSJ0129+38	37.3	?	?	$20.0-14.5$	?	[8], [15]
SDSSJ1240-01	37.4	$0.31-0.79$	$0.012-0.031$	$19.7-13.5$	$14.29^{+0.32}_{-0.32}$	[15], [16], [17]
SDSSJ0804+16	44.5	?	?	$19.0-17.8$?	?	[18]
SDSSJ1411+48	46.0	?	?	$19.7-19.4$	?	[19]
GP Com	46.6	$0.5-0.68$	$0.009-0.012$	$16.3-15.9$	$\leq 14.35^{+0.5\dagger}_{-0.5}$	[5]
SDSSJ0902+38	48.3	?	?	20.2	?	[20]
SDSSJ1208+35	52.6	?	?	$19.4-18.8$	?	[21]
SDSSJ1642+19	54.1	?	?	20.3	?	[20]
SDSSJ1552+32	56.3	?	?	$20.6-20.2$	?	[22]
V396 Hya	65.1	0.77	0.017	17.6	13.33	[17],[23],[24]

Table 4.1: The list of all AM CVn stars for which the orbital periods were determined up to date with the masses of the system components and their apparent brightness. The systems in red are in the persistently high state, in black are outbursting, in blue are persistently faint and in green are supposed to be the direct impact systems, (*) $\dot{M}_{\rm tr}$ is evaluated for the systems with estimated distances,†- upper limit. Ref: [1] Roelofs et al. (2010), [2] Copperwheat et al. (2011a), [3] Espaillat et al. (2005), [4] Fontaine et al. (2011), [5] Roelofs et al. (2007a), [6] Roelofs et al. (2007b), [7] Ramsay et al. (2010), [8] Ramsay et al. (2012), [9] Kato et al. (2000b), [10] Levitan et al. (2011), [11] Deloye et al. (2007), [12] Copperwheat et al. (2011b), [13] Armstrong et al. (2012), [14] Roelofs et al. (2006), [15] Shears et al. (2011), [16] Roelofs et al. (2005), [17] Ramsay et al. (2006), [18] Roelofs et al. (2009a), [19] Anderson et al. (2005), [20] Rau et al. (2010), [21] Anderson et al. (2008), [22] Roelofs et al. (2007c), [23] Thorstensen et al. (2008), [24] Ruiz et al. (2001).

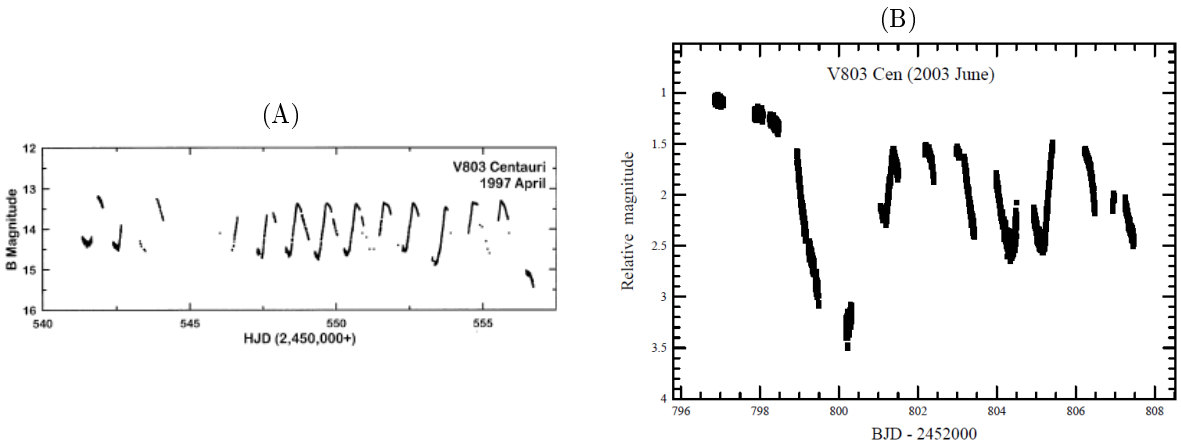

Figure 4.1: (A) The V803 Cen light curve during the standstill state in April 1997 taken from Patterson et al. (2000). (B) The superoutburst of the same system in June 2003 from Kato et al. (2004b).

ended one day later when the system brightened again and entered the state in which the rapid (with period $\sim 0.8 - 1$ d), low-amplitude (~ 1 mag) light variations started. This pattern composed of superoutburst maximum followed by the transient dip in brightness and the long-lasting state of oscillating light is also present in observations of other superoutbursts in V803 Cen and strongly resembles the superoutburst of WZ Sge in 2001. This state differs from the state observed in V803 Cen in April 1997 (in the latter there is no superoutburst-dip-cycling pattern and the superoutburst period is not detectable).

We follow the interpretation of Kato et al. (2004b) and define the *cycling state* as the state of the superoutburst 2003-type (or WZ Sge-type) while the state from April 1997 and after the superoutburst in 2000 we consider as the standstill-like with light variations which are not present in the standstills in dwarf novae.

Elements of the CR Boo light curve are similar to those of V803 Cen. The superoutbursts have maxima around $14.7 - 14.2$ mag and last usually $16 - 26$ d, and the short-lived rebrightenings appear during the periods of the low state (at V $\sim 16.0 - 17.0$ mag) with frequency of ~ 4 d. Usually the superoutbursts appear every 46.3 d, however in 2001 Kato et al. (2001) noticed the significant shortening of the supercycle to 14.7 d. As well as V803 Cen also CR Boo shows the transient dip during its superoutbursts, the periods which may be interpreted as standstills and cycling states. Peculiar for CR Boo is that sometimes the outburst preceding the superoutburst is very bright, even brighter than the superoutburst itself (Kato et al., 2000a).

In both stars the superhumps are detected during the superoutbursts and they are absent in the rebrightenings considered to be normal outbursts. The superhumps appear just at the peak phase of the superoutburst, they are detectable during the rapid decline phase from the superoutburst and possibly they are still present during the cycling state (Kato et al., 2000b).

The fact that the cycling state is observed only right after the occurrence of the superoutburst

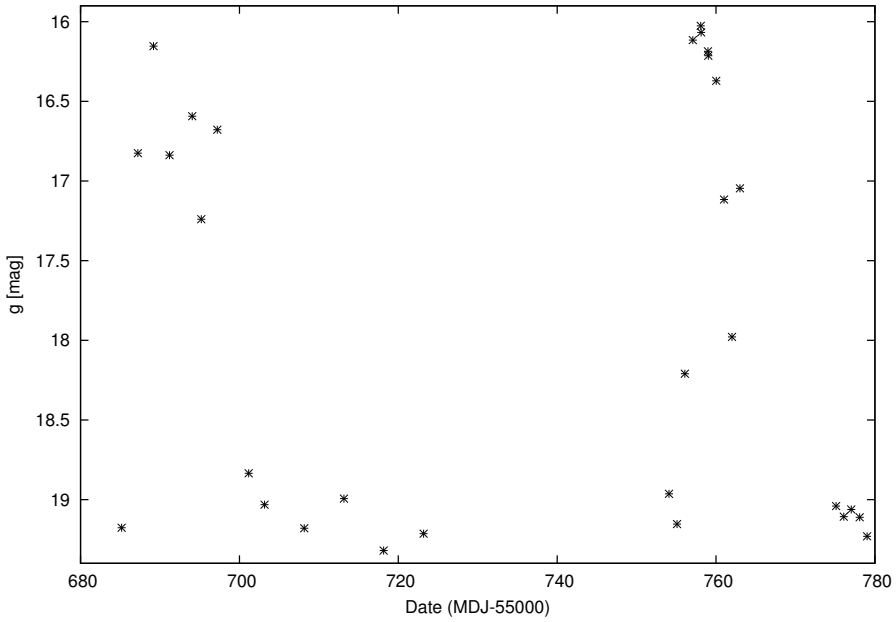

Figure 4.2: The light curve of KL Dra. Courtesy G.Ramsay.

suggests that those phenomena may be coupled.

4.2.2 KL Dra

The light curve of KL Dra consists mainly of superoutbursts of amplitude ~ 3.5 mag and duration ~ 14 d which appear almost regularly every $\sim 60 - 65$ d. At the beginning it seemed that no normal outbursts are present but now it is certain that at least two short eruptions took place. So far no cycling states or standstill has been observed but the ~ 2 mag dip during the better sampled superoutbursts is well pronounced. Very recently it appeared that the supercycle period has changed to 44 d (Ramsay et al., 2010, 2012).

4.2.3 PTF1J0719+4858

The latest published member of AM CVn group is PTF1J0719+4858 (in short PTF1J0719) and its light curve presents the new quality of AM CVn observations.

PTF1J0719 is the most similar to SU UMa among all observed AM CVn stars: both normal and superoutbursts are detected. Between two superoutbursts one observes about three normal outbursts of an amplitude ~ 2.5 d lasting about 1 d and repeating every 10.5 d. The ~ 20 day superoutburst is interrupted by a dip and there is no cycling state or standstill after it. After the system leaves the dip it reenters the slow fading phase and only after ~ 5 d quickly returns to quiescence. The most recent part of the light curve indicates that also in this case the supercycle duration change: initially

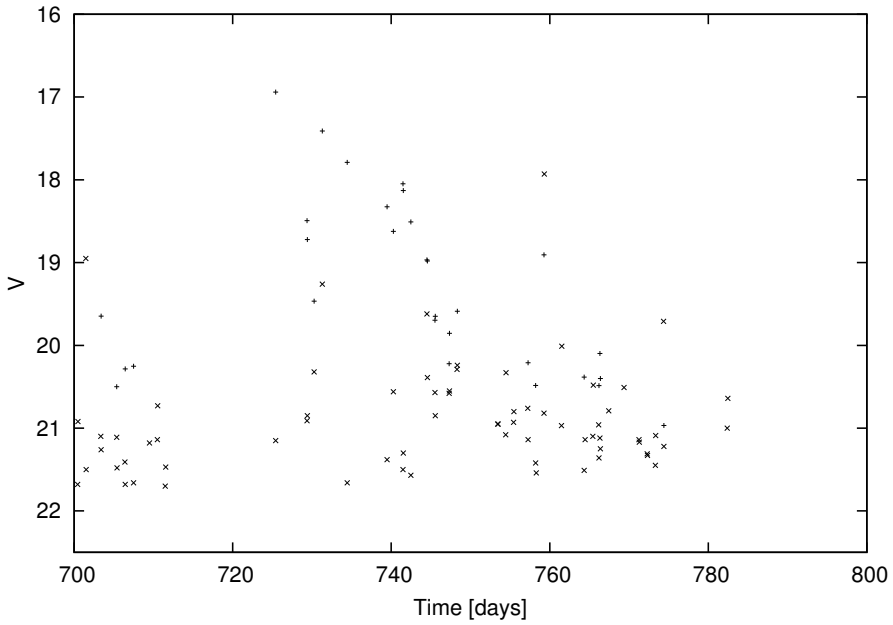

Figure 4.3: The light curve of PTF1J0719. Courtesy D. Levitan.

found to be ~ 65 d the latest one is prolongated to ~ 78 d.

4.2.4 Other outbursting AM CVns with characteristic light curves

1. **SDSS J0926:** During 4.5 year period of observations the system showed 6 outbursts of amplitudes $2 - 2.5$ mag with the average recurrence times $100 - 200$ d. This source is interesting as the only known eclipsing AM CVn star to date. Its inclination is determined to be 82.6 ± 0.3 deg (Copperwheat et al., 2011b). There is a characteristic feature in the observed eclipse profile: the small additional dimming at the egress. The width of the eclipse suggests that it is the accretion disc eclipse and the eclipse asymmetric profile is interpreted as the effect of the warped disc geometry (Copperwheat et al., 2011b).

2. **V406 Hya:** It was discovered as a supernova in year 2003, however the spectroscopic analysis indicated that it is rather a hydrogen-deficient dwarf novae. In May 2003 it was observed in its maximum brightness which was recognized as superoutburst plateau due to the presence of the superhumps. After several days it faded by about 3 mag and stopped about 2 mag above the quiescence level. The system stayed in this phase for about 20 d showing occasional eruptions of amplitude ~ 2 mag and about 1 day duration. Then the star declined to its low state. There is also a hint of the dip during the plateau phase of the superoutburst (similar to that in e.g. KL Dra) (Nogami et al., 2004). This superoutburst pattern again resembles the WZ Sge-type.

3. **SDSS J0129:** Discovered during its superoutburst on December 2009 this is another AM CVn

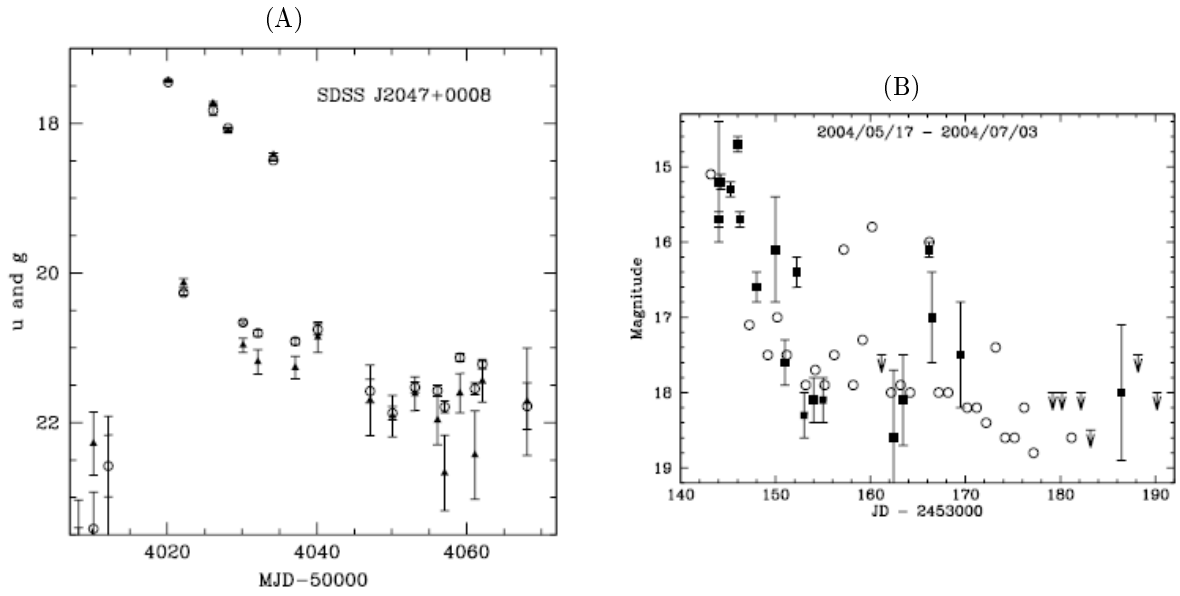

Figure 4.4: (A) The light curve of SDSS J2047 zoomed on the period when the superoutburst appeared. The plot is taken from Anderson et al. (2008). (B) The superoutburst of V406 Hya in May 2003 taken from Nogami et al. (2004).

star which has similar outburst activity to that of V803 Cen during its superoutburst in 2003. In this case six short rebrightenings in the time interval of $3-5$ d were detected right after the superoutburst maximum phase. After 41 days the SDSS J0129 was still at the level ~ 1.7 mag above the level of the minimum light (Shears et al., 2011).

4. **SDSS J2047:** The light curve of this system is yet poorly covered but the observed superoutburst is either followed by several rebrightenings or there appears a deep dip (Anderson et al., 2008).

4.3 The chemical composition

Since the disc is a mass spectrometer for the donor chemical composition it reflects the evolution history of the secondary and the binary as a whole. The determination of the disc chemical composition may help to verify their evolutionary tracks.

The observations clearly show that discs in AM CVn stars are not made of pure helium. One has to look closer at the observed AM CVn spectra to get a hint of what their disc metallicity might be.

The persistently faint systems or outbursting systems in quiescence show a spectrum consisting of a blue continuum and emission lines among which the strongest are HeI and HeII lines.

Unique for AM CVns is the triple-peak profile of the certain emission lines (e.g. HeI) in which the relative intensities of the central spike and the outer components differ from line to line. The ratio of the central component to the outer components rises for the lines which correspond to higher

excitation states (for HeII line the central part totally dominates the remaining two). It means that the emission arises in two independent sources: the outer components originate in the disc while the central spike comes from the region of very high temperatures, most probably from the accreting white dwarf or the boundary layer.

The two persistently faint systems – GP Com and V396 Hya – are very special. Unlike the other (outbursting or persistently bright) AM CVn stars, they show an unusual NV to CIV ratio indicating the significant overabundance of NV, in addition to a strong HeI and a weaker HeII line. They do not show the Si lines which are usually seen in other binaries of this type what may suggest the metal poor secondaries (Ruiz et al., 2001). All other binaries in a low state do not have such strong NV line and in addition show weak SiII and FeII lines.

In the spectra of three low state systems (SDSS J1552, SDSS J1208 and SDSS J1642) there is one more characteristic feature: a strong absorption in Mg which does not appear simultaneously with the absorption in Ca which would be expected if one wants to explain the Mg absorption by the metal-rich (DBZ type) accreting WD (T.Kupfer talk during 3rd AM CVn workshop in Warwick).

In the permanent high-state systems AM CVn or HP Lib the spectrum is dominated by the absorption lines, but sometimes emission in HeII is also detected. In the optical part of the spectrum the asymmetrical, broad absorption line of HeI dominates. The UV spectra show broad absorption lines of HeII, NV, NIV, SiIV, CIV (Wade et al., 2007). The spectra of the erupting systems, CR Boo and V803 Cen have similar characteristics during outbursts.

For GP Com (Strohmayer, 2004) it is estimated $Y = 0.99$ and $Z = 0.01$. Because GP Com and V396 Hya are the two metal-poor systems, we can consider $Z = 0.01$ as lower limit for an AM CVn disc metallicity. However, the exact metallicities of particular systems have not been well determined. They depend on the evolutionary channel: if it was the WD channel then the chemical composition would be roughly similar for the whole group and the potential differences would be induced by the mass of the progenitor and its stage in the CNO cycle; in turn if it was the He-star channel the abundances would be extremely different from $Z = 0.0$ to even $Z = 1.0$ depending on the moment when the mass transfer would have started (Nelemans et al. (2010), and Nelemans 2012 private communication).

Throughout, our fiducial model of outbursting AM CVn stars assumes $Y = 0.98$, $Z = 0.02$, but when discussing the general properties of the systems and the model we also consider other possibilities.

4.4 The stability limits

The preliminary verification of the DIM as the model of the outbursts in AM CVn stars is the to test the stability criteria predicted by the DIM versus the observed properties of these systems. The model should reproduce the observed relation between the luminosity state of the system and its orbital period: all high state AM CVns stars have $P_{\rm orb} < 20$ min, those outbursting have $P_{\rm orb}$ between 20 min and 40 min and those with $P_{\rm orb} > 40$ min are persistently in the low state.

The first to consider the stability of helium accretion discs in AM CVn systems was Cannizzo (1984).

In the standard version of the DIM the mass transfer rate $\dot{M}_{\rm tr}$ from the secondary is assumed to be constant and its value determines the stability of the disc. For pure helium discs the critical values of the accretion rate are:

$$\dot{M}^{+}_{\rm crit} = 1.01 \times 10^{17} \alpha_{0.1}^{-0.05} R_{10}^{2.68} M_1^{-0.89} \ {\rm g/s}, \tag{4.1}$$

$$\dot{M}^{-}_{\rm crit} = 3.17 \times 10^{16} \alpha_{0.1}^{-0.02} R_{10}^{2.66} M_1^{-0.89} \ {\rm g/s} \tag{4.2}$$

where $\alpha_{0.1} = \alpha/0.1$, R_{10} is the radius in units of 10^{10} cm and M_1 is the primary mass in solar masses.

We use the formulae for critical values of Σ, $T_{\rm c}$, $T_{\rm eff}$ and $\dot{M}_{\rm crit}$ for pure helium disc in their most recent version delivered us by Guillaume Dubus, who obtained them from the improved fitting procedures to the larger sample of points. Therefore, they slightly differ from those published in Lasota et al. (2008). The critical values for helium discs with $Z \neq 0$ have not been published before.

For $Y = 0.96$ $Z = 0.04$ critical $\dot{M}_{\rm accr}$ are:

$$\dot{M}^{+}_{\rm crit} = 4.76 \times 10^{16} \alpha_{0.1}^{-0.06} R_{10}^{2.65} M_1^{-0.88} \ {\rm g/s}, \tag{4.3}$$

$$\dot{M}^{-}_{\rm crit} = 1.74 \times 10^{16} \alpha_{0.1}^{-0.02} R_{10}^{2.61} M_1^{-0.87} \ {\rm g/s} \tag{4.4}$$

All formulae for critical values in discs of four different chemical compositions are given in Appendix A. The dependence on α in Eqs.(4.1) - (4.4) is clearly negligible.

To be in a hot (cold) stable equilibrium the accretion rate in a disc must be higher (lower) everywhere than the corresponding critical $\dot{M}_{\rm tr}$. Therefore, a stationary ($\dot{M}(R) = $ const.) disc is hot and stable when $\dot{M}_{\rm tr} > \dot{M}^{+}_{\rm crit}(R_{\rm d,max})$ and it is cold and stable when $\dot{M}_{\rm tr} < \dot{M}^{-}_{\rm crit}(R_{\rm in})$.

The comparison between the formulae (4.2) and (A) explains why there are no observed low state systems among hydrogen-rich CVs but they are among AM CVn stars: since $\dot{M}^{-}_{\rm crit}$ for helium is ~ 12 times higher than for solar composition discs the existence of cold stable hydrogen-deficient discs does not require so low mass-transfer rates as in the case of hydrogen-rich CVs, where it has to be lower than 8.0×10^{12} g/s.

The outer disc radius, $R_{\rm d}$, is calculated as a fraction of the primary Roche lobe radius given by Eggleton (1983)

$$\frac{R_{\rm RL1}}{a} = \frac{0.49\, q^{-2/3}}{0.6\, q^{-2/3} + \ln(1+q^{-1/3})} = \frac{0.49}{0.6 + q^{2/3} \ln(1+q^{-1/3})} \tag{4.5}$$

where a is the binary separation. It is assumed that in the outburst $R_{\rm d} \sim 0.9\, R_{\rm RL1}$. Eq.(4.5) is valid for $0 < M_2/M_1 < 0.8$ so it is a good approximation both for DN and AM CVns.

In the limit of very small values of q the expression $q^{2/3} \ln(1+q^{-1/3})$ in the denominator of Eq.(4.5) is very small (it tends to 0 for $q \to 0$). Since in AM CVn stars $0.0125 \leq q \leq 0.18$ the dependence of the maximal disc radius on mass ratio is rather weak and can be safely neglected. The inner radius is taken to be equal to the radius of the central white dwarf, $R_{\rm in} = R_1$, which is determined by the white dwarf mass M_1 through the $M - R$ relation (Nauenberg, 1972).

The plot of the estimated $\dot{M}_{\rm tr}$ versus $P_{\rm orb}$ for observed AM CVns compared with the model predictions is shown in Fig.4.5.

The color solid lines are the calculated critical mass transfer rates for two chemical compositions of the disc: $Y = 1.0$ and $Y = 0.96$ $Z = 0.04$, and two primary masses: $1.0\,{\rm M}_{\odot}$ and $0.6\,{\rm M}_{\odot}$. They show the general trend of $\dot{M}$ critical values: increase of the metals abundance in the disc lowers the values of $\dot{M}^{+}_{\rm crit}$ and $\dot{M}^{-}_{\rm crit}$ (compare for example line red (calculated for $Y = 1.0$ and $M_1 = 1.0\,{\rm M}_{\odot}$) with green (for $Y = 0.96$ $Z = 0.04$ and $M_1 = 1.0\,{\rm M}_{\odot}$)) while the lower primary mass leads to higher $\dot{M}^{+}_{\rm crit}$ and $\dot{M}^{-}_{\rm crit}$ (compare for example line red (calculated for $Y = 1.0$ and $M_1 = 1.0\,{\rm M}_{\odot}$) with blue (for $Y = 1.0$ and $M_1 = 0.6\,{\rm M}_{\odot}$)).

The permanently high-state systems ES Cet, SDSS J1908 and AM CVn lie well above the critical mass transfer limit regardless how low-mass CO white dwarf the primary would be. To be in accordance with observation the disc of HP Lib, which is another bright and steady system, should not be purely helium (and it is not, see Sect.4.3) and its M_1 should be close to its upper value estimated from observations: $0.8\ {\rm M}_{\odot}$ (Table 4.1).

The mass-transfer rates of CR Boo and V803 Cen are very close to the upper critical line, which might explain why these two outbursting systems have been alternately and confusedly classified as analogues of ER UMa, Z Cam, and (not consistent with their mass-transfer rate) of WZ Sge stars. Unless their disc are not very rich in metals they position on the $P_{\rm orb} - \dot{M}_{\rm tr}$ diagram agrees with the observations. SDSS J0926 and SDSS J1240 are outbursting and lie in the region between the stability limits.

V396 Hya and GP Com have shown no changes in their brightness till now, they are considered to be the low-state systems. V396 Hya lies below $\dot{M}^{-}_{\rm crit}$ line for $M_1 = 0.6\,M_{\odot}$ and above $\dot{M}^{-}_{\rm crit}$ line for $M_1 = 1.0\,M_{\odot}$. From Eq.(4.4) one can conclude that for V396 Hya the primary mass should lie in the range $0.6 - 1.0\,{\rm M}_{\odot}$. The value of $\dot{M}_{\rm tr}$ for GP Com marked on the plot is actually its upper limit and the uncertainties consider the estimation of this upper limit so the position of GP Com does not contradict the model predictions as it possible that it lies below $\dot{M}^{-}_{\rm crit}$ lines for reasonable set of the parameters.

4.5 AM CVn stars outbursts modeling

4.5.1 The quiescence problem

The still unsolved problem of dwarf novae light curves simulations is the discrepancy between the modeled and observed quiescence luminosity. In synthetic light curves the quiescence luminosity gradually rises (even by about 2.5 mag, e.g. Fig.2.9) while observations show that it should be approximately constant to within 0.1 mag (Smak, 2000). The same trouble concerns AM CVn stars.

The quiescence luminosity increase in the synthetic light curves can be explained by the dependence between disc surface density, effective temperature and luminosity: in quiescence the mass accumulates in the disc, the disc effective temperature rises with Σ what translates into the grow of the disc luminosity.

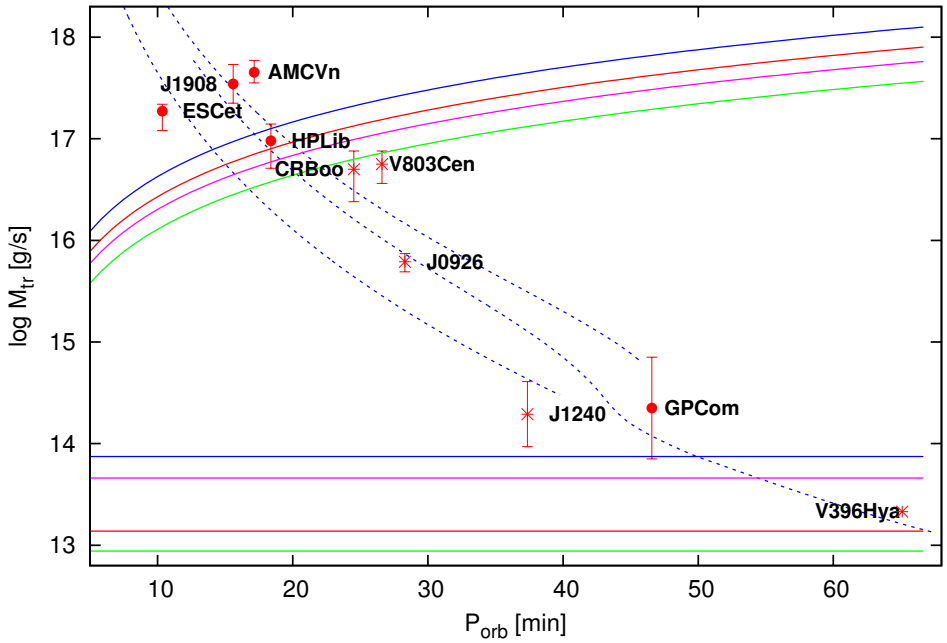

Figure 4.5: The $\log \dot{M}_{\rm tr} - P_{\rm orb}$ plane. Dots - persistent AM CVn systems with known distances; asterisks - outbursting AM CVn systems with known distances; solid lines are the upper and lower critical limits of $\dot{M}_{\rm tr}$- red: $M_1 = 1.0\,{\rm M}_\odot$, $Y = 1.0$; blue: $M_1 = 0.6\,{\rm M}_\odot$, $Y = 1.0$; green: $M_1 = 1.0\,{\rm M}_\odot$, $Y = 0.96$, $Z = 0.04$; pink: $M_1 = 0.6\,{\rm M}_\odot$, $Y = 0.96$, $Z = 0.04$. Dotted lines: evolution models for AM CVns through the WD channel (kindly provided by Chris Deloye)

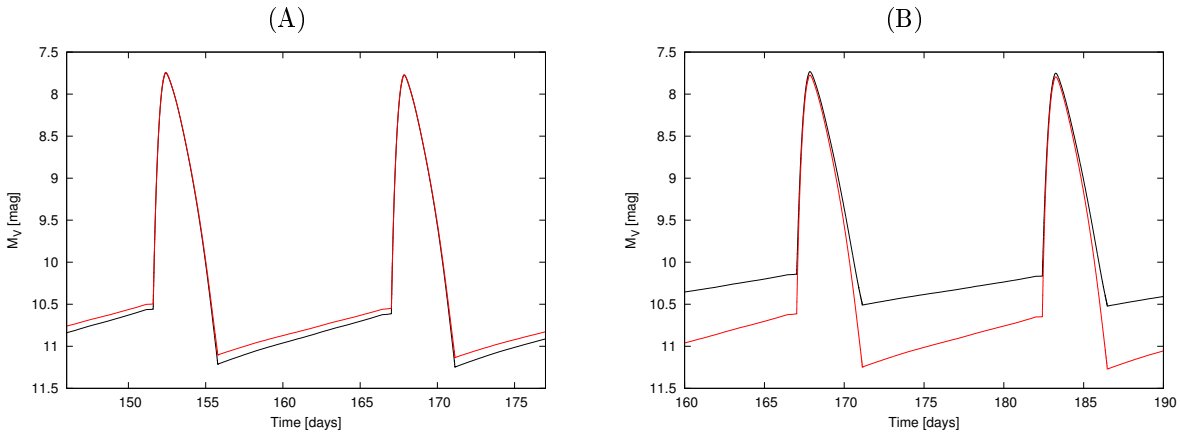

Figure 4.6: The light curves with additional components to the visual flux of the system in quiescence: (A) with the light from the secondary of $T_{\rm eff} = 5000$ K and $R_2 = 2.6 \times 10^9$ cm (red line), black line: without secondary contribution; (B) with hot spot contribution (black line) and without (red line). All light curves are calculated for $\alpha_{\rm c} = 0.02$, $\alpha_{\rm h} = 0.2$, $M_1 = 1.0\,{\rm M}_\odot$, $\dot{M}_{\rm tr} = 2.0 \times 10^{16}$ g/s and $\langle R_{\rm d} \rangle = 1.2 \times 10^{10}$ cm.

One can model the light curves with additional sources of light in quiescence: the light form the secondary and from the hot spot, to see if they cover the increase of disc luminosity. We assumed that the additional visual flux comes from the secondary of effective temperature 5000 K and radius 2.6×10^9 cm and/or from the hot spot. The contribution of the hot spot has been included according to Smak (2010) where the mean visual luminosity of the spot is

$$\langle L_{\rm spot} \rangle = \pi s^2 a^2 F(T_{\rm eff,spot}). \tag{4.6}$$

We adopted the dimensionless radius of the spot $s = 0.5$, the orbital separation between primary and secondary $a = 1.8 \times 10^{10}$ cm and the flux to be that of the black body $F(T_{\rm eff,spot}) = \sigma T^4_{\rm eff,spot}$ with $T_{\rm eff,spot} = 6800$ K. We use here the black body flux instead of the flux obtained from the model atmospheres (used in Smak (2010)) because we need just to see the influence of the hot spot light on quiescence and not to evaluate it quantitatively.

The results are plotted in Fig.4.6A and B. The impact of the secondary on the quiescence luminosity is negligible while the hot spot may increased its level by $\sim 0.5 - 1.0$ mag. Despite that the undesired luminosity increase is slightly reduced it is still noticeable and the problem remains.

4.5.2 Additional sources of disc heating

As described in Sect.4.2 all observed AM CVn stars show superoutbursts and the normal outbursts are rather occasional - the characteristics that is opposite to what is observed in DN. Before going further with the modifications of the standard DIM it is important to test the influence on helium discs of the sources of disc heating which are known to play a role in H-dominated CVs.

4.5.2.1 The magnetic field of a primary

So far no intermediate polars have been observed among helium dwarf novae. However, there is a candidate for the first system in this category - SDSS J080449.49+161624.8. The single-peaked, broad emission lines with series of ionized helium in its spectrum match strikingly to what is observed in optical spectra of magnetic CVs (Roelofs et al., 2009b). If it is a magnetic AM CVn star then the accretor magnetic field would be significant enough to affect the inner part of the disc.

In the quiescence the magnetic pressure which rapidly rises at small radii ($P_{\rm mag} \sim R^{-6}$) exceeds the gas and ram pressures of infalling matter up to radius R_M. It means that the matter flow is disrupted and the inner disc radius is pushed away from the white dwarf up to R_M (Frank et al., 2002):

$$R_{\rm in} = R_M = 9.8 \times 10^8 \dot{M}_{15}^{-2/7} M_1^{-1/7} \mu_{30}^{4/7} \text{ cm} \tag{4.7}$$

where μ_{30} is the magnetic moment in units of 10^{30} G cm^3, M_1 is the mass of the primary in solar masses and $\dot{M}_{15}$ is mass accretion rate in units of 10^{15} g/s.

During the outburst the situation changes - the mass accretion rate sharply rises the ram pressure of matter which dominates over the magnetic pressure and the inner edge of the disc approaches to the surface of the white dwarf.

The magnetic field strength of a white dwarf lies in a range $10^4 - 10^7$ G, so the magnetic moment range is $\mu_{30} \approx 1 - 10^3$ (El-Khoury and Li, 1999). It is possible that WD in non magnetic DN or AM CVn stars have a weak magnetic field up to 10^4 G (i.e.$\mu_{30} = 1.0$).

To test if and how the magnetic field of this order may influence the light curves we define the inner disc radius in the model by the formula (4.7) and present the results in Fig.4.7.

For lower $\dot{M}_{\rm tr}$ the presence of the primary white dwarf magnetic field prolongates the quiescence time because the disc has to accumulate more mass for the surface density to cross $\Sigma^-_{\rm crit}(R_{\rm in})$ and start the outburst. From the same reason it reduces the number of small outbursts.

For high $\dot{M}_{\rm tr}$ close to the upper critical value the magnetic truncation of the inner disc has the negligible impact on the synthetic light curves (panel (C) in Fig.4.7). The reason is that very high $\dot{M}_{\rm tr}$ trigger the outside-in instead of inside-out outbursts. Therefore, the different conditions imposed by magnetic pressure on the inner edge do not influence the propagation of the heating front. At the outburst maximum the inner radius extends to the accretor surface so the conditions are the same with and without the primary magnetic field and the outburst properties are not affected. There is a little difference in quiescence level because with WD magnetic fields included the cooling front ends at larger radii. The luminosity, however, is only slightly higher in this case because the dominant source of light in the low state are the outer parts of the disc.

4.5.2.2 Irradiation of the disc by the WD

The effective temperatures of white dwarfs in nonmagnetic DN are estimated at $\sim$ 15 000 K to $\sim$ 55 000 K (Sion and Godon, 2007). Since the hydrogen ionization takes place at $T^-_{\rm eff,crit} \sim$ 5 500 K

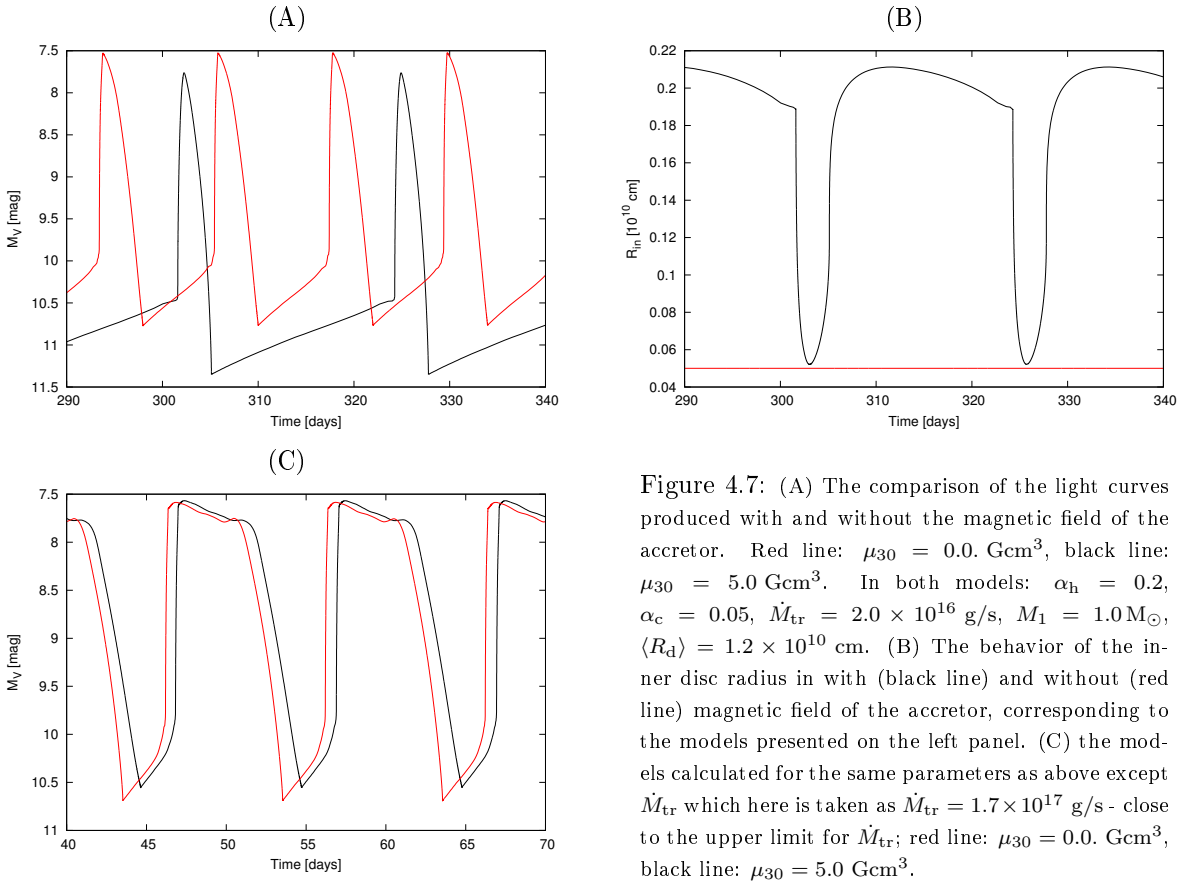

Figure 4.7: (A) The comparison of the light curves produced with and without the magnetic field of the accretor. Red line: $\mu_{30} = 0.0$. Gcm^3, black line: $\mu_{30} = 5.0$ Gcm^3. In both models: $\alpha_{\rm h} = 0.2$, $\alpha_{\rm c} = 0.05$, $\dot{M}_{\rm tr} = 2.0 \times 10^{16}$ g/s, $M_1 = 1.0\,{\rm M}_\odot$, $\langle R_{\rm d} \rangle = 1.2 \times 10^{10}$ cm. (B) The behavior of the inner disc radius in with (black line) and without (red line) magnetic field of the accretor, corresponding to the models presented on the left panel. (C) the models calculated for the same parameters as above except $\dot{M}_{\rm tr}$ which here is taken as $\dot{M}_{\rm tr} = 1.7 \times 10^{17}$ g/s - close to the upper limit for $\dot{M}_{\rm tr}$; red line: $\mu_{30} = 0.0$. Gcm^3, black line: $\mu_{30} = 5.0$ Gcm^3.

($T^{-}_{\rm c,crit} \sim 8\,200$ K) the radiative flux emerging from the hot central white dwarf, which modifies the surface temperature of the disc in the white dwarf vicinity, has an important influence on the disc stability in DN (Hameury et al., 1999).

The central white dwarfs in AM CVn-type binaries are supposed to have the effective temperatures similar to those in DN, i.e. between $\sim 12\,000$ K and $\sim 40\,000$ K (Sion et al., 2011), but the critical temperatures in helium discs are much higher than in hydrogen-dominated discs: $T^{-}_{\rm eff,crit} \sim 10\,000$ K ($T^{-}_{\rm c,crit} \sim 26\,800$ K). In the case of AM CVn stars the difference between temperatures of the irradiating flux and the disc is not so prominent and in fact the effect of the disc irradiation by the accretor is negligible as it is shown below.

The white dwarf should be treated as an extended source. A fraction $(1-\beta)$ of the radiative flux illuminating each side of the disc which is absorbed in the disc optically thick parts is given by (Friedjung, 1985; Smak, 1989a; Hameury et al., 1999)

$$T^4_{\rm ill} = (1-\beta)\, T^4_{\rm WD} \frac{1}{\pi} [\arcsin\rho - \rho(1-\rho^2)^{1/2}]$$

where $\rho = R_{\rm WD}/R$, $R_{\rm WD}$ and $T_{\rm WD}$ are radius and temperature of the white dwarf, and β is the disc albedo.

To incorporate this formula into numerical calculations of the vertical disc structure one has to modify the outer boundary condition:

$$\sigma T^4_{\rm s} = F_{\rm visc} + \sigma T^4_{\rm ill} \tag{4.8}$$

where $T_{\rm s}$ is the disc temperature at the photosphere. Then the Eq.(2.56) connecting the mid-plane temperature with the effective temperature becomes:

$$T^4_{\rm c} = \frac{3}{8}\sigma T^4_{\rm eff} + T^4_{\rm ill} \tag{4.9}$$

Also the prescription for change of α between hot and cold state during disc time evolution has to be changed with respect to Eq.(2.60):

$$\log(\alpha) = \log(\alpha_{\rm c}) + [\log(\alpha_{\rm h}) - \log(\alpha_{\rm c})] \times \left[1 + \left(\frac{2.5\times10^4\ {\rm K}}{(T^2_{\rm c} + 5T^2_{\rm ill})^{1/2}}\right)^8\right]^{-1} \tag{4.10}$$

The term $5T^2_{\rm ill}$ is added for technical reasons, similar to those presented in Sect.2.4 justifying $T_0 = T^{+}_{\rm c,crit}$ in the prescription for α change when no irradiation is taken into account. Here T_0 should account for the increase of temperature in the disc due to the irradiation in order to star changing α when the recombination in the disc matter starts.

As an input parameter it is used the whole term $\sqrt[4]{1-\beta}T_{\rm WD} = 25\,000\,{\rm K}$ to account for the disc albedo.

In DN the irradiation from WD rises the temperature of the inner disc region above the hydrogen ionization temperature. It also significantly lowers the value of maximum surface density $\Sigma^{-}_{\rm crit}(R)$

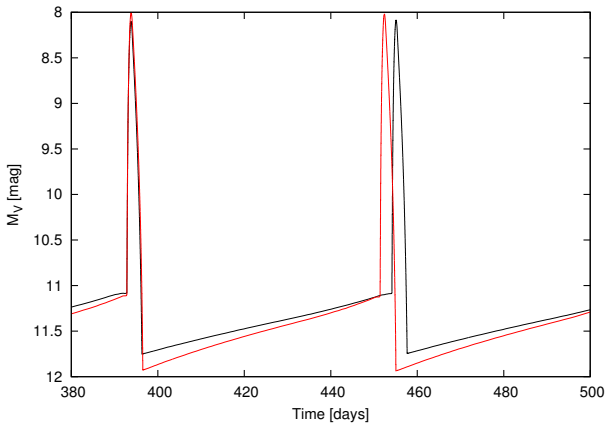

Figure 4.8: The light curves calculated with (black line) and without (red line) irradiation of the disc by a central white dwarf of temperature $\sim 25\,000$ K. The parameters if the models are: $\alpha_{\rm c} = 0.05$, $\alpha_{\rm h} = 0.1$, $\dot{M}_{\rm tr} = 1.0 \times 10^{16}$ g/s, $M_1 = 0.6\,{\rm M}_\odot$, $\langle R_{\rm d} \rangle = 1.2 \times 10^{10}$ cm.

up to the radius at which the irradiation flux no longer dominates over the local accretion flux. As a consequence lower mass transfer rate is sufficient to trigger the inside-out outbursts than in unirradiated case. In addition the amplitude of the outbursts is reduced as the irradiation lifts the disc brightness in the quiescence (Hameury et al., 1999).

While temperatures of accreting white dwarf are expected to be in the range $15\,000 - 35\,000\,{\rm K}$ (Sion et al., 2011) the helium disc midplane critical temperatures are expected to be $T^{-}_{\rm c,crit} \sim 18\,000 - 25\,000\,{\rm K}$ (depending on the disc parameters). This is the reason why in AM CVn this effect is marginal as can be seen from Fig.4.8 and we neglect it in the modeling of AM CVn stars light curves.

4.5.2.3 The outer disc heating by the hot spot

As the mass is transferred from the secondary its stream hits the outer ring of the accretion disc forming the so called hot spot and heating the outer parts of a disc.

To account for this phenomenon we consider the idealized situation when none of the impact energy is radiated away and all of it is changed into the heat in the disc outer region. In fact a major part of this energy may be radiated during the collision of the stream with the outer disc rim (Smak, 2002).

In the impact region the disc annulus of width $\Delta R_{\rm hs}$ is heated at a rate Q_i with efficiency η_i (Buat-Ménard et al., 2001a):

$$Q_i(R) = \eta_i \frac{GM_1\dot{M}_{\rm tr}}{2R_{\rm d}} \frac{1}{2\pi R_{\rm d}\Delta R_{\rm hs}} \exp\left(-\frac{R_{\rm d}-R}{\Delta R_{\rm hs}}\right) \tag{4.11}$$

where M_1 is the mass of the white dwarf, $\dot{M}_{\rm tr}$ is the mass transfer rate from the secondary and $R_{\rm d}$ is the outer radius of the disc.

When the disc is in a low state as much as half of a system visible light can be emitted from region

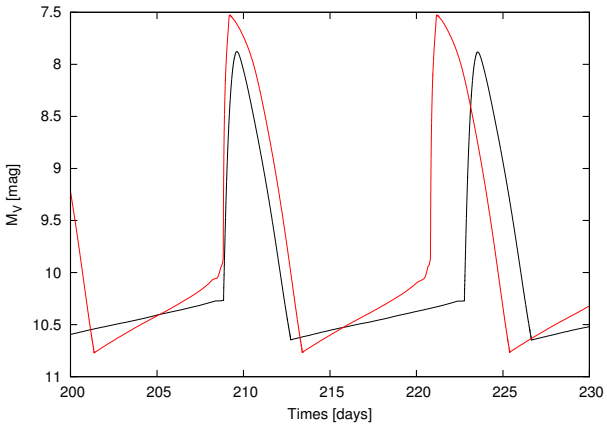

Figure 4.9: The light curves calculated for $\alpha_{\rm h} = 0.2$, $\alpha_{\rm c} = 0.05$, $\dot{M}_{\rm tr} = 2.0 \times 10^{16}$ g/s, $M_1 = 1.0\,{\rm M}_{\odot}$, $\langle R_{\rm d} \rangle = 1.2 \times 10^{10}$ cm. The red line corresponds to the model without the disc heating by the hot spot, the black line corresponds to the model in which disc heating by the hot spot is included.

of the stream impact (Smak, 2010) while in the outburst its contribution is negligible since most of the luminosity comes from the inner parts of hot accretion disc due to the high dissipation rate in the boundary layer.

The magnitude of the light coming from the hot spot during the quiescence depends on the inclination of the disc: smaller inclination means higher luminosity from the impact region.

The important result is that the additional heating of the outer edge reduces both critical values of $\Sigma^{\pm}_{\rm crit}$. This extends the lower limit of $\dot{M}_{\rm tr}$ for which the disc should be unstable and eases triggering of the outside-in outburst for moderate mass transfer rates. In Fig.4.9 it is showed that hot spot lowers the outburst amplitude and reduces the undesired grow of the luminosity during the quiescence.

According to Smak (2002) evaluations the contributions from the tidal heating and the stream impact heating are comparable. In what follows we use the stream heating only as representing the effects of both processes on the outer disc and outcoming light curves.

On the other hand Smak (2002) expressed doubts concerning the relevance of hot-spot heating noticing that most of the impact energy is radiated-away at the hot spot location.

4.5.3 Superoutbursts

Although they modify shapes of the synthetic light curves none of the additional disc heating sources discussed above leads to the superoutbursts corresponding to the observations. But again one can take advantage from the experiences from dwarf nova modeling for which the superoutbursts are reproduced when the enhanced mass transfer from secondary is applied in calculations (e.g. Hameury et al. (1997, 2000); Lasota (2001)).

In the space of years the discussion have been carried between the supporters of two models which were supposed to explain the origin of the superoutbursts i.e. the Tidal-Thermal Instability Model (hereafter TTI) and the Enhanced Mass Transfer Model (hereafter EMT).

In the following we claim that EMT is responsible for the superoutburst in AM CVn stars although the mechanism leading to the enhancement of the mass from the secondary is far from being understood. We briefly present the arguments of both sides and explain our choice.

4.5.3.1 The EMT Model vs the TTI Model

The idea of the mass transfer rate enhancement came directly from the observations.

The observations of VW Hyi, a non-eclipsing SU UMa-type dwarf nova, lead to the conclusion that the superoutbursts are always the consequence of the short outbursts. The observed enhancements in the hot spot brightness appear during the outbursts maxima or decline phases, never during the rise. Since the brightness of the hot spot comes from the reprocessed kinetic energy of the gas stream heating the disc then its enhancement has to be the reflection of enhanced force with which the stream hits the disc due to the enhanced mass transfer rate from the secondary (Vogt, 1983).

These observations lead to the formulations of the basics of the Enhanced Mass Transfer Model (Vogt, 1983; Osaki, 1985; Smak, 1991): the strong radiation emitted from the disc during the normal outburst heats up the gas in the region of the secondary photosphere exposed to this irradiation and the hot gas starts to flow through L_1 point at the enhanced rate. According to this model the radius of the disc expands during the superoutburst and then gradually decreases along the supercycle what is observed (Zola, 1989; Smak, 1991). The EMT model also predicts that the duration of the quiescence between the normal outbursts rises during the first phase of the supercycle but then it decreases in the several cycles just before the next superoutburst (Smak, 1991). These predictions have been confirmed even very recently in the extraordinarily detailed light curves of V1504 Cyg and V344 Lyr taken with *Kepler* telescope(Cannizzo et al., 2012) .

The alternative to the EMT model is the Tidal-Thermal Instability Model proposed by Osaki (1989). In contrast to the EMT model in the TTI model the mass transfer rate from a secondary is assumed to be constant. The superoutbursts are the consequence of the enhanced torque acting on the disc when it extends up to the $3:1$ resonance radius. There the enhanced tidal torque causes the more intensive dissipation in the outer part of the disc and prevents the formation of the cooling front (Osaki, 1989).

The TTI model predicts that after a superoutburst the disc radius considerably shrinks due to the high amount of mass which has been accreted from the disc during the superoutburst. Next the disc undergoes the series of small outbursts during which the disc mass builds up and during which the disc radius gradually rises again until the next superoutburst sets in. Contrary to the EMT model the TTI model does not predict the shortening of the normal cycles just before the onset of the superoutburst. The predicted by the TTI model behavior of the disc radius and of the normal cycles is in contradiction with what observations suggest (see above). This model was found relatively successful in reproducing the superhump periods and their relations with orbital period and mass ratio in the system, but not in reproducing their amplitudes which, in observed light curves, are ~ 0.3 mag, while the TTI simulations give the amplitudes an order of magnitude lower (Smak, 2009c).

The polemics between the supporters of both models has persisted for years. Osaki and Meyer

(2003) gave the counterarguments for the objections aimed at TTI model: (i) the observed brightenings in the humps of eclipsing binaries like WZ Sge, Z Cha or VW Hyi were interpreted as the superhumps in the early stage of their growth instead of brightening of the hot spot; (ii) to refute the argument that in observations the superhumps appear in delay to the superoutburst maximum (what is inconsistent with the origin of superoutbursts in this model), the 2 : 1 resonance radius was added to the model. The disc expands to 2 : 1 radius during the peak of the superoutburst and the superhumps are supposed to appear only after the disc contracts again to 3 : 1 resonance radius after the superoutbursts maximum.

However, the arguments from the series of articles Smak (2008a,b, 2009a,c,e,b,d, 2010, 2011) seem to tip the scales in favor of the EMT model. They can be summarized as follows:

1. the analysis of the eclipses (not contaminated by the superhumps) in the light curves of Z Cha and OY Car show the enhancement of the hot spot brightness during the superoutburst (Smak, 2007, 2008a) suggesting the enhanced $\dot{M}_{\rm tr}$ from the secondary,

2. as it was mentioned: the TTI model does not reproduce the observed amplitudes of the superhumps (Smak, 2009c),

3. the eccentricity of the disc during the superoutbursts of Z Cha, WZ Sge, OY Car and IY UMa has been questioned as based on not conclusive observational evidence(Smak, 2009a),

4. the alternative interpretation of the superhumps origin is given (that they are the results of variable irradiation of the secondary) which does not require the disc expanded to 3 : 1 radius (Smak, 2009b, 2011).

The most serious drawback of the EMT model is the efficiency of the heating mechanism of the secondary surface. The main problems pointed out by several authors, i.e. Osaki and Meyer (2003); Viallet and Hameury (2007), are: (i) the shadow casted by the disc on the broad region around L_1 point, (ii) the Coriolis force which may limit the diffusion of the heated matter from irradiated parts of the secondary photosphere to the cold shadowed parts and (iii) the high opacities of the secondary photosphere to the far UV and X radiation. The simulations done by Viallet and Hameury (2007, 2008) show that the gas from the parts of the secondary exposed to irradiation is able to flow into the vicinity of L_1 point but in the course of this flow it cools down to the temperature at which it is no longer able to account for $\dot{M}_{\rm tr}$ enhancement.

However, one has to pay attention to the assumptions which were made here. As was pointed out by Smak (2009b) the authors assume that the flowing gas cools in a isothermal layer what may overestimate the cooling rate in their simulations. Smak (2009d) proposed an additional phenomenon which should be taken into account and which changes the geometry of the secondary shielding - the tilt of an accretion disc.

The important point is that the EMT model works very well in reproducing all main features of the SU UMa-type dwarf novae light curves (see Schreiber et al. (2004a); Hameury and Lasota (2005); Buat-Ménard and Hameury (2002); Hameury et al. (2000, 1997); Ramsay et al. (2010)) and it seems that it is necessary in the context of the AM CVn stars light curves simulations what is shown below.

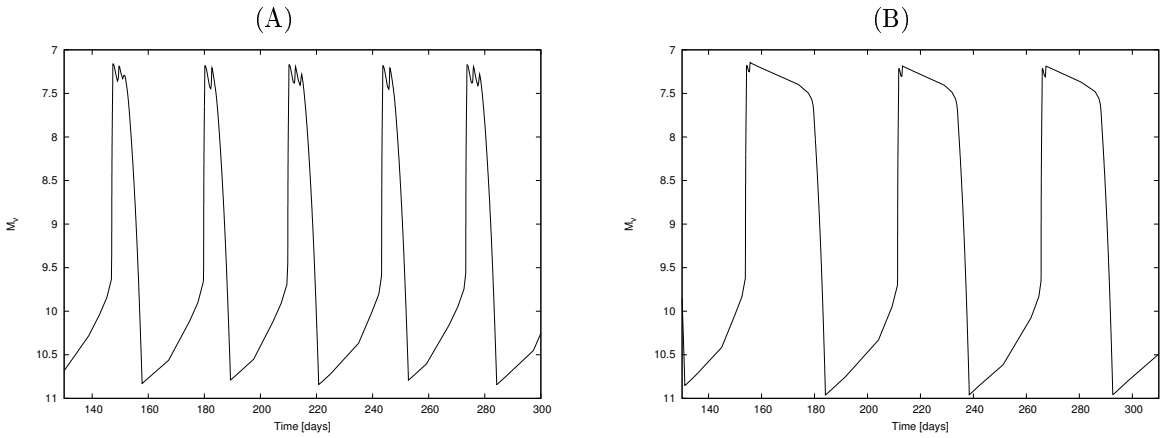

Figure 4.10: The example of γ-parameter influence on the modeled light curves. The models are calculated for pure helium disc for (A) $\gamma = 0.4$, and (B) $\gamma = 0.8$, in both cases other parameters are: $\alpha_{\rm h} = 0.1$, $\alpha_{\rm c} = 0.05$, $\dot{M}_{\rm tr} = 1.0 \times 10^{17}$ g/s, $M_1 = 1.0\,{\rm M}_{\odot}$, $\langle R_{\rm d} \rangle \approx 1.2 \times 10^{10}$ cm, $\mu_{30} = 2.0$.

4.5.3.2 Helium SU UMa stars - KL Dra and PTF1J0719

The general properties of the relatively simple light curves of KL Dra and PTF1J0719 can be reproduced by using the simple prescription for accretion-irradiation mass-transfer rate increase originally proposed by Hameury et al. (1997):

$$\dot{M}_{\rm tr} = \max(\dot{M}_{\rm tr,0}, \gamma\,\dot{M}_{\rm accr}) \tag{4.12}$$

where γ is the parameter of proportionality between $\dot{M}_{\rm tr}$ and $\dot{M}_{\rm accr}$ in the range from 0 to 1, $\dot{M}_{\rm tr,0}$ corresponds to the "secular" (non-enhanced) mass-transfer rate and $\dot{M}_{\rm accr}$ is the accretion rate onto the primary.

The influence of the γ-parameter on the outbursts as its value approaches unity can be seen in Fig.4.10 - it prolongates the outburst while the outburst amplitude is unchanged. The small light variations during the outburst maximum in Fig.4.10A are the outcome of the moderately enhanced mass transfer rate which causes that the outer parts of the disc are marginally stable - the cooling front starts to develop there but it is stopped just few moments later by the heating front immediately developing behind it.

Dealing with better-sampled multi-wavelength light curves such as that of VY Hyi, Schreiber et al. (2004b) used a more "refined" prescription using $\langle \dot{M}_{\rm accr} \rangle$ suitably averaged over time which takes into account that the fraction of the accretion luminosity may heat up the primary white dwarf. We decided to use the simpler version given by Eq.(4.12) because the AM CVn light curve are not of similar quality and because the prescription with $\langle \dot{M}_{\rm accr} \rangle$ does not influence the dwarf novae light curves noticeably (Schreiber et al., 2004b).

As for hydrogen-dominated dwarf novae the light curve properties depend on the mass-transfer rate, the mass of the primary, and the viscosity parameters, as well as on the assumed white dwarf's

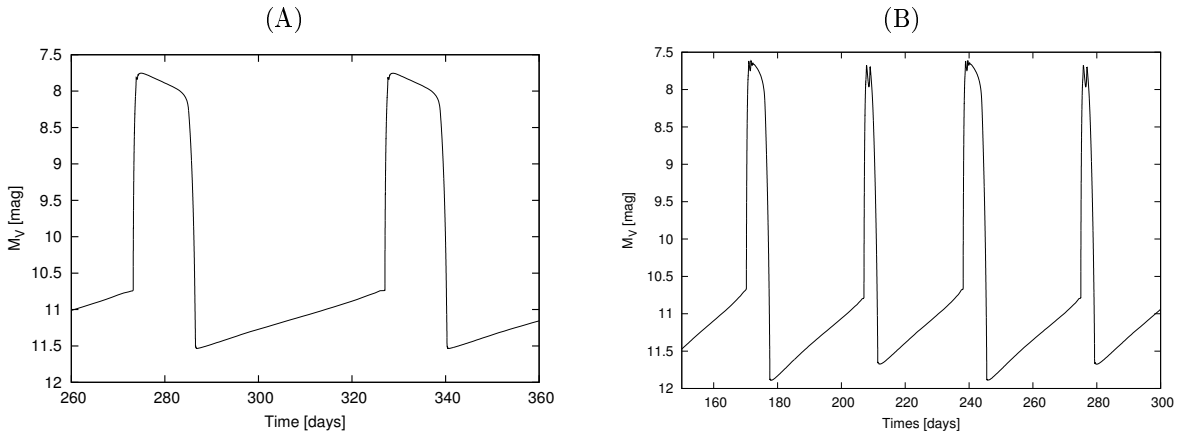

Figure 4.11: (A) The model of KL Dra in the case where no normal outbursts are present. The disc is assumed to be $Y = 0.98$ $Z = 0.02$ and the parameters are $\alpha_{\rm h} = 0.2$, $\alpha_{\rm c} = 0.035$, $\dot{M}_{\rm tr} = 2.0 \times 10^{16}$ g/s, $M_1 = 0.6\,{\rm M}_\odot$, $\langle R_{\rm d} \rangle \approx 1.1 \times 10^{10}$ cm, $\gamma = 0.8$, $\mu_{30} = 1.0$ and hot spot heating is included. (B) The model with the same parameters as (A) but with $\mu_{30} = 0.0$ and without the hot spot heating.

magnetic moment and the value of the parameter γ (Hameury et al., 2000). In AM CVns one has additionally to fix the chemical composition, i.e. the metallicity which we will assume to be $Y = 0.98$ $Z = 0.02$ unless stated otherwise.

Until recently KL Dra was thought to show only the superoutbursts. In the calculations we used the parameters suggested in Ramsay et al. (2010) for this binary: $\dot{M}_{\rm tr} = 2.0 \times 10^{16}$ g/s, $M_1 = 0.6\,{\rm M}_\odot$. The light curve consisting only of the superoutbursts of amplitudes $A_{\rm s} \sim 3.5$ mag lasting $t_{\rm s} \sim 15$ d and appearing every $T_{\rm recc,s} \sim 57$ d was possible to obtain only by turning on the magnetic field of the primary of magnetic moment $\mu_{30} = 1.0$ (corresponding to $B \sim 1.5 \times 10^3$ G) in the model, setting the viscosity parameters $\alpha_{\rm c} = 0.035$, $\alpha_{\rm h} = 0.2$, enhancing $\dot{M}_{\rm tr}$ with $\gamma = 0.8$ and including the heating of the outer disc edge by the hot spot. The resulting supercycles presented in Fig.4.11A reproduce quite well the observed ones in which $A_{\rm s,obs} \sim 3.5$ mag, $t_{\rm s,obs} \sim 14$ d and $T_{\rm recc,s,obs} \sim 63$ d shown in Fig.4.2.

Essential for obtaining the light curve in Fig.4.11A is the magnetic field of the primary and the heating by the hot spot which both stabilize the disc. The magnetic field truncates the disc inner parts, increasing $\Sigma^-_{\rm crit}(R_{\rm in})$ and enforcing the disc to accumulate more mass before triggering the inside-out outburst. On the opposite disc edge the hot spot heating, in turn, lowers $\Sigma^+_{\rm crit}(R_{\rm d})$ so that more mass has to be accreted before the cooling front can form. Both effects contribute to the suppression of the normal outbursts and favor the appearance of the superoutburst instead.

In reality, as mentioned above, KL Dra could have normal outbursts that have been missed during observational campaigns and recently the detection of two short and faint eruptions has been confirmed (Ramsay 2012, private communication).

With no hot spot heating and the primary magnetic field included and with the same model parameters, the light curve consists of narrow and wide outbursts which last ~ 5 d and ~ 9 d respectively. The recurrence times of the outbursts of both types are approximately the same: ~ 68 d, the time

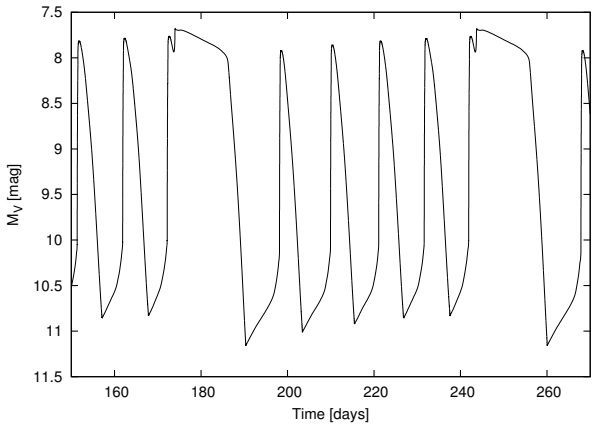

Figure 4.12: The model of PTF1J0719 light curve: $\alpha_{\rm h} = 0.1$, $\alpha_{\rm c} = 0.02$, $\dot{M}_{\rm tr} = 6.0 \times 10^{16}$ g/s, $M_1 = 1.0\,{\rm M}_{\odot}$, $\langle R_{\rm d} \rangle \approx 1.1 \times 10^{10}$ cm, $\gamma = 0.6$. The disc is $Y = 0.98$ $Z = 0.02$.

elapsing from the onset of the wide outburst to the onset of the narrow is ~ 37 d and from the onset of narrow to the onset of the wide one is ~ 30 d (Fig.4.11B). The quiescence luminosity after the wide outbursts is about 0.2 mag lower because more mass has been accreted than during the narrow outburst. The light curve presented in Fig.4.11B is far for resembling that of KL Dra.

The short outbursts observed in KL Dra light curve are strong argument in favor that KL Dra is the helium SU UMa star, just as PTF1J0719. Since the periods of quiescence in KL Dra light curve are not well covered and the overall appearance of the light curve is highly uncertain, we do not focus on tuning the parameters of the models (without the hot spot heating and $\mu_{30} = 0.0$) to obtain the light curve potentially corresponding to KL Dra. Instead, to consider the light curves of the SU UMa-type helium dwarf novae, we rather focus on modeling of the PTF1J0719 light curve.

Except for its orbital period (26.8 min) not much is known about the parameters of PTF1J0719 which is the first observed helium system to show clearly the outburst activity typical for SU UMa-type dwarf novae. The best result in reproducing its light curve has been obtained with the model parameters: $\dot{M}_{\rm tr} = 6.0 \times 10^{16}$ g/s, $M_1 = 1.0\,{\rm M}_{\odot}$, $\alpha_{\rm h} = 0.1$, $\alpha_{\rm c} = 0.02$, $\gamma = 0.6$ for disc of chemical composition $Y = 0.98$ $Z = 0.02$. We also drop in this case the stabilizing mechanisms which were present the model of KL Dra (i.e. we set $\mu_{30} = 0.0$ and not include hot spot heating) and let the normal outbursts develop. The result is presented in Fig.4.12.

Between superoutbursts one notices a slight gradual increase of the minimum and maximum luminosity of the four consecutive normal outbursts. This happens because during each normal outburst $\dot{M}_{\rm tr}$ is enhanced due to the γ-prescription - the disc gains more mass than it looses due to accretion. In consequence, during the sequence of the normal outbursts, the mass is gradually accumulated in the disc and Σ rises everywhere in the disc. This effect is one of the typical features of the EMT model (it is also present for slightly different reasons in the TTI version (Schreiber et al., 2004b; Tsugawa and Osaki, 1997a)). While the general luminosity rise in quiescence is not observed in real systems and is one of the weaknesses of the DIM (Smak, 2000) the increase of the normal outburst peak luminosity

might have been observed in some systems (e.g. V1504 Cyg, V344 Lyr, see Cannizzo et al. (2012).

The superoutburst precursor is typical of both the EMT and TTI models (Schreiber et al., 2004b). Owing to mass accumulation, the disc arrives to a state where after the rise of a normal outburst the cooling front is no longer able to propagate - the disc becomes stuck in the hot state and a superoutburst begins. This last normal outburst leading to a superoutburst appears as its precursor in the light curve.

However, there is the problem with such normal outburst appearing between superoutbursts. When one compares the model light curve to that of PTF1J0719 one notes that in our model the amplitude of normal outbursts is larger by 0.5 mag and their duration is four times longer. The normal outburst duration is extended by the $\dot{M}_{\rm tr}$ enhancement and the high amplitude is the result of the assumed α-ratio - a lower ratio would result in a lower amplitude. However, lowering this ratio would also lower the superoutburst amplitude and shorten the recurrence times. Tuning the parameters to obtain a better agreement does not make much sense in view of the arbitrariness of the mass transfer prescription and of the uncertainties of the DIM itself.

4.5.3.3 The light curves inspired by CR Boo and V803 Cen

The mass-transfer rates attributed to both CR Boo and V803 Cen (see Table 4.1) are very close to the critical ones and a phenomenon analogous to Z Cam standstills could be expected for this systems. The main difference is that Z Cam stars have no superoutbursts. We will test the Z Cam model (Buat-Ménard et al., 2001b) by combining its mass-transfer modulations with the EMT. Dips might or might not be related to the cycling states. They are very similar to those observed during the decay from superoutbursts in WZ Sge-type stars. If common to both systems, the dip origins are not connected to the value of the mass-transfer rate but would instead result from the very compact size of their orbit. We tested a simple hypothesis based on this assumption.

Adapting the Z Cam models from Buat-Ménard et al. (2001b) to AM CVn stars, we assumed the mass-transfer to be modulated as $\Delta\dot{M}_{\rm tr}/\dot{M}_{\rm tr} = 40\%$ around an average rate close to the critical ($\langle\dot{M}_{\rm tr}\rangle = 1.1 \times 10^{17}$ g/s) with the modulations occurring at $t = 10 + k \cdot 70$ d. In other words we force $\dot{M}_{\rm tr}$ to increase by 40% ($\dot{M}_{\rm trmod} = \langle\dot{M}_{\rm tr}\rangle + 40\%\langle\dot{M}_{\rm tr}\rangle = 1.54 \times 10^{17}$ g/s) and keefuture workp this level for 10 d. Next $\dot{M}_{\rm tr,mod}$ falls to the value by 40% lower than the average value $\langle\dot{M}_{\rm tr}\rangle$ (i.e. to $\dot{M}_{\rm tr,mod} = 0.66 \times 10^{17}$ g/s) and maintains it for 70 d after which it is forced to rise again. To take into account the presence of irradiation-induced superoutbursts, we combined this modulation with the mass-transfer modulations given by Eq.(4.12) with the actual value of the mass-transfer rate instead of $\dot{M}_{\rm tr,0}$ (we put $\dot{M}_{\rm tr,0} = \dot{M}_{\rm tr,mod}$ into Eq.(4.12)). Choosing as typical parameters $\alpha_{\rm c} = 0.04$, $\alpha_{\rm h} = 0.2$, $M_1 = 1.0\,{\rm M}_\odot$, $\langle R_{\rm d}\rangle = 1.0 \times 10^{10}$ cm and $\gamma = 0.7$ we obtained the light curve shown in Fig.4.13A, Fig.4.13B shows the modulation of $\dot{M}_{\rm tr}$.

This light curve shows superoutbursts and standstills, as expected, but features resulting from the superposition of both types of modulations are also present in the form of "dips". The hypercycle (the cycle between two consecutive superoutbursts followed by a standstill) starts with a major $\dot{M}_{\rm tr}$ enhancement due to γ (about day 70 in Fig.4.13A). During the decay from the superoutburst maximum,

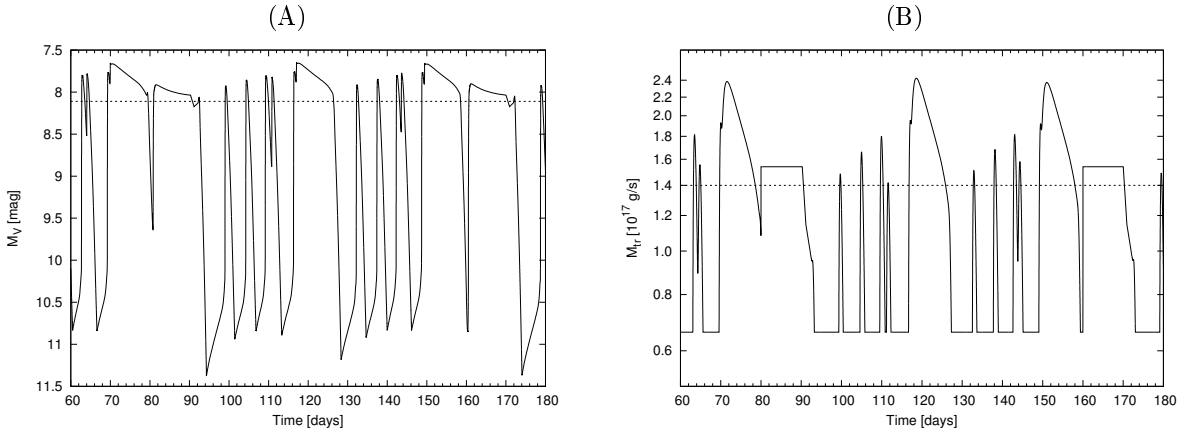

Figure 4.13: Light curve of a superoutbursting helium "Z Cam" star. The parameters are:$\alpha_{\rm c} = 0.04$, $\alpha_{\rm h} = 0.2$, $M_1 = 1.0\,{\rm M}_\odot$, $\langle \dot{M}_{\rm tr} \rangle = 1.1 \times 10^{17}$ g/s, $\Delta \dot{M}_{\rm tr} = 0.4\,\langle \dot{M}_{\rm tr} \rangle$, $t_{\rm high} = 10$ d, $t_{\rm low} = 70$ d, $\gamma = 0.7$, $\langle R_{\rm d} \rangle = 1.0 \times 10^{10}$ cm. The dotted lines correspond to the hot stability limit. (A): the model light curve, (B): $\dot{M}_{\rm tr}$ modulations.

the fall of $\dot{M}_{\rm tr}$ is quenched by a rising modulation through $\langle \dot{M}_{\rm tr} \rangle + \Delta \dot{M}_{\rm tr}$. The mass-transfer rate then rises again (around day 80) and the decay from maximum is reversed by a resulting outside-in heating front that catches up with the propagating cooling front before the latter reaches the inner disc edge - hence a dip-like feature. During the following superoutburst a slight difference in phase of the two mass-transfer modulations allows the cooling front to propagate almost to the disc's inner end. A similar mechanism produces the dip in narrow outburst preceding the superoutburst.

This suggest that dips and cycling-state features might result from mass transfer modulations triggering cooling/heating front "catching" and not from reflections. On the other hand, the indentation at the end of the standstill is the result of cooling front reflection (as described e.g. in Dubus et al. (1999)). In any case, the presumed Z Cam-effect mechanism applied to outbursting AM CVns produced the required type of light curve combining superoutbursts with standstills (and normal outbursts).

Since in AM CVn light curves other peculiar features are present in addition to standstills, we tried other simple forms of mass transfer rate modulations.

Then we tried to modify Eq.(4.12) with the *sine* function

$$\dot{M}_{\rm tr} = \max(\dot{M}_{\rm tr,0}(1 + A \sin(C + \pi t/\tau), (\gamma \dot{M}_{\rm accr}))) \tag{4.13}$$

where A, C (dimensionless) and τ (time) are adjustable constants; t is the time coordinate.

With $M_1 = 1.0\,{\rm M}_\odot$, $\dot{M}_{\rm tr} = 1.1 \times 10^{17}$ g/s and $\langle R_{\rm d} \rangle = 1.0 \times 10^{10}$ cm, $\alpha_{\rm c} = 0.04$, $\alpha_{\rm h} = 0.2$, choosing $A = 0.5$, $C = 2.0$, $\tau = 1$ d and $\gamma = 0.8$, one obtains the light curve shown in Fig.4.14A, the $\dot{M}_{\rm tr}$ modulations are shown in Fig.4.14B. One remarks superoutbursts with amplitude $A_{\rm s} \sim 3$ mag, duration $T_{\rm s} \sim 15$ d and recurrence time of $T_{\rm recc,s} \sim 27$ d. These are "standard" EMT, γ-enhancement triggered outbursts.

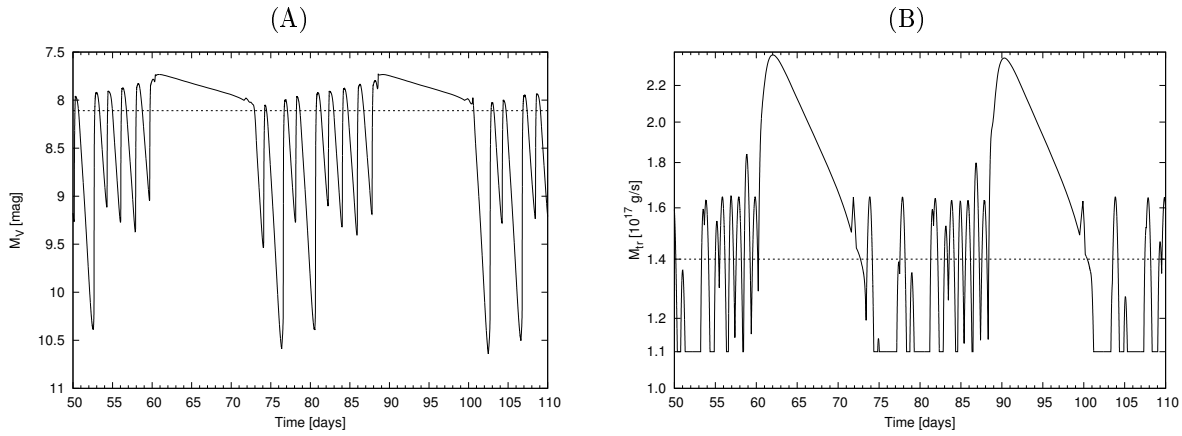

Figure 4.14: Light curve corresponding to sinusoidal+γ modulations of the mass-transfer rate. The parameters are $\alpha_{\rm h} = 0.2$, $\alpha_{\rm c} = 0.04$, $\dot{M}_{\rm tr,0} = 1.1 \times 10^{17}$ g/s, $M_1 = 1.0\,{\rm M}_\odot$, $\langle R_{\rm d} \rangle = 1.0 \times 10^{10}$ cm, $\gamma = 0.8$, $A = 0.5$, $C = 2.0$, $\tau = 1$ d. The dotted lines correspond to the hot stability limit. (A): the model light-curve. (B): $\dot{M}_{\rm tr}$ modulations.

In addition, short outbursts with a repetition time of ~ 1.8 d and an amplitude $\sim 1.2 - 2.4$ mag appear during the decay from superoutburst and persist until the following one. One is of course tempted to identify them with the cycling states of CR Boo or V803 Cen. The origin of these short outbursts is quite simple to understand. At the end of the decay of $\dot{M}_{\rm tr}$ from the superoutburst value, the sinusoidal enhancement of $\dot{M}_{\rm tr}$ dominates over the γ-induced $\dot{M}_{\rm tr}$ fluctuations. This short enhancement of $\dot{M}_{\rm tr}$ results in a low-amplitude, short outburst (starting at day ~ 73 in Fig.4.14A) because the cooling front that switches off the superoutburst is quenched by a freshly triggered outside-in heating front. This happens because the post-cooling front Σ is still close to the critical value due to $\dot{M}_{\rm tr}$ enhancement through the sinusoidal modulation. However, since the disc's mass is decreasing, after one day a new cooling front forms immediately and this time it succeeds in propagating till the inner disc's rim but, because of mass accumulating, a new outburst starts immediately. All heating fronts are triggered by mass-transfer enhancement and therefore are of the outside-in type. Their maximum brightness is slightly increasing because of mass accumulation. Their amplitude depends on the combined strengths of the sinusoidal plus γ enhancement. If the enhancement brings $\dot{M}_{\rm tr}$ above $\dot{M}^{+}_{\rm crit}$, the resulting short outburst will have a small amplitude as the outside-in heating front forms easily and promptly catches up with the cooling front that quenches it. But when the disc's mass is still quite low and the $\gamma + sine$ enhancement is not powerful enough to bring $\dot{M}_{\rm tr}$ above $\dot{M}^{+}_{\rm crit}$, the cooling front will propagate unhindered till the low-luminosity level (see e.g. day 81).

We tried also the simpler version of Eq.(4.14) to test the sinusoidal $\dot{M}_{\rm tr}$ modulations alone. We take $\dot{M}_{\rm tr}$ as

$$\dot{M}_{\rm tr} = \dot{M}_{\rm tr,0}(1 + A\sin(C + \pi t/\tau)) \tag{4.14}$$

The other examples of light curves which can be obtained using either of the two prescriptions for $\dot{M}_{\rm tr}$, Eq.(4.13) or Eq.(4.14) by playing with the parameters are presented in Fig.4.16 and Fig.4.15.

There are several observations to be made:

1. The *sine*-modulation favors the appearance of many short rebrightenings of various amplitudes. The reason is the gradual increase of $\dot{M}_{\rm tr}$ which takes place not only during the outburst maximum but also during the outburst decay and quiescence and which destabilizes the outer parts of the disc as was described above. In the case when the amplitude A of the *sine* function is high (i.e. $A > 1$) (e.g. Fig.4.16B) more mass is added to the disc and the resulting outbursts tend to be longer and less frequent.

2. The truncation of the inner disc by the primary white dwarf magnetic field stabilizes the disc because in this case Σ in the disc is in general higher - the rapid eruptions disappear - Fig. 4.15B, Fig. 4.16C. The effect of the hot spot heating is not so noticeable (the hot spot is added in all models but one in Fig. 4.14B).

3. While the *sine*-enhancement of $\dot{M}_{\rm tr}$ leads to periodic recurrence of the light curve pattern, the interplay between γ and *sine* modulations in Eq.(4.13) leads to high irregularity and the variety of features which can be obtained in the light curves (compare light curves in Fig.4.14 and in Fig.4.15).

4. The dip arises when the γ-induced superoutburst decay is stopped by the sinusoidal increase of $\dot{M}_{\rm tr}$ - Fig.4.15A and B.

5. The problem is the quiescence - due to the considerable $\dot{M}_{\rm tr}$ enhancements it is short or completely disappears.

One concludes, therefore that suitable modulations of the mass transfer rate can produce various observed features of outbursting AM CV light curves even with the simplest assumptions about their shapes. However, the mechanisms that are able to produce mass-transfer modulations are still to be firmly identified. There is no doubt that mass-transfer rates in close binaries are highly variable, in some cases with huge amplitudes. Although irradiation of the secondary is the usual suspect, in many cases the observed variability (e.g. of AM Her or VY Scl stars, see Warner (2003)) is not caused by variable irradiation. A periodic modulation of mass transfer rate could be also achieved through the presence of a warped/tilted disc (Smak, 2011). The sinusoidal variation of Eq.(4.13) or (4.14) could be considered an attempt to represent the effect of the variable irradiation if the modulation time $\tau = 1$ d could find a convincing interpretation in this context. The observation of negative superhumps in outbursting AM CVn stars would be the additional argument for the tilted discs and EMT model acting in those systems (Smak, 2009d).

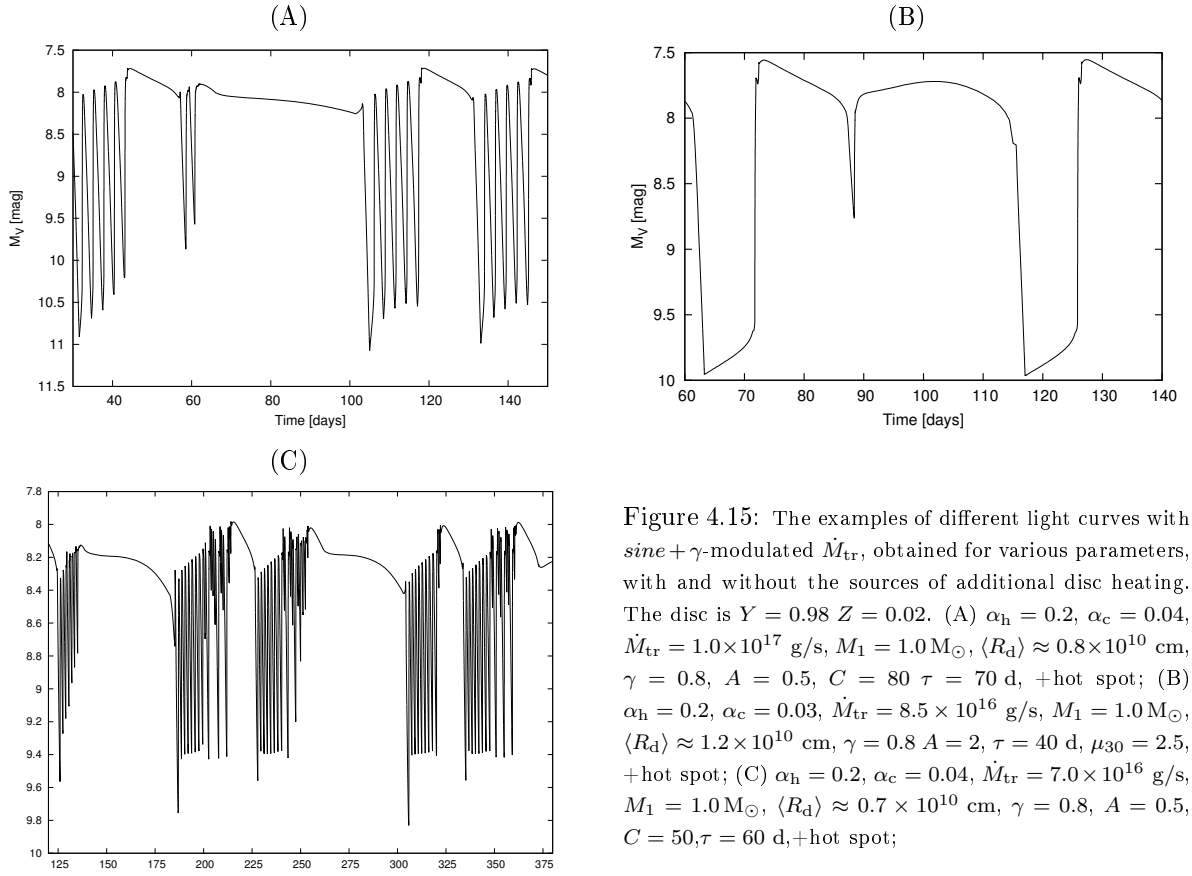

Figure 4.15: The examples of different light curves with *sine*+γ-modulated $\dot{M}_{\rm tr}$, obtained for various parameters, with and without the sources of additional disc heating. The disc is $Y = 0.98$ $Z = 0.02$. (A) $\alpha_{\rm h} = 0.2$, $\alpha_{\rm c} = 0.04$, $\dot{M}_{\rm tr} = 1.0{\times}10^{17}$ g/s, $M_1 = 1.0\,{\rm M}_{\odot}$, $\langle R_{\rm d}\rangle \approx 0.8{\times}10^{10}$ cm, $\gamma = 0.8$, $A = 0.5$, $C = 80$ $\tau = 70$ d, +hot spot; (B) $\alpha_{\rm h} = 0.2$, $\alpha_{\rm c} = 0.03$, $\dot{M}_{\rm tr} = 8.5 \times 10^{16}$ g/s, $M_1 = 1.0\,{\rm M}_{\odot}$, $\langle R_{\rm d}\rangle \approx 1.2{\times}10^{10}$ cm, $\gamma = 0.8$ $A = 2$, $\tau = 40$ d, $\mu_{30} = 2.5$, +hot spot; (C) $\alpha_{\rm h} = 0.2$, $\alpha_{\rm c} = 0.04$, $\dot{M}_{\rm tr} = 7.0{\times}10^{16}$ g/s, $M_1 = 1.0\,{\rm M}_{\odot}$, $\langle R_{\rm d}\rangle \approx 0.7 \times 10^{10}$ cm, $\gamma = 0.8$, $A = 0.5$, $C = 50$,$\tau = 60$ d,+hot spot;

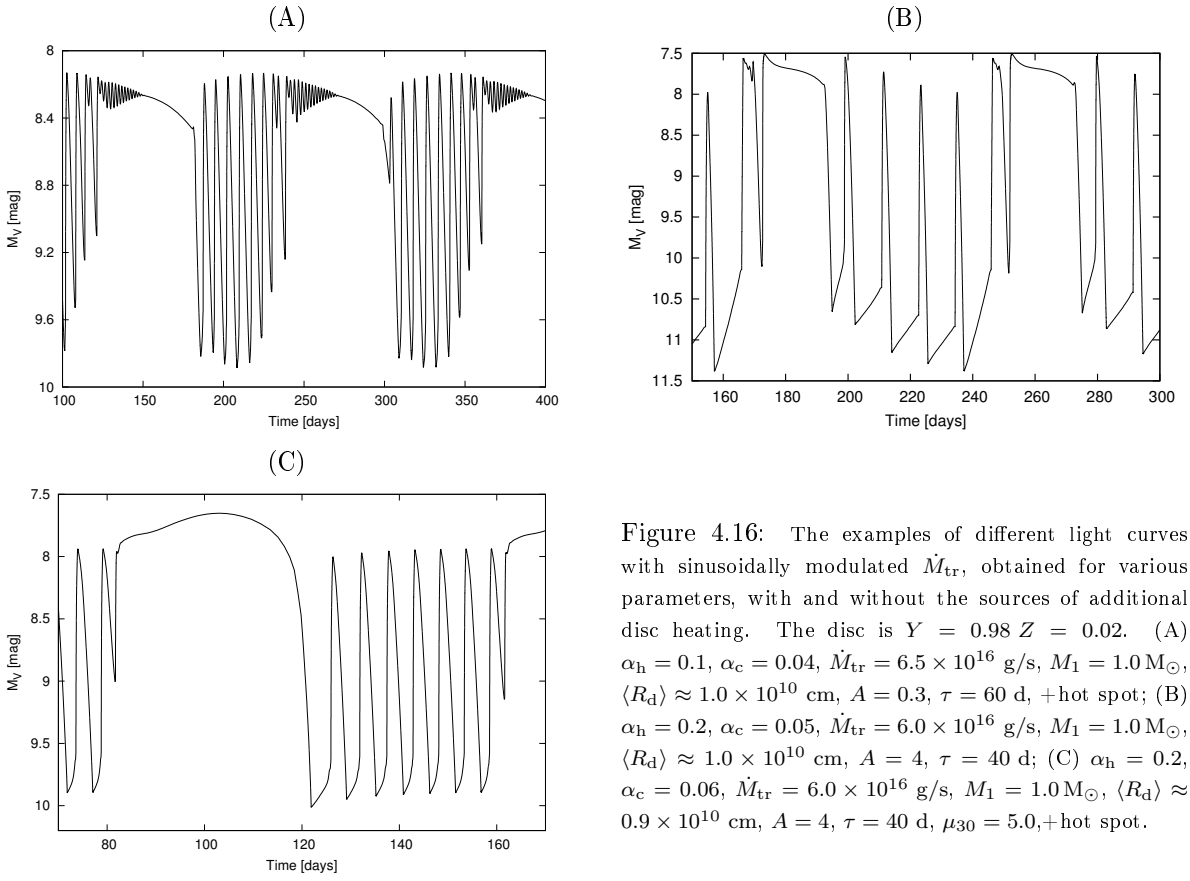

Figure 4.16: The examples of different light curves with sinusoidally modulated $\dot{M}_{\rm tr}$, obtained for various parameters, with and without the sources of additional disc heating. The disc is $Y = 0.98$ $Z = 0.02$. (A) $\alpha_{\rm h} = 0.1$, $\alpha_{\rm c} = 0.04$, $\dot{M}_{\rm tr} = 6.5 \times 10^{16}$ g/s, $M_1 = 1.0\,{\rm M}_\odot$, $\langle R_{\rm d} \rangle \approx 1.0 \times 10^{10}$ cm, $A = 0.3$, $\tau = 60$ d, +hot spot; (B) $\alpha_{\rm h} = 0.2$, $\alpha_{\rm c} = 0.05$, $\dot{M}_{\rm tr} = 6.0 \times 10^{16}$ g/s, $M_1 = 1.0\,{\rm M}_\odot$, $\langle R_{\rm d} \rangle \approx 1.0 \times 10^{10}$ cm, $A = 4$, $\tau = 40$ d; (C) $\alpha_{\rm h} = 0.2$, $\alpha_{\rm c} = 0.06$, $\dot{M}_{\rm tr} = 6.0 \times 10^{16}$ g/s, $M_1 = 1.0\,{\rm M}_\odot$, $\langle R_{\rm d} \rangle \approx 0.9 \times 10^{10}$ cm, $A = 4$, $\tau = 40$ d, $\mu_{30} = 5.0$,+hot spot.

Chapter 5

α in accretion discs

The mechanism of the angular momentum transport has been a matter of debate since the very beginning of the theory of accretion discs. The Shakura-Sunyaev α-parametrization does not explains it but it gives the tool to investigate the disc properties without the need of answering this question.

The theory which will describe the viscosity in the disc has to be consistent with the observations, in particular it has to predict the values of α which are appropriate for outbursts of dwarf novae.

Unfortunately , the values of α found from the MRI, which is so far the best candiate for the mechanisms explaining the viscosity in the disc, are an order of magnitude lower ($\alpha_{\rm MRI} \sim 0.01$) than those deduced from observations for hot discs ($\alpha \sim 0.1-0.2$) (Hirose et al., 2009). Another problem is that MRI does not predict how much the different the values of α for quiescence and outburst should be. The simulations clearly show that the amplitude of dwarf novae outbursts may be reproduced only when $\alpha_{\rm c}$ in the cold disc is $\sim 4-5$ times smaller than $\alpha_{\rm h}$ the hot disc. In some AM CVn stars $\alpha_{\rm h}/\alpha_{\rm c} \approx 2$ is sufficient.

The first to evaluate α from observations was Smak (1999) (hereafter S99). We verify the observation-deduced values of α using new set of data and methods which in part are different from those used in Smak (1999).

First we estimate $\alpha_{\rm h}$ from the comparison between observational light curves and models. This method was used by Smak (1999) with the result that $\alpha_{\rm h}$ is ≈ 0.2. We also derive the decay time semi-analytically and check what α we need in the calculations to arrive to the decay times comparable with those measured from observations. Next from the DIM we determine an amplitude vs recurrence-time relation and compare it to the empirical Kukarkin-Parenago relation (hereafter K-P relation) between the same, but observed, quantities.

5.1 The decay time

The values of α which can be deduced from observations of dwarf-nova decay from outburst maximum are almost model-independent. Basically one only assumes that the decay time is determined by the

viscous timescale $t_{\rm visc}$ in the hot disc.

Since $t_{\rm visc} \sim R^2/\nu$, assuming that the kinematic viscosity coefficient $\nu \sim \alpha c_{\rm s} H$, where $c_{\rm s}$ is the sound speed and H the disc semi-thickness, determining the decay time allows estimating α. To do that one has to estimate the disc radius e.g. from the binary's orbital period (Eq.(5.1) and (5.2)). Using this method S99 obtained an observational relation between the outburst decay rate $\tau_{\rm dec}$ (or alternatively the outburst width W) and the orbital period $P_{\rm orb}$: $\tau_{\rm dec}(P_{\rm orb})$ and $W(P_{\rm orb})$. Comparing these relations with the relations of the same type found from the fits to data from the numerical models he concluded that the best agreement between observation and models is obtained for $\alpha_{\rm h} = 0.2$. Below, we determine the viscosity parameter using a different DN sample and different numerical models.

5.1.1 The decay rate vs. the disc radius relation

To assure that the result is independent from the choice of the observational data we took into account 21 systems among which only 9 are in common with S99. The systems included in our sample of dwarf novae are listed in Table 5.1: U Gem- type binaries (rows $1-8$) and the decay rates for the normal outbursts in SU UMa-type binaries (rows $14-20$) are taken from Ak et al. (2002); in rows $9-13$ are 7 U Gem-type dwarf novae not included in Ak et al. (2002) for which we have measured the decay rates ($\tau_{\rm dec}$) from their light curves obtained from AFOEV database. We have measured $\tau_{\rm dec}$ as the time it takes the system brightness to decline by ~ 1 mag starting from the level 1 mag below the maximum. The last row stands for the only AM CVn-type star for which the existence of the normal outbursts have been confirmed (Levitan et al., 2011). S99 uses dwarf novae with measured decay rates and orbital periods ($P_{\rm orb}$) given in van Paradijs (1983) and Warner (2003) including all types of DNs: U Gem, SU UMa and Z Cam.

First, we mark all 21 systems on the $\tau_{\rm dec} - P_{\rm orb}$ plane and find the coefficient C_τ of the linear fit to the data of the form $\tau_{\rm dec} = C_\tau P_{\rm orb}$ to confront it with the coefficient $C_{\tau,{\rm S99}}$ obtained by S99. The fit to our data gives $C_\tau = 0.37 \pm 0.03$ with dispersion $rms = 0.698$ which compares nicely with the result of S99: $C_{\tau,{\rm S99}} = 0.38 \pm 0.02$ with $rms = 0.54$.

Considering the more general case when the $\tau_{\rm dec} - P_{\rm orb}$ relation takes the power-law form $\tau_{\rm dec} = C^1_\tau {P_{\rm orb}}^\beta$ we get $C^1_\tau = 0.69 \pm 0.17$ and $\beta = 0.66 \pm 0.14$ with dispersion $rms = 0.64$. The S99 result is $C^1_{\tau,{\rm S99}} = 0.61 \pm 0.07$ and $\beta_{\rm S99} = 0.71 \pm 0.09$ with dispersion $rms = 0.48$. Our results are similar to those of S99 within the uncertainty of the fit coefficients.

To compare the model decay times with those observed during dwarf-nova outbursts we have to convert orbital periods of observed systems into the disc radii because models are calculated not for a given $P_{\rm orb}$ but for a given disc radius.

The outer disc radius in dwarf novae expands up to $R_{\rm d,max} \sim 0.9 R_{\rm R1}$ (see e.g. Smak (2001)) during the outbursts. $R_{\rm R1}$ is the radius of a primary Roche lobe given by Eggleton (1983):

$$R_{\rm R1} = a \left(\frac{0.49}{0.6 + q^{2/3} \ln\left(1 + q^{-1/3}\right)} \right) \tag{5.1}$$

	System	$P_{\rm orb}$	M_1	M_2	$R_{\rm d,max}$	W	${\tau_{\rm dec}}^o$	${\tau_{\rm dec}}^t_{0.2}$
1	BV Cen	14.67	1.24	1.1	9.76	20.9	5.7	5.47
2	AT Ara	9.02	0.53	0.42	5.354	4.1	2.3	1.98
3	RU Peg	8.99	1.21	0.94	7.05	7.2	3.2	2.75
4	Mu Cen	8.21	1.2	0.99	6.586	7.9	3.1	4.15
5	SS Cyg	6.6	0.81	0.55	5.069	6.4	2.5	1.89
6	TW Vir	4.38	0.91	0.4	4.168	3.7	0.8	1.82
7	SS Aur	4.33	1.08	0.39	4.462	4.3	1.6	1.48
8	UGem	4.25	1.2	0.42	4.58	3.2	1.3	1.32
9	EY Cyg	11.02	1.1	0.49	8.201	14.3	4.29	2.83
10	DX And	10.57	1.2	0.8	7.923	12.5	3.47	2.90
11	EX Dra	5.04	0.75	0.56	4.097	?	2.63	2.01
12	BD Pav	4.30	1.15	0.73	4.307	?	2.96	1.54
13	IP Peg	3.797	1.16	0.55	4.077	?	2.16	1.75
14	CU Vel	1.884	1.23	0.15	2.988	4.5	1.1	1.05
15	WX Hyi	1.796	0.9	0.16	2.519	4.0	0.9	1.55
16	Z Cha	1.788	0.84	0.13	2.503	3.7	1.0	1.24
17	VW Hyi	1.783	0.67	0.11	2.292	4.0	0.7	0.90
18	OY Car	1.515	0.64	0.086	2.07	4.7	0.8	0.74
19	Ek TrA	1.509	0.46	0.09	1.775	3.0	0.7	0.50
20	SW UMa	1.364	0.71	0.1	1.987	7.6	0.6	0.49
21	PTF1J0719	0.446	0.5	0.05	0.871	1.0	0.25	0.79

Table 5.1: The orbital period $P_{\rm orb}$ is in hr, the primary and secondary masses, M_1 and M_2 , are in $\rm M_\odot$ units, the observed outburst width W is in days, ${\tau_{\rm dec}}^o$, ${\tau_{\rm dec}}^t_{0.2}$ are the observational decay rate and theoretical decay rate calculated for $\alpha_{\rm h} = 0.2$ respectively in days per magnitude and maximum disc radius $R_{\rm d,max}$ is in 1.0×10^{10} cm. Rows: $1-8$: U Gem stars from Ak et al. (2002), $9-13$: U Gem stars with $\tau_{\rm dec}$ calculated by authors from light curves from AFOEV database, $14-20$: SU UMa stars fromAk et al. (2002), 21: AM CVn star from Levitan et al. (2011); $P_{\rm orb}$, M_1 and M_2 are taken from Ritter and Kolb (2003); $R_{\rm d,max}$ is calculated according to Eqs. (5.1) & (5.2).

where

$$a = 2.3 \times 10^9 M_1^{1/3} (1+q)^{1/3} P_{\rm min}^{2/3} \ {\rm cm} \tag{5.2}$$

is the orbital separation, $q = M_2/M_1$ and $P_{\rm min}$ is the orbital period in minutes.

A primary and a secondary masses (M_1 and M_2) are taken from the most recent version (November 2011) of Ritter and Kolb (2003). For PTF1J0719 M_1 and M_2 remain unknown so their values have been guessed according to what is expected for AM CVn stars.

Once the system's orbital periods are converted into the maximum radii of their discs the linear fit to all data from Table 5.1 of the form $\tau_{\rm dec} = A_1 R_{\rm d,max}$ gives $A_1 = 0.48 \pm 0.02$ with dispersion $rms = 0.56$.

It is interesting to check if the $\tau_{\rm dec} - R_{\rm d,max}$ relation is independent of the class of systems exhibiting normal outbursts and chemical composition of the disc. Since the basic DIM (with no mass transfer rate enhancement or the additional sources of a disc heating) is able to reproduce normal outbursts only (see Sect.4 and e.g. Lasota (2001)) we find it reasonable to start with U Gem-type systems, where only normal outbursts are present and then we enrich the sample with SU UMa stars and the PTF1J0719.

The $\tau_{\rm dec} - R_{\rm d,max}$ relation for U Gem-type binaries is to a good approximation linear. For the linear fit one obtains $A_1 = 0.49 \pm 0.03$ with dispersion $rms = 0.68$. The coefficients for the general relation $\tau_{\rm dec} = B_1 {R_{\rm d,max}}^{\gamma}$ are $B_1 = 0.27 \pm 0.12$ and $\gamma = 1.32 \pm 0.22$ with $rms = 0.66$. In this case, similar to what was noticed by S99, the rms dispersions do not differ significantly for the linear and non-linear fit, moreover the errors of B_1 and γ are rather large. Therefore we limit our further considerations to the simpler, linear case.

According to the model, the outbursts appearing between superoutbursts of SU UMa stars have the same origin as those in U Gem-type binaries. As expected, their measured $\tau_{\rm dec}$ marked on the $\tau_{\rm dec} - R_{\rm d,max}$ plane extrapolate the $\tau_{\rm dec} - R_{\rm d,max}$ relation for U Gem to the regime of orbital periods shorter than 2 hr. The coefficient A_1 of the linear fit for the sample including the normal outbursts of U Gem-type and SU UMa-type DN is $A_1 = 0.48 \pm 0.03$ with dispersion $rms = 0.57$.

As discussed in Kotko et al. (2012) and Sect.4.2 PTF1J0719 is the only system in the AM CVn class of binaries where short outbursts can be firmly classified as "normal" and the system considered as a helium counterpart of an SU UMa-type DN. With PTF1J0719 taken into account the coefficient of the linear fit remains almost unchanged ($A_1 = 0.48 \pm 0.02$). We conclude that the $\tau_{\rm dec} - R_{\rm d,max}$ relation is universal for normal outbursts of all classes of cataclysmic variables.

To estimate the $\alpha_{\rm h}$ parameter one needs to find the relevant $\tau_{\rm dec} - R_{\rm d,max}$ relation for model light curves calculated with different $\alpha_{\rm h}$ and compare the results with observations. We have chosen 4 values of $\alpha_{\rm h}$: 0.05, 0.1, 0.2, 0.3 and for each of them the set of models with different mass transfer rates $\dot{M}_{\rm tr}$ (from 10^{15} to 10^{17} g/s), primary masses M_1 (from 0.6 to 1.2 $M_\odot$) and maximum disc radii $R_{\rm d,max}$ ($0.3 - 3.0 \times 10^{10}$ cm) have been calculated. The decay rates of the synthetic outbursts have been measured in the same manner as in the observational case.

Although our code (Sect.3.2) differs from the code used by S99 (for example the input parameters are different and in our code the adaptive grid enables high resolution of the fronts) the differences

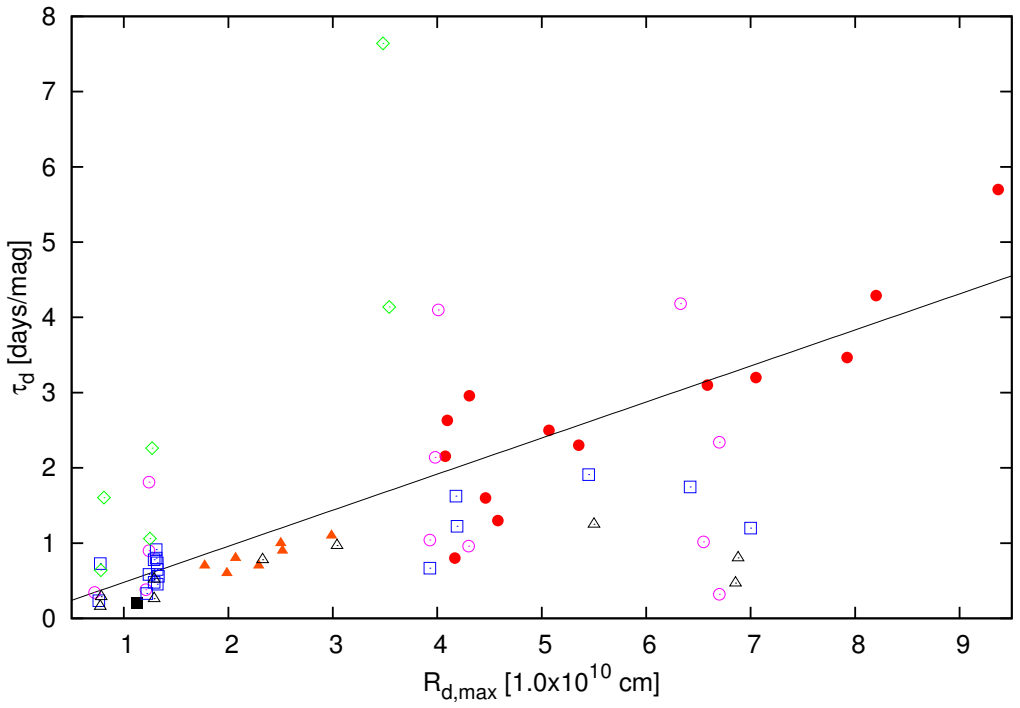

Figure 5.1: The decay rate-maximum disc radius relation. Filled symbols: U Gem-type systems (red circles), normal outbursts of SU UMa-type systems (orange triangles) and PTF1J0719 (black square). Open symbols: models with $\alpha_{\rm h} = 0.05$ (green diamonds), $\alpha_{\rm h} = 0.1$ (pink circles), $\alpha_{\rm h} = 0.2$ (blue squares), $\alpha_{\rm h} = 0.3$ (black triangles). The solid line - linear fit to the observational data (filled symbols) in the form $\tau_{\rm dec} = A_1 R_{\rm d,max}$ with $A_1 = 0.48$.

should not affect modeling of the decay phase of the outburst.

When measuring $\tau_{\rm dec}$ of the outbursts for a wide range of model parameters one has to pay attention to the several problems:

(a) For large discs ($R_{\rm d,max} > 5.0 \times 10^{10}$ cm) and high primary masses ($M_1 > 1.0\,{\rm M}_\odot$) the reflares appear during the decline from maximum (Sect.2.23). In this case the model outburst cannot be considered as normal.

(b) In large discs and for high values of $\alpha_{\rm h}$ inside-out heating fronts may not be able to propagate up to the outer disc edge because such values of the viscosity parameter decrease the value of $\Sigma^{+}_{\rm crit}$ (see the formulae in Appendix A) and, with increasing R, increases the possibility that a cooling front will form right behind the heating front. In this case the cooling front will start at $R \ll R_{\rm d,max}$ and the decay rate will not be connected with the real extent of the disc.

(c) Models with the same parameters except for $\alpha_{\rm h}$ have different stability limits.

Those properties of the DIM have their reflection in the distribution of the model points in Fig.5.1. For large $R_{\rm d,max}$ models with higher $\alpha_{\rm h}$ tend to deviate more from the empirical $\tau_{\rm dec} - R_{\rm d,max}$ relation.

Linear fits to the $\tau_{\rm dec} = A_\alpha R_{\rm d,max}$ relation obtained for the models with different $\alpha_{\rm h}$ give:

$A_{0.05} = 1.624 \pm 0.235$ for $\alpha_{\rm h} = 0.05$

$A_{0.1} = 0.525 \pm 0.128$ for $\alpha_{\rm h} = 0.1$

$A_{0.2} = 0.338 \pm 0.036$ for $\alpha_{\rm h} = 0.2$

$A_{0.3} = 0.151 \pm 0.031$ for $\alpha_{\rm h} = 0.3$

The coefficients A_α show a clear tendency to decrease when a higher $\alpha_{\rm h}$ is set in the model. The comparison with A_1 obtained from the fits to empirical data shows that $\alpha_{\rm h} \in [0.1, 0.2]$, with no unambiguous preference for one of these values, thus confirming conclusions obtained by S99.

SU UMa-type stars and their superoutbursts provide another piece of interesting information. The decay from superoutburst may be divided in least into two phases: (i) a plateau and (ii) a fast decay phase. According to the EMT model (Sect.4.5.3.1), during the plateau phase the slow decline of the system luminosity is caused by accretion-driven depletion of the excess matter provided by the enhanced mass transfer from the secondary. This phase ends when a cooling front forms and so the following fast decline is caused by the same mechanism which produces normal outbursts. Based on this, we measured $\tau_{\rm dec}$ during the fast decay phase of SU UMa superoutbursts and found that they are approximately the same as $\tau_{\rm dec}$ measured for their normal outbursts. The same is true of the superoutbursts and normal outbursts in the models calculated with the prescription for the enhancement given in $\dot{M}_{\rm tr}$ (Hameury et al., 1997), Sect.4.5.

The decay rate in the fast decline phase was measured as the time interval between the time the system luminosity was 1 mag below the start of the decline phase to the time when the system was 2 mag below it.

This conclusion is very promising in the context of evaluation of $\alpha_{\rm h}$ in AM CVn stars. As was already mentioned, the normal outbursts in AM CVn stars are rarely detected and the outburst cycle is dominated by superoutbursts. However, with well observed fast decay phases of the superoutbursts in AM CVn stars it will be possible to estimate $\alpha_{\rm h}$ in helium-dominated discs more precisely. Unfortunately the currently available data are not of sufficient quality to permit such investigations.

5.1.2 The outburst width-orbital period relation

In van Paradijs (1983) it is showed that there exists a positive correlation between the outburst width W and the orbital period but it is concluded, however, that narrow and wide outbursts should be considered separately.

To determine consistently the outburst width in various systems the magnitude level at which it is measured has to be defined. Following van Paradijs (1983) S99 defines W as the time interval during which the system luminosity is above the level set at 2 mag below the outburst maximum.

Using data from van Paradijs (1983), S99 finds the coefficients for:

- the linear dependence in the form $W = C_{W,\rm S99} P_{\rm orb}$: $C_{W,\rm S99} = 1.39 \pm 0.06$

- the non-linear dependence in the form $W = C_{W,\mathrm{S99}} {P_{\mathrm{orb}}}^{\beta_{\mathrm{S99}}}$: $C_{W,\mathrm{S99}} = 2.01 \pm 0.29$ and $\beta_{\mathrm{S99}} = 0.78 \pm 0.11$.

Since, as S99, we find the linear fit to be of superior quality, in what follows we will not use the non-linear fitting formula. We shall also use only narrow outbursts as "generic" normal outbursts.

The linear fit to our data (which now contains 18 systems for which the measurement of the outburst width was possible) gives $C_W = 0.99 \pm 0.12$ thus the agreement with S99 is not as good as for the decay times. The analogous procedure applied to different subsets of our data gives:

- for U Gem stars from Ak et al. (2002) only: $C_W = 0.79 \pm 0.07$
- for U Gem stars from Ak et al. (2002) complemented with our measurements: $C_W = 0.90 \pm 0.10$.

One concludes that C_W depends on the choice of the DN sample.

The measurements of the outbursts width are clearly more vulnerable to uncertainties connected with the precise determination of the outburst maximum and with usually sparser data coverage of the outburst rise in comparison to the outburst decay. Moreover, except for systems observed intensively for a long time (such as the already mentioned SS Cyg or U Gem) the straightforward assessment of which outbursts are narrow and which are wide may be problematic. Nevertheless it is worth comparing observations with models as has been done in Sect.5.1.1 for τ_{dec}.

The width W of synthetic outbursts has been defined in the same manner as in observational case. Applying the linear dependence $W = C_\alpha R_{\mathrm{d,max}}$ to the same set of models as in Sect.5.1.1 one obtains:

$C_{0.05} = 3.222 \pm 1.132$ for $\alpha_{\mathrm{h}} = 0.05$

$C_{0.1} = 1.794 \pm 0.285$ for $\alpha_{\mathrm{h}} = 0.1$

$C_{0.2} = 1.502 \pm 0.112$ for $\alpha_{\mathrm{h}} = 0.2$

$C_{0.3} = 0.872 \pm 0.165$ for $\alpha_{\mathrm{h}} = 0.3$.

The comparison of the above listed C_α's with $C_1 = 1.496 \pm 0.135$ determined from the observed relation $W = C_1 R_{\mathrm{d,max}}$ favors again $\alpha_{\mathrm{h}} \in [0.1, 0.2]$ with even stronger indication of $\alpha_{\mathrm{h}} = 0.2$.

The model and observational data with fitted linear dependence between W and $R_{\mathrm{d,max}}$ are presented on Fig.5.2.

Even if W is not well enough determined to provide a firm value of α_{h} from the $W = C_1 R_{\mathrm{d,max}}$ relation, the results obtained totally preclude $\alpha_{\mathrm{h}} \ll 0.1$.

5.1.3 The decay time from the DIM

The decrease of the luminosity after the outburst maximum is the effect of two mechanisms: (1) the depletion of the matter from the disc due to the accretion onto the central object and (2) the propagation of the cooling front through the disc (Sect.2.5).

The decay time t_{dec} is the time it takes the system luminosity to drop from the maximum to the quiescence level and it may be written approximately as

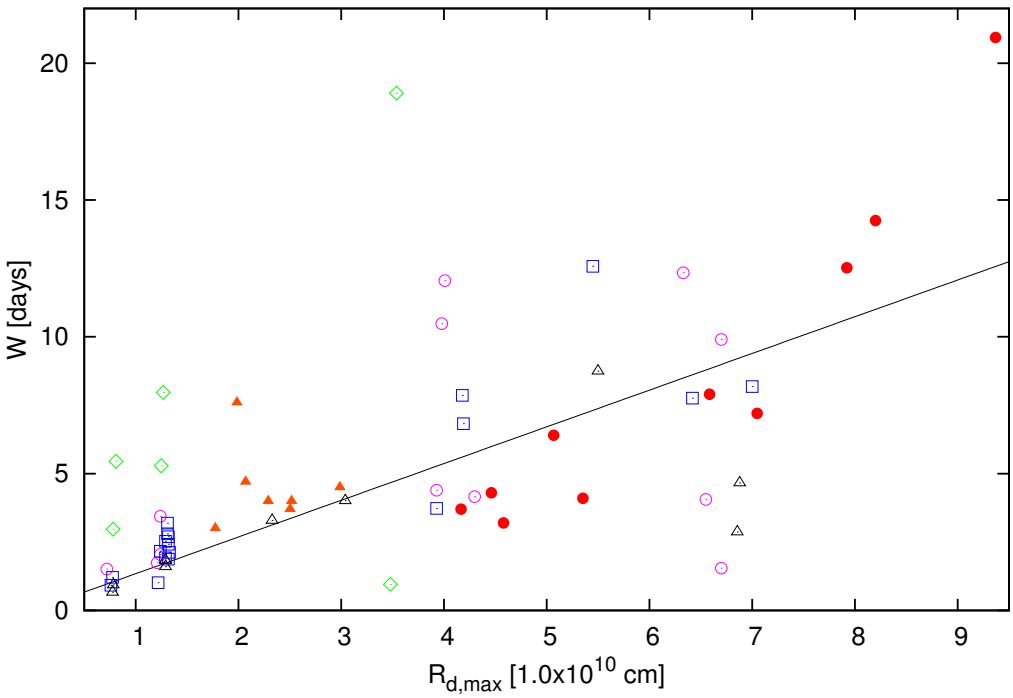

Figure 5.2: The $W - R_{\rm d,max}$ relation. Filled symbols: U Gem-type systems (red circles), normal outbursts of SU UMa- type systems (orange triangles). Open symbols: models with $\alpha_{\rm h} = 0.05$ (green diamonds), $\alpha_{\rm h} = 0.1$ (pink circles), $\alpha_{\rm h} = 0.2$ (blue squares), $\alpha_{\rm h} = 0.3$ (black triangles). The dotted line - linear fit to the observational data (filled symbols) with a coefficient $C_1 = 1.496$.

$$t_{\rm dec} \approx \frac{R_{\rm d,max}}{{\rm v}_{\rm dec}} \tag{5.3}$$

where (as before) $R_{\rm d,max}$ is the maximum disc radius and ${\rm v}_{\rm dec}$ is the decline velocity.

There are two contributions to ${\rm v}_{\rm dec}$: (a) the velocity at which the hot matter ahead the front diffuses inwards (${\rm v}_{\rm visc}$) and the velocity at which the matter outflows from the hot region into the cold region what takes place at the cooling front (${\rm v}_{\rm F}$). Therefore, ${\rm v}_{\rm F}$ rises the depletion rate of the matter from the hot region of the disc and so rises the rate at which the luminosity of the disc decreases. ${\rm v}_{\rm visc}$ and ${\rm v}_{\rm F}$ are independent velocities, in a sense that ${\rm v}_{\rm F}$ includes the effect of radial drift of matter at the front, while ${\rm v}_{\rm visc}$ defines the rate at which matter diffuses inwards in the whole hot region. Therefore, $|{\rm v}_{\rm dec}| \approx |{\rm v}_{\rm visc} + {\rm v}_{\rm F}|$.

Since ${\rm v}_{\rm visc} \approx \nu/R$, from Eq.(2.8) one has

$${\rm v}_{\rm visc} \approx \frac{2}{3}\alpha_{\rm h} c_{\rm s}^2 \frac{1}{\Omega_{\rm K} R} \tag{5.4}$$

where $c_{\rm S}^2 = P/\rho$ and P is the total pressure.

It is important to stress that H is the disc's (semi)scale-height and not the disc's actual (e.g. photospheric) height which can be larger by a factor of few. Unfortunately S99 uses the height z_0 corresponding to the optical depth ~ 1 hence the use of his formula would result in $\alpha_{\rm S99}$ that does not correspond to the α-parameter defined by the Shakura-Sunyaev prescription. Fortunately, however, S99 does not calculate $\alpha_{\rm h}$ directly from his analytical formula, only compares the theoretical and empirical dependence between the outburst decay rate (or the outburst width) and the orbital period, thus his conclusions about the value of the viscosity parameter in hot accretion discs remain valid.

From numerical simulations Menou et al. (1999) find that ${\rm v}_{\rm F} \sim 1/7\,\alpha_{\rm h} c_{\rm s}$. We confirmed this result for cooling front velocity in solar composition discs and found that it applies also to helium-dominated disc (Sect.2.7.2.2).

We take ${\rm v}_{\rm visc}$ and ${\rm v}_{\rm F}$ as the "average" velocities. In other words we assume that ${\rm v}_{\rm F}$ is approximated by its value in the asymptotic regime and that viscous velocity is the same at each radius and is approximated by its value calculated at $R_{\rm d,max}$.

The final formula for "average" $t_{\rm dec}$ is thus

$$t_{\rm dec} \approx \frac{7 R_{\rm d,max}}{\alpha_{\rm h} c_{\rm s} (1 + 14/3 (c_{\rm s} \Omega_{\rm K} R_{\rm d,max}))} \tag{5.5}$$

The speed of sound can be expressed in terms of the central temperature in the disc: $c_{\rm s} = \sqrt{kT_{\rm c}/m_{\rm H}}$, where k is the Boltzmann constant and $m_{\rm H}$ is hydrogen molecular mass (in the case of helium disc it should be replaced by helium molecular mass). The numerical fit to the temperature at the cooling front found from models of solar-composition discs gives

$$T_{\rm c} \approx 4.7 \times 10^4 \text{ K} \tag{5.6}$$

with no dependence on disc parameters.

For AM CVn stars, e.g. PTF1J0719, the chemical composition ($Y = 0.98$ $Z = 0.02$) gives

$$T_{\rm c} \approx 1.1 \times 10^5 \text{ K} \tag{5.7}$$

From Eq.(5.5) it is clear that $t_{\rm dec}$ depends on $R_{\rm d,max}$, M_1 and $\alpha_{\rm h}$. The primary mass M_1 determines the white dwarf radius R_1 through $M-R$ relation (Nauenberg, 1972). M_1 and $R_{\rm d,max}$ define the disc extend since the model assumes that the inner disc radius $R_{\rm in} = R_1$.

To compare the observational outbursts decay rates ${\tau_{\rm dec}}^o$ with the analytical decay rates ${\tau_{\rm dec}}^t$, the derived $t_{\rm dec}$ has to be divided by the amplitude of the outburst $A_{\rm n}$. For each system with measured $P_{\rm orb}$ and estimated M_1 and M_2 (necessary for calculating $R_{\rm d,max}$) there is only one free parameter left: $\alpha_{\rm h}$. Thus the conformity between the observed decay rate ${\tau_{\rm dec}}^o$ and ${\tau_{\rm dec}}^t$ calculated from Eq.(5.5) can be attained by adjusting $\alpha_{\rm h}$. We assumed $\alpha_{\rm h} = 0.2$. The calculation results are summarized in Table 5.1 and presented in Fig.5.3.

Fig.5.3 shows the dependence of decay rate $\tau_{\rm dec}$ on $R_{\rm d,max}$ for observational systems listed in Table 5.1 (red crosses) and the calculated decay rates using Eq.(5.5) for $\alpha_{\rm h} = 0.2$ (blue stars) and $\alpha_{\rm h} = 0.1$ (green crosses).

It can be seen that decay rates calculated from Eq.(5.5) follow quite close the observational ${\tau_{\rm dec}}^o(R_{\rm d,max})$ and that in most cases the calculated time for $\alpha_{\rm h} = 0.2$ is close to the observed one (Table 5.1). In few cases the discrepancy is large. It is not clear if it is due to the imprecision in measuring the decline time, the peculiar nature of the outbursts, or to the non-universal value of $\alpha_{\rm h}$. After all, since MRI does not give the correct value of this parameter we do not really know what is the physical mechanism driving accretion in hot dwarf nova discs. Hence there is no reason to assume that it is "generic".

One should keep in mind, however, that the significant impact on $\alpha_{\rm h}$ has the determination accuracy of the observed outbursts amplitudes. An underestimate of $A_{\rm n}$ may be the cause of significantly higher $\alpha_{\rm h}$ for TW Vir, WX Hyi and PTF1J0719.

5.2 The Kukarkin-Parenago relation

The first to notice the relation between an outburst amplitude $A_{\rm n}$ and its recurrence time $T_{\rm n}$ were Kukarkin and Parenago (1934). However, as their sample was based on the outbursts both in recurrent novae and dwarf novae, its relevance has been questioned (Bath and Shaviv, 1978) and it has not been used since then in its original form.

First to conclude that the $A_{\rm n}(T_{\rm n})$ correlation exists for the normal outbursts of dwarf novae was van Paradijs (1985), even though a look at Fig.5.5 induces rather skeptical attitude to this idea (see e.g. Payne-Gaposchkin (1977)).

Nowadays, for historical reasons the relation between amplitude and recurrence time of the normal outbursts in dwarf novae is still called the Kukarkin-Parenago relation (hereafter K-P relation) and its most recent form is presented in Warner (2003)

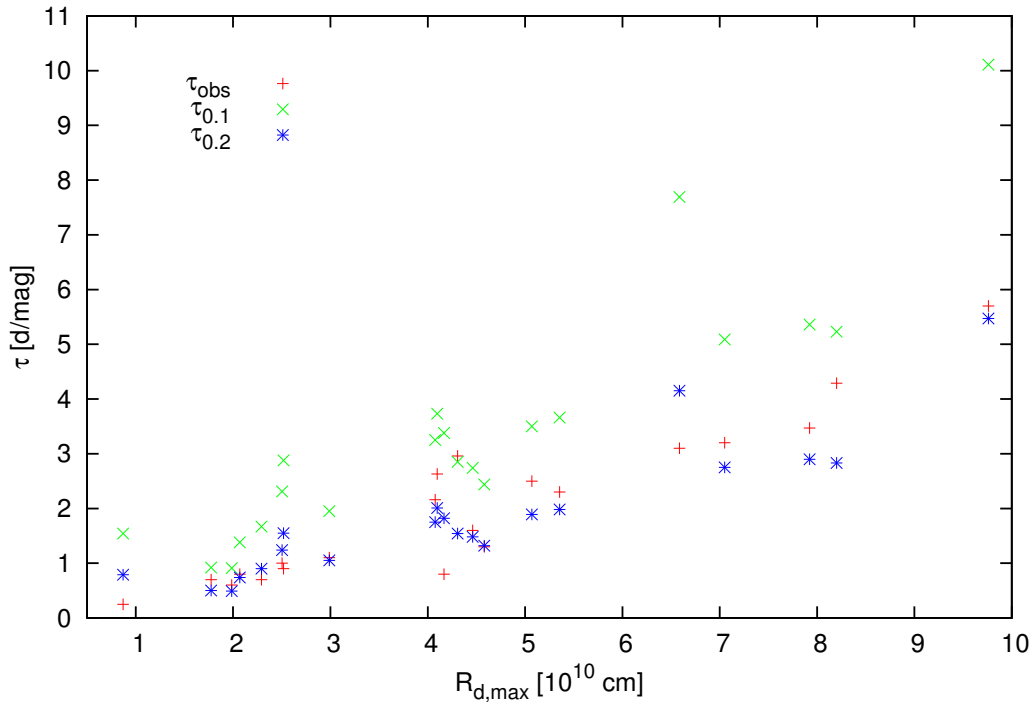

Figure 5.3: The relation between decay rate τ and maximum radius of the disc $R_{\mathrm{d,max}}$ for observational decay rate ${\tau_{\mathrm{dec}}}^{o}$ (red crosses), decay rate ${\tau_{\mathrm{dec}}}^{t}_{0.1}$ calculated from Eq. (5.5) for $\alpha_{\mathrm{h}} = 0.1$ (green crosses) and ${\tau_{\mathrm{dec}}}^{t}_{0.2}$ calculated for $\alpha_{\mathrm{h}} = 0.2$ (blue stars). ${\tau_{\mathrm{dec}}}^{t}_{0.1}$ is calculated for the same systems and system parameters as ${\tau_{\mathrm{dec}}}^{t}_{0.2}$. ${\tau_{\mathrm{dec}}}^{t}_{0.2}$ and ${\tau_{\mathrm{dec}}}^{o}$ are listed in Table 5.1.

$$A_{\rm n} = (0.7 \pm 0.43) + (1.9 \pm 0.22) \log T_{\rm n} \tag{5.8}$$

where $T_{\rm n}$ is in days and $A_{\rm n}$ in magnitudes.

Since it has been argued that the K-P relation might represent some global and average properties of DN outbursts van Paradijs (1985) it is worth trying to establish if it follows from the DIM.

While the other relations, connecting different quantities characterizing the binary system and their light curves (e.g. the $M_{\rm V,max}(P_{\rm orb})$ or the $\tau_{\rm dec}(P_{\rm orb})$ relations, see Warner (2003)) follow directly from the DIM model, the derivation of the K-P relation is not so straightforward.

Of course as the outburst amplitude is related to the mass of the disc and the mass of the disc with the accumulation time, a relation of the K-P style could be in principle expected. For example, van Paradijs (1985) speculated that the average amount of mass $\Delta M_{\rm quies}$ transferred during an average recurrence time $T_{\rm n}$: $\Delta M_{\rm quies} = T_{\rm n}\dot{M}_{\rm quies}$ is constant over the dwarf nova population but also warned about possible selection effects and model dependence. Here, we try to examine what $A_{\rm n}(T_{\rm n})$ relation can be deduced from the DIM in its simplest (and when possible simplified) form.

The mass accumulation starts during the terminal phase of the decay of the previous outburst (point 1 in Fig.5.4A) but since very little mass is accumulate during this very short short phase one can safely assume that the mass accumulation in the disc takes place during quiescence and the rise of an outburst. As can be seen from the Fig.5.4C there is no mass accretion at the disc inner edge during the quiescence, it starts to rise slightly during the rise of the outburst but the rapid depletion of the mass from the disc takes place during the outburst decay (between point 2 and 3 in Fig.5.4B).

For simplicity we will assume that accumulation rate $\dot{M}_{\rm accum}$ of the mass in the disc during quiescence is approximately equal to the mass transfer rate from the secondary $\dot{M}_{\rm tr}$ (this assumes no truncation of the inner edge of the disc; no "leaky" disc), and that the mean accretion rate during the outburst is about half the maximum accretion rate during outburst $\langle \dot{M}_{\rm outb} \rangle \approx \frac{1}{2}\dot{M}_{\rm accr,max}$.

The former is the upper limit for the mass accumulation rate, as the disc can not accumulate mass faster than it receives it, and the latter can be assumed from the shape of the function $\dot{M}_{\rm accr}(t)$ in the model which is rapidly rising and approximately exponentially decreasing during the outburst (Fig.5.4C).

It is important to recall here that one can not approximate$\dot{M}_{\rm accr,max}$ by $\dot{M}^{+}_{\rm crit}(R_{\rm d,max})$ as it is usually assumed for the hot discs, it can be seen from Fig.5.4C where green horizontal line represents $\dot{M}^{+}_{\rm crit}(R_{\rm d,max})$ which in this case is 3 times smaller than $\dot{M}_{\rm accr,max}$. The simulations clearly show that the mass accretion reaches its maximum after the cooling front starts to propagate (see Sect.2.5.3).

In the following we assume that $\dot{M}_{\rm accr,max} \approx \epsilon \dot{M}^{+}_{\rm crit}(R_{\rm d,max})$, where $\epsilon \sim 3$.

The amount of mass accreted during the outburst decay is equal to the mass accumulated in the disc during the quiescence and the rise of the outburst: $\Delta M_{\rm accr} = \Delta M_{\rm accum}$. Therefore,

$$\langle \dot{M}_{\rm outb} \rangle t_{\rm dec} = \dot{M}_{\rm tr}(t_{\rm quiesc} + t_{\rm rise}) \tag{5.9}$$

where $t_{\rm quiesc}$ is the duration of the quiescence, $t_{\rm rise}$ is the time it takes the outburst to reach its

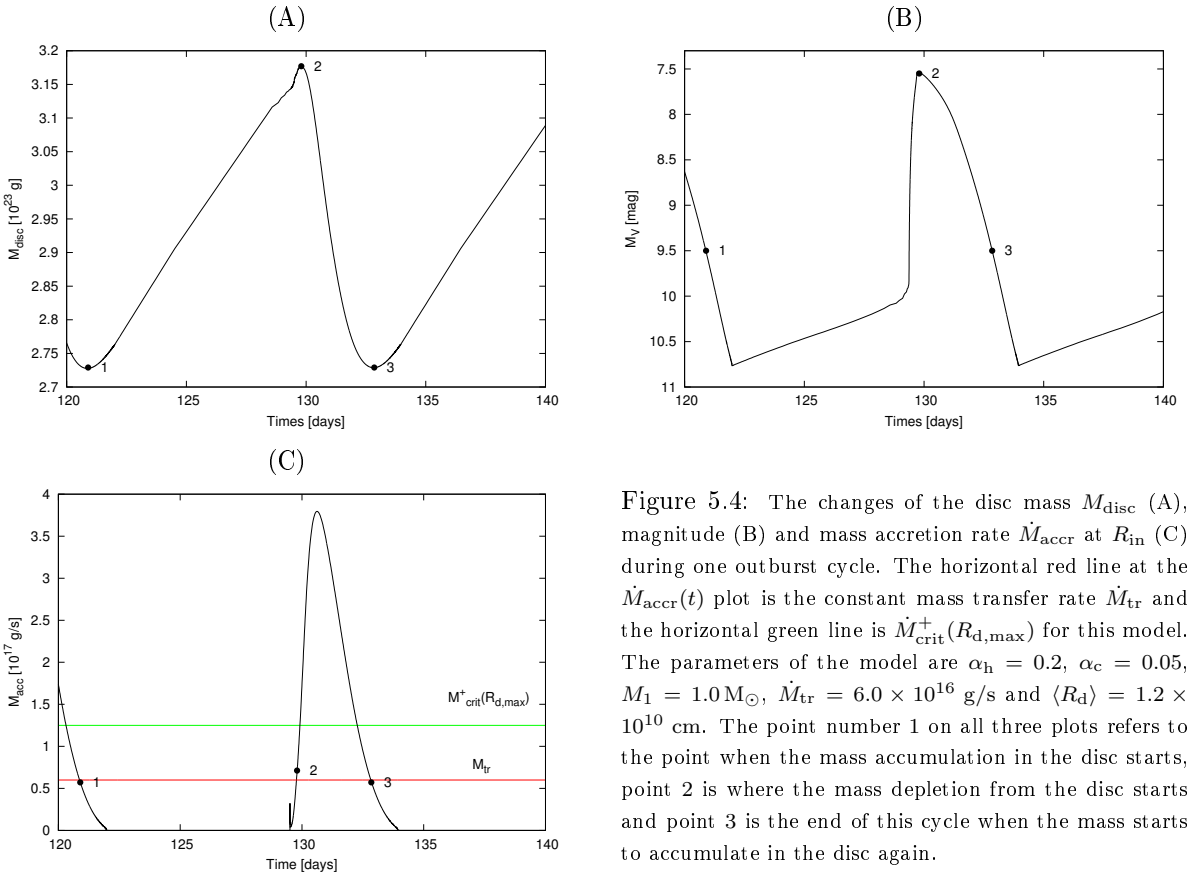

Figure 5.4: The changes of the disc mass $M_{\rm disc}$ (A), magnitude (B) and mass accretion rate $\dot{M}_{\rm accr}$ at $R_{\rm in}$ (C) during one outburst cycle. The horizontal red line at the $\dot{M}_{\rm accr}(t)$ plot is the constant mass transfer rate $\dot{M}_{\rm tr}$ and the horizontal green line is $\dot{M}^{+}_{\rm crit}(R_{\rm d,max})$ for this model. The parameters of the model are $\alpha_{\rm h} = 0.2$, $\alpha_{\rm c} = 0.05$, $M_1 = 1.0\,{\rm M}_\odot$, $\dot{M}_{\rm tr} = 6.0 \times 10^{16}$ g/s and $\langle R_{\rm d} \rangle = 1.2 \times 10^{10}$ cm. The point number 1 on all three plots refers to the point when the mass accumulation in the disc starts, point 2 is where the mass depletion from the disc starts and point 3 is the end of this cycle when the mass starts to accumulate in the disc again.

luminosity maximum and $t_{\rm dec}$ is the duration of the outburst decay to the quiescence level.

The decay time $t_{\rm dec}$ is calculated as it is described in Sect.5.1.

The outburst recurrence time $T_{\rm n}$ is counted from the onset of the outburst to the onset of the following one: $T_{\rm n} = t_{\rm rise} + t_{\rm dec} + t_{\rm quiesc}$ while the accumulation time is $t_{\rm accum} = t_{\rm quiesc} + t_{\rm rise}$ ($t_{\rm rise}$ is non negligible and it is important to include it to be able to account for the "cycling state" outbursts where no quiescence stage is present). Substituting $T_{\rm n}$ and $t_{\rm accum}$ to Eq. (5.9) gives

$$T_{\rm n} = \left(\frac{\langle \dot{M}_{\rm outb} \rangle}{\dot{M}_{\rm tr}} + 1 \right) t_{\rm dec} = \left(\frac{\dot{M}_{\rm accr,max}}{2\dot{M}_{\rm tr}} + 1 \right) t_{\rm dec} \tag{5.10}$$

Since $\dot{M}_{\rm accr,max} \approx \epsilon \dot{M}^{+}_{\rm crit}(R_{\rm d})$ and the instability condition requires $\dot{M}_{\rm tr} < \dot{M}^{+}_{\rm crit}(R_{\rm d})$ then the ratio in the brackets is $\dot{M}^{+}_{\rm crit}(R_{\rm d})/(2\dot{M}_{\rm tr}) \gg 1$ and one can take

$$T_{\rm n} \approx \frac{\epsilon \dot{M}^{+}_{\rm crit}(R_{\rm d})}{2\dot{M}_{\rm tr}} t_{\rm dec} \tag{5.11}$$

The visual luminosity in the maximum of an outburst is determined by the radiation produced in the whole hot disc:

$$L_{\rm max} = 2 \int_{R_{\rm in}}^{R_{\rm d,max}} Q^{+}(R)\, 2\pi R dR \tag{5.12}$$

From Eq.(2.55) in Sect.2.3.2 and assuming that for the discs in DN or AM CVn stars $R_1/R_{\rm d,max} \ll 1$ is a reasonable approximation, the luminosity at the outburst maximum can be taken as

$$L_{\rm max} \approx \frac{GM_1 \epsilon \dot{M}^{+}_{\rm crit}(R_{\rm d})}{2R_1} \tag{5.13}$$

where R_1 is a white dwarf radius and M_1 is its mass.

In the quiescence it is mainly the outer region of the disc which contributes to the luminosity at minimum light (we do not consider here the contributions from the hot spot and the secondary).

Since the disc in the quiescence is in thermal equilibrium but it is not in the viscous equilibrium ($\dot{M}_{\rm accr} \neq$ const) the equation (2.53) can not be applied to calculate $L_{\rm min}$.

From the equations describing non stationary disc (Sect.2.3) the radial velocity $\mathrm{v_R}$ is given by

$$\mathrm{v_R} = -\frac{3}{\Sigma\sqrt{\mathrm{R}}} \frac{\partial}{\partial \mathrm{R}} [\nu\Sigma\sqrt{\mathrm{R}}]. \tag{5.14}$$

From Eq.(5.14) and the definition of the mass accretion rate $\dot{M}_{\rm accr} \equiv 2\pi R \Sigma\, \mathrm{v_R}$ ($\mathrm{v_R} < 0$) one obtains

$$\dot{M}_{\rm accr} = 3\pi\nu\Sigma \left(2\frac{\partial \ln(\nu\Sigma)}{\partial \ln R} + 1 \right) \tag{5.15}$$

The Eq.(5.15) is the linear inhomogeneous differential equation with respect to $\nu\Sigma$ and taking into account the boundary condition at the disc inner edge $\nu\Sigma(R_1) = 0$ its solution may be written in the

form

$$\nu\Sigma = u(R,t)\left(1-\sqrt{\frac{R_1}{R}}\right). \tag{5.16}$$

Substituting $\nu\Sigma$ given by Eq.(5.16) to Eq.(5.15) and rearranging the terms gives

$$\dot{M}_{\rm accr} = 3\pi\nu\Sigma\left[2\frac{\partial \ln u(R,t)}{\partial \ln R} + \left(1-\sqrt{\frac{R_1}{R}}\right)^{-1}\right] = 3\pi\nu\Sigma\tilde{g}. \tag{5.17}$$

Now substituting $\nu\Sigma$ defined by Eq.(5.17) to the Eq.(2.38) the viscous heating is given by

$$Q^+(R) \approx \frac{3GM_1\dot{M}_{\rm accr}}{8\pi R^3\tilde{g}} \tag{5.18}$$

and the estimated minimum disc luminosity is

$$L_{\rm min} \approx \frac{GM_1\dot{M}_{\rm tr}}{2R_{\rm d}\tilde{g}} \tag{5.19}$$

where $\tilde{g}\sim 2$ (Idan et al., 1999).

The amplitude $A_{\rm n}$ is the difference between the magnitudes at maximum $M_{\rm V,max}$ and minimum $M_{\rm V,min}$

$$A_{\rm n} = M_{\rm V,min} - M_{\rm V,max} + BC_-^+ = 2.5\log\frac{L_{\rm max}}{L_{\rm min}} + BC_-^+ \tag{5.20}$$

where BC_-^+ is the difference between the bolometric corrections at maximum and minimum. From Eq.(5.11), (5.13) and (5.19) we thus get

$$A_{\rm n} \approx C_1 + 2.5\log T_{\rm n} \tag{5.21}$$

where

$$C_1 = 2.5\log\,2\tilde{g} - 2.5\log t_{\rm dec} + BC_{\rm max} - BC_{\rm min} \tag{5.22}$$

The last step is to calculate the bolometric corrections BC_{max} and $BC_{\rm min}$.

From definition $BC_{\rm max} = M_{\rm bol,max} - M_{\rm V,max} = M_{\rm bol,max} + 2.5\log(L_{\rm V,max}/L_\odot)$.

Following Smak (1989b) we calculate the visual luminosity in maximum $L_{\rm V,max}$ with spectral energy distribution of a black body disc integrated over the band frequencies appropriate for Johnson V-filter where the effective wavelength is $\lambda_{\rm eff}\approx 545$ nm and the bandwidth is ~ 85 nm. This translates into the frequency range from $\nu_1 = 5.966\times10^{14}$ Hz to $\nu_2 = 5.102\times10^{14}$ Hz

$$L_{\rm V,max} = \frac{45}{\pi^4}\frac{GM_1\dot{M}_{\rm accr,max}}{2R_1}\int_{\nu_1}^{\nu_2}d\nu\int_1^{4x_d}\frac{1}{\nu_*}\frac{xdx}{\exp\left(\frac{\nu}{\nu_*}x^{3/4}(1-x^{-1/2})^{-1/4}\right)-1} \tag{5.23}$$

Model	C_1	$\alpha_{\rm h}$	$R_{\rm d,max}$	M_1
1	-2.5	0.01	2	1
2	-0.95	0.2	0.6	0.6
3	-0.2	0.2	2	1
4*	0.1	0.2	0.7	1
5	1.2	0.2	5	1.2
6*	1.3	0.2	0.8	1.2

Table 5.2: The table shows 6 sets of parameters for which the theoretical K-P relation has been calculated. The parameters listed in the table are: $\alpha_{\rm h}$ - the viscosity parameter in the hot disc, $R_{\rm d,max}$ - maximum disc radius in 10^{10} cm, M_1 - primary mass in $M_\odot$ and C_1 - the constant from Eq. (5.22) calculated for a given set of parameters. Models 2 and 5 correspond to the lower and upper limits of the theoretical K-P relation for solar discs with $\alpha_{\rm h} = 0.2$; models marked with "$*$" are calculated for helium discs ($Y = 0.98$ $Z = 0.02$): model 4* is supposed to give the K-P relation for PTF1J0719, model 6* is supposed to give the K-P relation for CR Boo and V803 Cen in their cycling states. The comparison between model 1 and 3 shows how the relation changes when $\alpha_{\rm h}$ is decreased from $\alpha_{\rm h} = 0.2$ to $\alpha_{\rm h} = 0.01$ in solar disc. The models are plotted with lines in Fig. 5.5.

where

$$x_d = \frac{R_{\rm d}}{R_1} \quad \nu_* = \frac{k}{h}\left(\frac{3}{8\pi\sigma}\frac{GM_1\dot{M}_{\rm accr,max}}{R_1^3}\right)^{1/4}. \tag{5.24}$$

As can be seen $L_{\rm V,max}$ (and so $BC_{\rm max}$) depends on M_1, R_1, $R_{\rm d}$ and $\dot{M}_{\rm accr,max}$.

The precise calculations of $L_{\rm V,max}$ should be performed using the fluxes from the models of stellar atmospheres (e.g. from The Kurucz Stellar Atmospheres Atlas), however, the black body approximation gives almost the same results within an error of 0.1 mag (Smak, 1989b) so it seems to be sufficient in this context.

$BC_{\rm min}$ can be estimated from spectral energy distribution, calculated for the model of a quiescent disc, which effective temperature is ~ 5500 K. We used spectra calculated by Irit Idan (2011 private communication; see Idan et al. (2010)) to determine the luminosity of the cold disc in the V-band. Assuming that the main contribution to the bolometric luminosity in quiescence comes from the outer parts of the disc ($\sim 40\%$ of the total disc surface, say) we eventually estimate that $BC_{\rm min} \approx -0.4$.

Eq.(5.21) does not correspond exactly to the K-P relation (see Eqs.5.8, 5.25). The slope of the theoretical relation is always 2.5 (by construction) as compared with ~ 2 obtained from fits to observations. Considering the typical spread of parameters, in hydrogen dominated discs C_1 is contained between ~ -1.0 and ~ 1.2 and is between ~ -0.2 and 1.3 in helium discs (see Table 5.2), to be compared with C_1 between 0.3 and 2.0 for the K-P relation. Considering the very large scatter of observational data this can be considered a rather satisfactory result. This is true only of the theoretical relation obtained assuming $\alpha_{\rm h} = 0.2$. The same relation with $\alpha_{\rm h} = 0.01$ gives a totally unacceptable representation of the $A_{\rm n}(T_{\rm n})$ relation thus confirming the conclusion of the previous Sections that $\alpha_{\rm h} \approx 0.2$.

The various $A_{\rm n}(T_{\rm n})$ relations are plotted in Fig.5.5. We also marked on this diagram the values of $A_{\rm n}(T_{\rm n})$ for a subset of dwarf novae and outbursting AM CVn stars. The sample of the systems

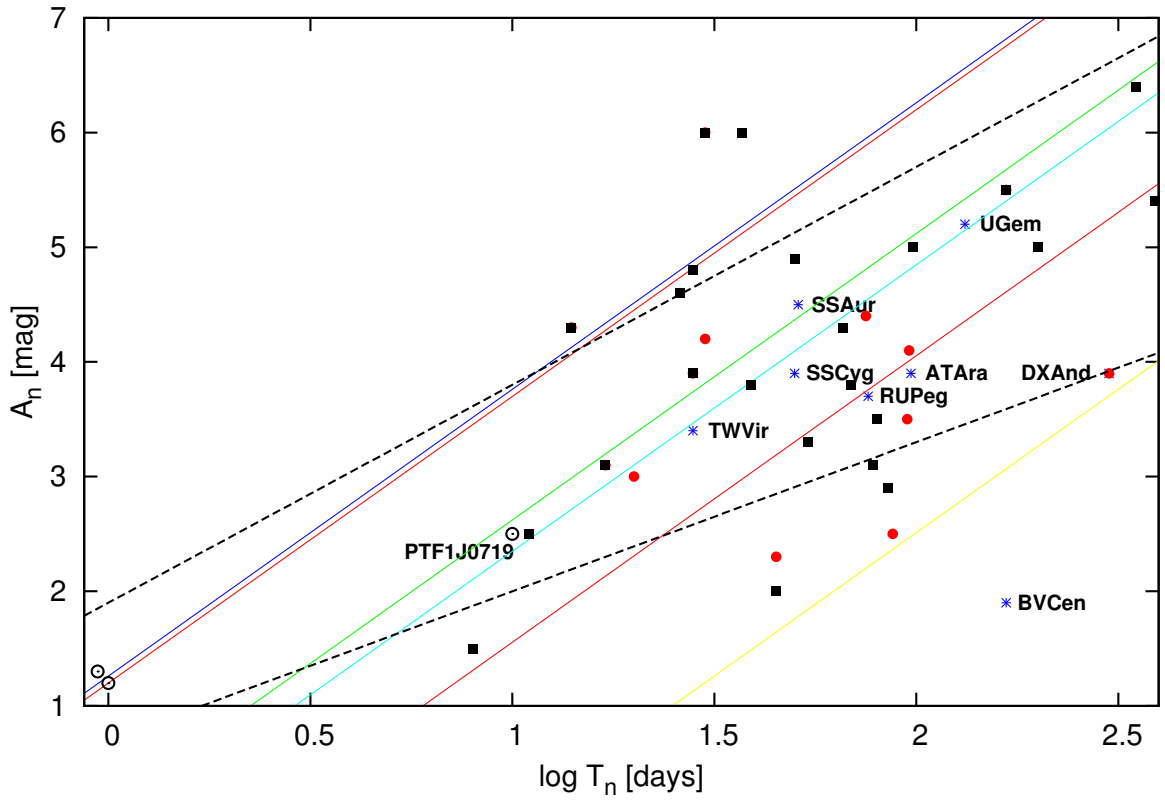

Figure 5.5: Various $A_{\rm n}(T_{\rm n})$ relations. The line colors correspond to the row numbers in Table 5.2: yellow - (1), red - (2), light blue - (3), green - (4), pink - (5), blue - (6). The red and pink lines correspond respectively to the "lower and upper limits" (see text) deduced from the theoretical relation for solar-abundance discs with $\alpha_{\rm h} = 0.2$ ($C_1 = -0.95$ and 1.2). Helium disc theoretical relations are represented by the lines green and blue ($C_1 = 0.1$ and 1.3). Lines yellow and light blue illustrate the $\alpha_{\rm h}$ dependence of the $A_{\rm n}(T_{\rm n})$ relation: for the same binary parameters they correspond to $\alpha_{\rm h} = 0.01$ and $\alpha_{\rm h} = 0.2$ respectively. The upper and lower uncertainty of observational K-P relation fitted to the systems are marked with black, dashed lines. The sample of binaries marked on the plot consists of U Gem-type systems listed in Table 5.1 (full circles and asterisk), AM CVn systems: PTF1J0719, CR Boo and V803 Cen (both in cycling state outbursts) (open circles) and SU UMa stars (normal outbursts only, full squares) from Ak et al. (2002) and updated Cataclysmic Binaries Catalog (Ritter and Kolb, 2003).

presented in Fig. 5.5 consists of U Gem-type binaries taken from Ak et al. (2002) and listed in Table 5.1, SU UMa-type binaries taken from Ak et al. (2002) (also listed in Table 5.1) and from updated Cataclysmic Binaries Catalog (Ritter and Kolb, 2003) (non listed in Table 5.1) and three AM CVn-type stars for which $A_{\rm n}$ and $T_{\rm n}$ were measured from their light curves. For CR Boo and V803 Cen (open circles in the left, bottom corner of Fig. 5.5) the measured $A_{\rm n}$ and $T_{\rm n}$ relate to the outbursts in the cycling state (Patterson et al., 2000).

In this sample 15 systems out of 43 are the same as used in Warner (2003). The linear fit to our sample gives

$$A_{\rm n} = (1.3 \pm 0.6) + (1.6 \pm 0.3) \log T_{\rm n} \tag{5.25}$$

Upper and lower uncertainties of this relation are marked as dashed lines in Fig.5.5. Some of the U Gem-type binaries in Fig.5.5 are marked with asterisks and their names as examples to show how observed systems correspond to the theoretical lines. For the same purpose the name of one of AM CVn stars is shown on the plot.

The amplitudes of the systems common to Ak et al. (2002) and Warner (2003) have been corrected and correspond to amplitudes of the disc luminosities alone. In maximum the main source of the optical luminosity is the disc, in quiescence the contribution of the hot spot may have a meaning only in the case of high inclinations, while the contribution from the primary WD may be significant (the boundary layer contributes mainly to wavelengths shorter than V).

The difference between Warner's corrected amplitudes and those taken from Ritter Catalog for the same systems differ by 0.8 mag on average. Taking into account all the simplifications and approximations in our derivation, as well as the uncertainties of the observational measurements of the outbursts amplitudes and uncertainties in determination of the WD temperature in a given system and its contribution to the total light, we believe that the fact that the amplitudes of other systems have not been corrected does not influence significantly our conclusions about the order of magnitude of α.

The independence of the theoretical K-P relation from $\dot{M}_{\rm tr}$ is the consequence of the assumption $\dot{M}_{\rm accr,max} \approx \epsilon \dot{M}^{+}_{\rm crit}(R_{\rm d,max})$ since $\dot{M}^{+}_{\rm crit}(R_{\rm d,max})$ does not depend on $\dot{M}_{\rm tr}$. Systems with larger (more extended) discs and more massive M_1 have higher $A_{\rm n}$ for a given $T_{\rm n}$ than systems with small discs or less massive primaries (compare lines red-pink, blue-green in Fig.5.5). Despite the simplifications and approximations assumed in the derivation, the theoretical K- P relation follows the observational data reasonably well. One concludes that normal dwarf nova outbursts are indeed the results of filling and emptying of an accretion disc, as assumed in the model. The parameter that has the deciding influence on the recurrence time and amplitude of normal outbursts is the disc's extent.

Chapter 6

Summary and outlook

In this thesis we showed that the Disc Instability Model is universal as the explanation of dwarf-nova-type outbursts. On the other hand its properties differ between the discs dominated by different chemical elements. This gives a unique opportunity to investigate the accretion disc response to changes of chemical compositions by the of numerical simulations of dwarf nova and AM CVn star light curves. The results brings new information about the conditions in which the thermal-viscous instability develops in the disc, about the connection of angular momentum transport in the disc with its microphysics and about what can be read out from the observed light curves of systems erupting in dwarf-nova manner.

The consequences of the change of the main disc matter component from hydrogen to helium were presented in Chapter 2. The high temperatures of helium ionization change the ranges of $T_{\rm c}$ and Σ at which the thermal-viscous instability operates in the disc. These high temperatures also imply that contrary to hydrogen-dominated disc even a small addition of metals ($\gtrsim 2\%$) affects the critical values of $T_{\rm c}$ and Σ and has noticeable influence on the disc behavior. Although the chemical composition of the disc manifest itself in the observed light curves, as has been proved with simulations in Sect.2.7.3, there are still too many uncertainties concerning the other disc parameters which shape the outbursts (e.g. the α-parameter) to state that one could infer the disc composition from observations of dwarf novae or AM CVn star light curves.

The atomic structure of helium gives rise to two possible ionization states. We analyzed how this modifies the opacities dependence on temperature (and so the critical values of Σ and $T_{\rm c}$) in helium discs taking into account also various metal fractions. Our results show also that changing α in the simulations of helium discs may have similar effect on the synthetic light curves as changing Z (Sect.2.7.1).

At this point one may ask the question about the relevance of different values of α for a hot and cold disc since it may be suspected that this would be no longer necessary in

the disc with hydrogen-less chemical composition. However, according to our results to obtain the outburst amplitudes corresponding to observed ones α still has to be changed in simulations of AM CVn stars.

The presence of two electrons in the helium atom gives rise to a wide range of atomic transitions which are absent in hydrogen. We found that this has the consequences for the structure and velocities of the heating and cooling fronts propagating in the disc (Sect.2.7.2): the fronts in helium discs are slower than those in solar-composition discs and their profiles show "humps" at the temperatures which may be identified with different atomic transitions in helium. There are no similar features in the profiles of fronts in hydrogen-rich discs.

In Chapter 4 it was shown that the DIM predictions for helium discs stability limits are in agreement with the observations of the AM CVn stars luminosity states with respect to their orbital periods. Thus it is reasonable to consider it as the model describing dwarf-nova-like outbursts in these systems. The analysis of the influence of helium disc parameters on the modeled light curves (including different Z) clearly shows that the basic version of the DIM has to be supplemented with additional components to reproduce the complex AM CVn star light curves. Among those which have been tested (the additional disc heating sources, a primary white dwarf magnetic field, the enhanced mass transfer rate from the secondary) the crucial one are the enhancements of mass transfer rate from the donor which is irradiated in a variable manner. As there is no agreement about the nature of such irradiation mechanism three ad hoc prescriptions have been used. This approach allowed to reproduce superoutbursts, standstills, the cycling states and dips in the modeled light curves which resemble the features seen in AM CVn star light curves. We found that the most successful is the prescription for mass transfer enhancement which in a very rough way may correspond to the precessing warped/tilted disc which temporary unveils the secondary to irradiation.

In the last part of this thesis the value of α in hot accretion discs has been investigated. The methods concern the comparison between the widths W and the decay time rates $\tau_{\rm dec}$ measured in the observed outbursts with those measured in the model light curves. Those methods are a repetition of what has been done by Smak (1999) but with the use of the different set of data. This set comprises of two types of dwarf novae (U Gem and SU UMa) and contains one AM CVn star (PTF1J0719+4858), the only one with well-observed normal outbursts. From the obtained relations $W - P_{\rm orb}$, $\tau_{\rm dec} - P_{\rm orb}$ and $W - R_{\rm disc}$, $\tau_{\rm dec} - R_{\rm disc}$ it can be inferred that $\alpha_{\rm h} = 0.1 - 0.2$ with preference for 0.2. These values are independent of the dwarf nova type. Though there is only one helium system included, it follows these relations close enough to conclude that they presumably do not depend on the disc chemical composition.

To verify the above-mentioned results we have derived the decay time of an outburst in a semi-analytical way. It has been taken into account that the decay time of the disc

luminosity is defined not by the propagation velocity of the cooling front in the disc but by the viscous diffusion of the hot disc matter and by the rate at which the matter outflows from the hot to the cold part of the disc. The derived expression depends on the quantities which can be estimated observationally and on $\alpha_{\rm h}$. The decay times calculated with this formula for the systems with known parameters and compared with the measured decay times of the outbursts in these systems indicates in most cases that $\alpha_{\rm h} = 0.2$ (Sect.5.1).

In the last part of this thesis the Kukarkin-Parenago relation (K-P relation) was considered. It has been known for a long time as the empirical relation between the amplitude and the recurrence time of the normal outbursts in dwarf novae. Here it is shown that corresponding relation can be derived from the DIM (Sect.5.2). This gives two pieces of information: (i) it confirms that the DIM is the model of normal outbursts in dwarf novae and (ii) if an outburst follows this relation it should be of normal type. This leads to farther conclusions that since the small outbursts in the cycling states of two AM CVn stars: CR Boo and V803 Cen follow the K-P relation they are the result of the same mechanism as normal outbursts.

To test the dependence of the empirical K-P relation on the disc chemical composition we fit the relation to our set of U Gem-type dwarf novae and check if the normal outbursts of PTFJ0719_4858 fit it. The fact that they follow it very closely and the previous conclusion about cycling states in AM CVn stars suggests that K-P relation is presumably independent of disc chemical composition and that DIM is the universal model explaining normal outbursts.

The derived K-P relation can be used as another method to deduce $\alpha_{\rm h}$ on the same principle as the formula for the decay time of an outburst - by comparing the amplitudes calculated for known parameters of the systems and assumed $\alpha_{\rm h}$ with the measured amplitudes of the outbursts in these systems. Again the results suggest that $\alpha_{\rm h} \sim 0.1 - 0.2$.

All the methods used in Chapter 5 as well as the simulations of the dwarf novae and AM CVn light curves rule out the values of $\alpha_{\rm h}$ much lower than 0.1. It has its consequences for the results of simulations performed in the framework of Magneto-Rotational-Instability model which give $\alpha_{\rm h} \sim 0.01 - 0.02$ which is an order of magnitude too small.

The results obtained in this thesis suggest the possible directions for further investigations:

1. The verification of the possible relation between α and the disc chemical composition - performing the simulations of disc behavior for wider range of chemical compositions, also with the dominant contribution of metals. The chemical composition in AM CVn stars is determined by their evolutionary path. The He-star channel allows the disc to be even completely comprised of metals ($Z = 1.0$). Verifying the behavior of the disc for so extreme abundances may set constrains on possible evolution of those binaries.

2. Joining the simulations of AM CVn star light curves with the simulations of their spectra - there are very few attempts of simulations of helium disc spectra and none of them are considering

optically thick discs with convection. The simulations of the evolution of spectra during the outburst cycle in helium discs, similar to those performed for hydrogen-rich discs (Idan et al., 2010) would be very valuable.

3. More detailed analysis of the problem of the precessing tilted disc geometry and its application to variable irradiation of the secondary - this complicated problem may give clues not only about the possible mechanism of complicated outburst patter in AM CVn stars but also about the nature of superhumps. The subject of enhanced mass transfer rate deserves even more attention as it is passed over by dwarf novae community despite arguments which seem to give evidence in its favor.

4. Verification of the obtained results with new, more detailed AM CVn stars database - the ongoing (e.g. Palomar Transient Factory) and planned (e.g. Gaia) surveys, in which AM CVn stars are important targets, are very promising. Higher sensitivity of the instruments and growing attention paid to these systems has already resulted in doubling the number of binaries classified as AM CVn stars. The better covered and more numerous light curves of helium systems will allow to verify our conclusions considering α in helium disc and explanation of their light curves.

5. The modeling of the discs in X-ray binaries - it is tempting to take advantage from the experience gained during the work on this thesis, extrapolate it to simulations of light curves of systems with more compact primaries and trying to reproduce complicated features of X-ray binaries light curves taking into account the conclusions from AM CVn light cuvres simulations.

6. The discrepancy between α deduced from MRI and dwarf nova simulations seems to be undeniable, taking into account that new methods still suggest that value of α in the hot discs of dwarf novae is ~ 0.2 . It is then reasonable to analyze closer the MRI assumptions as there may lie the problem and its solution.

Bibliography

Ak, T., Ozkan, M. T., and Mattei, J. A. (2002). Statistical analysis of the long-term visual light curve parameters of dwarf novae. A&A, 389:478–484.

Alexander, D. R. and Ferguson, J. W. (1994). Low-temperature Rosseland opacities. ApJ, 437:879–891.

Anderson, S. F., Becker, A. C., Haggard, D., Prieto, J. L., Knapp, G. R., Sako, M., Halford, K. E., Jha, S., Martin, B., Holtzman, J., Frieman, J. A., Garnavich, P. M., Hayward, S., Ivezić, Ž., Mukadam, A. S., Sesar, B., Szkody, P., Malanushenko, V., Richmond, M. W., Schneider, D. P., and York, D. G. (2008). Two More Candidate AM Canum Venaticorum (am CVn) Binaries from the Sloan Digital Sky Survey. AJ, 135:2108–2113.

Anderson, S. F., Haggard, D., Homer, L., Joshi, N. R., Margon, B., Silvestri, N. M., Szkody, P., Wolfe, M. A., Agol, E., Becker, A. C., Henden, A., Hall, P. B., Knapp, G. R., Richmond, M. W., Schneider, D. P., Stinson, G., Barentine, J. C., Brewington, H. J., Brinkmann, J., Harvanek, M., Kleinman, S. J., Krzesinski, J., Long, D., Neilsen, Jr., E. H., Nitta, A., and Snedden, S. A. (2005). Ultracompact AM Canum Venaticorum Binaries from the Sloan Digital Sky Survey: Three Candidates Plus the First Confirmed Eclipsing System. AJ, 130:2230–2236.

Armstrong, E., Patterson, J., and Kemp, J. (2012). Two photometric periods in the AM CVn system CP Eridani. MNRAS, 421:2310–2315.

Balbus, S. A. and Hawley, J. F. (1998). Instability, turbulence, and enhanced transport in accretion disks. *Reviews of Modern Physics*, 70:1–53.

Bath, G. T. and Shaviv, G. (1978). The space density, recurrence rate and classification of novae. MNRAS, 183:515–522.

Bildsten, L., Townsley, D. M., Deloye, C. J., and Nelemans, G. (2006). The Thermal State of the Accreting White Dwarf in AM Canum Venaticorum Binaries. ApJ, 640:466–473.

Buat-Ménard, V. and Hameury, J.-M. (2002). Superoutbursts, superhumps and the tidal-thermal instability model. A&A, 386:891–898.

Buat-Ménard, V., Hameury, J.-M., and Lasota, J.-P. (2001a). The nature of dwarf nova outbursts. A&A, 366:612–622.

Buat-Ménard, V., Hameury, J.-M., and Lasota, J.-P. (2001b). Z Cam stars: A particular response to a general phenomenon. A&A, 369:925–931.

Cannizzo, J. K. (1984). Accretion disk limit cycle mechanism in twin-degenerate interacting binaries. Nature, 311:443.

Cannizzo, J. K., Ghosh, P., and Wheeler, J. C. (1982). Convective accretion disks and the onset of dwarf nova outbursts. ApJ, 260:L83–L86.

Cannizzo, J. K., Smale, A. P., Wood, M. A., Still, M. D., and Howell, S. B. (2012). The Kepler Light Curves of V1504 Cygni and V344 Lyrae: A Study of the Outburst Properties. ApJ, 747:117.

Cannizzo, J. K., Still, M. D., Howell, S. B., Wood, M. A., and Smale, A. P. (2010). The Kepler Light Curve of V344 Lyrae: Constraining the Thermal-viscous Limit Cycle Instability. ApJ, 725:1393–1404.

Cannizzo, J. K. and Wheeler, J. C. (1984). The vertical structure and stability of alpha model accretion disks. ApJS, 55:367–388.

Copperwheat, C. M., Marsh, T. R., Dhillon, V. S., Littlefair, S. P., Woudt, P. A., Warner, B., Patterson, J., Steeghs, D., Kemp, J., Armstrong, E., and Rea, R. (2011a). The photometric period in ES Ceti. MNRAS, 413:3068–3074.

Copperwheat, C. M., Marsh, T. R., Littlefair, S. P., Dhillon, V. S., Ramsay, G., Drake, A. J., Gänsicke, B. T., Groot, P. J., Hakala, P., Koester, D., Nelemans, G., Roelofs, G., Southworth, J., Steeghs, D., and Tulloch, S. (2011b). SDSS J0926+3624: the shortest period eclipsing binary star. MNRAS, 410:1113–1129.

Deloye, C. J., Taam, R. E., Winisdoerffer, C., and Chabrier, G. (2007). The thermal evolution of the donors in AM Canum Venaticorum binaries. MNRAS, 381:525–542.

Dubus, G., Lasota, J.-P., Hameury, J.-M., and Charles, P. (1999). X-ray irradiation in low-mass binary systems. MNRAS, 303:139–147.

Eggleton, P. P. (1971). The evolution of low mass stars. MNRAS, 151:351.

Eggleton, P. P. (1983). Approximations to the radii of Roche lobes. ApJ, 268:368.

El-Khoury, W. and Li, J. (1999). A magnetic field in AM CVn? In Hellier, C. and Mukai, K., editors, *Annapolis Workshop on Magnetic Cataclysmic Variables*, volume 157 of *Astronomical Society of the Pacific Conference Series*, page 393.

Elvius, A. (1975). Variable blue object with a peculiar spectrum. A&A, 44:117–121.

Espaillat, C., Patterson, J., Warner, B., and Woudt, P. (2005). The Helium-rich Cataclysmic Variable ES Ceti. PASP, 117:189–198.

Faulkner, J., Lin, D. N. C., and Papaloizou, J. (1983). On the evolution of accretion disc flow in cataclysmic variables. I - The prospect of a limit cycle in dwarf nova systems. MNRAS, 205:359–375.

Fontaine, G., Brassard, P., Green, E. M., Charpinet, S., Dufour, P., Hubeny, I., Steeghs, D., Aerts, C., Randall, S. K., Bergeron, P., Guvenen, B., O'Malley, C. J., Van Grootel, V., Østensen, R. H., Bloemen, S., Silvotti, R., Howell, S. B., Baran, A., Kepler, S. O., Marsh, T. R., Montgomery, M. H., Oreiro, R., Provencal, J., Telting, J., Winget, D. E., Zima, W., Christensen-Dalsgaard, J., and Kjeldsen, H. (2011). Discovery of a New AM CVn System with the Kepler Satellite. ApJ, 726:92.

Frank, J., King, A., and Raine, D. J. (2002). *Accretion Power in Astrophysics: Third Edition*.

Friedjung, M. (1985). Accretion disks heated by luminous central stars. A&A, 146:366–368.

Grevesse, N. and Noels, A. (1993). Atomic data and the spectrum of the solar photosphere. *Physica Scripta Volume T*, 47:133–138.

Hameury, J., Lasota, J., and Hure, J. (1997). A model for WZ SGE with 'standard' values of alpha. MNRAS, 287:937–940.

Hameury, J., Lasota, J., and Warner, B. (2000). The zoo of dwarf novae: illumination, evaporation and disc radius variation. A&A, 353:244–252.

Hameury, J.-M. and Lasota, J.-P. (2005). Tidal torques, disc radius variations, and instabilities in dwarf novae and soft X-ray transients. A&A, 443:283–289.

Hameury, J.-M., Lasota, J.-P., and Dubus, G. (1999). Hot white dwarfs and the UV delay in dwarf novae. MNRAS, 303:39–44.

Hameury, J.-M., Menou, K., Dubus, G., Lasota, J.-P., and Hure, J.-M. (1998). Accretion disc outbursts: a new version of an old model. MNRAS, 298:1048–1060.

Harrop-Allin, M. K. and Warner, B. (1996). Accretion disc radii in eclipsing cataclysmic variables. MNRAS, 279:219–228.

Hirose, S., Krolik, J. H., and Blaes, O. (2009). Radiation-Dominated Disks are Thermally Stable. ApJ, 691:16–31.

Honeycutt, R. K. and Robertson, J. W. (1998). Multiyear Photometry and a Spectroscopic Orbital Period Search for the VY SCULPTORIS Type Cataclysmic Variable V794 Aquilae. AJ, 116:1961–1965.

Idan, I., Lasota, J. P., Hameury, J.-M., and Shaviv, G. (1999). Radiation from dwarf nova discs. Phys. Rep., 311:213–223.

Idan, I., Lasota, J.-P., Hameury, J.-M., and Shaviv, G. (2010). Accretion-disc model spectra for dwarf-nova stars. A&A, 519:A117.

Iglesias, C. A. and Rogers, F. J. (1996). Updated Opal Opacities. ApJ, 464:943.

Ishioka, R., Uemura, M., Matsumoto, K., Ohashi, H., Kato, T., Masi, G., Novak, R., Pietz, J., Martin, B., Starkey, D., Kiyota, S., Oksanen, A., Moilanen, M., Cook, L., Kral, L., Hynek, T., Kolasa, M., Vanmunster, T., Richmond, M., Kern, J., Davis, S., Crabtree, D., Beaulieu, K., Davis, T., Aggleton, M., Gazeas, K., Niarchos, P., Yushchenko, A., Mallia, F., Fiaschi, M., Good, G. A., Boyd, D., Sano, Y., Morikawa, K., Moriyama, M., Mennickent, R., Arenas, J., Ohshima, T., and Watanabe, T. (2002). First detection of the growing humps at the rapidly rising stage of dwarf novae AL Com and WZ Sge. A&A, 381:L41–L44.

Jetsu, L., Porceddu, S., Lyytinen, J., Kajatkari, P., Lehtinen, J., Markkanen, T., and Toivari-Viitala, J. (2012). Did the ancient egyptians record the period of the eclipsing binary Algol - the Raging one? *ArXiv e-prints*.

Kato, T. (2001). Changing Supercycle of the ER UMa-Type Star V1159 Ori. PASJ, 53:L17–L19.

Kato, T., Nogami, D., Baba, H., Hanson, G., and Poyner, G. (2000a). CR Boo: the 'helium ER UMa star' with a 46.3-d supercycle. MNRAS, 315:140–148.

Kato, T., Nogami, D., Matsumoto, K., and Baba, H. (2004a). Superhumps and Repetitive Rebrightenings of the WZ Sge-Type Dwarf Nova, EG Cancri. PASJ, 56:109.

Kato, T., Reszelski, M., Poyner, G., Simonsen, M., Muyllaert, E., Dubovsky, P. A., McGee, H., Ripero, J., and Itoh, H. (2001). The Second Supercycle of the Helium ER UMa Star, CR Boo. *Information Bulletin on Variable Stars*, 5120:1.

Kato, T., Stubbings, R., Monard, B., Butterworth, N. D., Bolt, G., and Richards, T. (2004b). V803 Centauri: Helium Dwarf Nova Mimicking a WZ Sge-Type Superoutburst. PASJ, 56:89.

Kato, T., Stubbings, R., Monard, B., and Pearce, A. (2000b). V803 Cen - the Second "Helium ER UMa Star". *Information Bulletin on Variable Stars*, 4915:1.

Kippenhahn, R. and Weigert, A. (1990). *Stellar Structure and Evolution*.

Kotko, I., Lasota, J.-P., Dubus, G., and Hameury, J.-M. (2012). Models of AM CVn star outbursts. *ArXiv e-prints*.

Kukarkin, B. and Parenago, P. (1934). *Var. Star. Bull.*, 4:44.

Landau, L. D. and Lifshitz, E. M. (1975). *The classical theory of fields*.

Lasota, J.-P. (2001). The disc instability model of dwarf novae and low-mass X-ray binary transients. New A Rev., 45:449–508.

Lasota, J.-P., Dubus, G., and Kruk, K. (2008). Stability of helium accretion discs in ultracompact binaries. A&A, 486:523–528.

Levitan, D., Fulton, B. J., Groot, P. J., Kulkarni, S. R., Ofek, E. O., Prince, T. A., Shporer, A., Bloom, J. S., Cenko, S. B., Kasliwal, M. M., Law, N. M., Nugent, P. E., Poznanski, D., Quimby, R. M., Horesh, A., Sesar, B., and Sternberg, A. (2011). PTF1 J071912.13+485834.0: An Outbursting AM CVn System Discovered by a Synoptic Survey. ApJ, 739:68.

Lin, D. N. C. and Papaloizou, J. (1979). Tidal torques on accretion discs in binary systems with extreme mass ratios. MNRAS, 186:799–812.

Ludwig, K. and Meyer, F. (1998). Fine mesh calculations of dwarf nova outbursts. A&A, 329:559–570.

Mason, K. O., Cordova, F. A., Watson, M. G., and King, A. R. (1988). The discovery of orbital dips in the soft X-ray emission of U GEM during an outburst. MNRAS, 232:779–791.

Menou, K., Hameury, J.-M., and Stehle, R. (1999). Structure and properties of transition fronts in accretion discs. MNRAS, 305:79–89.

Meyer, F. (1984). Transition waves in accretion disks. A&A, 131:303–308.

Meyer, F. and Meyer-Hofmeister, E. (1981). On the Elusive Cause of Cataclysmic Variable Outbursts. A&A, 104:L10.

Mineshige, S. and Osaki, Y. (1983). Disk-instability model for outbursts of dwarf novae Time-dependent formulation and one-zone model. PASJ, 35:377–396.

Nauenberg, M. (1972). Analytic Approximations to the Mass-Radius Relation and Energy of Zero-Temperature Stars. ApJ, 175:417.

Nelemans, G., Portegies Zwart, S. F., Verbunt, F., and Yungelson, L. R. (2001). Population synthesis for double white dwarfs. II. Semi-detached systems: AM CVn stars. A&A, 368:939–949.

Nelemans, G., Yungelson, L. R., van der Sluys, M. V., and Tout, C. A. (2010). The chemical composition of donors in AM CVn stars and ultracompact X-ray binaries: observational tests of their formation. MNRAS, 401:1347–1359.

Nogami, D., Monard, B., Retter, A., Liu, A., Uemura, M., Ishioka, R., Imada, A., and Kato, T. (2004). The Peculiar 2004 Superoutburst in the Helium Dwarf Nova, 2003aw. PASJ, 56:L39–L43.

Osaki, Y. (1985). Irradiation-induced mass-overflow instability as a possible cause of superoutbursts in SU UMa stars. A&A, 144:369–380.

Osaki, Y. (1989). A model for the superoutburst phenomenon of SU Ursae Majoris stars. PASJ, 41:1005–1033.

Osaki, Y. and Meyer, F. (2003). Is evidence for enhanced mass transfer during dwarf-nova outbursts well substantiated? A&A, 401:325–337.

Paczyński, B. (1969). Envelopes of Red Supergiants. Acta Astron., 19:1.

Paczyński, B. (1971). Evolutionary Processes in Close Binary Systems. ARA&A, 9:183.

Paczynski, B. (1976). Common Envelope Binaries. In Eggleton, P., Mitton, S., and Whelan, J., editors, *Structure and Evolution of Close Binary Systems*, volume 73 of *IAU Symposium*, page 75.

Papaloizou, J. and Pringle, J. E. (1977). Tidal torques on accretion discs in close binary systems. MNRAS, 181:441–454.

Patterson, J., Masi, G., Richmond, M. W., Martin, B., Beshore, E., Skillman, D. R., Kemp, J., Vanmunster, T., Rea, R., Allen, W., Davis, S., Davis, T., Henden, A. A., Starkey, D., Foote, J., Oksanen, A., Cook, L. M., Fried, R. E., Husar, D., Novák, R., Campbell, T., Robertson, J., Krajci, T., Pavlenko, E., Mirabal, N., Niarchos, P. G., Brettman, O., and Walker, S. (2002). The 2001 Superoutburst of WZ Sagittae. PASP, 114:721–747.

Patterson, J., Walker, S., Kemp, J., O'Donoghue, D., Bos, M., and Stubbings, R. (2000). V803 Centauri: A Helium-rich Dwarf Nova. PASP, 112:625–631.

Payne-Gaposchkin, C. (1977). Past and Future Novae. In Friedjung, M., editor, *Novae and Related Stars*, volume 65 of *Astrophysics and Space Science Library*, page 3.

Podsiadlowski, P. (2008). The Evolution of Close Binaries. In Evans, A., Bode, M. F., O'Brien, T. J., and Darnley, M. J., editors, *RS Ophiuchi (2006) and the Recurrent Nova Phenomenon*, volume 401 of *Astronomical Society of the Pacific Conference Series*, page 63.

Podsiadlowski, P., Han, Z., and Rappaport, S. (2003). Cataclysmic variables with evolved secondaries and the progenitors of AM CVn stars. MNRAS, 340:1214–1228.

Postnov, K. A. and Yungelson, L. R. (2006). The Evolution of Compact Binary Star Systems. *Living Reviews in Relativity*, 9:6.

Pringle, J. E. (1981). Accretion discs in astrophysics. ARA&A, 19:137–162.

Ramsay, G., Barclay, T., Steeghs, D., Wheatley, P. J., Hakala, P., Kotko, I., and Rosen, S. (2012). The long-term optical behaviour of helium-accreting AM CVn binaries. MNRAS, 419:2836–2843.

Ramsay, G., Groot, P. J., Marsh, T., Nelemans, G., Steeghs, D., and Hakala, P. (2006). XMM-Newton observations of AM CVn binaries: V396 Hya and SDSS J1240-01. A&A, 457:623–627.

Ramsay, G., Kotko, I., Barclay, T., Copperwheat, C. M., Rosen, S., Jeffery, C. S., Marsh, T. R., Steeghs, D., and Wheatley, P. J. (2010). Multiwavelength observations of the helium dwarf nova KL Dra through its outburst cycle. MNRAS, 407:1819–1825.

Rau, A., Roelofs, G. H. A., Groot, P. J., Marsh, T. R., Nelemans, G., Steeghs, D., Salvato, M., and Kasliwal, M. M. (2010). A Census of AM CVn Stars: Three New Candidates and One Confirmed 48.3-Minute Binary. ApJ, 708:456–461.

Ritter, H. (2008). Formation and Evolution of Cataclysmic Variables. *ArXiv e-prints*.

Ritter, H. and Kolb, U. (2003). Catalogue of cataclysmic binaries, low-mass X-ray binaries and related objects (Seventh edition). A&A, 404:301–303.

Roelofs, G. H. A., Groot, P. J., Benedict, G. F., McArthur, B. E., Steeghs, D., Morales-Rueda, L., Marsh, T. R., and Nelemans, G. (2007a). Hubble Space Telescope Parallaxes of AM CVn Stars and Astrophysical Consequences. ApJ, 666:1174–1188.

Roelofs, G. H. A., Groot, P. J., Marsh, T. R., Steeghs, D., and Nelemans, G. (2005). SDSS J1240-01: A New AM CVn Star with a 37-Minute Orbital Period. In Koester, D. and Moehler, S., editors, *14th European Workshop on White Dwarfs*, volume 334 of *Astronomical Society of the Pacific Conference Series*, page 443.

Roelofs, G. H. A., Groot, P. J., Marsh, T. R., Steeghs, D., and Nelemans, G. (2006). Phase-resolved spectroscopy of the helium dwarf nova 'SN 2003aw' in quiescence. MNRAS, 365:1109–1113.

Roelofs, G. H. A., Groot, P. J., Nelemans, G., Marsh, T. R., and Steeghs, D. (2007b). On the orbital periods of the AM CVn stars HP Librae and V803 Centauri. MNRAS, 379:176–182.

Roelofs, G. H. A., Groot, P. J., Steeghs, D., Marsh, T. R., and Nelemans, G. (2007c). The long-period AM CVn star SDSS J155252.48+320150.9. MNRAS, 382:1643–1647.

Roelofs, G. H. A., Groot, P. J., Steeghs, D., Rau, A., de Groot, E., Marsh, T. R., Nelemans, G., Liebert, J., and Woudt, P. (2009a). SDSSJ080449.49+161624.8: a peculiar AM CVn star from a colour-selected sample of candidates. MNRAS, 394:367–374.

Roelofs, G. H. A., Groot, P. J., Steeghs, D., Rau, A., de Groot, E., Marsh, T. R., Nelemans, G., Liebert, J., and Woudt, P. (2009b). SDSSJ080449.49+161624.8: a peculiar AM CVn star from a colour-selected sample of candidates. MNRAS, 394:367–374.

Roelofs, G. H. A., Rau, A., Marsh, T. R., Steeghs, D., Groot, P. J., and Nelemans, G. (2010). Spectroscopic Evidence for a 5.4 Minute Orbital Period in HM Cancri. ApJ, 711:L138–L142.

Ruiz, M., Rojo, P., Garay, G., and Maza, J. (2001). CE 315: A New Interacting Double-Degenerate Binary Star. ApJ, 552:679–684.

Rutkowski, A., Olech, A., Wiśniewski, M., Pietrukowicz, P., Pala, J., and Poleski, R. (2009). CURious Variables Experiment (CURVE): CCD photometry of active dwarf nova DI Ursae Majoris. A&A, 497:437–444.

Schreiber, M. R., Hameury, J.-M., and Lasota, J.-P. (2004a). Delays in dwarf novae II: VW Hyi, the tidal instability and enhanced mass transfer models. A&A, 427:621–635.

Schreiber, M. R., Hameury, J.-M., and Lasota, J.-P. (2004b). Delays in dwarf novae II: VW Hyi, the tidal instability and enhanced mass transfer models. A&A, 427:621–635.

Shakura, N. I. and Sunyaev, R. A. (1973). Black holes in binary systems. Observational appearance. A&A, 24:337–355.

Shears, J., Brady, S., Koff, R., Goff, W., and Boyd, D. (2011). Superhumps and post-outburst rebrightening episodes in the AM CVn star SDSS J012940.05+384210.4. *ArXiv e-prints*.

Sion, E. M. and Godon, P. (2007). Properties of White Dwarfs in CVs Above the Period Gap. In Napiwotzki, R. and Burleigh, M. R., editors, *15th European Workshop on White Dwarfs*, volume 372 of *Astronomical Society of the Pacific Conference Series*, page 563.

Sion, E. M., Linnell, A. P., Godon, P., and Ballouz, R.-L. (2011). The Hot Components of AM CVn Helium Cataclysmics. ApJ, 741:63.

Smak, J. (1967). Light variability of HZ 29. Acta Astron., 17:255.

Smak, J. (1982). Accretion in cataclysmic binaries. I - Modified alpha-disks with convection. Acta Astron., 32:199–211.

Smak, J. (1983). Accretion in cataclysmic binaries. III - Helium binaries. Acta Astron., 33:333–337.

Smak, J. (1984). Accretion in cataclysmic binaries. IV - Accretion disks in dwarf novae. Acta Astron., 34:161–189.

Smak, J. (1989a). On the irradiation of disks in cataclysmic binaries. Acta Astron., 39:201–207.

Smak, J. (1989b). On the M(V)-M relation for accretion disks in cataclysmic binaries. Acta Astron., 39:317–321.

Smak, J. (1999). Dwarf Nova Outbursts. III. The Viscosity Parameter alpha. Acta Astron., 49:391–401.

Smak, J. (2000). Unsolved problems of dwarf nova outbursts. New A Rev., 44:171–175.

Smak, J. (2002). On the Structure of the Outer Parts of Accretion Disks in Close Binary Systems. Acta Astron., 52:263–272.

Smak, J. (2007). Superoutbursts of Z Chameleontis. Detection of the Hot Spot. Acta Astron., 57:87–101.

Smak, J. (2008a). Superoutbursts of Z Cha and their Interpretation. Acta Astron., 58:55–64.

Smak, J. (2008b). The Hot Spot in OY Car during its Superoutburst. Acta Astron., 58:65–67.

Smak, J. (2009a). Are Disks in Dwarf Novae during their Superoutbursts Really Eccentric? Acta Astron., 59:89–101.

Smak, J. (2009b). New Interpretation of Superhumps. Acta Astron., 59:121–130.

Smak, J. (2009c). On the Amplitudes of Superhumps. Acta Astron., 59:103–107.

Smak, J. (2009d). On the Origin of Tilted Disks and Negative Superhumps. Acta Astron., 59:419–430.

Smak, J. (2009e). Z Cha and its Superhumps. Acta Astron., 59:109–120.

Smak, J. (2010). On the Mass Transfer Rate in SS Cyg. Acta Astron., 60:83–89.

Smak, J. (2011). Direct Evidence for Modulated Irradiation of Secondary Components in Dwarf Novae during Superoutbursts. Acta Astron., 61:59–69.

Smak, J. (2012). Stream Overflow in Z Cha and OY Car during Quiescence. *ArXiv e-prints*.

Smak, J. and Waagen, E. O. (2004). The 1985 Superoutburst of U Geminorum. Detection of Superhumps. Acta Astron., 54:433–442.

Smak, J. I. (1991). On the models for superoutbursts in dwarf novae of the SU UMa type. Acta Astron., 41:269–277.

Smak, J. I. (2001). U Gem - Rediscussion of Radial Velocities and System Parameters. Acta Astron., 51:279–293.

Strohmayer, T. (2004). Detection of Nitrogen and Neon in the X-Ray Spectrum of GP Comae Berenices with XMM/Newton. ApJ, 608:L53–L56.

Thorstensen, J. R., Lépine, S., and Shara, M. (2008). Parallax and Distance Estimates for Twelve Cataclysmic Variable Stars. AJ, 136:2107–2114.

Tohline, J. E. (2002). The Origin of Binary Stars. ARA&A, 40:349–385.

Trampedach, R. and Stein, R. F. (2011). The Mass Mixing Length in Convective Stellar Envelopes. ApJ, 731:78.

Tsugawa, M. and Osaki, Y. (1997a). Disk Instability Model for the AM Canum Venaticorum Stars. PASJ, 49:75–84.

Tsugawa, M. and Osaki, Y. (1997b). Disk Instability Model for the AM Canum Venaticorum Stars. PASJ, 49:75–84.

van Paradijs, J. (1983). Superoutbursts - A general phenomenon in dwarf novae. A&A, 125:L16–L18.

van Paradijs, J. (1985). Recurrence behaviour of dwarf novae - The Kukarkin-Parenago relation. A&A, 144:199–201.

Viallet, M. and Hameury, J.-M. (2007). Hydrodynamic simulations of irradiated secondaries in dwarf novae. A&A, 475:597–606.

Viallet, M. and Hameury, J.-M. (2008). Mass transfer variation in the outburst model of dwarf novae and soft X-ray transients. A&A, 489:699–706.

Vishniac, E. T. and Wheeler, J. C. (1996). The Speed of Cooling Fronts and the Functional Form of the Dimensionless Viscosity in Accretion Disks. ApJ, 471:921.

Vogt, N. (1983). VW Hydri revisited - Conclusions on dwarf nova outburst models. A&A, 118:95–101.

Wade, R. A., Eracleous, M., and Flohic, H. M. L. G. (2007). New Ultraviolet Observations of AM CVn. AJ, 134:1740–1749.

Warner, B. (1995). Systematics of Superoutbursts in Dwarf Novae. Ap&SS, 226:187–211.

Warner, B. (2003). *Cataclysmic Variable Stars*.

Wood, M. A., Winget, D. E., Nather, R. E., Hessman, F. V., Liebert, J., Kurtz, D. W., Wesemael, F., and Wegner, G. (1987). The exotic helium variable PG 1346 + 082. ApJ, 313:757–771.

Zola, S. (1989). Disc radius versus time relations in Z Cha. Acta Astron., 39:45–49.

Appendix A

A.1 Y=1.0 Z=0.0

$$\Sigma^{-}_{\rm crit} = 5.28 \times 10^{2} \alpha_{0.1}^{-0.81} R_{10}^{1.07} M_{1}^{-0.36} \tag{A.1}$$

$$\Sigma^{+}_{\rm crit} = 1.62 \times 10^{2} \alpha_{0.1}^{-0.84} R_{10}^{1.19} M_{1}^{-0.40} \tag{A.2}$$

$$T^{+}_{\rm c,crit} = 7.70 \times 10^{4} \alpha_{0.1}^{-0.20} R_{10}^{0.08} M_{1}^{-0.03} \tag{A.3}$$

$$T^{-}_{\rm c,crit} = 1.78 \times 10^{4} \alpha_{0.1}^{-0.13} R_{10}^{-0.03} M_{1}^{0.01} \tag{A.4}$$

$$T^{+}_{\rm eff,crit} = 1.30 \times 10^{4} \alpha_{0.1}^{-0.01} R_{10}^{-0.08} M_{1}^{0.03} \tag{A.5}$$

$$T^{-}_{\rm eff,crit} = 9.70 \times 10^{3} \alpha_{0.1}^{-0.01} R_{10}^{-0.09} M_{1}^{0.03} \tag{A.6}$$

$$\dot{M}^{+}_{\rm crit} = 1.01 \times 10^{17} \alpha_{0.1}^{-0.05} R_{10}^{2.68} M_{1}^{-0.89}$$

$$\dot{M}^{-}_{\rm crit} = 3.17 \times 10^{16} \alpha_{0.1}^{-0.02} R_{10}^{2.66} M_{1}^{-0.89}$$

A.2 Y=0.98 Z=0.02

$$\Sigma^{+}_{\rm crit} = 3.80 \times 10^{2} \alpha_{0.1}^{-0.78} R_{10}^{1.06} M_{1}^{-0.35} \tag{A.7}$$

$$\Sigma^{-}_{\rm crit} = 6.12 \times 10^{2} \alpha_{0.1}^{-0.82} R_{10}^{1.10} M_{1}^{-0.37} \tag{A.8}$$

$$T^{+}_{\rm c,crit} = 7.14 \times 10^{4} \alpha_{0.1}^{-0.21} R_{10}^{0.08} M_{1}^{-0.03} \tag{A.9}$$

$$T^{-}_{\rm c,crit} = 2.36 \times 10^{4} \alpha_{0.1}^{-0.14} R_{10}^{-0.00} M_{1}^{0.00} \tag{A.10}$$

$$T^{+}_{\rm eff,crit} = 1.15 \times 10^{4} \alpha_{0.1}^{-0.01} R_{10}^{-0.08} M_{1}^{0.03} \tag{A.11}$$

$$T^{-}_{\rm eff,crit} = 8.69 \times 10^{3} \alpha_{0.1}^{-0.00} R_{10}^{-0.09} M_{1}^{0.03} \tag{A.12}$$

$$\dot{M}^{+}_{\rm crit} = 6.22 \times 10^{16} \alpha_{0.1}^{-0.05} R_{10}^{2.67} M_{1}^{-0.89} \tag{A.13}$$

$$\dot{M}^{-}_{\rm crit} = 2.04 \times 10^{16} \alpha_{0.1}^{-0.02} R_{10}^{2.62} M_{1}^{-0.87} \tag{A.14}$$

A.3 Y=0.96 Z=0.04

$$\Sigma^{+}_{\rm crit} = 3.22 \times 10^{2} \alpha_{0.1}^{-0.78} R_{10}^{1.04} M_{1}^{-0.35} \tag{A.15}$$

$$\Sigma^{-}_{\rm crit} = 4.59 \times 10^{2} \alpha_{0.1}^{-0.81} R_{10}^{1.08} M_{1}^{-0.36} \tag{A.16}$$

$$T^{+}_{\rm c,crit} = 6.68 \times 10^{4} \alpha_{0.1}^{-0.22} R_{10}^{0.07} M_{1}^{-0.02} \tag{A.17}$$

$$T^{-}_{\rm c,crit} = 2.51 \times 10^{4} \alpha_{0.1}^{-0.14} R_{10}^{0.00} M_{1}^{-0.00} \tag{A.18}$$

$$T^{+}_{\rm eff,crit} = 1.07 \times 10^{4} \alpha_{0.1}^{-0.01} R_{10}^{-0.09} M_{1}^{0.03} \tag{A.19}$$

$$T^{-}_{\rm eff,crit} = 8.35 \times 10^{3} \alpha_{0.1}^{-0.00} R_{10}^{-0.10} M_{1}^{0.03} \tag{A.20}$$

$$\dot{M}^{+}_{\rm crit} = 4.76 \times 10^{16} \alpha_{0.1}^{-0.06} R_{10}^{2.65} M_{1}^{-0.88} \tag{A.21}$$

$$\dot{M}^{-}_{\rm crit} = 1.74 \times 10^{16} \alpha_{0.1}^{-0.02} R_{10}^{2.61} M_{1}^{-0.87} \tag{A.22}$$